Techno-economic assessment of decarbonisation technologies for the iron and steel industry

by

Abhinav Bhaskar

Thesis submitted in fulfilment of
the requirements for the degree of
PHILOSOPHIAE DOCTOR
(PhD)

Faculty of science and technology

Institute of energy and petroleum technology
2023

University of Stavanger
NO-4036 Stavanger
NORWAY
www.uis.no

ISBN: Click to enter ISBN.
ISSN: Click to enter ISSN.
PhD: Thesis UiS No. Click to enter PhD No.

Acknowledgements

I would like to express my deepest gratitude to my supervisor, Professor Mohsen Assadi, for his unwavering guidance, support, and encouragement throughout the course of my doctoral research. His vast knowledge and expertise in the field of energy transition has been an invaluable asset to my work. I am deeply grateful for his dedication to my research and his willingness to provide feedback and advice at every stage of my work. I would also like to thank Dr. Homam Nikpey, and Mr. Oystein Arild, for their support and encouragement throughout my studies. I am thankful to the ENSYSTRA team for a cross-disciplinary learning experience, which has made me aware of challenges and opportunities across different disciplines of the energy transition.

I would like to extend my gratitude to my family, my parents, especially my wife, Rekha, for her love, support and understanding throughout the years of my research. Her unwavering support and encouragement have been a source of strength and motivation for me. I am truly grateful for the sacrifices she has made throughout this journey. It is safe to say that I would not have been able to finish my PhD without her support. My Parent's unwavering belief in me has been a constant source of inspiration for me. I would also like to thank my friends, who have always been there for me, providing support and encouragement. Their presence in my life has been a constant source of inspiration and motivation.

I am deeply grateful to all the people who have supported me throughout this journey, and I could not have done it without their guidance and support.

Abstract

Rapid decarbonisation of all segments of the economy is essential to limit the global mean surface temperature rise to 1.5ºC. Industries contribute to approximately a quarter of the global energy related emissions but have not received the same level of attention as the power and transport segment. The heterogeneity of industrial processes, use of fossil fuels as chemical feedstock and source of high-temperature heat, and the competitive nature of global commodity markets makes it difficult to implement decarbonisation solutions. Improving energy efficiency of existing processes has been the primary focus to reduce emissions from the industrial processes and has led to significant decline in energy and emission intensity of industrial segments.

Approximately 1.8 billion tonnes of steel is produced every year globally. The iron and steel industry is the backbone of modern civilization and is indispensable for the development of robust and resilient infrastructure, and the production of automobiles, buildings, household appliances etc. Primary production of steel through the blast furnace basic oxygen furnace route has high energy and emission intensity. The steel industry contributes to 7-8% of the global greenhouse gas emissions. Incremental improvements in the existing production process could be insufficient to meet the emission reduction targets. Innovative production technologies such as hydrogen direct reduction of iron ore, electrolysis of iron ore, use of carbon capture utilization and storage with blast furnace etc. have the potential to substantially reduce the emission footprint of the iron and steel industry.

In this work, a techno-economic assessment framework was used to assess the feasibility of the hydrogen direct reduced iron production route. A market analysis was conducted as the first step. It was found that the demand for low-emission steel in different end-use segments could be the key driver for the adoption of the technology. Policies and

regulations to support the innovative low-carbon production technologies i.e., carbon border adjustment mechanism, carbon contracts for difference etc., along with the increase in emission prices could lead to an increased rate of adoption of the technology. Approximately 60 Kg of hydrogen is required to produce one ton of liquid steel. Specific energy consumption of 4.25 MWh per ton of liquid steel for the process is comparable to the energy required by the blast furnace basic oxygen furnace route. Direct emissions from the process are 90% lower than the current primary production route. The levelized cost of production for was found to be in the range of 620-720 USD per ton of liquid steel. Electricity price and iron ore price were the most important parameters affecting the economic feasibility of the process. Other important parameters are the discount rate, electrolyzer capex and efficiency.

The rapid adoption of the technology by steel producers could be facilitated by policy measures intended to promote reductions in industrial emissions, such as capex subsidies for industrial decarbonization projects, high emission prices, carbon contracts for difference for energy-intensive industries, carbon border adjustment mechanism, hydrogen-related subsidies like the inflation reduction act, and general measures to ensure the competitiveness of the industrial segments in the EU and US. Other industrial actors have expressed interest in and plans to use the technology to create low emission steel, including China, Oman, and Indonesia. Technology adoption could be made possible by proximity to an area with access to high-grade iron ore and availability of good quality renewable resources like solar, wind, hydro, etc.

List of papers

I. Bhaskar, A.; Assadi, M.; Nikpey Somehsaraei, H. Decarbonization of the Iron and Steel Industry with Direct Reduction of Iron Ore with Green Hydrogen. *Energies* **2020**, *13*, 758. https://doi.org/10.3390/en13030758

II. Abhinav Bhaskar, Mohsen Assadi, Homam Nikpey Somehsaraei, Can methane pyrolysis based hydrogen production lead to the decarbonisation of iron and steel industry?, Energy Conversion and Management: X, Volume 10,2021,100079, ISSN 2590-1745, https://doi.org/10.1016/j.ecmx.2021.100079

III. Abhinav Bhaskar, Rockey Abhishek, Mohsen Assadi, Homam Nikpey Somehesaraei, Decarbonizing primary steel production : Techno-economic assessment of a hydrogen based green steel production plant in Norway, Journal of Cleaner Production, Volume 350, 2022, 131339, ISSN 0959-6526, https://doi.org/10.1016/j.jclepro.2022.131339

Table of Contents

Table of Figures

List of Tables

1 Introduction

Global carbon dioxide (CO2) emissions which have a direct impact on the radiative forcing resulting in the increase of global mean surface temperature have been rapidly increasing over the past few decades, as shown in Figure 1. Increasing emissions from all segments of the economy could lead to catastrophic impacts on our biosphere and all parts of the living world. Anthropogenic climate change is one of the biggest challenges to the human civilization. To mitigate the impacts of climate change rapid decarbonisation of all segments of the economy is required. While the focus up to now has been on reducing emissions from the energy system it is becoming increasingly evident that other sectors such as industries, and transport, often referred to as hard-to-abate segments, need to be decarbonized as well, as shown by the International energy agency in its recent report on net zero emission pathways (shown in Figure 2). Majority of the investments required to achieve the decarbonization goals are in the end-use segments like buildings, industry etc. Increased investments in infrastructure and end-use technologies for electrification and production and distribution of hydrogen will be required in the next decades to ensure complete decarbonization, as shown in Figure 3.

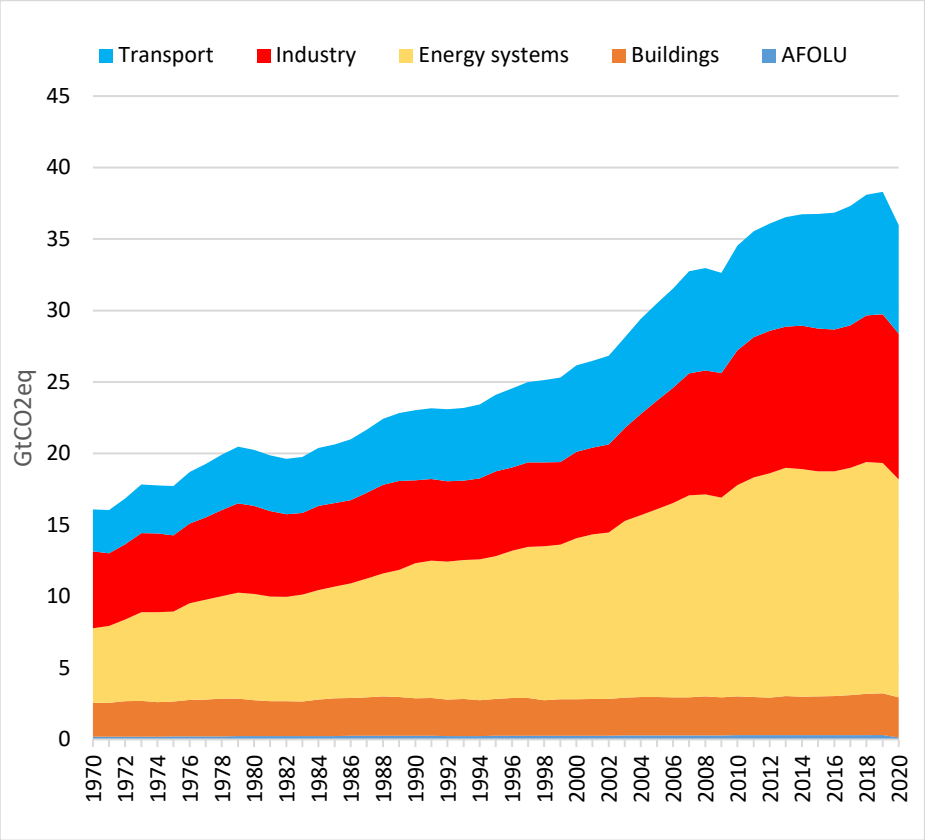

Figure 1 Global anthropogenic emissions growth from 1970 to 2019, CO_2-Land use-land use change – forestry (LULUCF) emissions are excluded (IPCC, 2022a)

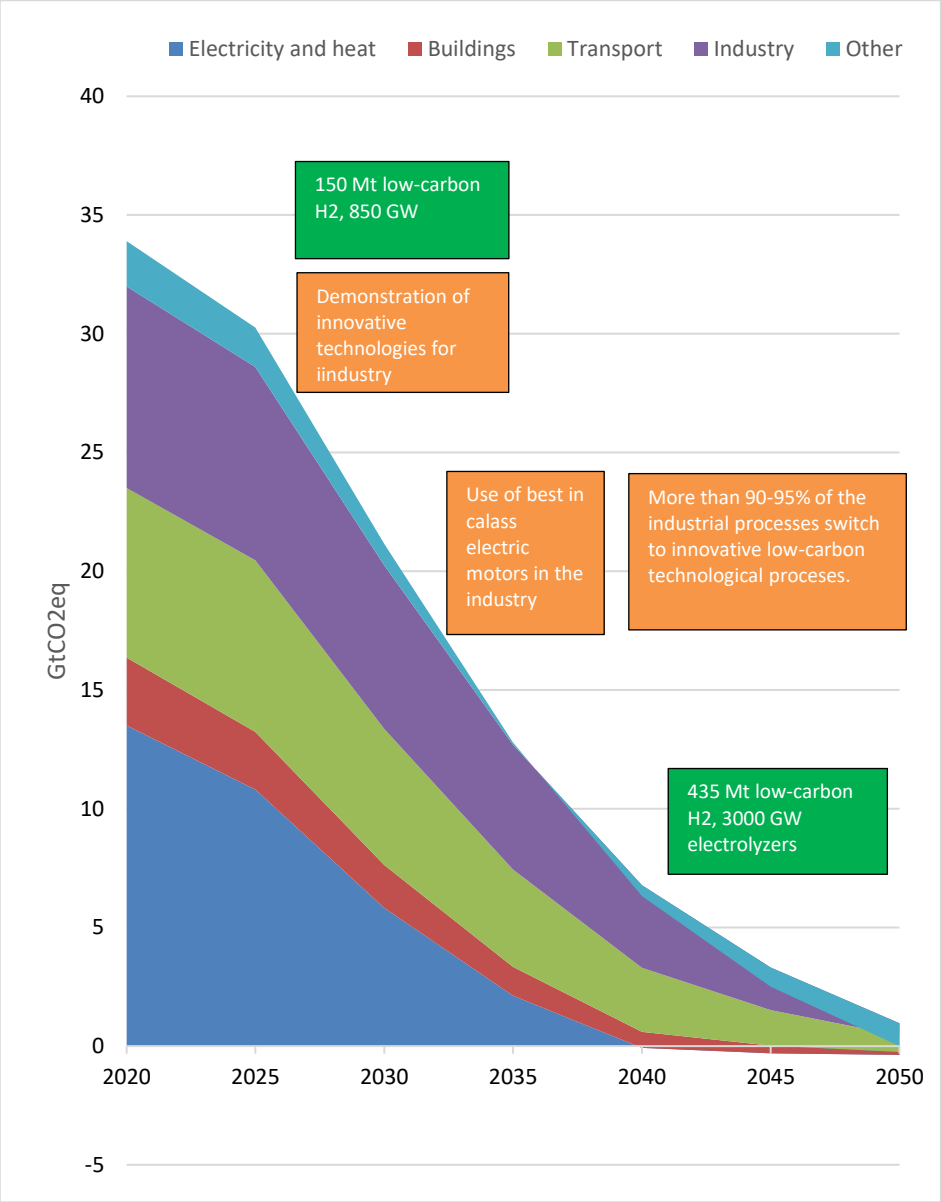

Figure 2 Selected global milestones for policies, infrastructure, and technology deployment in the Net-Zero emission scenarios (IEA, 2021b). Introduction of innovative low-carbon production technologies

in the industrial sector is contingent on the availability of large quantities of low-carbon hydrogen.

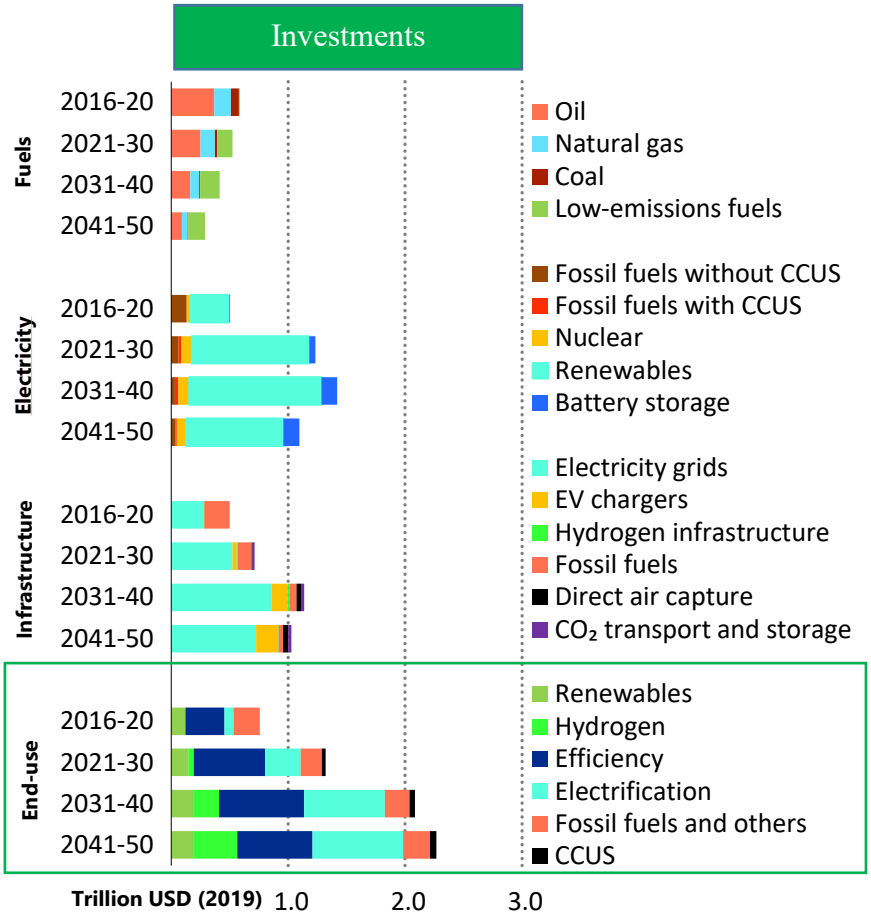

Figure 3 Investments required in different technologies to decarbonize the different segments of the economy by 2050 (IEA, 2021a).

To visualize the available solutions and their inter-dependence on the energy system, six academic institutions, across different North-sea countries launched a project called ENSYSTRA (energy systems in transition). The project was funded by the European commission under the innovative training network program (ITN). The focus of the program was to train fifteen early-stage researchers (ESR) in the different aspects of the energy transition, through open-source energy system modelling, technological evaluation, and understanding of the social and policy aspects. The current research was conducted under the work package 2 of the ENSYTRA project dealing with the techno-economic assessment of innovative technologies, specially focused on the techno-economic assessment of innovative production technologies for the decarbonization of energy intensive industries in the North-sea region.

Production of metals such iron, aluminum, copper, etc., is energy and emission intensive. Metallurgical processes require high-temperature heat supplied by fossil fuels. Fossil fuels are used as a chemical feedstock in some processes i.e., reduction of iron ore to iron, which is carried out by reacting the iron oxide at high temperature with carbon produced from coal. As depicted in Figure 4, emissions from the metal segments have been increasing significantly since 1970's. One of the major contributors to the emissions from the metal segments is the iron and steel sector and is the focus of the current research. The primary reasons for selecting the iron and steel segment lie in its huge contribution to the global CO_2 emissions, its significant role in the energy transition, and the presence of the iron and steel industry in the North-sea region (Figure 7). The rest of the thesis is structured as follows; a brief introduction to the global steel industry and the different decarbonization pathways is presented in subsequent sections of Chapter 1. The methodology is described briefly in Chapter 2. Research articles published as part of the doctoral research are summarized in Chapter 3, 4, and 5. Concluding remarks and future research suggestion are presented in Chapter 6.

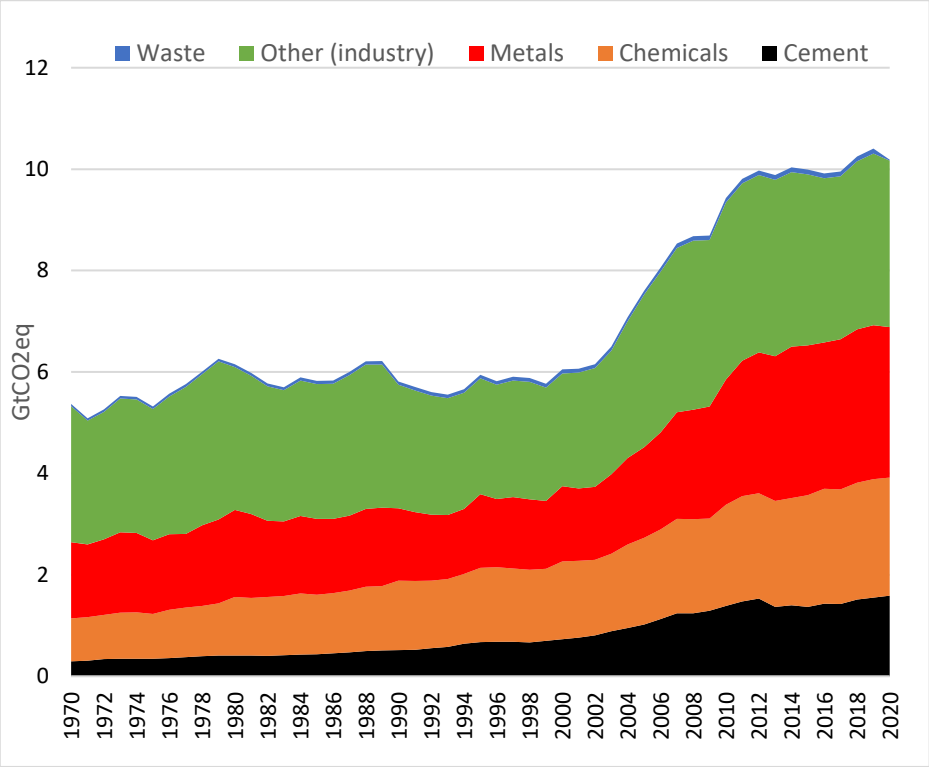

Figure 4 Industrial sector emissions from 1970-2020 (IEA, 2022d)

1.1 Global steel industry

Demand for materials has increased to provide services and infrastructure supporting the higher living standards of the society. The demand for materials such as steel, concrete, aluminium, copper, plastics, chemicals, etc., has increased considerably in the past few decades. Steel is ubiquitous and is one of the major building blocks for the modern economies. It finds application in a variety of end-use sectors. Steel mills across the globe produced 1.85 billion tonnes of steel in the year 2021, which is more than double of the 800 million tons they produced in the year 2000 (Energy Transition Commission, 2022). The surge in production is linked to the rapid economic growth of China, which produces more than half of the global steel. Crude steel produced is converted into a variety of products such as coils, sheets, strips, wires, bars, rods, tubes, pipes, rails and into plated and coated version which find application in specialized applications where corrosion resistance is required. Construction sector is the major driver for the increased demand for steel, and 40% of the steel produced is used for the construction of commercial and residential buildings. 20% of it is used in manufacturing industrial equipment; 18% for making consumer products (refrigerators, dish washers, washing machines etc.);13% for infrastructure (bridges etc.); and the remaining 10% is used in the automobile industry (IEA, 2022c).

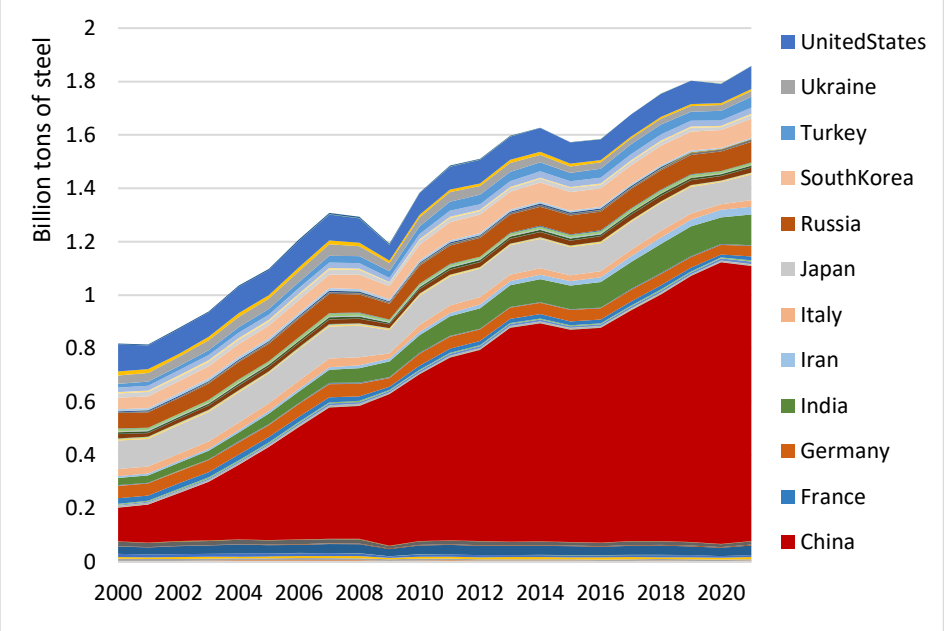

Figure 5 Global steel production from 2000-2021(WorldSteel, 2022)

Increase in steel production is closely linked to economic growth. The global steel industry is heavily fragmented with many regional producers. The top ten producers along with their production capacities are depicted in Figure 6.

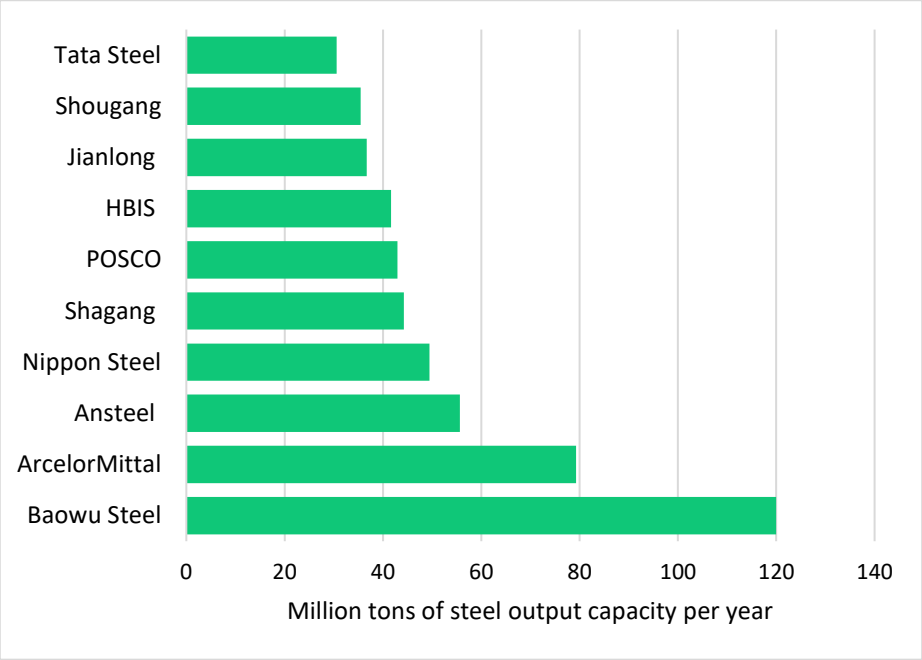

Figure 6 Largest producers of steel in 2021(WorldSteel, 2022)

There has been a significant overcapacity in the steel markets especially after the meteoric rise of steel production in China. The steel production in the EU-27 and the UK is going through a declining trend. The close relationship between GDP growth and steel production is shown in Figure 5. There was a steep reduction in production output in 2008-09 due to the financial crisis. The impact of covid-19 pandemic resulted in reduced production of steel in 2020. Although production has picked up, it is still lower than the peak reached in 2006-07. European steel production has declined over the years, as it has been facing stiff competition from developing countries which have cheaper production costs (Figure 6). Germany is the largest producer of steel in the EU closely followed by Italy and France. Majority of the steel is produced through the secondary steel production route in Italy (EUROFER, 2022).

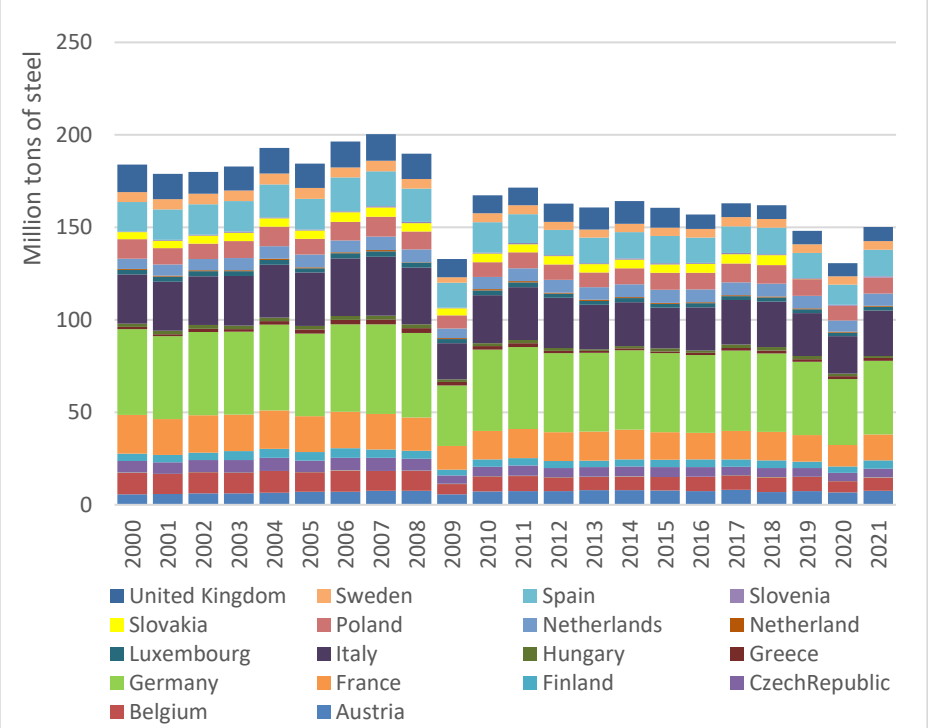

Figure 7 Steel production in EU-27 and UK (Energy Transition Commission, 2022; EUROFER, 2022)

1.2 Steel Production pathways

There are two dominant production pathways for the global steel industry based on the type of metallic input used. Primary steel production refers to the use of iron ore and its subsequent reduction using coal or natural gas. The use of steel scrap for production of crude steel by using electricity as a source of energy and heat is referred to as secondary steelmaking. In 2019, 71.1 % of the crude steel was produced by the primary steelmaking route whereas the remaining 28.9% was produced by the secondary steel making route in electric arc and induction furnaces (IEA, 2022d). The regional differences in the overall production mixes are more nuanced and are affected by the availability of scrap, price of iron ore, energy sources, etc. The distribution of the production pathways

in the twenty largest steel producing countries is presented in Figure 8. It is important to note that in countries with large quantities of direct reduced iron (DRI) production (i.e., Iran, India, Russia, Egypt, Saudi Arabia, etc.) electric arc furnaces are also used for primary steel production. Scrap and DRI are mixed in varying proportions as the input feed to the Electric arc furnace (EAF). Developing countries like China have lesser material stock returning for secondary production and are currently reliant on primary steel production routes to meet their steel demand. In developed economies like Italy and Germany, secondary steel making is increasing its market share. In the EU-27 countries EAF based steel production had an average market share of 43.9% in 2021(EUROFER, 2022).

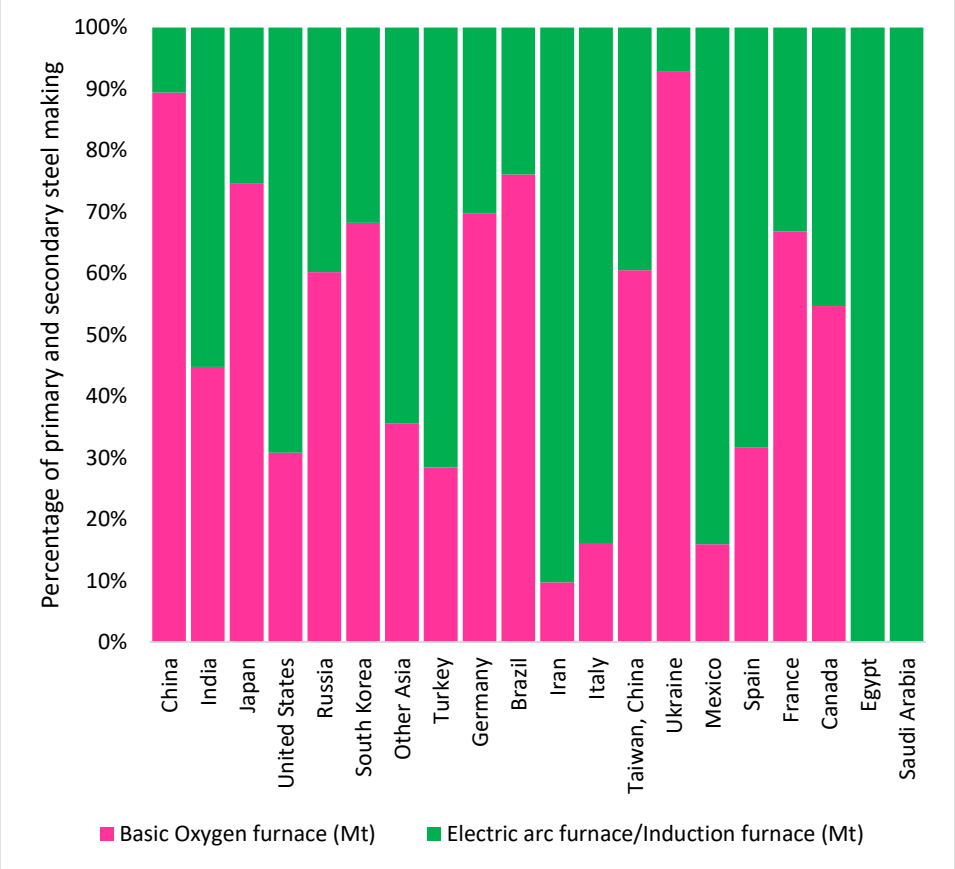

Figure 8 Crude steel produced from different production pathways for the twenty leading steel producers (WorldSteel, 2022)

1.2.1 Primary steelmaking

Primary steelmaking incorporates three main steps i.e., raw material production/preparation, ironmaking, and steelmaking, as has been depicted in Figure 9 . The raw materials required for primary steelmaking are iron ore, lime fluxes (limestone and dolomite to remove impurities), reducing agent (coke, natural gas, biomass etc.,) and energy source (for high temperature heat and mechanical drives such as pumps, compressors etc.).

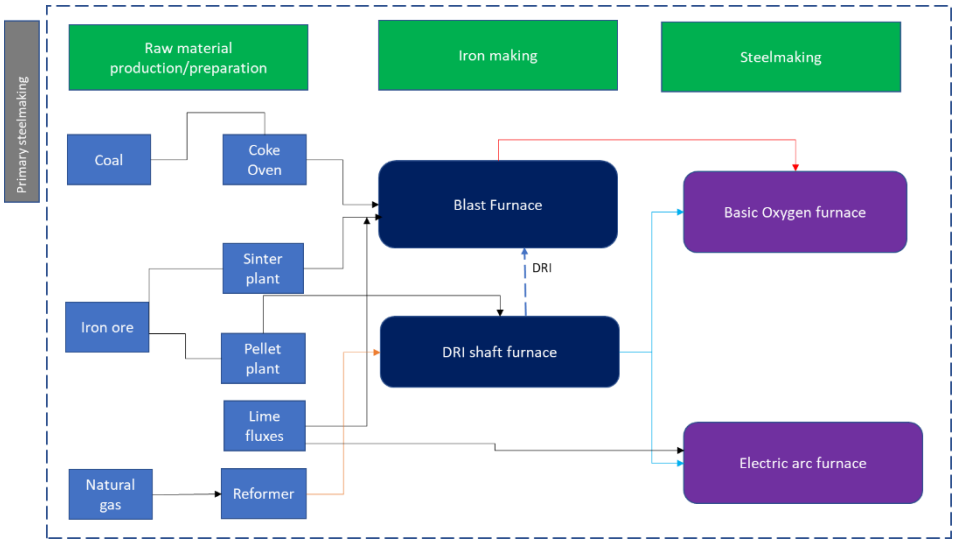

Figure 9 Production pathways of primary steel (Energy Transition Commission, 2022)

Iron is one of the most abundant materials. It forms 5% of the earth's crust. Iron is found in the form of its oxides i.e., Hematite (Fe_2O_3) or Magnetite (Fe_3O_4) in nature, along with impurities such as alumina, silica, phosphorus, sulfur etc. The raw iron ore needs to be processed to remove the impurities. During the beneficiation process raw iron ore is screened, crushed and grinded into fine particles often called as iron ore fines. Iron ore fines go through the process of agglomeration (sintering or pelletizing) before they can go through the reduction process. Sintering has traditionally been used in the blast furnace-based steel production route. Iron ore, slag forming agent, fluxes, and solid fuel (coke) are thermally agglomerated at a temperature of 1300-1400 °C (Fernández-González et al., 2017). Sintering allows the control of thermal, mechanical, and chemical properties of the input feed to the blast furnace and allows optimal operations. Pellets are made in three steps i.e., feed preparation and mixing (iron ore concentrates, anthracite, coke, dolomite, binding agent); balling or rolling process which produces spherical balls of 8-16 mm diameter with optimal moisture content; the

final step is called induration in which the spherical pellets produced from the rolling process are heated to a high temperature at controlled heating rates. The induration step imparts the physical and metallurgical properties required for handling, transportation, and final application(Fernández-González et al., 2018). The binding agent used in the pellet making process is bentonite, which is composed of alumina and silica. Substituting bentonite with organic binding agents is an active area of research. It can improve the performance of the reduction process by reducing the amount of alumina and silica in the feed (de Moraes et al., 2020). Pellets can be divided into blast furnace (BF) and direct reduction (DR) grade pellets (Pal, 2019). The distinction is made based on their iron content, where DR grade pellets have a higher iron content of 66% or higher, compared to 62-65% of BF grade pellets (Halt & Kawatra, 2014). DR grade pellets must have lower impurity content. The direct reduction process does not have a slag removal step, as iron is formed in the solid state. It must be noted that there is significant variation in the composition of the iron ore agglomerates depending on the mines. In the iron ore markets, ores with higher iron or metallic content attracts a price premium. The amount of sulfur should be very low for DR grade pellets especially the ones that are fed to DR furnaces with an external reformer such as the MIDREX reactors (Alhumaizi et al., 2012).

Iron ore is a globally traded commodity and is one of the most important commodities for bulk trade through the sea-borne route. Australia is one of the largest exporters of iron ore. China and Japan are the largest importers of the iron ore from Australia owing to the geographical proximity. Fortescue metals group (FMG), Rio Tinto, Vale, BHP Billiton etc. are the largest producers and exporters of iron ore globally.

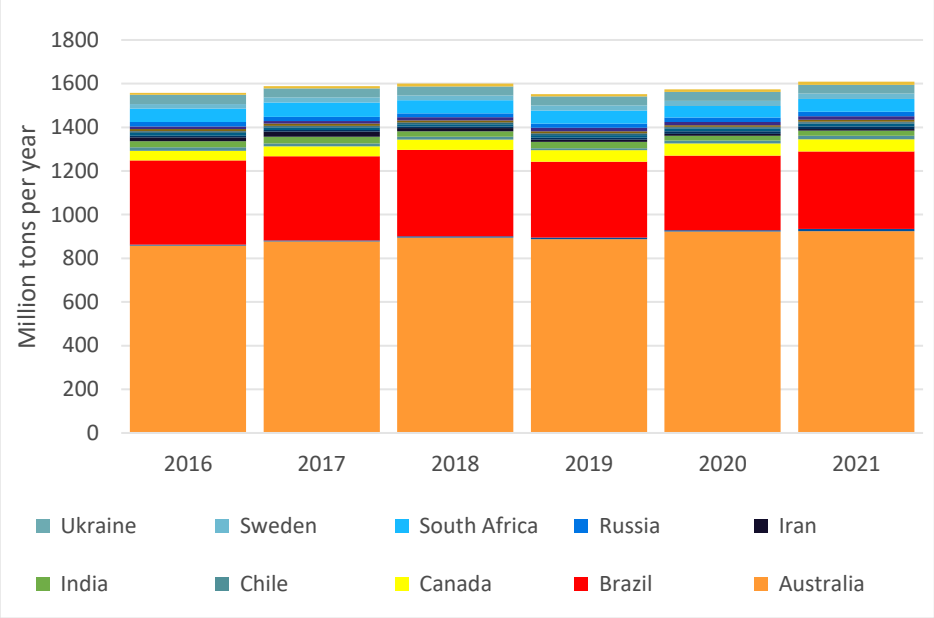

Figure 10 Largest iron ore exporters globally(WorldSteel, 2022)

Almost 90% of the primary steel is produced through the blast furnace basic oxygen furnace (BF-BOF) route, where iron ore is reduced to iron in a blast furnace and is subsequently converted to steel in a basic oxygen furnace. In some countries such as Russia and Ukraine, open hearth furnaces are still being used to convert iron to steel, but they have primarily been replaced with basic oxygen furnace in most other countries (Muslemani et al., 2021; WorldSteel, 2022). Coke has traditionally been used for the reduction of iron oxide to iron in a blast furnace. Coking coal has higher carbon content compared to thermal coal. Coke is produced by heating coking coal to a temperature of 1100-1300°C in the absence of air in a coke oven (Naito et al., 2015). The heat addition removes the volatile components of coal which are released from the coke oven as coke oven gas. The coke oven gas is rich in hydrogen, methane, and carbon monoxide, has a high calorific value and is often used for power or heat production in an integrated steel mill. There are many steel mills in China which produce methanol from the

coke oven gases (IEA, 2022c). Iron ore sinters and coke are fed to the blast furnace from the top. Blast furnace is a counter current heterogenous reactor operating at a temperature higher than 1650 °C (Treptow & Jean, 1998). Hot air is blown into the blast furnace from the bottom which combusts the coke, producing large quantities of carbon monoxide (CO). The iron ore is reduced by CO in the reduction zone. Exhaust gases from the blast furnace are released from the top of the furnace. In some plants the exhaust gases are used for heat and power generation owing to the high-energy content of the exhaust stream. Limestone ($CaCO_3$) fed into the furnace decomposes into lime and CO_2. Lime (CaO) reacts with silica and other impurities in the iron ore to form slag. The reduced iron or pig iron which has a high carbon content of 4-5% is transferred from the blast furnace to the basic oxygen furnace (Worrell et al., 1999). Excess carbon is removed from the iron in this step. Other material such as chromium, vanadium etc. can be added to steel to induce the desired properties. The molten steel is further processed into the desired end-products in the product finishing steps. The overall reactions in the shaft furnace are presented in **Error! Reference source not found.** to Equation 3. Heat generated from the oxidation of the coke is used to maintain the high temperature inside the reactor to maintain favorable kinetics for the reduction reaction.

Equation 1 Exothermic coke oxidation

$$C_{(s)} + ½\ O_{2(g)} \rightarrow CO_{(g)}$$

Equation 2 Decomposition of limestone

$$CaCO_{3(s)} \rightarrow CaO_{(s)} + CO_{2(g)}$$

Equation 3 Iron ore reduction

$$Fe_2O_{3(s)} + 3CO_{(g)} \rightarrow 2Fe_{(s)} + 3CO_{2(g)}$$

Direct reduction

Direct reduction (DR) refers to the reduction of iron ore in its solid state resulting in the production of direct reduced iron (DRI) or hot briquetted iron (HBI). Carbon monoxide and hydrogen are the reducing gases and are primarily produced from the reforming of natural gas. Coal gasification has been used to produce reducing gas but currently only one such plant i.e., Jindal steel, Angul, Odisha is functional. Coke oven gases have also been used in some plants as they are rich in CO and H_2. Production of DRI at a commercial scale started in the 1970's and the installed capacity has been increasing in the recent years especially in regions with access to cheap natural gas such as Russia, Iran, Algeria, United States etc. Iron ore reduction is carried out at a temperature of 900-1000 °C in reduction shaft furnace which is a counter current heterogenous reactor. Iron ore pellets are fed from the top of the furnace while the reducing gas is fed from the bottom of the reactor. Hematite in the iron ore is first converted into Magnetite, subsequently to Wustite and finally to metallic iron (Heidari et al., 2021) . The metallization rate of DRI shaft furnace is in the range of 90-94% (Spreitzer & Schenk, 2019). DRI produced from the shaft furnace is converted to steel in an electric arc furnace or a basic oxygen furnace. DRI can be fed to a blast furnace to improve the metallic output. DRI can be converted to steel at the same location or transported to another location depending on the requirements. Transport of DRI is generally avoided as it is highly susceptible to oxidation and is generally converted to HBI. The global production of DRI in 2021 grew more than two times from 2000 to 108.1 Mt/year

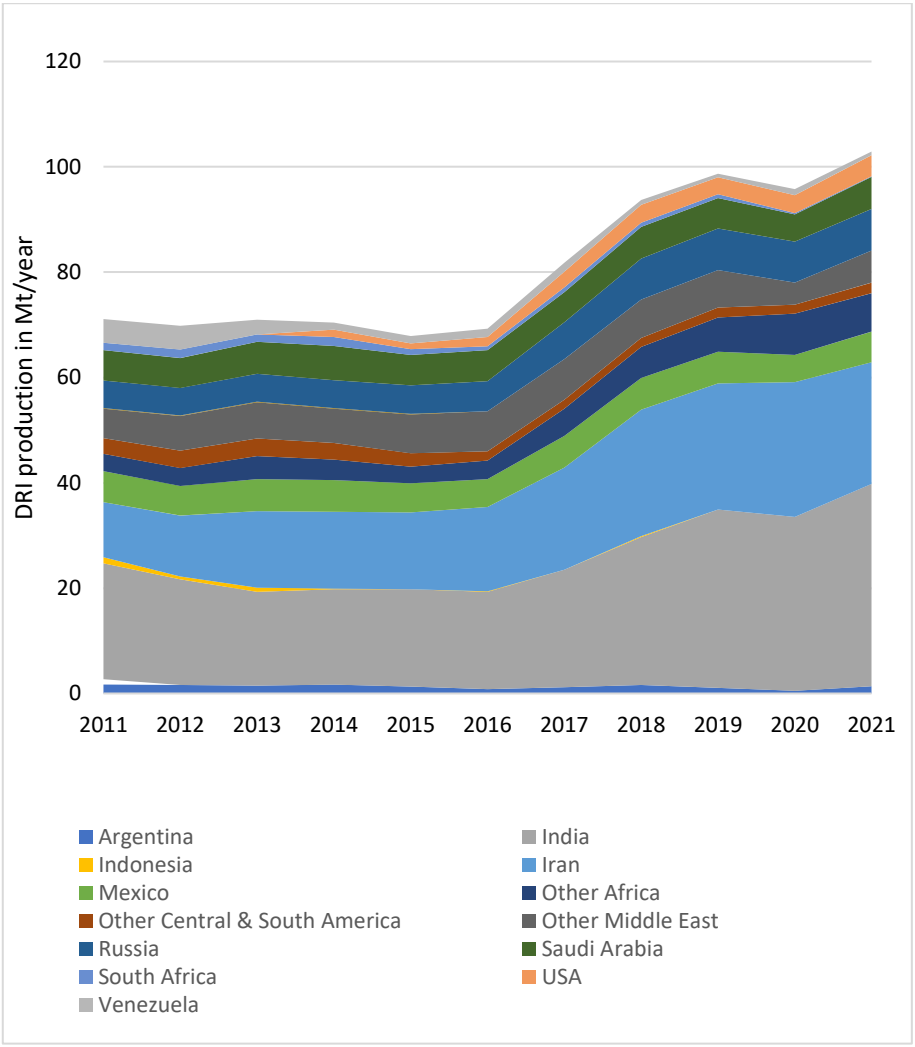

Figure 11 Global DRI production in Mt per year from 2000-2021 (WorldSteel, 2022)

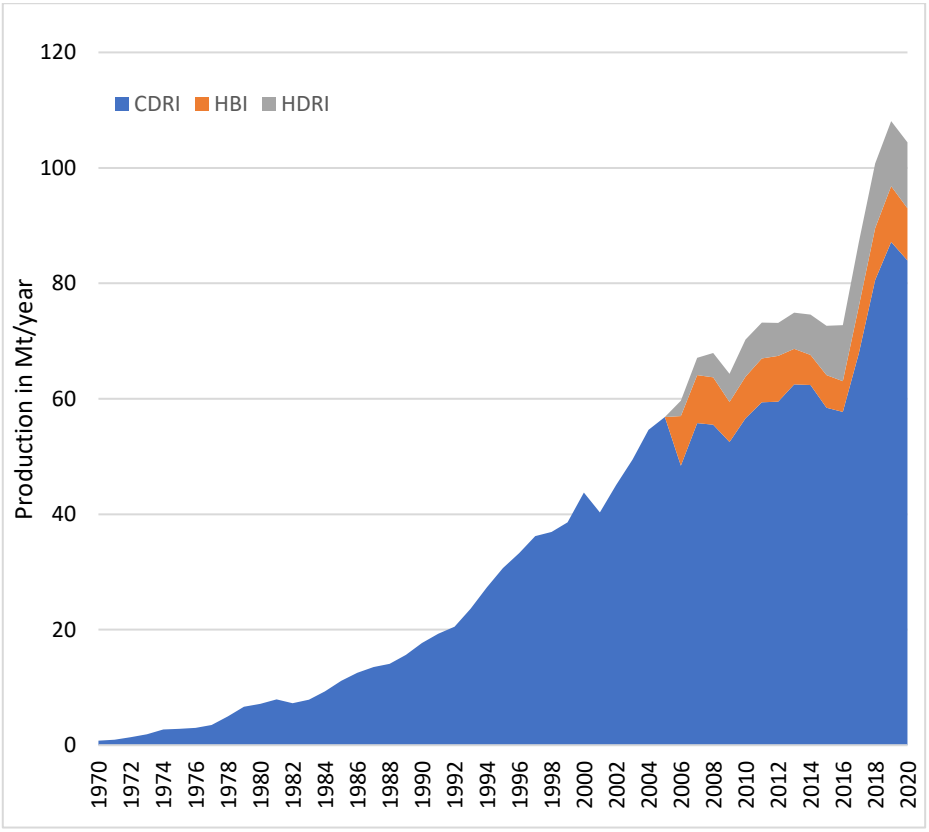

Figure 12 Production statistics of cold DRI (CDRI), Hot DRI (HDRI) and HBI from 1970-2020(WorldSteel, 2022)

1.2.2 Secondary steelmaking (Recycling)

Steel scrap collected from end-of-life products, discarded materials during production, and metal produced as waste from the manufacturing industry can be converted back to steel by melting it in an electric arc furnace (Fan & Friedmann, 2021). The furnace consists of a refractory-lined vessel, typically water-cooled, that is filled with steel scrap. The scrap is heated by an electric arc, which is created by connecting the scrap to a high-power electric current. The intense heat generated by the arc melts the scrap, and the molten steel can then be poured into molds

or castings to create new steel products. EAFs are commonly used in secondary steelmaking because they can melt steel quickly and efficiently and they can process a wide range of scrap materials (Pfeifer & Kirschen, 2003).

1.3 *Energy consumption and emissions from the steel industry*

1.3.1 Energy consumption

The iron and steel industry is one of the most energy intensive industries and uses approximately one-fifth of the global industrial energy. In 2019, the iron and steel industry used 21.91 EJ of energy, which corresponds to 5% of the global energy consumption and 18% of the industrial energy consumption (IEA, 2022e). Fossil fuels are the major source of energy. Coal is the dominant source of energy and is a feedstock for production of coke used as a reducing agent for the reduction of iron oxide to iron. Natural gas is used in the direct reduction plants as a source of carbon monoxide and hydrogen and is also used in secondary steelmaking processes for pre-heating the scrap. Natural gas is used in the subsequent processing of steel into a finished product as a source of high temperature heat. Electricity is majorly used in the secondary steelmaking processes where it is used to power the electric arc and induction furnaces. It is also used for powering the motor drives, pumps, and auxiliary units in the plant. The average energy consumption from different fuel sources is presented in Figure 13. The average specific energy consumption of the iron and steel industry has been improving. In the EU energy efficiency improvements and use of off-gases in power generation has resulted in a decline in the energy intensity of blast furnace-based steelmaking from 19.5 GJ/ton of finished product to 17.26 GJ/ton. Majority of the energy is consumed in the blast furnace and basic oxygen furnace where the iron

oxides are reduced to iron and is subsequently converted to steel by the removal of unwanted carbon. Iron ore agglomeration steps such as sintering, and palletization contribute 10-12% of the total specific energy consumption. Average specific energy consumption of an integrated steel plant in EU from 2000-2015 is shown in Figure 14. The data for the analysis has been taken from Mantzos et al. (Mantzos et al., 2017).

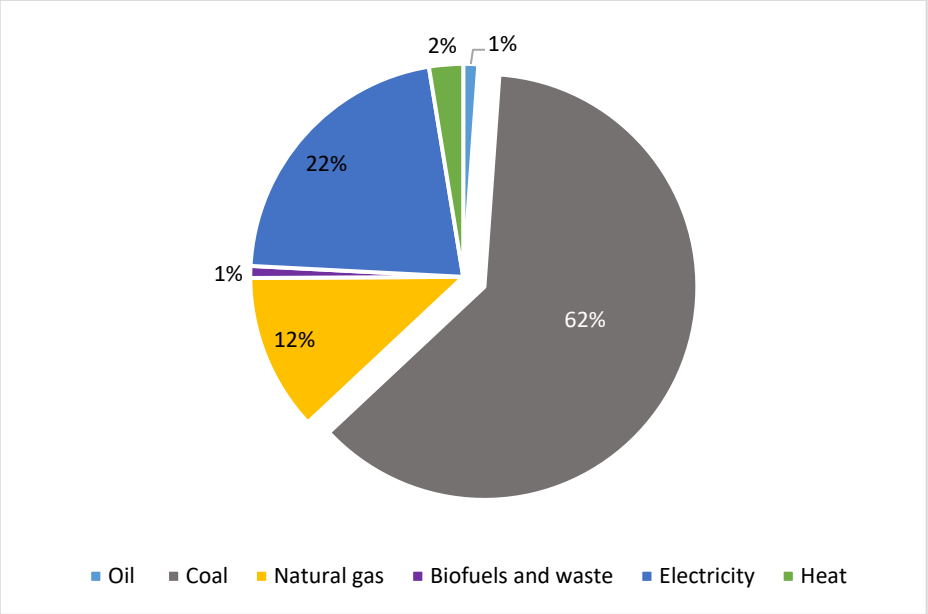

Figure 13 Energy consumption from the global iron and steel industry (IEA, 2022e)

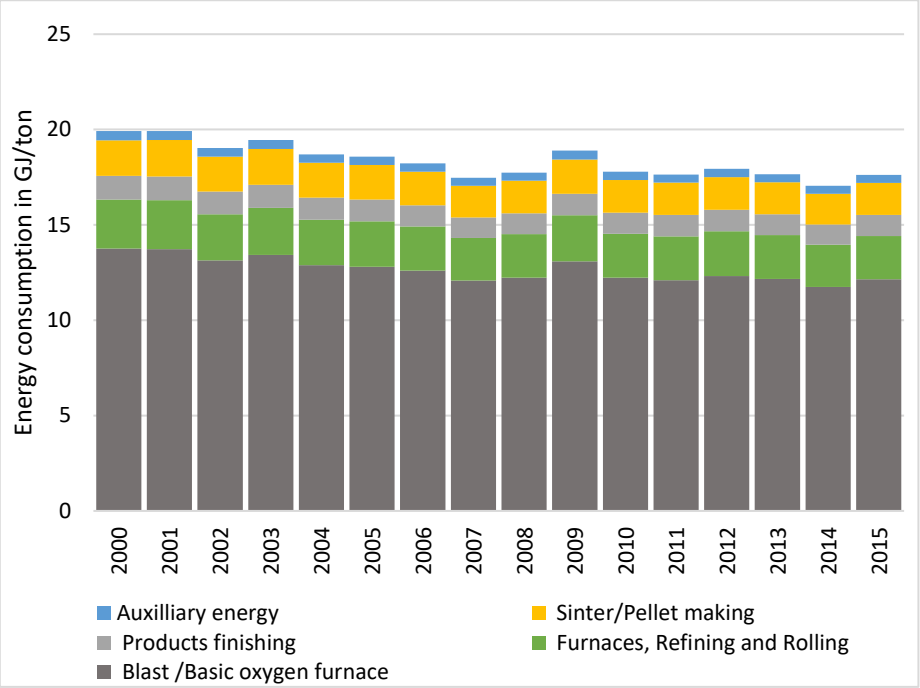

Figure 14 Average specific energy consumption in GJ/ton from an integrated steel plant in EU (2000-2015)

Since the most energy intensive step of iron production is not present in secondary steelmaking it has the advantage of using less energy. Secondary steelmaking uses one-fourth of the energy to produce one ton of finished steel. More than 40% of the total energy is used to raise the temperature of the metal to the melting temperature of steel (>1550 °C). The remaining energy is required to power the rolling, refining, smelters, and product finishing operations. Approximately 4.80 GJ/ton of energy was required to produce one ton of finished steel in the EU countries in 2015, as depicted in Figure 15. The energy consumption in electric arc furnace varies significantly based on the type of input and its chemical composition as large amount of energy for melting the metal burden is supplied from the exothermic chemical reactions inside the furnace (Kirschen et al., 2011).

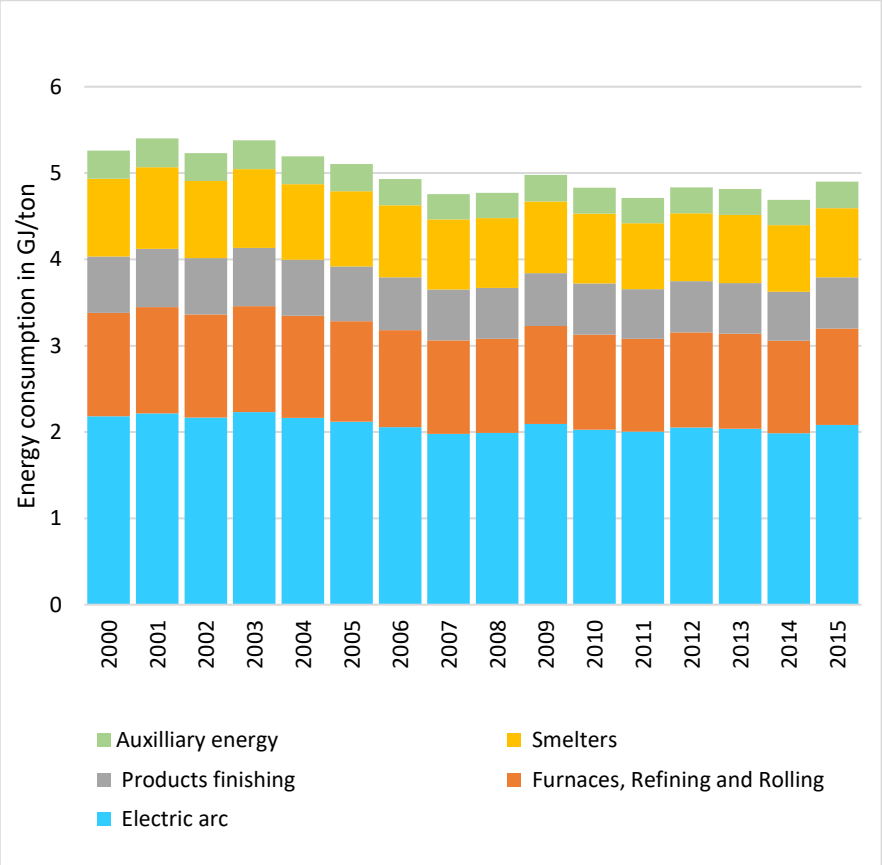

Figure 15 Average specific energy consumption for secondary steel production in EU countries from 2000-2015 (Mantzos et al., 2017)

1.3.2 *Emissions from steel production*

The steel industry contributes to 7-8% of the global greenhouse gas emissions. In 2019 the steel sector had a direct emission of 2.6 $GtCO_2$. According to the IEA an additional 1.1 $GtCO_2$ could be attributed to the

iron and steel sector if indirect emissions from the power sector (electricity used for secondary steelmaking) and emissions from the combustion of steel off gases are included (IEA, 2022c). The total energy related emissions in 2019 were 37 $GtCO_2$ (IEA, 2021a). Considering the additional emissions means that 10% of the global energy related emissions were emitted by the steel industry. Fugitive methane emissions from fossil fuel production is a cause of serious concern due to the higher global warming potential of methane than CO_2 (28 times higher than CO2 over a 100-year period) (Ju et al., 2016; Sadavarte et al., 2021). Coal mining contributed to 42 Mt of methane emissions in 2021, which excludes emissions from abandoned coal mines (IEA, 2022b). Quantification of methane emissions from coal mining is challenging and has started getting increased attention from researchers and authorities recently (Neininger et al., 2021). Metallurgical coal is a key input to the steel industry and has a higher specific emission than thermal coal as it is produced in deeper mines.

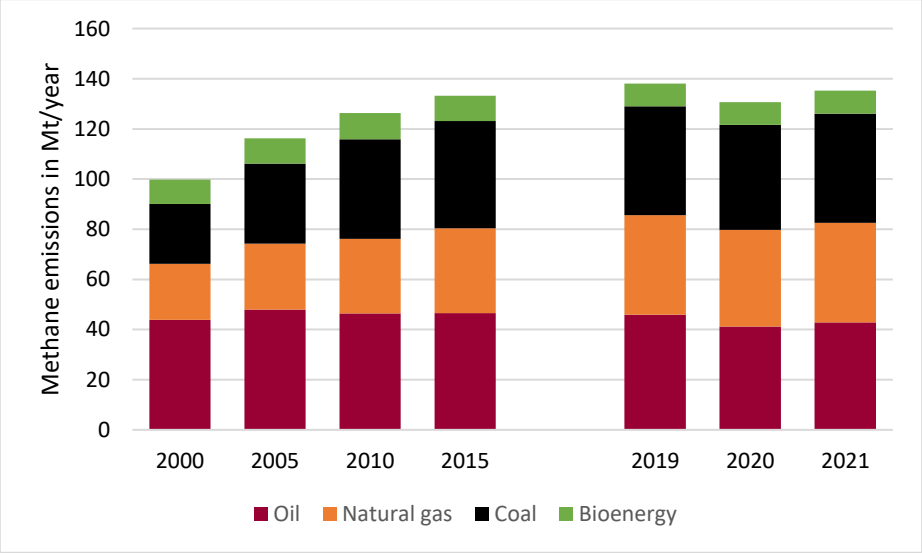

Figure 16 Global methane emissions (IEA, 2022a)

Specific emissions from the primary and second production of steel in EU countries is presented in the **Error! Reference source not found.** and **Error! Reference source not found.** respectively. Energy efficiency enhancement and process integration along with the use of waste heat for district heating in some plants has reduced the emissions intensity of steelmaking in the EU countries (Moya et al., 2010). More than 70% of the emissions come from the use of coal for heating and carrying out the reduction reaction in the blast furnace to produce iron from the iron ore and its conversion to steel in the basic oxygen furnace. Emissions from the secondary steelmaking plant do not consider the indirect emissions from the production of electricity. Use of natural gas for pre-heating the scrap, and its use in the rolling and section mills is the major source of emissions. The reduction of FeO inside the electric arc furnace and oxidation of carbon incase pig iron or DRI is used as an input could also lead to release of process emissions in secondary steelmaking.

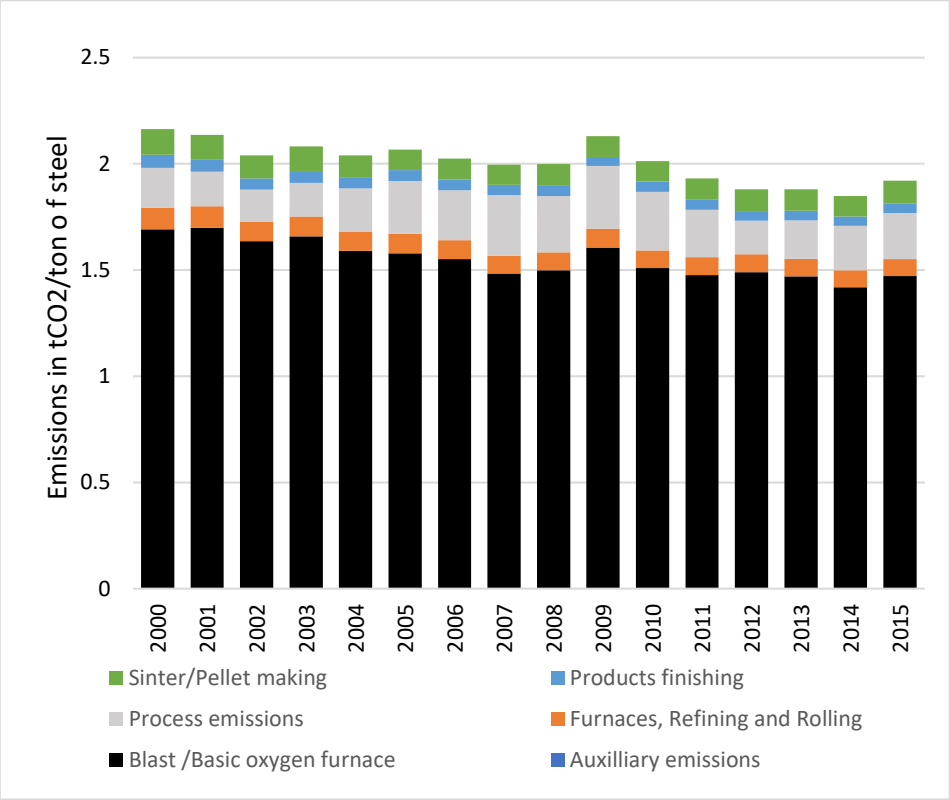

Figure 17 Specific emissions from primary steel production in EU countries from the integrated steelmaking route through 2000-2015 in tCO2/ton of finished steel product(Mantzos et al., 2017)

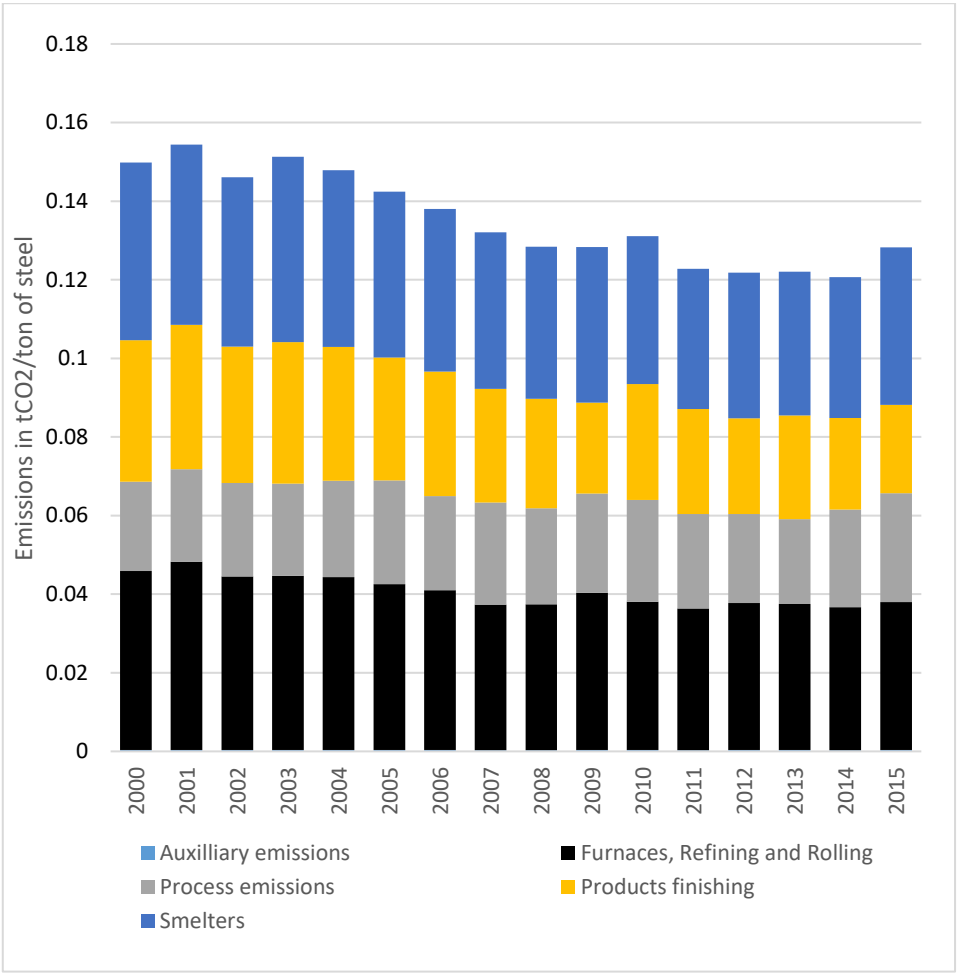

Figure 18 Specific emissions from secondary steel production in EU countries from 2000-2015 in tCO2/ton of finished steel. Emission numbers do not include emissions from the electricity used in the process (Mantzos et al., 2017)

1.4 Future steel demand and its implication on global GHG emissions

Steel demand is likely to grow by 30% by 2050 to meet the demand of the increasing population and to support the increase in living standards.

Energy transition has necessitated a massive build out of new infrastructure such as solar and wind plants, transmission lines, zero emission vehicles, public transport infrastructure, pipelines etc. which will all require large quantities of steel. If the steel industry continues to produce steel with the same emissions intensity as today, it will consume more than 25% of remaining carbon budget, as shown in

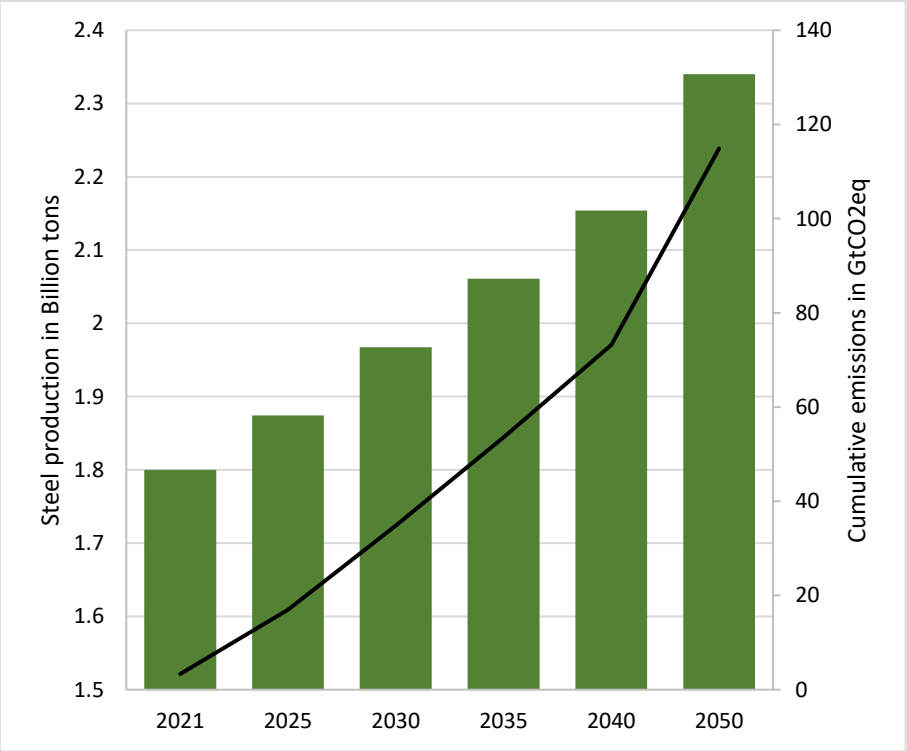

Figure 19 Emissions from the unabated steel industry considering the same emission intensity

1.5 Decarbonization pathways

To achieve the CO_2 emission reduction targets, keep the global means surface temperature increase below 1.5°C, and to mitigate the adverse

impacts of climate change, all segments of the economy, including energy intensive industries like the iron and steel industry need to be decarbonized (UNFCCC Conference of the Parties (COP), 2015) (International energy agency, 2021). The iron and steel industry is one of the major contributors of greenhouse gas emissions, as discussed in section 1.3.2. However, the steel sector has not received as much attention as the energy and transport sector in the decarbonization dialogues even though emissions from the steel segment have contributed to 147 $GtCO_2eq$ of emissions from 1900-2015 (Wang et al., 2021). Incremental efficiency improvements have largely been negated by a more than 44-fold increase in global demand for steel. Difficulties associated with decarbonization of the steel segment can be summarized as follows:

1. Increase in demand for steel to meet the requirements for building new infrastructure and services.
2. CO2 emissions in the steel sector are from the use of fossil fuels for high temperature heat generation, and their use as chemical feedstock for reduction of iron ore to iron.
3. Existing facilities for primary steel production, which are capital intensive, and have a lifetime of at least 40 years are relatively young, which creates a carbon-lock in.
4. Use of steel in buildings, infrastructure etc. which have long-lifetime (50-70 years) hence the return of steel for recycling is relatively slow.
5. Steel is a globally traded commodity, and any increase in the production prices could make the segment uncompetitive.
6. Steel sector employs more than 6 million people globally. Relocation of steel mills could have an adverse impact on the local/regional economy, which creates hurdles in introducing stringent environmental regulations (WorldSteel, 2022).

The decarbonization pathways for the steel segment could be divided into two broad categories as depicted in Figure 20. Demand side

measures such as material efficiency, product service life extension, and material substitution could reduce the demand for steel and hence reduce the associated emissions (Allwood et al., 2011). On the supply side, the focus has traditionally been on incremental improvements in efficiency etc., however to reach the goals of complete decarbonization of steel segment alternative technological options for production such as blast furnace combined with carbon capture and storage/ utilization (BF-CCUS), use of 100% hydrogen in direct reduction shaft furnace (H_2-DRI), use of CCS or CCUS in DRI shaft furnaces, and use of electrolysis (both molten metal and low-temperature electrolysis) (Fischedick et al., 2014). The different supply and demand side alternatives are discussed in the following sections.

To mitigate the adverse impacts of climate change decarbonization of all segments of the economy will be required (International energy agency, 2021). Given the significant contribution of the steel industry in the global greenhouse gas emissions various strategies, technologies and policies could be needed to decarbonize it. The choice of decarbonization pathways and the associated development of technologies and enabling policies would differ significantly based on demand forecast and structural issues of a country/region's economy. While developed economies are witnessing decoupling of their economies and steel demand, developing countries could see an upward tick in steel demand, as the demand for infrastructure and services continue to increase in these regions/countries (Wang et al., 2021).

The decarbonization pathways for the steel industry could be divided into two broad segments as shown in Figure 20. Demand side measures refer to technological and policy-based interventions required to reduce the demand of iron and steel. This could be achieved through a combination of actions such as material efficiency improvements, extending the life of products so that the same amount of materials can provide services for a longer duration of time, substitution of steel with other materials such as increased use of plastics in the automobile industry, and broad demand

reduction measures such as the use of digitalization etc. to reduce the demand of services such as transportation i.e., work from home initiatives or improvement of public transport infrastructure to reduce the demand for new vehicles. In section 1.5.1 each of these demand side measures are discussed in detail.

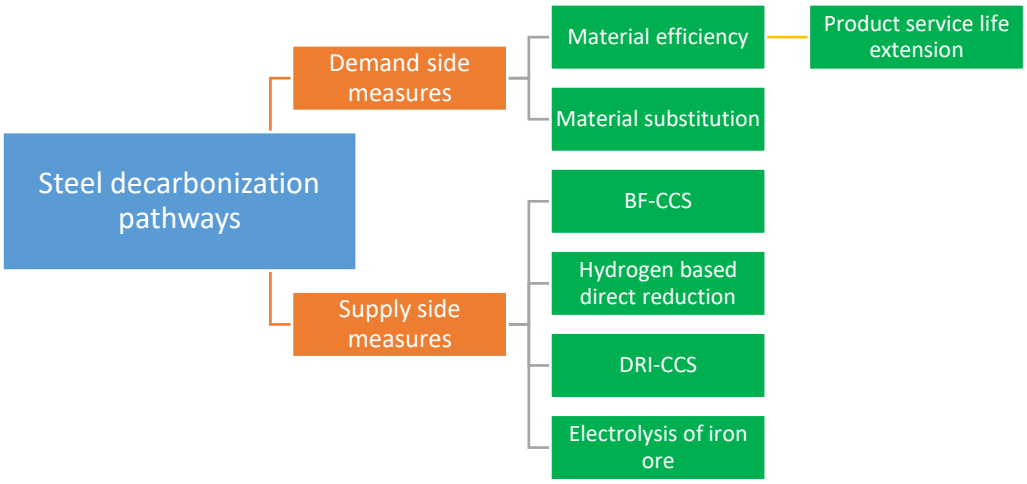

Figure 20 Decarbonization pathways for the global steel industry

1.5.1 Demand side measures

Reducing the demand for material could reduce emissions from the material segment, reduce the risks associated with material shortage, reduce dependence of a country/region in imports and reduce scope 2 and scope 3 emissions (automobile industry, buildings, shipping etc.) for many industries. Material efficiency improvements could significantly reduce the demand for steel. In the next sections, different measures which can be deployed to reduce the steel demand are discussed.

1.5.1.1 Material efficiency

Worrell et al. identified four major strategies for reducing material demand through material efficiency i.e., design of longer-lasting products; use of modularization and remanufacturing; component re-use; and designing products with less material (Allwood et al., 2011). The IEA has highlighted the importance of material efficiency across the value chain of materials and has segregated the material efficiency strategies into four stages (IEA, 2019).

- **Design stage:** Most significant contribution to reduce demand for new materials could be done in the design phase. The product could be designed for a longer lifetime (i.e., ensuring that the household appliances like washing machines, dishwashers etc. last for a longer time and can be repaired) (Laitala et al., 2021), use of lightweight materials (i.e., use of thinner sheets of steel to get the same structural strength), design for reuse of material after the end of product lifetime, and design to minimize waste production during fabrication (use of standard size of materials in the components and building structures).
- **Fabrication stage:** Crude steel undergoes multiple transformations before it can be used i.e., conversion into hot or cold rolled coils, rods, beams, pipes etc. There are losses associated with each step of the transformation. The end user uses steel products of standard sizes to meet his/her needs. Ensuring that the losses at the fabrication stage are minimized could save significant quantities of steel.
- **Use stage:** More intense use of products i.e., use of vehicles to transport a larger number of people or extending the use of commercial buildings beyond working hours (Allwood, 2013; Ruuska & Häkkinen, 2014; Wolfram et al., 2021).
- **End of life:** Ensuring that the materials are reused either directly or after going through the recycling process could reduce demand for new materials.

To facilitate the uptake of material efficiency measures at different stages of a product enabling policies and regulations need to be implemented.

- Policy measures oriented towards an increase in data collection for life cycle assessments and benchmarking of processes. Develop regulations to make it mandatory for manufacturers to reveal their life cycle emissions i.e., environmental product declaration from steel producers. Sharing of benchmarking data, comparison of impacts of the material efficiency measures on the product and service could also facilitate development of enabling regulations.
- Making it mandatory to consider life cycle emissions in the design phase of a product development process could facilitate deployment of material efficiency measures.
- Develop regulatory frameworks and incentives to support material efficiency such as use of performance-based standards, green certification programs and use of material efficiency measures in public procurement. Regulations to make it easier for products to be repaired could help in reducing material demand.
- Increase spending on communicating the benefits of circular economy and material efficiency could help in developing a willingness to pay for products, which have been designed and produced keeping material efficiency improvements as an important consideration.

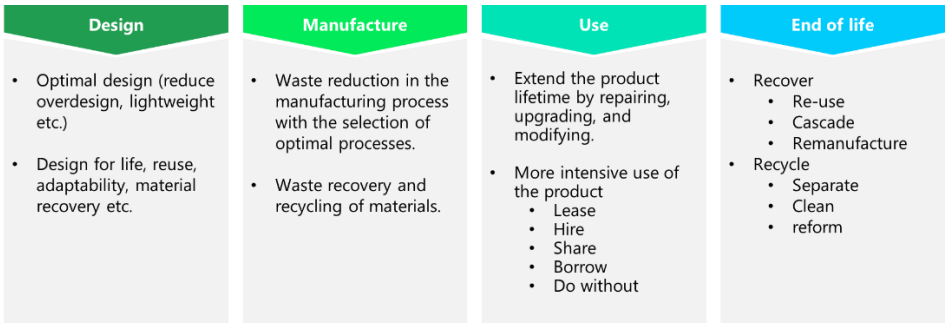

Figure 21 Material efficiency improvements at different stages of product life-cycle (Bashmakov et al., 2022)

1.5.1.2 Material substitution

Material substitution refers to the use of alternative materials to get the same level of service. Increase in the use of plastics as a packaging material compared to steel sheets is an example of material substitution. Chen et al. conducted a life cycle assessment to compare the environmental impact of using cross laminated timber (CLT) as a substitute to traditional building materials like steel and concrete for a functionally equivalent building in China. Their analysis revealed that use of CLT could reduce GHG emissions by 25% compared to the base case (C. X. Chen et al., 2022). Liang et al. found even higher emission reduction potential of 70% from the baseline by considering the sequestered emissions in the timber (Z. Chen et al., 2020). Hart et al. used material flow analyses and LCA to calculate the environmental impact of substituting steel with CLT globally. They found that the potential emission reduction range in the next thirty years is 20 to 80 $MtCO_2$ per year (D'Amico et al., 2021). The automobile industry has paid considerable attention to reduce the overall weight of the automobiles to improve fuel efficiency, and consequently reduce emissions. While more compact designs are important, material substitution such as replacement of steel with aluminum, high-strength steel, and plastics and composite is also a viable strategy (Czerwinski, 2021). The cumulative emission reduction potential from 2010 to 2050

through persistent light-weighting of passenger cars was calculated by Modaresi et al. They estimated an emission reduction potential of 9-18 $GtCO_2eq$ compared to the business-as-usual scenario (Modaresi et al., 2014). They indicated that after 2030 increased recycling of metals could further reduce emissions by 4-6 $GtCO_2eq$. These numbers were calculated based on the continued use of internal combustion engine powered vehicles and could be lower in a world with higher penetration of battery electric and other zero emission vehicles (Czerwinski, 2021).

1.5.2 Supply side measures

While demand side measures and structural changes in the economy could bring down the demand significantly it is estimated that demand for steel could increase by 30% by 2050 (Karakaya et al., 2018; Rechberger et al., 2020a). In the past few decades, the steel industry and the research community have focused their attention on the use of incremental efficiency and productivity improvement technologies to reduce the energy and emission intensity of steel production. However, the efficiency improvements have stagnated as most of the modern plants operate close to the theoretical efficiency limits (Bashmakov et al., 2022; Bataille et al., 2018; IPCC, 2022a; Jai et al., 2020). To decarbonize the steel sector while increasing the production would require the use of alternative low-carbon production technologies (Arens & Vogl, n.d.).

Several technologies for decarbonization of the iron and steel sector were investigated under the Ultra-low CO_2 based steel making program of the EU (Quader et al., 2016). Other initiatives such as AISI technology roadmap program in US, COURSE 50 in Japan, POSCO CO_2 breakthrough framework in South Korea, BlueScope steel in Australia investigated different technologies for steel decarbonization (IEA, 2022c). Decarbonization technologies for ore-based steel production can be divided into two broad groups. Carbon abatement technologies refer to the use of carbon capture and storage or utilization technologies (CCUS), which can be deployed on existing production systems. Their

major characteristics is the continued use of carbon or carbon monoxide as the primary reductant. The CO_2 released in the process is captured and stored in geological reservoirs or used in other processes such as enhanced oil recovery. Other alternative is to use the CO_2 rich gas to produce value-added chemicals. An example of this is the use of CCUS to convert blast furnace exhaust gases to ethanol or methanol. On the other hand, carbon direct avoidance technologies rely on the use of hydrogen and electrons as the reductant. Use of hydrogen in the gaseous or plasma form to reduce iron ore to iron has garnered a lot of attention in the recent years. Electrons can be used as a reductant to reduce iron ore either at low-temperatures or at temperatures above the melting point of iron.

The joint research center of the European commission assessed the different technologies to decarbonize the EU steel industry; and found CCUS, DRI-EAF and iron ore electrolysis to be the three main routes being pursued by the steelmakers(Somers, 2022). The CCS and CCUS route are becoming the less preferred option among majority of the EU steelmakers owing to the complexity involved in capturing CO_2 in an integrated steel plant and public acceptance of CO_2 transport and storage. Although theoretical capture efficiency of more than 95% have been discussed, such high levels have not been achieved at commercial scale yet. Within an integrated steel plant there are multiple sources of CO_2 emissions, i.e., blast furnace, coke oven, basic oxygen furnace, power plant etc. The low concentration of CO_2 and high levels of process integration pose significant challenges in deploying CCS and CCUS technologies. There are challenges associated with the social acceptance of CCS in Europe (Witte, 2021).

The IPCC AR6 report on climate change mitigation has identified several technologies to decarbonize the iron and steel sector, as depicted in Table 1 (IPCC, 2022b). The technologies are compared based on their technology readiness level (TRL), mitigation cost per ton of CO_2, and year of availability. Hydrogen based DRI for iron making and its

conversion to steel in an electric arc furnace has the highest emission reduction potential, lowest mitigation cost and is likely to be available commercially by 2025 or sooner. Fischedick et al. conducted a techno-economic assessment of three innovative ore-based routes for steel production i.e., BF-CCS, DRI-EAF, and iron ore electrolysis (electrowinning), under three different scenarios, and found that DRI-EAF based route to have a high potential in decarbonizing the steel sector (Fischedick et al., 2014). Wiegel et al. extended the comparative analysis to include twelve additional criteria segmented by technology, society and politics, economy, safety and vulnerability, and ecology. They concluded that the DRI-EAF and EW route have the maximum potential in decarbonizing the steel segment while the BF-CCS option would be hard to implement due to the lack of social acceptability of CCS solutions and constraints on the geological storage sites for the captured CO_2(Weigel et al., 2016). In the following sections each of these technologies will be described briefly. Use of biomass in steelmaking, has not been discussed. Biomass availability could be constrained owing to the competition between different end-use segments for biomass i.e., biofuels, bio-methanol etc. (Suopajärvi et al., 2018).

Table 1 Technology potential for deep decarbonization of the steel industry (adapted from (IPCC, 2022b)).

Current Intensity (TCO2eq per ton)	Potential GHG reduction	TRL	Cost per tonne CO2 - eq (2019 USD tco2-eq for % of emissions)	Year available assuming policy push	Reference
All steel	1.83				
BF-BOF (average)	2.3	9			
BF-BOF(Best)	1.8	9			
NG-DRI (with net-zero electricity)	0.7	9			
EAF (depends on current intensity)	>=0.05	9			

Material efficiency	up to 40%	9	Not quantified	Today	(Allwood, 2013; Allwood et al., 2011; IEA, 2019)
More recycling; depends on stock availability, recycling network; quality of scrap; availability of DRI for dilution	Highly regional; growing with time	9		Today	(Material Economics et al., 2019)
BF-BOF with top gas recirculation and CCU/s	60%	7	70-130	2025-30	(Wyns & Axelson, 2016)
Syngas (H2 and CO) DRI EAF with concentrated flow CCU/s	90%	9	>=40	Today	(Wyns & Axelson, 2016)
Hisarna with concentrated CO2 capture	80-90%	6-7	40-70		(van Boggelen et al., 2022)
Hydrogen DRI-EAF; H2 produced from SMR-CCS or water electrolysis	up to 99%	7	35-70 (depends on electricity price)	2025	(Rechberger et al., 2020b)
Aqueous (SIDERWIN) or Molten oxide electrolysis	up to 99%	3-5	Not quantified	2035-40	(Wiencke et al., 2018)

Friedmann et al. reviewed the different technology options for deep decarbonization of the steel sector and found that the optimal solution will vary with location, resource availability, policies, and regulations.

They found DRI based routes to be most promising for steel decarbonization (Fan & Friedmann, 2021). Based on their assessment they have provided suggestions to policy makers which includes the following:

1. Providing incentives in the form of grants, feed-in tariffs, and contracts for differences, or capital treatments, such as tax credits.
2. Providing elevated prices for greener products in public procurement especially for military and infrastructure.
3. Development of low-carbon production standards; facilitate the implementation of carbon border adjustment mechanisms to protect the domestic industry.
4. Bring structural shift in steel production, forcing the shut-down of polluting units and providing support for secondary steelmaking.
5. Creating a consortium of buyers of greener products, for exchange of best practices etc. which will help in creating a commonly used standard for green steel.

1.6 Decarbonization efforts of steel producers

Global steel industry is responding to the challenge of decarbonizing its operations and most of the large steel producers have explicit carbon neutrality goals by 2050. The intermediate goals for reduction in emissions, such as emission reduction by 2030, could allow companies to track progress of their decarbonization efforts. In Table 2, decarbonization pledges of the largest steel producers is listed.

Table 2 Decarbonization pledges by the global steel producers, adapted from (Vogl et al., 2021).

Company	Country	Production capacity in Mtpa	2030 Target	2050 Target

Baowu Steel Group	China	115.29	Not stated	Carbon neutrality
ArcelorMittal	Luxembourg	78.46	25% reduction (baseline 2018)	Carbon neutrality
HBIS	China	43.76	30% reduction (baseline 2022)	Carbon neutrality
Nippon Steel	Japan	41.58	30% reduction (baseline 2013)	Carbon neutrality
POSCO	South Korea	40.58	20% reduction (baseline undefined)	Carbon neutrality
Tata Steel Europe	England	28.07	30% reduction (baseline 2020)	Carbon neutrality
JFE Steel	Japan	24.36	20% reduction (baseline 2013)	Carbon neutrality
Hyundai Steel	South Korea	19.81	Not stated	Carbon neutrality
NLMK	Russia	15.75	Not stated	Not stated
China Baotou Steel	China	15.46	30% reduction (baseline 2023)	Carbon neutrality
JSW Steel	India	14.86	>40% reduction (baseline 2005)	Not stated
China Steel Corporation	Taiwan	14.11	Not stated	Carbon neutrality
Evraz	UK	13.63	20% reduction (baseline 2019)	Not stated
US Steel	USA	11.55	20% reduction (baseline 2018)	Carbon neutrality
Severstal	Russia	11.31	Not stated	Not stated
Thyssenkrupp	Germany	10.73	30% reduction (baseline 2018)	Carbon neutrality
MetInvest	Ukraine	10.16	15% reduction (baseline undefined)	Not stated

To reach their ambitious goals of decarbonizing steel production, steel companies have announced many projects. An overview of the important projects and the type of technology being deployed is presented in Table 3. Majority of the projects are based in European countries, owing to the strong focus on decarbonization in the region. Higher emission prices, and development of enabling policies such as carbon border adjustment

mechanism has enabled steel producers to take rapid decarbonization measures (UNCTAD, 2021).

Table 3 Decarbonization projects by steel companies (Vogl et al., 2021)

Company	Country (in which project/investment is taking place)	Location	Project scale	Technology category	Year online
ArcelorMittal	Belgium	Ghent	Full scale	HDRI-EAF	2030
ArcelorMittal	Canada	Dofasco	Full scale	HDRI-EAF	2028
ArcelorMittal	France	Dunkirk	Full scale	HDRI	2027
ArcelorMittal	France	Maizières-lès-Metz	Pilot	Electrolysis	2022
ArcelorMittal	Germany	Bremen	Full scale	HDRI-EAF	2026
ArcelorMittal	Germany	Hamburg	Demo	HDRI	2024
ArcelorMittal	Spain	Gijon	Full scale	HDRI-EAF	2025
Boston Metal	USA	Boston	Demo	Electrolysis	2024
Fortescue Metals	Australia	Pilbara	Full scale	HDRI	2023
H2 Green Steel	Sweden	Svartbyn	Full scale	HDRI	2024
Liberty Steel	Australia	Whyalla	Full scale	HDRI	2024

Liberty Steel	France	Dunkirk	Full scale	HDRI	Not stated
Liberty Steel	Romania	Galati	Full scale	HDRI	2024
Metalloinvest	Russia	Kursk region	Full scale	HDRI	2024
POSCO	South Korea	N/A	Full scale	HDRI	Not stated
Salzgitter	Germany	Salzgitter	Demo	HDRI	2022
SSAB	Sweden	Gällivare	Demo	HDRI-EAF	2026
Tata Steel	Netherlands	Ijmuiden	Full scale	HDRI-EAF	2030
Thyssenkrupp	Germany	Duisburg	Full scale	HDRI-EAF	2025

1.7 Research Focus

A combination of demand side interventions and use of innovative production technologies could allow the steel sector to decarbonize (Bashmakov et al., 2022; Energy Transition Commission, 2022; IEA, 2022d). While demand reduction would largely be driven by structural changes in the economy, adoption of circular economy principles, push from the policymakers, and changes in the end-use segments such as construction, the use of innovative production technologies could be driven by both global and regional drivers. Use of HDRI-EAF based 'green steel' production has become the technology of choice for many steelmakers (Table 3). Drivers for the quick uptake of the technology are listed below:

- **Technological maturity:** Natural gas based DRI production has been used commercially since 1970's. Shaft furnace reactors used

for the natural gas based DRI production can be used for 100% H_2 based DRI production. At present the reducing gas has up to 50% or more of H_2, and the remaining is CO by volumetric composition (Kawasaki et al., 1962; Oh & Noh, 2017). Although H2 has better reducing properties than CO, the reduction reaction between iron oxide and H2 is endothermic, and this would require design changes in the current set-up, along with changes in the operations (Spreitzer & Schenk, 2019). The reducing gas is currently produced from reforming of natural gas. Electrolytic hydrogen production could be used for producing the reducing gas. A pilot plant with 100% H2 based DRI has been operated in Sweden under the HYBRIT project since August 2020 (Pei et al., 2020). Production of steel in an EAF is a proven technology. Majority of the EAF producers use DRI (either hot or cold) or hot briquetted iron (HBI) as a feedstock for steel production. Suppliers of the DRI shaft furnace technology i.e., MIDREX and TENOVA have publicly stated that conversion of their shaft furnaces to run on 100% hydrogen is technically feasible.

- **Economics:** In a carbon constrained world with high emission prices, HDRI-EAF technology could become economically competitive. The CO_2 abatement cost of HDRI-EAF technology is in the range of 34-68 EUR/tCO2eq, at an electricity price of 40 EUR/MWh, which is one of the lowest among other decarbonization technologies(Bashmakov et al., 2022; Vogl et al., 2018).
- **Social acceptance:** Unlike use of CCS, which faces issues with social acceptance of transport and storage of CO_2, HDRI-EAF technology does not face such issues. It is likely to create new job opportunities in regions with access to good renewable resources, iron ore etc.
- **Development of hydrogen economy:** Rapid decline in the price of renewable electricity, and the focus on decarbonization of hard-to-abate sectors has put hydrogen at the forefront of climate

change mitigation discussions (IRENA, 2022a, 2022b). The demand for hydrogen is expected to increase approximately three times by 2030, from the current 70-80 Mtpa to more than 210 Mtpa (IEA, 2021b). Increased deployment of hydrogen technologies could drive down cost of production equipment like electrolyzer, power electronics etc., expedite the development of required infrastructure for transport and storage of hydrogen, making it easier for steel producers to switch to HDRI-EAF based production (IRENA, 2020, 2022a, 2022b).

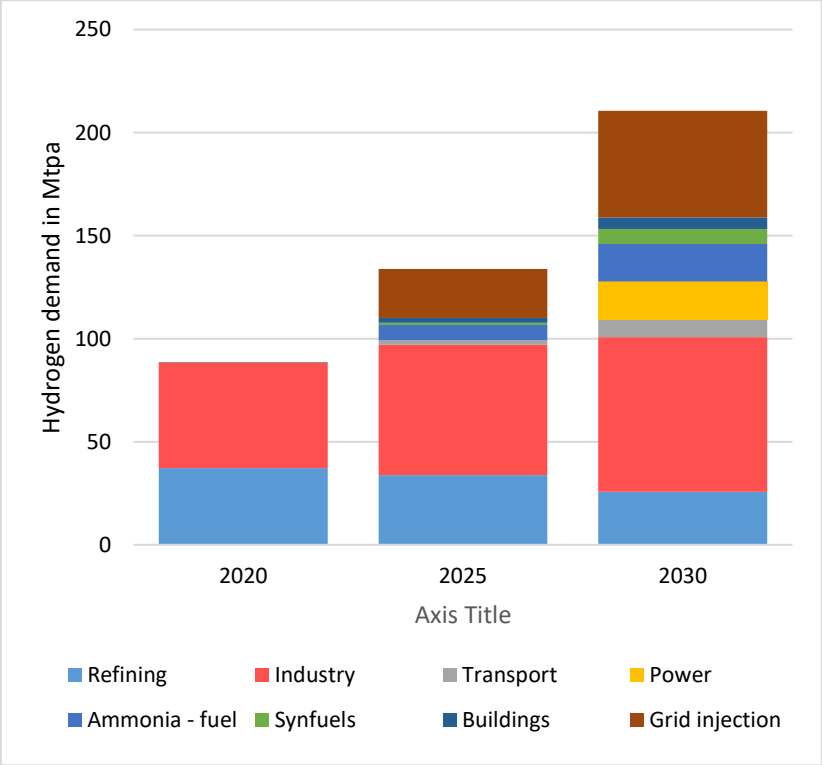

Figure 22 Demand for hydrogen in the Net-zero emission scenario (IEA, 2021b).

- **Enabling policies:** Government policies towards industrial decarbonization could lead to faster uptake of the HDRI-EAF technology. The use of carbon contracts for difference (CCFD)

to promote uptake of cleaner technologies, use of industrial decarbonization fund in Germany to fund the demonstration plant at Hamburg, hydrogen strategies and policies, and implementation of carbon border adjustment mechanism by the EU are examples of policy measures which have resulted in quicker uptake of HDRI-EAF technologies (Agora industry et al., 2022).

However, there are still questions which need to be answered to take financial decisions by industry and for development of adequate policy measures to support the industry towards the adoption of HDRI-EAF technology at scale. The most important questions are listed below:

1. What are the market drivers for the uptake of HDRI-EAF based steel production in selected geographies?
2. What are the material and energy flows for a HDRI-EAF based steel production unit? How do they different components interact with each other?
3. Are there any technological barriers towards the large-scale implementation of HDRI-EAF technology for steel production?
4. How does the specific energy consumption and specific emission of HDRI-EAF based steel production compare with the baseline steel production technologies? Which are the main factors affecting the energy and emission profiles?
5. Is HDRI-EAF based steel production economically feasible? Which factors contribute to the uncertainty in estimation of economic feasibility of the technology?
6. How can policymakers ensure a faster uptake of the technology?

A techno-economic assessment model was developed to answer the research questions listed above. First, a literature review was conducted on the current state of the HDRI-EAF technology. An open-source python-based model was developed to calculate the material and energy balance of a 100% H2 based DRI-EAF reactor was developed as the first

step (Bhaskar et al., 2020). Hydrogen was produced from water electrolysis. Specific energy consumption, and specific emissions from the technology were compared to baseline primary steel production technologies. In the next step, the techno-economic assessment was extended to include detailed economic assessment of the HDRI-EAF technology (Bhaskar et al., 2021). Molten metal methane pyrolysis was compared as an alternative hydrogen production technology and its integration with the steelmaking process. Uncertainty quantification methods were used to find the factors affecting the uncertainty in the economic parameters. A linear optimization framework, using day-ahead electricity prices in Northern Norway as the cost function, was developed in the last step to find the optimal annual electricity consumption for a 100% H2 based HDRI-EAF unit, where H2 was made from water electrolysis (Bhaskar et al., 2022). The methodology is discussed in Section 2. The main results of the research articles are published in the Sections 3,4,5 respectively and summarized in Figure 23.

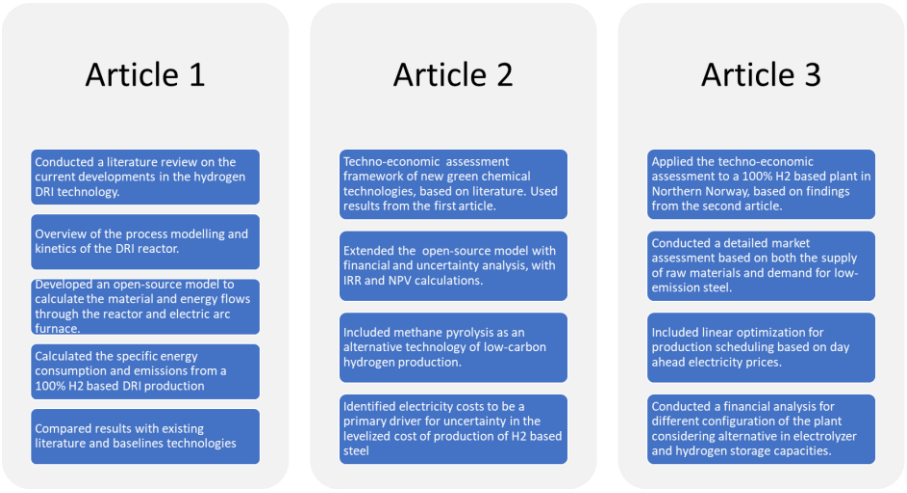

Figure 23 Main outcomes of the three journal articles and their connection to each other

2 Methodology

HDRI-EAF based steel making is a green technology at low technology readiness level. To evaluate the techno-economic feasibility and to compare it with the baseline technologies, a techno-economic assessment framework developed by Thomassen et al. for green chemical production technologies at low technology readiness level was used (Thomassen et al., 2019). The different steps, their objectives and the methods used for the analysis are presented in Table 4.

Open-source scientific computation software have been used in this work to increase reproducibility of results , and allow the integration of to energy system models. The Pandas library was used for retrieving and analyzing tabular data (McKinney, 2010). Numpy was used for creating arrays and data handling (van der Walt et al., 2011). Matplotlib was used for data visualization, and creation of plots (Hunter, 2007). The Ipython notebook environment was used to write the python scripts. The optimization model was written in Python, using PYOMO, which is an open-source optimization framework (Bynum et al., 2021). Gurobi was used to solve the optimization problem (Gruobi, 2021).

Table 4 The different steps of the techno-economic assessment framework (Thomassen et al., 2019)

	Steps	Objective	Methods used
1	Market Analysis	What are the main drivers? Is the defined case feasible	Market reports, environmental reports

2	Material and energy balance	Key input and output parameters for different material and energy flows, and to identify the conceptual process flow diagram.	System boundary definition, material and energy balance model based on conceptual process flow model
3	Economic analysis	Find the economic feasibility of the technology from an investor's perspective	Calculation of the NPV and IRR
4	Environmental analysis	To calculate the impact of the new technology on the environment	CO2 footprint calculation for the background and foreground processes within the system boundary
5	Uncertainty analysis	Find the key parameters, quantify uncertainty, find optimal value of parameters	Sensitivity analysis, contribution analysis, one-factor optimization

2.1 Market analysis

EU countries used more than 150 million tons of steel in 2019 (EUROFER, 2022). Construction sector contributes to one-third of the demand. The automobile and machinery sector are the two other major

demand segments. There has been an increased scrutiny of the embodied emissions of buildings and structures, which includes structural steel used in the construction sector. A global coalition of public and private organizations, called the Industrial deep decarbonization initiative (IDDI) was set up recently to stimulate demand for low carbon industrial materials (UNIDO, 2021). The objectives of IDDI include encouraging governments, and the private sector to buy low carbon steel and cement, and to share data and resources to set common standards and targets across member states. These goals were reiterated during the conference of parties organized in Egypt in November 2022. The recent announcements to lower the cap in the EU emission trading system, carbon border adjustment taxes, and emphasis on the use of climate-neutral industrial products could result in an increased demand for green steel (Agora industry et al., 2022). Leading automobile manufacturers are moving towards green steel. Volvo, which is a leading automobile manufacturer, and steel producer SSAB have signed a collaboration agreement on research, development, serial production and commercialization of the world's first vehicles to be made of hydrogen reduction-based steel. Volvo plans to start the production of concept vehicles and components from hydrogen based green steel by 2021 (Volvo, 2021). Similar, plans have been announced by the Mercedes group, which has invested in an upcoming 5 Mtpa steel production facility in Sweden (Schäfer, 2021). Orsted, a leading wind energy developer has joined the SteelZero global initiative to drive market demand for net-zero emission steel (Stougaard, 2021). A summary of the pledges made by leading shipping, construction, automobile and renewable developer and equipment suppliers is presented in Table 5.

Table 5 Pledges made by participants of the SteelZero initiative

Company	Segment	100% steel requirement to be met with green steel	50% steel requirement to be met with green steel

A.P. Moller - Maersk	Shipping	2050	2030
Barrett Steel Limited	Steel supplier and stockholder	2050	2030
BHC	Construction: structural steelwork	2050	2030
Billington Structures Ltd.	Construction: structural steelwork	2050	2030
B+M Steel	Construction: structural steelwork	2050	2030
Bourne Group	Construction: structural steelwork	2050	2030
Deconstruct UK	Construction	2050	2030
Eiffage Métal, France	Construction	2050	2030
Grosvenor Property UK	Construction	2050	2030
Iberdrola	Renewable developer	2050	2030
Landsec	Construction	2050	2030
Lendlease	Construction	2040	2030
Mace Group	Construction	2040	2030
Met Structures	Construction: structural steelwork	2050	2030
Morrow + Lorraine	Architecture and construction	2050	2030
Multiplex Construction Europe	Construction	2050	2030

Ørsted	Renewable developer	2040	2030
Severfield plc	Construction: structural steelwork	2050	2030
Siemens Gamesa	Renewable developer	2040	2030
Smulders	Construction: structural steelwork	2050	2030
Skanska UK	Construction	2050	2030
SKF	Automotive components	2050	2030
Vattenfall BA Wind	Renewable developer	2050	2030
ViaCon Group	Construction	2050	2030
Volvo Cars	Automotive	2050	2030

2.2 Material and energy balance model

Hydrogen based steel production can be divided into three distinct sub-processes i.e., the production and storage of reducing agent (hydrogen), direct reduced iron production in the shaft furnace, and its subsequent conversion to steel in the EAF. A conceptual model of the system is presented in Figure 24. Material and energy flows through the different components of the sub-systems were calculated to produce one ton liquid steel. The specific heat and enthalpy of the different species were calculated using the Shomate equation (Bhaskar et al., 2021). The coefficients of the Shomate equations were taken from NIST webbook (Chase, 1998).

The DRI shaft furnace is counter current solid-gas reactor, where the reduction of iron ore pellets is carried out in three steps. Hematite

($Fe_2O_{3(s)}$) is first converted to Magnetite $Fe_3O_{4(s)}$(Heidari et al., 2021). In the subsequent steps, magnetite is converted to Wustite (FeO), and finally metallic iron (Fe). Kim et al. found that the easy nucleation, and fast diffusion through the iron oxide product layer are the main reasons for the fast reduction kinetics of hematite to Wustite conversion (Kim et al., 2021). The conversion from Wustite to metallic iron is an order of magnitude slower due to sluggish mass transport, particularly of the oxygen through the iron layers. The reduction kinetics of is positively correlated with temperature in the range of 800-1000 C. Increase in kinetics is attributed to the increase in diffusivity and reaction rate (Heidari et al., 2021). Reduction kinetics of H_2 was found to be higher than CO and could result in reactors with smaller dimensions. The reduction reaction between hydrogen and iron oxide is endothermic, requiring 99.5 KJ/mol of energy (Ranzani Da Costa et al., 2013). The reduction steps and kinetics of the reduction reaction are presented in (Bhaskar et al., 2020). The methodology along with a detailed process description is presented in (Bhaskar et al., 2022).

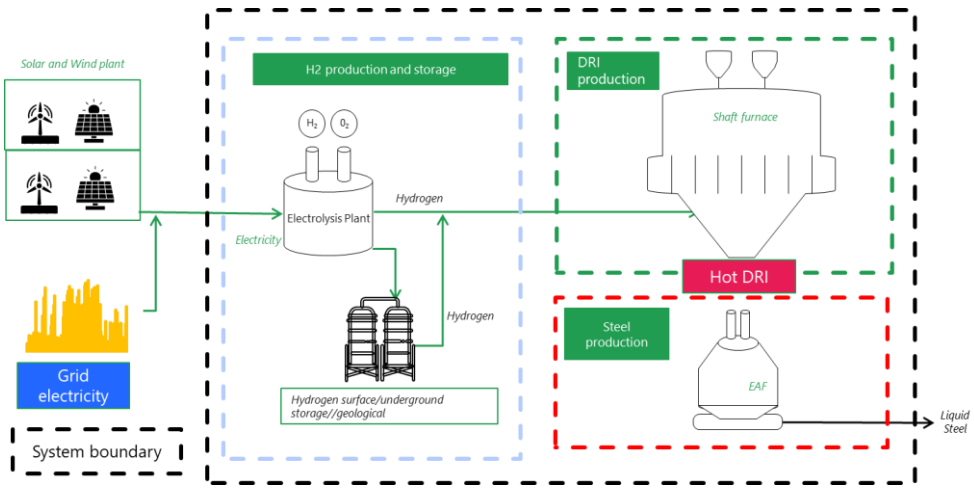

Figure 24 Conceptual model of the HDRI-EAF based steelmaking system.

2.3 Economic analysis

A discounted cash flow analysis was conducted to calculate the levellized cost of production for the proposed system, based on the preliminary material and energy balance. Detailed assumptions on the capital, operational, maintenance costs etc. are provided in (Bhaskar et al., 2022). The model is made available on the Zenodo repository in the form of Jupyter notebooks (Bhaskar, 2021).

2.4 Environmental Analysis

The material and energy balance model were used to calculate the CO2 emission footprint of the processes. Emissions associated with electricity consumption are secondary emission. Details about the system boundaries and grid emission factors used for the analysis are presented in the individual articles.

2.5 Uncertainty analysis

Local and global sensitivity analysis were conducted to apportion the uncertainty in the model output to different model inputs (Saltelli et al., 2010). There are different sources of uncertainty in the model inputs. They arise from the fluctuations in the price of internationally traded commodities (iron ore, natural gas, carbon price etc.), and price of input parameters such as electricity cost, emission costs etc. The technologies analyzed in this work are at a low TRL, hence values of input parameters such as electrolyser efficiency, their capex values and other values remain highly uncertain. The NPV and IRR of the system were selected as the target variables.

A global sensitivity analysis was conducted using the sobol sensitivity indices approach to ascertain the uncertainty of the NPV and IRR values, based on the global uncertainty in the input parameter values (Sobol, 2001). Sobol sensitivity analysis determines the contribution of each

input parameter, and their interactions to the overall model output variance. The global sensitivity analysis was carried out using the SALib library to evaluate the Sobol first-order and Sobol total-order sensitivity indices (Herman & Usher, 2017).

3 Decarbonization of the Iron and Steel Industry with Direct Reduction of Iron Ore with Green Hydrogen

DOI: 10.3390/en13030758

Model and Python codes: 10.5281/zenodo.3562399

The aim of the first article was to present the material and energy balance for a HDRI-EAF based system running on hydrogen produced from water electrolysis. The material and energy flows across different components of the system were calculated and overall energy and emission profiles were presented (Bhaskar et al., 2020). The main findings of the article were that HDRI-EAF is a viable alternative to BF-BOF based steel production, but adoption of the technology would depend on the future cost of electrolyzers and electricity. It was found that electrolyzer efficiency is the most important factor affecting the system energy consumption. The system emissions were linearly correlated with grid emission factor. Recent improvements in the performance of electrolyzers could reduce the energy consumption and emissions from the HDRI-EAF based steel production. The iron and steel industry could play a major role in the transition to the hydrogen economy by creating a demand for large quantities of hydrogen, which could lead to the development of infrastructure for generation, storage, and safe transport of hydrogen. The use of hydrogen in steel making coupled with hydrogen storage could provide flexibility to the electricity grid to integrate intermittent renewable energy sources and open new opportunities for revenue generation for steel companies by participating in the power reserve markets. Other strategies for flexible operation of the HDRI-EAF system could be explored by storing the DRI and operating the EAF according to electricity prices. Dynamic modeling of

the HDRI-EAF system could quantify the potential of the steel industry to participate in the demand response market.

3.1 Key results

Local sensitivity analysis was carried out by varying the input parameters by ±5%, ±10%, ±15%, ±20%, one-at-a-time and keeping other parameters fixed (Hamby, 1994). Hydrogen mass flow rate (λ), electrolyzer efficiency, hydrogen input temperature(T3), EAF input temperature (T4), adsorber efficiency and the grid emission factor were selected for the parametric sensitivity analysis. The results of the sensitivity analysis are presented in Figure 25.

Electrolyzer efficiency had the largest impact on the overall energy consumption of the DRI-EAF system. Another important parameter affecting the electricity consumption is λ, which is a ratio of the actual hydrogen required for production of one ton of liquid steel to the stoichiometric requirement of hydrogen. The value of λ is related to the design of the shaft furnace reactor and operating conditions. Electricity requirement of the system decreases as the adsorption efficiency increases in the pressure swing adsorption system.

Since the system is assumed to be grid connected, the emissions from the system, which are a combination of the primary and secondary emissions, are strongly correlated with the grid emission factor. Electrolyzer output, lambda and the adsorption factor are important factors, which decide the overall emissions from the system, as they are related to the electricity consumption of the HDRI-EAF system. Hydrogen input temperature (T3) and the EAF input temperature (T4) do not have a major impact on the energy requirement and emissions from the HDRI-EAF system

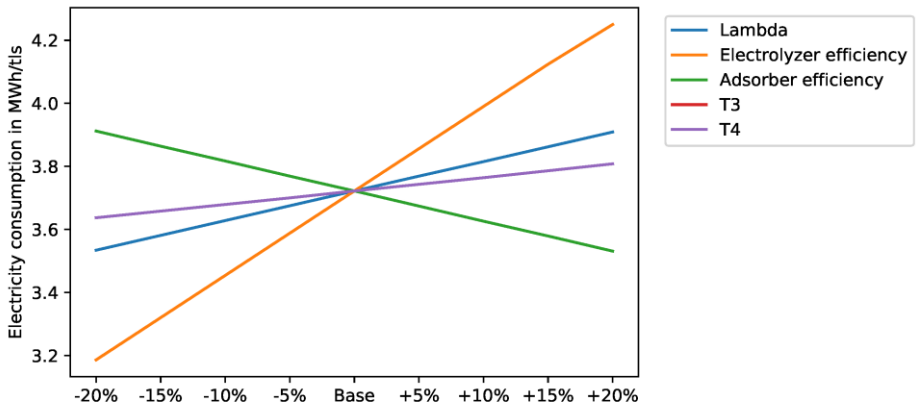

(a)

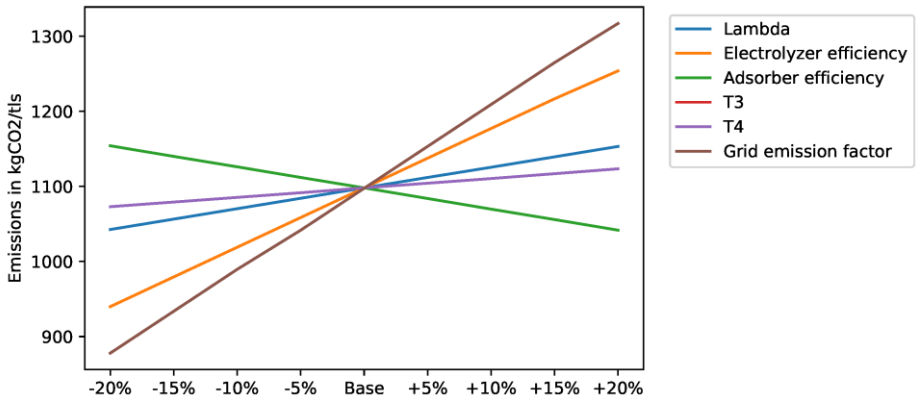

(b)

Figure 25 Sensitivity analysis to identify the parameters affecting the electricity requirements of the HDRI-EAF system. (b) Sensitivity analysis to identify the most important parameters affecting the CO2 emission from the HDRI-EAF system.

4 Can methane pyrolysis-based hydrogen production lead to the decarbonisation of iron and steel industry?

DOI: 10.1016/j.ecmx.2021.100079

Model and Python codes: 10.5281/zenodo.4504841

In this work, results from the techno-economic assessment of a H_2-SF connected to an electric arc furnace (EAF) for steel production are presented under two scenarios. In the first scenario H2 is produced from molten metal methane pyrolysis in an electrically heated liquid metal bubble column reactor. Grid connected low-temperature alkaline electrolyser was considered for H2 production in the second scenario. In both cases, 59.25 kgH2 was required to produce one ton of liquid steel (tls). The specific energy consumption (SEC) for the methane pyrolysis-based system was found to be 5.16 MWh/tls. The system used 1.51 MWh/tls of electricity, and required 263 kg/tls of methane, corresponding to an energy consumption of 3.65 MWh/tls. The water electrolysis-based system consumed 3.96 MWh/tls of electricity, at an electrolyser efficiency of 50 KWh/kgH2. Both systems have direct emissions of 129.4 kgCO2/tls. The indirect emissions are dependent on the source of natural gas, pellet making process and the grid-emission factor. Indirect emissions for the electrolysis-based system could be negligible if the electricity is generated from renewable energy sources. The levelized cost of production (LCOP) was found to be $631, and $669 respectively at a discount rate of 8%, for a plant-life of 20 years. The LCOP of a natural gas reforming based direct reduction steelmaking plant of operating under similar conditions was found to be $414. Uncertainty analysis was conducted for the NPV and IRR values (Bhaskar et al., 2021).

4.1 Key result

The methane pyrolysis-based system was found to have a lower levelized cost of production (LCOP) of 631 $/t, compared to the LCOP of 669 $/t for the electrolyser based H2-SF-EAF system. The NG reformer based DRI-EAF system has a much lower LCOP of 414 $/t. The break-up of the LCOP is presented in Figure 26. The annual operational costs contribute to more than 50% of the production costs in all three scenarios. Annualized capital costs have a significant contribution to the LCOP of methane pyrolysis-based system. Compared to the low-carbon steel production routes, emission costs have the highest impact on the production costs of the NG reformer based DRI-EAF system. In a carbon constrained world, rising emission prices could increase production costs significantly for the NG reformer based DRI-EAF systems.

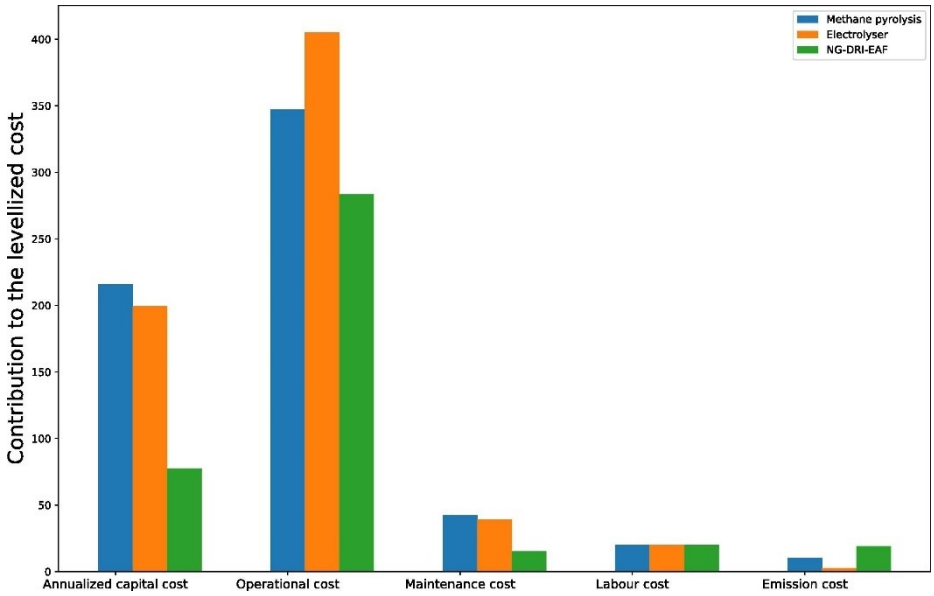

Figure 26 Breakup of levelized cost of production of steel for methane pyrolysis and electrolysis-based hydrogen production, coupled with the DRI-EAF process. The costs are compared with a natural gas reformer based DRI-EAF based system, operating under similar conditions.

5 Decarbonizing primary steel production: Techno-economic assessment of a hydrogen based green steel production plant in Norway

DOI : 10.1016/j.jclepro.2022.131339

Model and Python codes: 10.5281/zenodo.5908635

High electricity cost is the biggest challenge faced by the steel industry in transitioning to hydrogen-based steelmaking. A steel plant in Norway could have access to cheap, emission free electricity, high-quality iron ore, skilled manpower, and the European market. An open-source model for conducting techno-economic assessment of a hydrogen-based steel manufacturing plant, operating in Norway has been developed in this work. Levelized cost of production (LCOP) for two plant configurations; one procuring electricity at a fixed price, and the other procuring electricity from the day-ahead electricity markets, with different electrolyzer capacity were analyzed. LCOP varied from $622/tls to $722/tls for the different plant configurations. Procuring electricity from the day-ahead electricity markets could reduce the LCOP by 15%. Increasing the electrolyzer capacity reduced the operational costs, but increased the capital investments, reducing the overall advantage. Sensitivity analysis revealed that electricity price and iron ore price are the major contributors to uncertainty for configurations with fixed electricity prices. For configurations with higher electrolyzer capacity, changes in the iron ore price and parameters related to capital investment were found to affect the LCOP significantly(Bhaskar et al., 2022).

5.1 Key results

LCOP of $714/t was calculated for the configuration with fixed electricity price of $60/MWh. For the systems procuring electricity from the day-ahead markets, the LCOP varied from $622-$722/t. The LCOP values, for all configurations, were found to be significantly higher than the LCOP of the plants based on BF-BOF process. LCOP of the different configurations is shown in Figure 27. The configurations are shown on the X-axis, according to their hydrogen output capacity. The right most column(7.55-ppa) represents the configuration with a hydrogen output capacity of 7.55 t/h, while purchasing electricity at a fixed power purchase agreement. Almost 73% of the LCOP is comprised of the operational cost, which is primarily composed of the electricity costs and iron ore costs. While the operational costs have the maximum contribution to the production costs at lower hydrogen output capacities, the contributions from capex become more prominent for the configurations with higher electrolyzer capacities. The maintenance costs increase with higher capacities, while the labor and emission costs remain constant for all configurations at $20 million and $7.64 million respectively. The emission costs were calculated only for the direct emissions from the H2-SF-EAF system.

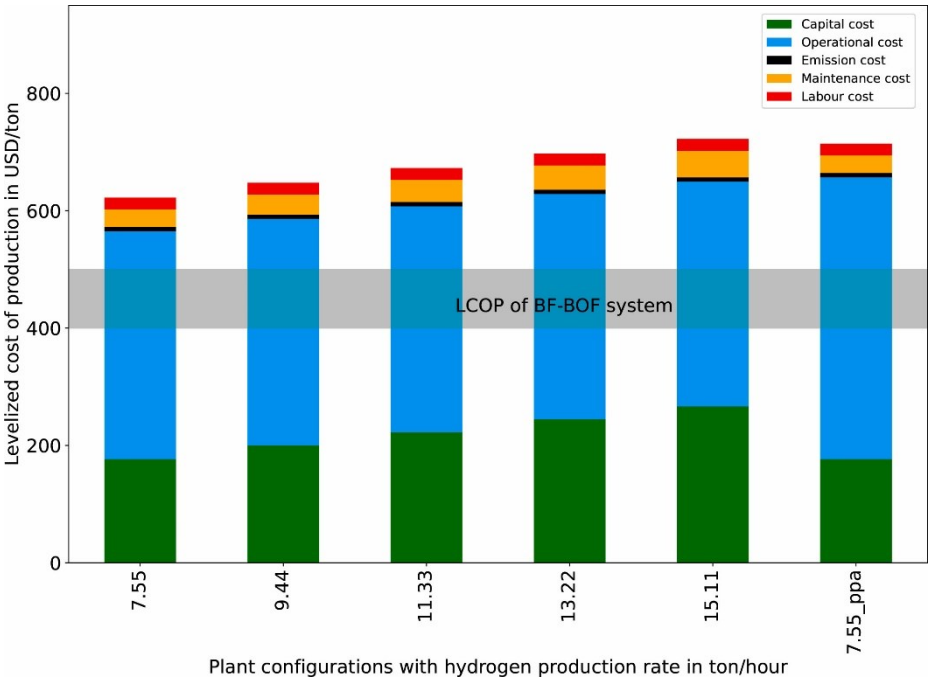

Figure 27 Levelized cost of production for different plant configurations.

5.2 Marginal abatement carbon cost (MACC)

The emission price at which an alternatively technology could become economically feasible is often used as a metric to evaluate competing decarbonizing technologies. The CO_2 mitigation cost range for the different configurations is presented in Figure 28. The mitigation costs were found to vary from \$68/tCO2 to \$180/tCO2. The emission trading price in the EU has increased from \$40/tCO2 to \$90/tCO_2 in the past year, and the increasing trend is likely to continue in the coming years, on the back of ambitious climate policies.

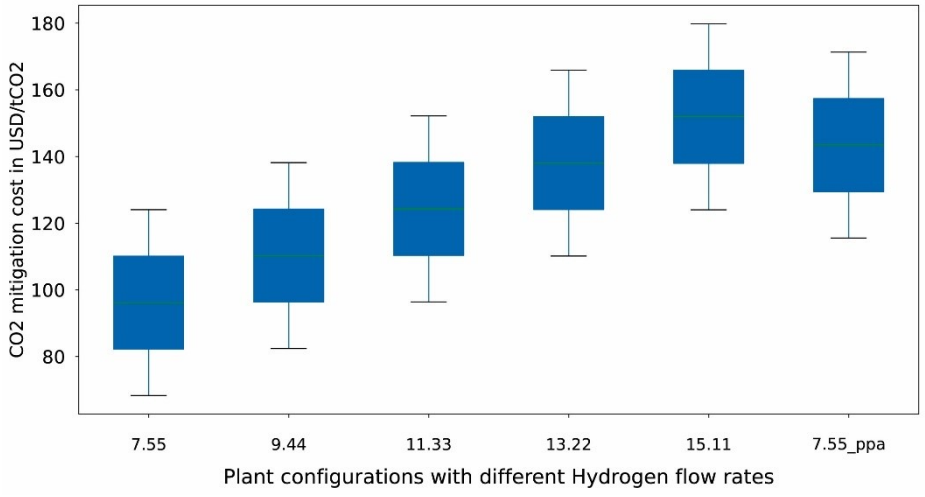

Figure 28 CO_2 mitigation costs for different configurations.

6 Conclusions and future work

HDRI-EAF based steel production is an innovative production technology with a low carbon footprint and can play a pivotal role in reducing emissions from the global steel industry. A techno-economic assessment of the technology was conducted to understand the feasibility of the technology, and the key factors underlying its future uptake by the steel industry. The specific energy consumption was found to vary from 3.48 to 4.25 MWh/tls. The wide range of estimates pertains to the use of different electrolyzer types, electrolyzer efficiency (depends on the projected installation year of the plant), use of scrap in the EAF, thermal energy requirements of the shaft-furnace, purge-gas requirements etc. Water electrolysis was found to consume more than 75% of the total energy. Direct emissions from the HDRI-EAF system were found to be approximately twenty-five times lower than the BF-BOF based steel production system. The LCOP for an HDRI-EAF system operational in the year 2025, at a fixed electricity price of 60 USD/MWh was found to be significantly higher than the baseline technologies for steel production. Operational costs including the price of iron ore and electricity are the major contributor to the production costs for a grid connected electrolyzer based HDRI-EAF system.

Increased ambitions to reduce the anthropogenic ambitions is the key driver for faster uptake of the technology. Policy measures designed to facilitate reduction in industrial emissions i.e., capex subsidies for industrial decarbonization projects, high emission prices, carbon contracts for difference for energy intensive industries, carbon border adjustment mechanism, hydrogen related subsidies like the inflation reduction act, and general measures to ensure competitiveness of the industrial segments in EU and US could facilitate the fast uptake of the HDRI-EAF by steel producers. Access to good quality renewable

resources like solar, wind, hydro etc. and proximity to a region with access with high-quality DRI grade iron ore could enable technology adoption. Policy measures incentivizing use of greener materials in end use products could create a market demand for low emission steel and increase the speed of transition of the steel industry.

Future work

The research presented in this thesis has focused on techno-economic assessment of HDRI-EAF based steelmaking as an alternative technology to decarbonize the steel industry. The techno-economic assessment model has been developed for a grid connected electrolyzer based H_2 production system. There are many areas in which further research is needed to fully realize the potential of this technology. Potential areas of future work include:

1. Integrating HDRI-EAF based steel production in open-source energy system models like PyPSA (Brown et al., 2018) to evaluate the impact of the uptake of the technology on the overall energy system.
2. Evaluate the economic feasibility of developing off-grid facilities in regions with high renewable potential to produce low-emission steel, and intermediate metallic products such as hot briquetted iron or pig iron.
3. The integration of the renewable generators, energy storage in the form of batteries or hydrogen storage (surface or geological storage), and the HDRI-EAF system and developing an optimal system design for such a plant considering the physical characteristics and operational constraints of individual components.
4. DR grade iron ore is a scarce commodity, and adoption of HDRI-EAF technology could be hampered by the availability of high-quality iron ore. Assessing the impact of iron ore quality on the DRI properties, impact on the downstream processes in the EAF

and investigations into the use of catalysts etc. to facilitate the use of low-quality iron ore in the DRI shaft furnace and bring down production costs.

5. Technological solutions to efficiently heat hydrogen to the reactor temperature could be beneficial for the technology deployment and could have potential synergies in many other high-temperature industrial applications.
6. Examining the potential for hydrogen-based steelmaking to be integrated with other industrial processes, such as cement and chemical production, to create more efficient and sustainable integrated industrial systems.

7 References

Agora industry, FutureCamp, & Wuppertal Institute. (2022). *Transforming industry through carbon contracts*. agora-industry.org

Alhumaizi, K., Ajbar, A., & Soliman, M. (2012). Modelling the complex interactions between reformer and reduction furnace in a midrex-based iron plant. *Canadian Journal of Chemical Engineering*, *90*(5), 1120–1141. https://doi.org/10.1002/cjce.20596

Allwood, J. M. (2013). Transitions to material efficiency in the UK steel economy. *Philosophical Transactions of the Royal Society A: Mathematical, Physical and Engineering Sciences*, *371*(1986). https://doi.org/10.1098/rsta.2011.0577

Allwood, J. M., Ashby, M. F., Gutowski, T. G., & Worrell, E. (2011). Material efficiency: A white paper. *Resources, Conservation and Recycling*, *55*(3), 362–381. https://doi.org/10.1016/j.resconrec.2010.11.002

Arens, M., & Vogl, V. (n.d.). *Can we find a market for green steel? Technological change and industrial energy efficiency-Exploring the low-carbon transformation of the German iron and steel industry View project HYBRIT RP1 (HYdrogen BReakthrough Ironmaking Technology) and CAST (Circular And sustainable Steel Transitions) View project*. www.steeltimesint.com

Bashmakov, I. A., Nilsson, L. J., Acquaye, A., Bataille, C., Cullen, J. M., de La Rue Du Can, S., Fischedick, M., Geng, Y., & Tanaka, K. (2022). *Climate Change 2022: Mitigation of Climate Change. Contribution of Working Group III to the Sixth Assessment Report of the Intergovernmental Panel on Climate Change*. https://doi.org/10.1017/9781009157926.013

Bataille, C., Åhman, M., Neuhoff, K., Nilsson, L. J., Fischedick, M., Lechtenböhmer, S., Solano-Rodriquez, B., Denis-Ryan, A., Stiebert, S., Waisman, H., Sartor, O., & Rahbar, S. (2018). A review of technology and policy deep decarbonization pathway options for making energy-intensive industry production consistent with the Paris Agreement. *Journal of Cleaner Production*, *187*, 960–973. https://doi.org/10.1016/j.jclepro.2018.03.107

Bhaskar, A. (2021). *Decarbonizing primary steel production : Techno-economic assessment of green steel production in Norway* (1.0). Zenodo. https://doi.org/10.5281/zenodo.5485274

Bhaskar, A., Abhishek, R., Assadi, M., & Somehesaraei, H. N. (2022). Decarbonizing primary steel production : Techno-economic assessment of a hydrogen based green steel production plant in Norway. *Journal of Cleaner Production*, *350*, 131339. https://doi.org/10.1016/J.JCLEPRO.2022.131339

Bhaskar, A., Assadi, M., & Somehsaraei, H. N. (2021). Can methane pyrolysis based hydrogen production lead to the decarbonisation of iron and steel industry? *Energy Conversion and Management: X*, *10*(March), 100079. https://doi.org/10.1016/j.ecmx.2021.100079

Bhaskar, A., Assadi, M., & Somehsaraei, H. N. H. N. (2020). Decarbonization of the iron and steel industry with direct reduction of iron ore with green hydrogen. *Energies*, *13*(3), 1–23. https://doi.org/10.3390/en13030758

Brown, T., Schlachtberger, D., Kies, A., Schramm, S., & Greiner, M. (2018). Synergies of sector coupling and transmission reinforcement in a cost-optimised, highly renewable European energy system. *Energy*, *160*, 720–739. https://doi.org/10.1016/j.energy.2018.06.222

Bynum, M. L., Hackebeil, G. A., Hart, W. E., Laird, C. D., Nicholson, B. L., Siirola, J. D., Watson, J.-P., & Woodruff, D. L. (2021). *Pyomo : Optimization Modeling in Python* (Vol. 67). Springer International Publishing. https://doi.org/10.1007/978-3-030-68928-5

Chase, M. W. (1998). NIST-JANAF thermochemical Tables. In *Journal of Physical and Chemical Reference Data* (4th ed., Vol. 9). American Chemical Society;American institute of Physics for the National institute of standards and technology.

Chen, C. X., Pierobon, F., Jones, S., Maples, I., Gong, Y., & Ganguly, I. (2022). Comparative life cycle assessment of mass timber and concrete residential buildings: A case study in China. *Sustainability (Switzerland)*, *14*(1). https://doi.org/10.3390/su14010144

Chen, Z., Gu, H., Bergman, R. D., & Liang, S. (2020). Comparative life-cycle assessment of a high-rise mass timber building with an equivalent reinforced concrete alternative using the athena impact estimator for buildings. *Sustainability (Switzerland)*, *12*(11). https://doi.org/10.3390/su12114708

Czerwinski, F. (2021). *materials Current Trends in Automotive Lightweighting Strategies and Materials*. https://doi.org/10.3390/ma14216631

D'Amico, B., Pomponi, F., & Hart, J. (2021). Global potential for material substitution in building construction: The case of cross laminated timber. *Journal of Cleaner Production*, *279*, 123487. https://doi.org/10.1016/J.JCLEPRO.2020.123487

de Moraes, S. L., Lima, J. R. B. de, Neto, J. B. F., Fredericci, C., & Saccoccio, E. M. (2020). Binding Mechanism in Green Iron Ore Pellets with an Organic Binder. *Mineral Processing and Extractive*

Metallurgy Review, *41*(4), 247–254. https://doi.org/10.1080/08827508.2019.1604521

Energy Transition Commission. (2022). *Making Net-Zero Steel Possible*.

EUROFER. (2022). *European Steel in Figures*. eurofer.eu

Fan, Z., & Friedmann, S. J. (2021). Low-carbon production of iron and steel: Technology options, economic assessment, and policy. In *Joule* (Vol. 5, Issue 4, pp. 829–862). Cell Press. https://doi.org/10.1016/j.joule.2021.02.018

Fernández-González, D., Piñuela-Noval, J., & Verdeja, L. F. (2018). Iron Ore Agglomeration Technologies. In *Iron Ores and Iron Oxide Materials*. InTech. https://doi.org/10.5772/intechopen.72546

Fernández-González, D., Ruiz-Bustinza, I., Mochón, J., González-Gasca, C., & Verdeja, L. F. (2017). Iron Ore Sintering: Process. *Mineral Processing and Extractive Metallurgy Review*, *38*(4), 215–227. https://doi.org/10.1080/08827508.2017.1288115

Fischedick, M., Marzinkowski, J., Winzer, P., & Weigel, M. (2014). Techno-economic evaluation of innovative steel production technologies. *Journal of Cleaner Production*, *84*(1), 563–580. https://doi.org/10.1016/j.jclepro.2014.05.063

Gruobi. (2021). *Gurobi Optimizer Reference Manual*.

Halt, J. A., & Kawatra, S. K. (2014). Review of organic binders for iron ore concentrate agglomeration. In *MINERALS & METALLURGICAL PROCESSING* (Vol. 31, Issue 2).

Hamby, D. M. (1994). A review of techniques for parameter sensitivity analysis of environmental models. *Environmental Monitoring and Assessment*, *32*(2), 135–154. https://doi.org/10.1007/BF00547132

Heidari, A., Niknahad, N., Iljana, M., & Fabritius, T. (2021). A Review on the Kinetics of Iron Ore Reduction by Hydrogen. *Materials*, *14*(24), 7540. https://doi.org/10.3390/ma14247540

Herman, J., & Usher, W. (2017). SALib: An open-source Python library for Sensitivity Analysis. *The Journal of Open Source Software*, *2*(9), 97. https://doi.org/10.21105/joss.00097

Hunter, J. D. (2007). Matplotlib: A 2D graphics environment. *Computing in Science and Engineering*, *9*(3), 99–104. https://doi.org/10.1109/MCSE.2007.55

IEA. (2019). *Material efficiency in clean energy transitions*. https://www.iea.org/reports/material-efficiency-in-clean-energy-transitions

IEA. (2021a). *IEA (2021), Global Energy Review 2021, IEA, Paris*. https://www.iea.org/reports/global-energy-review-2021

IEA. (2021b). *Net Zero by 2050 - A Roadmap for the Global Energy Sector*. www.iea.org/t&c/

IEA. (2022a). *Global methane emissions from the energy sector over time, 2000-2021, IEA*. https://www.iea.org/data-and-statistics/charts/global-methane-emissions-from-the-energy-sector-over-time-2000-2021

IEA. (2022b). *Global Methane Tracker 2022, IEA, Paris*. https://www.iea.org/reports/global-methane-tracker-2022/estimating-methane-emissions

IEA. (2022c). *Iron and Steel Technology Roadmap Towards more sustainable steelmaking Part of the Energy Technology Perspectives series*. https://iea.blob.core.windows.net/assets/eb0c8ec1-3665-4959-97d0-187ceca189a8/Iron_and_Steel_Technology_Roadmap.pdf

IEA. (2022d). *World Energy Outlook 2022*. www.iea.org/t&c/

IEA. (2022e, August). *IEA World energy balance* . IEA (2021), World Energy Balances: Overview, IEA, Paris . https://www.iea.org/reports/world-energy-balances-overview

International energy agency. (2021). *Net Zero by 2050 - A Roadmap for the Global Energy Sector*. https://www.iea.org/reports/net-zero-by-2050

IPCC. (2022a). *Mitigation of Climate Change Climate Change 2022 Working Group III contribution to the Sixth Assessment Report of the Intergovernmental Panel on Climate Change*. https://www.ipcc.ch/site/assets/uploads/2018/05/uncertainty-guidance-note.pdf.

IPCC. (2022b). *Mitigation of Climate Change Climate Change 2022 Working Group III contribution to the Sixth Assessment Report of the Intergovernmental Panel on Climate Change*. https://doi.org/10.1017/9781009157896

IRENA. (2020). *Green Hydrogen Cost Reduction: Scaling up Electrolysers to Meet the 1.5^{0}C Climate Goal*.

IRENA. (2022a). *Geopolitics of the Energy Transformation: The Hydrogen Factor*. www.irena.org/publicatons

IRENA. (2022b). *World Energy Transitions Outlook 2022: 1.5°C Pathway*. www.irena.org

Jai, D., Pandit, K., Watson, M., & Qader, A. (2020). *Reduction of Greenhouse Gas Emissions in Steel Production Final Report Reduction of Greenhouse Gas Emissions in Steel Production i Commercial in Confidence Acknowledgement*. www.co2crc.com.au

Ju, Y., Sun, Y., Sa, Z., Pan, J., Wang, J., Hou, Q., Li, Q., Yan, Z., & Liu, J. (2016). A new approach to estimate fugitive methane emissions from coal mining in China. *Science of The Total Environment*, *543*, 514–523. https://doi.org/10.1016/J.SCITOTENV.2015.11.024

Karakaya, E., Nuur, C., & Assbring, L. (2018). Potential transitions in the iron and steel industry in Sweden: Towards a hydrogen-based future? *Journal of Cleaner Production*, *195*, 651–663. https://doi.org/10.1016/j.jclepro.2018.05.142

Kawasaki, E., Sanscrainte, J., & Walsh, T. J. (1962). Kinetics of reduction of iron oxide with carbon monoxide and hydrogen. *AIChE Journal*, *8*(1), 48–52. https://doi.org/10.1002/aic.690080114

Kim, S. H., Zhang, X., Ma, Y., Souza Filho, I. R., Schweinar, K., Angenendt, K., Vogel, D., Stephenson, L. T., El-Zoka, A. A., Mianroodi, J. R., Rohwerder, M., Gault, B., & Raabe, D. (2021). Influence of microstructure and atomic-scale chemistry on the direct reduction of iron ore with hydrogen at 700°C. *Acta Materialia*, *212*. https://doi.org/10.1016/j.actamat.2021.116933

Kirschen, M., Badr, K., & Pfeifer, H. (2011). Influence of direct reduced iron on the energy balance of the electric arc furnace in steel industry. *Energy*, *36*(10), 6146–6155. https://doi.org/10.1016/j.energy.2011.07.050

Laitala, K., Klepp, I. G., Haugrønning, V., Throne-Holst, H., & Strandbakken, P. (2021). Increasing repair of household appliances, mobile phones and clothing: Experiences from consumers and the repair industry. *Journal of Cleaner Production*, *282*. https://doi.org/10.1016/j.jclepro.2020.125349

Mantzos, L., Wiesenthal, T., Matei, N.-A., Tchung-Ming, S., Rozsai, M., Russ, H. P., & Soria Ramirez, A. (2017). *JRC-IDEES: Integrated*

Database of the European Energy Sector: Methodological note. https://doi.org/10.2760/182725

Material Economics, Wuppertal institute, & Institute of European studies. (2019). *Industrial Transformation 2050 Pathways to Net-Zero Emissions from EU Heavy Industry*. https://materialeconomics.com/publications/industrial-transformation-2050

McKinney, W. (2010). Data Structures for Statistical Computing in Python. In S. van der Walt & J. Millman (Eds.), *Proceedings of the 9th Python in Science Conference* (pp. 51–56).

Modaresi, R., Pauliuk, S., Løvik, A. N., & Müller, D. B. (2014). Global carbon benefits of material substitution in passenger cars until 2050 and the impact on the steel and aluminum industries. *Environmental Science and Technology*, *48*(18), 10776–10784. https://doi.org/10.1021/es502930w

Moya, J. A., Pardo, N., Mercier, A., J. Moya, N. Pardo, A. M., Moya, J. A., Pardo, N., & Mercier, A. (2010). Energy Efficiency and CO 2 Emissions : Prospective Scenarios for the Cement Industry. In *Publications Office of the European Union*. https://doi.org/10.2790/25732

Muslemani, H., Liang, X., Kaesehage, K., Ascui, F., & Wilson, J. (2021). Opportunities and challenges for decarbonizing steel production by creating markets for 'green steel' products. *Journal of Cleaner Production*, *315*, 128127. https://doi.org/10.1016/J.JCLEPRO.2021.128127

Naito, M., Takeda, K., & Matsui, Y. (2015). Ironmaking technology for the last 100 years: Deployment to advanced technologies from introduction of technological know-how, and evolution to next-generation process. In *ISIJ International* (Vol. 55, Issue 1, pp. 7–

35). Iron and Steel Institute of Japan. https://doi.org/10.2355/isijinternational.55.7

Neininger, B. G., Kelly, B. F. J., Hacker, J. M., LU, X., & Schwietzke, S. (2021). Coal seam gas industry methane emissions in the Surat Basin, Australia: comparing airborne measurements with inventories. *Philosophical Transactions of the Royal Society A: Mathematical, Physical and Engineering Sciences*, *379*(2210), 20200458. https://doi.org/10.1098/rsta.2020.0458

Oh, J., & Noh, D. (2017). The reduction kinetics of hematite particles in H2 and CO atmospheres. *Fuel*, *196*. https://doi.org/10.1016/j.fuel.2016.10.125

Pal, J. (2019). Innovative Development on Agglomeration of Iron Ore Fines and Iron Oxide Wastes. In *Mineral Processing and Extractive Metallurgy Review* (Vol. 40, Issue 4, pp. 248–264). Taylor and Francis Inc. https://doi.org/10.1080/08827508.2018.1518222

Pei, M., Petäjäniemi, M., Regnell, A., & Wijk, O. (2020). Toward a fossil free future with hybrit: Development of iron and steelmaking technology in Sweden and Finland. *Metals*, *10*(7), 1–11. https://doi.org/10.3390/met10070972

Pfeifer, H., & Kirschen, M. (2003). Thermodynamic analysis of EAF energy efficiency and comparison with a statical model of electric energy model of demand. *Engineering*, 1–16.

Quader, M. A., Ahmed, S., Dawal, S. Z., & Nukman, Y. (2016). *Present needs , recent progress and future trends of energy-ef fi cient Ultra-Low Carbon Dioxide (CO 2) Steelmaking (ULCOS) program*. *55*, 537–549. https://doi.org/10.1016/j.rser.2015.10.101

Ranzani Da Costa, A., Wagner, D., & Patisson, F. (2013). Modelling a new, low CO2 emissions, hydrogen steelmaking process. *Journal*

of Cleaner Production, *46*, 27–35. https://doi.org/10.1016/J.JCLEPRO.2012.07.045

Rechberger, K., Spanlang, A., Sasiain Conde, A., Wolfmeir, H., & Harris, C. (2020a). Green Hydrogen-Based Direct Reduction for Low-Carbon Steelmaking. *Steel Research International*, *91*(11). https://doi.org/10.1002/srin.202000110

Rechberger, K., Spanlang, A., Sasiain Conde, A., Wolfmeir, H., & Harris, C. (2020b). Green Hydrogen-Based Direct Reduction for Low-Carbon Steelmaking. *Steel Research International*, *91*(11). https://doi.org/10.1002/SRIN.202000110

Ruuska, A., & Häkkinen, T. (2014). Material efficiency of building construction. *Buildings*, *4*(3), 266–294. https://doi.org/10.3390/buildings4030266

Sadavarte, P., Pandey, S., Maasakkers, J. D., Lorente, A., Borsdorff, T., Denier van der Gon, H., Houweling, S., & Aben, I. (2021). Methane Emissions from Superemitting Coal Mines in Australia Quantified Using TROPOMI Satellite Observations. *Environmental Science & Technology*, *55*(24), 16573–16580. https://doi.org/10.1021/acs.est.1c03976

Saltelli, A., Annoni, P., Azzini, I., Campolongo, F., Ratto, M., & Tarantola, S. (2010). Variance based sensitivity analysis of model output. Design and estimator for the total sensitivity index. *Computer Physics Communications*, *181*(2), 259–270. https://doi.org/10.1016/j.cpc.2009.09.018

Schäfer, M. (2021). *From 2025: "Green" steel for Mercedes-Benz*. https://www.daimler.com/sustainability/climate/green-steel.html

Sobol, I. M. (2001). Global sensitivity indices for non-linear mathematical models and their Monte carlo estimates. *Mathematics and Computers in Sumulation*, *5*(2), 271–280.

Somers, J. (2022). *Technologies to decarbonise the EU steel industry.* https://data.europa.eu/doi/10.2760/069150

Spreitzer, D., & Schenk, J. (2019). Reduction of Iron Oxides with Hydrogen—A Review. *Steel Research International*, *90*(10), 1900108. https://doi.org/10.1002/srin.201900108

Stougaard, A. (2021). *Ørsted joins the SteelZero initiative to support transition to low-carbon steel*. https://orsted.com/en/media/newsroom/news/2020/12/633975720078575

Suopajärvi, H., Umeki, K., Mousa, E., Hedayati, A., Romar, H., Kemppainen, A., Wang, C., Phounglamcheik, A., Tuomikoski, S., Norberg, N., Andefors, A., Öhman, M., Lassi, U., & Fabritius, T. (2018). Use of biomass in integrated steelmaking – Status quo, future needs and comparison to other low-CO2 steel production technologies. *Applied Energy*, *213*, 384–407. https://doi.org/10.1016/J.APENERGY.2018.01.060

Thomassen, G., van Dael, M., van Passel, S., & You, F. (2019). How to assess the potential of emerging green technologies? Towards a prospective environmental and techno-economic assessment framework. *Green Chemistry*, *21*(18), 4868–4886. https://doi.org/10.1039/c9gc02223f

Treptow, R. S., & Jean, L. (1998). The Iron Blast Furnace: A Study in Chemical Thermodynamics. *Journal of Chemical Education*, *75*(1), 43. https://doi.org/10.1021/ed075p43

UNCTAD. (2021). *A European Union Carbon Border Adjustment Mechanism : Implications for developing countries* (Issue July). https://unctad.org/system/files/official-document/osginf2021d2_en.pdf

UNFCCC. Conference of the Parties (COP). (2015). Paris Climate Change Conference-November 2015, COP 21. *Adoption of the Paris Agreement. Proposal by the President.*, *21932*(December), 32. https://doi.org/FCCC/CP/2015/L.9/Rev.1

UNIDO. (2021). *Industrial Deep Decarbonisation Initiative*. https://www.unido.org/IDDI

van Boggelen, J., Hage, H., Meijer, K., & Zeilstra, C. (2022). HIsarna: A Technology to Meet Both the Climate and Circularity Challenges for the Iron and Steel Industry. In A. Lazou, K. Daehn, C. Fleuriault, M. Gökelma, E. Olivetti, & C. Meskers (Eds.), *REWAS 2022: Developing Tomorrow's Technical Cycles (Volume I)* (pp. 595–600). Springer International Publishing.

van der Walt, S., Colbert, S. C., & Varoquaux, G. (2011). The NumPy array: A structure for efficient numerical computation. *Computing in Science and Engineering*, *13*(2), 22–30. https://doi.org/10.1109/MCSE.2011.37

Vogl, V., Åhman, M., & Nilsson, L. J. (2018). Assessment of hydrogen direct reduction for fossil-free steelmaking. *Journal of Cleaner Production*, *203*, 736–745. https://doi.org/10.1016/j.jclepro.2018.08.279

Vogl, V., Sanchez, F., Gerres, T., Lettow, F., Bhaskar, A., Swalec, C., Mete, G., Åhman, M., Lehne, J., Schenk, S., Witecka, W., Olsson, O., & Rootzén, J. (2021). *Green Steel Tracker*. https://www.sei.org/featured/green-steel-tracker/

Volvo. (2021). *Volvo Group and SSAB to collaborate on the world's first vehicles of fossil-free steel*. https://www.volvogroup.com/en/news-and-media/news/2021/apr/news-3938822.html

Wang, P., Ryberg, M., Yang, Y., Feng, K., Kara, S., Hauschild, M., & Chen, W. Q. (2021). Efficiency stagnation in global steel

production urges joint supply- and demand-side mitigation efforts. *Nature Communications*, *12*(1). https://doi.org/10.1038/S41467-021-22245-6

Weigel, M., Fischedick, M., Marzinkowski, J., & Winzer, P. (2016). Multicriteria analysis of primary steelmaking technologies. *Journal of Cleaner Production*, *112*(May 2013), 1064–1076. https://doi.org/10.1016/j.jclepro.2015.07.132

Wiencke, J., Lavelaine, H., Panteix, P. J., Petitjean, C., & Rapin, C. (2018). Electrolysis of iron in a molten oxide electrolyte. *Journal of Applied Electrochemistry*, *48*(1), 115–126. https://doi.org/10.1007/s10800-017-1143-5

Witte, K. (2021). Social acceptance of carbon capture and storage (Ccs) from industrial applications. In *Sustainability (Switzerland)* (Vol. 13, Issue 21). MDPI. https://doi.org/10.3390/su132112278

Wolfram, P., Tu, Q., Heeren, N., Pauliuk, S., & Hertwich, E. G. (2021). Material efficiency and climate change mitigation of passenger vehicles. *Journal of Industrial Ecology*, *25*(2), 494–510. https://doi.org/10.1111/jiec.13067

WorldSteel. (2022). *2022 World Steel in Figures*.

Worrell, E., Martin, N., & Price, L. (1999). *Energy Efficiency and Carbon Dioxide Emissions Reduction Opportunities in the U.S. Iron and Steel Sector*.

Wyns, T., & Axelson, M. (2016). The Final Frontier – Decarbonising Europe's energy intensive industries. *Institute for European Studies*, 64. https://doi.org/10.1017/CBO9781107415324.004

A. Appendices

I. Abbreviations

EU	European Union
USA	United States of America
UK	United Kingdom
IDDI	Industrial deep decarbonization initiative1
DRI	Direct reduced iron
HBI	Hot briquetted iron
SF	Shaft furnace
HDRI	Hydrogen direct reduced iron
HYFOR	Hydrogen-based fine-ore reduction
NIST	National institute of standards
EAF	Electric arc furnace
BF-BOF	Blast furnace basic oxygen furnace
SMR	Steam methane reforming
CAC	Corrected Arc Crossings
LCOP	Levelized cost of production
IPCC	Inter-governmental panel on climate change
SSAB	Svenskt Stål AB
LKAB	Luossavaara-Kiirunavaara Aktiebolag
MMBTU	Metric Million British Thermal Unit
IDDI	Industrial deep decarbonization initiative
SEC	Specific energy consumption
tls	Ton of liquid steel

$kgCO_2$	Kilogram of carbon dioxide
tCO_2	Tonn of carbon dioxide
$GtCO_2$	Gigaton of carbon dioxide
kg	Kilogram
kJ	KiloJoule
GJ	GigaJoule
kW	kilowatt
kW_{el}	kilowatt electric
MW	Megawatt
GW	Gigawatt
KWh	Kilowatthour
MWh	Megawatthour
TWh	Terrawatthour
Mtpa	Million ton per annum
mol	moles
L	Liter
NM^3	Normal cubic meter
h	hour
CO	Carbon Monoxide
H2	Hydrogen
O2	Oxygen
Al2O3	Aluminum oxide (Alumina)
SiO2	Silicon dioxide(Sillica)
Fe2O3	Hematite
Fe3O4	Magnetite
Fe	Iron
FeO	Iron Oxide

Fe_3C	Iron carbide
C	Carbon
CO_2	Carbon dioxide
NO_2	Nitrous Oxide
MgO	Magnesium Oxide
CaO	Calcium Oxide
Symbols	
$	US Dollar
USD	US Dollar
°C	Celsius
€	Euro

II. Research Articles

Decarbonization of the Iron and Steel Industry with Direct Reduction of Iron Ore with Green Hydrogen

Can methane pyrolysis based hydrogen production lead to the decarbonisation of iron and steel industry?

Decarbonizing primary steel production: Techno-economic assessment of a hydrogen based green steel production plant in Norway

1. Bhaskar, A.; Assadi, M.; Nikpey Somehsaraei, H. Decarbonization of the Iron and Steel Industry with Direct Reduction of Iron Ore with Green Hydrogen. *Energies* **2020**, *13*, 758. https://doi.org/10.3390/en13030758

energies

IMPACT FACTOR 3.252

CITESCORE 5.0

Article

Decarbonization of the Iron and Steel Industry with Direct Reduction of Iron Ore with Green Hydrogen

Abhinav Bhaskar, Mohsen Assadi and Homam Nikpey Somehsaraei

MDPI

https://doi.org/10.3390/en13030758

energies

MDPI

Article

Decarbonization of the Iron and Steel Industry with Direct Reduction of Iron Ore with Green Hydrogen

Abhinav Bhaskar *,†, Mohsen Assadi and Homam Nikpey Somehsaraei

University of Stavanger, Faculty of Science and Technology, Instiute of Energy and Petroleum Engineering, 4036 Stavanger, Norway; mohsen.assadi@uis.no (M.A.); homam.nikpey@uis.no (H.N.S.)

* Correspondence: abhinav.bhaskar@uis.no

† Current address: University of Stavanger, 4036 Stavanger, Norway.

Received:11 December 2019; Accepted: 3 February 2020; Published: 9 February 2020

Abstract: Production of iron and steel releases seven percent of the global greenhouse gas (GHG) emissions. Incremental changes in present primary steel production technologies would not be sufficient to meet the emission reduction targets. Replacing coke, used in the blast furnaces as a reducing agent, with hydrogen produced from water electrolysis has the potential to reduce emissions from iron and steel production substantially. Mass and energy flow model based on an open-source software (Python) has been developed in this work to explore the feasibility of using hydrogen direct reduction of iron ore (HDRI) coupled with electric arc furnace (EAF) for carbon-free steel production. Modeling results show that HDRI-EAF technology could reduce specific emissions from steel production in the EU by more than 35%, at present grid emission levels (295 kgCO_2/MWh). The energy consumption for 1 ton of liquid steel (tls) production through the HDRI-EAF route was found to be 3.72 MWh, which is slightly more than the 3.48 MWh required for steel production through the blast furnace (BF) basic oxygen furnace route (BOF). Pellet making and steel finishing processes have not been considered. Sensitivity analysis revealed that electrolyzer efficiency is the most important factor affecting the system energy consumption, while the grid emission factor is strongly correlated with the overall system emissions.

Keywords: hydrogen; direct reduction of iron ore; green steel production; industrial decarbonization

1. Introduction

Anthropogenic climate change is one of society's greatest challenges. Decarbonization of all sectors of the energy system is essential to mitigate climate change. Although the industrial sector consumes one-third of the primary energy resources and releases one-quarter of the energy-related greenhouse gas emissions, it has not received as much attention from researchers and policy-makers as other demand sectors like electricity generation, buildings and transport etc. The non-homogeneity of industrial plants and the use of fossil fuels as feedstock makes it difficult to find effective strategies to decarbonize industries. Iron and steel, chemicals, cement, non-ferrous metals, paper, and pulp etc. are referred to as energy-intensive industries (EII) because they use energy resources as primary raw material. Energy efficiency has played a major role in reducing the industrial sector's energy intensity and emissions. Nonetheless, incremental changes in current industrial production technologies would not reach the emission reduction goals needed to avoid catastrophic effects of anthropogenic climate change [1,2].

Steel is the backbone of modern civilization. It is used in buildings, transport, packaging, shipping and infrastructure etc. Approximately 1.73 billion tons of crude steel was produced in 2017 [3]. The apparent steel use per capita (finished steel products) was 216.3 kg in 2017. Industrialized countries like Germany have a high apparent steel use per capita of approximately 500 kg. India, a developing

country, on the other hand, has a per capita steel consumption of 66.3 kg. As the standard of living in developing countries increases, demand for steel will grow further. The demand for steel will increase until 2050 [4]. Steel could be produced by reducing iron ore or by recycling steel scrap in an electric arc furnace (EAF). Iron and steel sector releases seven percent of the total CO_2 emission and 16% of the total industrial emission of CO_2 globally [5,6]. Limited availability of scrap and demand for special grades of steel, which can not be produced from steel recycling, would lead to an increased demand for ore based steel production in the future. More than 80% [3] of the ore based steel is produced through the BF-BOF route. The BF-BOF route uses approximately 18 GJ/t of energy supplied from coal [7], and has an emission intensity of approximately 1870 $kgCO_2/tls$ [4,8] (considering pellet making, steel rolling and finishing steps). Majority of the emissions is released from the blast furnace (61%) and coke making plant (27%) [9].

Some of the alternative processes with significantly reduced carbon footprint are BF-BOF with carbon capture and storage (CCS), direct reduction of iron ore (DRI) with CCS, electrowining (electrolysis of iron ore) [10] and green hydrogen-based DRI production. Integration of CCS in steelmaking processes is being explored under the ultra–Low carbon dioxide(CO_2) steelmaking (ULCOS) [11,12] project. However, concerns over the safe transport and storage of captured makes CCS options less attractive. Electrowining or molten electrolysis of iron ore is a relatively new technology and is quite far from reaching commercial feasibility. Hydrogen direct reduction of iron ore (HDRI)-EAF based steel production is the most viable alternative to BF-BOF based steel production, as the production of hydrogen with intermittent renewable energy generators has an additional benefit of providing flexibility to the electricity grid [7]. Hydrogen, as an energy carrier, has applications in other sectors of the energy system, like chemical production, heavy transport, aviation, shipping etc. Large scale production, storage and transport of hydrogen to cater to the demands of the steel industry will reduce the price of hydrogen for other industries like chemical production, transportation, buildings and district heating etc. [13–15]. The use of green hydrogen in the iron and steel sector, has the potential to reduce emissions by 2.3 gigatonnes of carbon dioxide per year ($GtCO_2/y$) [16] globally.

The first HDRI based steel production unit was commissioned in the year 1999 in Trinidad. Production was based on fluidized bed reactors [17]. The plant produced steel with 95% metallization rate, at a production capacity of 65 tonnes of liquid steel per hour (tls/hr) [18]. Energiron, which is a commercial supplier of natural gas-based DRI shaft furnaces, tested direct reduction of iron ore with more than 90% hydrogen in its test facility at Hysla, Monterrey [19].The pilot plant had a capacity of 36 tls/day of hot and cold DRI production. A high metallization rate of 94–96% was achieved. The company claims that their shaft furnace reactors could be easily optimized to use 100% hydrogen for the reduction of iron ore. It is supplying shaft furnace reactors to many European demonstration projects for hydrogen-based steel production. The higher cost of hydrogen compared to fossil fuel resources is a roadblock for further development of the technology. There is a renewed interest in the hydrogen economy among researchers, policy-makers and industries, on the back of declining prices of renewable electricity generators and demand for more flexibility in the electricity grid to integrate intermittent renewable energy generators [16]. Techno-economic modeling of hydrogen and ammonia production using water electrolysis was carried out by [20]. They found that the cost of green hydrogen could reduce to 2 USD/Kg, which is comparable to hydrogen produced from fossil fuel sources. Researchers at the Technical University of Munich and Stanford University found that the cost of hydrogen produced from renewable electricity has decreased to €3.23 kg^{-1} and will further decrease to €2.50 kg^{-1} in Germany and Texas [21] within the next decade. The cost of producing hydrogen from renewable electricity could fall 30% by 2030 as a result of declining costs of renewable energy and the scaling up of hydrogen production [22]. In the HYBRIT project [23], hydrogen-based steel production would be demonstrated by Luossavaara-Kiirunavaara Aktiebolag (LKAB), Svenskt Stål AB (SSAB), Vattenfall along with Swedish energy agency. Voestalpine is testing a six-megawatt proton exchange membrane electrolyzer (PEM) developed by Siemens for hydrogen production [24]. Under the Salcos [25] project along with GrInHy2 [26] and Windh2 [27], the feasibility of integrating

30 MW of wind electricity generators with solid oxide electrolyzers for hydrogen production at a steel production facility in Germany is being explored. Tata steel Europe, Nouryon and the port of Amsterdam have partnered to develop the largest green hydrogen cluster in Europe [28]. Arcelormittal is building a demonstration HDRI unit, with a production capacity of 100,000 t/year [29]. The plant will use grey hydrogen produced from natural gas until green hydrogen becomes cost-competitive. Midrex technologies will supply the shaft furnace reactor for the plant [30]. Thyssenkrupp has begun testing of hydrogen-based steel production at its production facility in Duisburg, Germany. Coke has been replaced with hydrogen in one of the nine blast furnaces. If the results from the pilot study are favorable, hydrogen could replace coke in all blast furnaces [31].

There have been many discussions about the use of 100% hydrogen as reducing agent DRI based steel production [7,9,32–35] in the scientific literature. However, energy consumption and emissions values reported in the literature vary significantly. There is a lack of clarity about system configuration and boundaries. In this work, system boundary has been clearly defined, making it easier to compare the energy and emission intensity of BF-BOF and HDRI-EAF based steelmaking process. More details about the process parameters are included in this model than other comparable models available in the literature. The model codes are written in an open-source software and are available to the scrutiny of other researchers [36]. Theoretical concepts and the chemical reactions, along with discussions on the reaction kinetics are presented in Section 2. The HDRI-EAF model, along with mass and energy flows through the different components are discussed in Section 3. Modelling results are presented in the Section 4, followed by the conclusions in Section 5 and discussions on future work in Section 6.

2. Concept

Direct reduction of iron ore refers to the conversion of solid iron ore to metallic iron without conversion to the liquid phase [37]. Majority of the direct reduced iron (DRI) [38] is produced by reacting iron oxide with hydrocarbon-based reducing gases produced from reforming natural gas or coal gasification [39–42]. DRI technology has been deployed commercially and five percent of the total global steel is produced through the DRI route [43]. Lower capital investment, space requirements, and simpler design and operation make it easier to build and operate a DRI plant [33]. With the declining price of shale gas, there has been an upsurge in the installation of DRI plants in the US [44]. Shaft furnaces, rotary kilns, rotary hearth furnaces and fluidized bed reactors are used for direct reduction of iron ore. Most of the DRI plants use shaft furnace reactors developed by MIDREX [43] and HYL-Energiron [45] technologies. Shaft furnaces are moving bed counter-current reactors. Rotary hearth furnaces are used, when coal is used as the source for production of reducing gases [33]. Kinetic studies have revealed that the reduction of hematite occurs in stages, it is first converted to magnetite and at temperatures above 570 °C, wustite is formed [46]. At temperatures below 570 °C, magnetite is converted to iron directly [35] as wustite is not stable below 570 °C. Reduction reactions occurring inside the shaft furnace, with syngas as the reducing gas are depicted in Equations (1) and (2). Exothermic reduction of Hematite by CO [42,47]:

$$Fe_2O_3(s) + 3\,CO(g) \longrightarrow 2\,Fe(s) + 3\,CO_2(g). \quad (1)$$

Endothermic reduction of Hematite by H_2:

$$Fe_2O_3(s) + 3\,H_2(g) \longrightarrow 2\,Fe(s) + 3\,H_2O(g). \quad (2)$$

Natural gas is converted to a mixture of CO and H_2 using steam methane reforming (SMR). The reaction is endothermic and has a reaction enthalpy of 206 $kJmol^{-1}$ [48], as shown in Equation (3).

$$CH_4(g) + H_2O(g) \longrightarrow CO(g) + 3\,H_2(g). \quad (3)$$

Countries with large reserves of natural gas such as Saudi Arabia, Qatar, USA(shale gas) and Iran have deployed the technology for steel production [43]. The DRI produced from the shaft furnace can either be fed to an EAF as hot DRI or cooled and briquetted for transport. Addition of DRI in the EAF reduces the dependence on scrap and improves the quality of the steel produced [49–51].

Hydrogen Direct Reduction of Iron Ore

In the HDRI-EAF system, hydrogen is used as the reducing gas in a moving bed shaft furnace. The DRI is fed to an EAF for steel production. The reduction reactions are depicted in Equations (4)–(6) [52]. The reduction reaction is endothermic and energy in the form of heat needs to be supplied to carry the reaction forward [37]. The reaction propagation and the different processes involved in the reaction are depicted in Figure 1.

$$3\,Fe_2O_3(s) + H_2(g) \longrightarrow 2\,Fe_3O_4(s) + H_2O(g) \quad (4)$$

$$(1-x)\,Fe_3O_4(s) + (1-4x)\,H_2(g) \longrightarrow 3\,Fe_{1-x}O(s) + (1-4x)\,H_2O(g) \quad (5)$$

$$Fe_{1-x}O(s) + H_2(g) \longrightarrow (1-x)\,Fe(s) + H_2O(g). \quad (6)$$

As depicted in Figure 1, the chemical reaction occurs by adsorption of hydrogen gas on the iron oxide interface. At high temperatures, the rate of chemical reaction is higher than the transport rate or mass transfer rate of reactants and products. This observation is in accordance with the Arrhenius equation [37]. In a solid-gas reaction at high temperatures, diffusion of reactants and products is often the rate-limiting step. The porosity of the pellets is an important factor, as higher porosity of the raw material leads to higher permeability and diffusivity of the reactants and products. The size and geometry of the pellets and temperature of the inlet gas have a strong influence on the reaction rate. The reaction rate varies inversely with the size of the pellets [53]. The reaction rate is faster with hematite ore than magnetite ore as the porosity of intermediate reaction products formed by hematite is higher [54]. Addition of biomass in the iron ore pellets could increase the porosity of the pellets and reduce the apparent activation energy required for the reduction reaction [55]. Water vapor formed during the reduction of iron oxide has a lower adsorption and desorption rate than hydrogen. At lower temperatures, this could affect the rate of reaction. Experimental studies have shown that the rate of iron ore reduction reaction is higher with pure hydrogen than with traditionally used syngas (mixture of CO and H_2) [56] between 700–900 °C. Higher reduction rates could lead to a more compact design of the shaft furnace for the same DRI output, which could reduce capital costs and lower the heat losses from the shaft furnace, owing to a smaller surface area available for heat transfer. The addition of small amounts of CO in the reducing gas mixture can slow down the reduction reaction significantly, as CO reduces the diffusivity of the reducing gases [57]. By conducting experiments on hematite reduction with hydrogen at different temperatures, it was found that at temperatures higher than 900 °C, the reaction rate decreases because of sintering and formation of a dense outer layer on the iron ore pellets [46]. The values for apparent activation energy for the reduction reaction varies from 11 kJ mol^{-1} to 246 kJ mol^{-1}. The large variation in the values of apparent activation energies is due to its dependence on multiple factors. Thermo-physical properties of the input material, reducing gas composition, reduction temperature, particle size and the experimental set-up are some of the variables listed by [37]. There is a need for a more thorough investigation to evaluate the apparent activation energy required for iron ore reduction reaction with pure hydrogen.

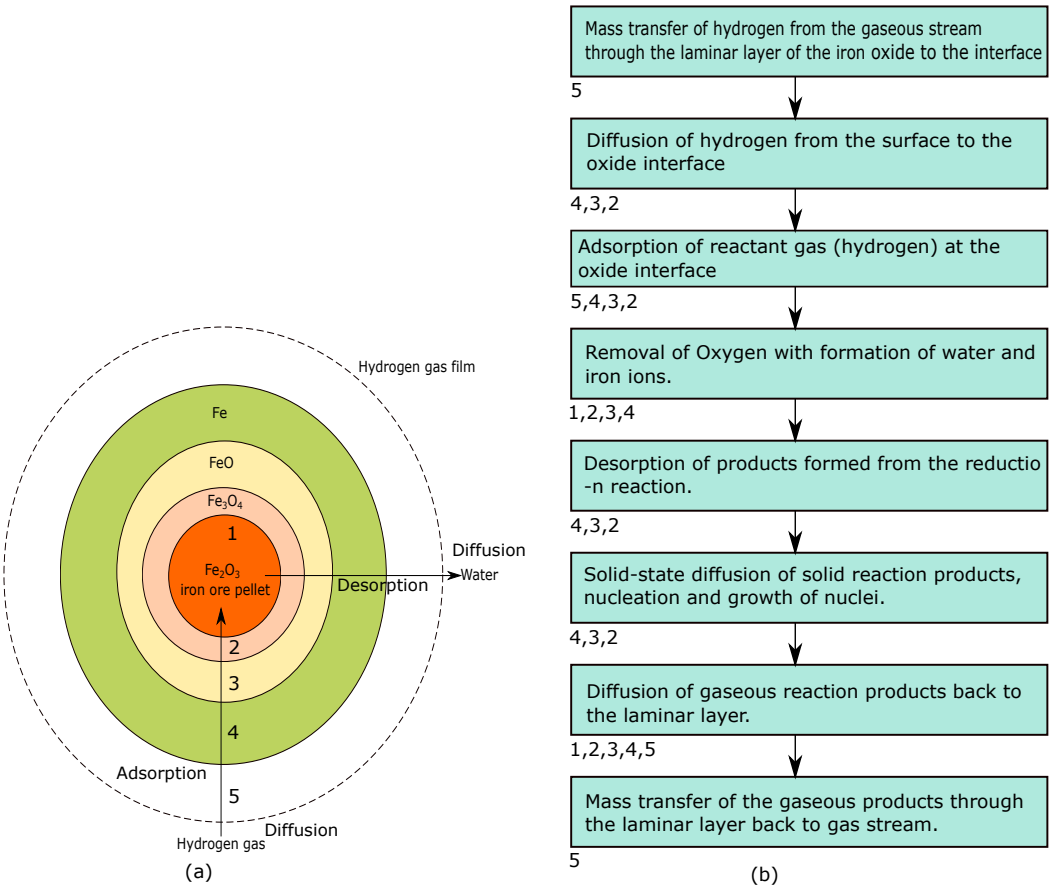

Figure 1. (**a**) Shrinking core model depicting the evolution of iron ore reduction reaction with hydrogen [56]. (**b**) Process steps in the reduction of iron ore pellets with hydrogen [37]. The location of the process steps is represented from numbers 1 to 5 (1b), which are also depicted in the shrinking core model (1a).

3. Methodology

The objective of this analysis is to improve the understanding of the impact of different process parameters on the energy and emission intensity of the steel production system. A new system configuration was modeled and analyzed in this work. The system configuration is shown in Figure 2. Other configurations with different technologies for hydrogen production, pellet pre-heating, adsorption of hydrogen from the waste gas stream etc. are also possible and should be explored. Energy consumption and emissions related to iron ore mining, pellet making and downstream steel finishing steps have not been considered in this model. Modeling assumptions are presented in Appendix A. The model has been developed using Python, which is open-source software. The codes were written in the Jupyter notebook [58] environment. NumPy [47] and Pandas [59] libraries have been used for calculations and data visualization. The graphs and bar charts have been plotted using matplotlib [60] library. All these libraries could be used with the standard anaconda [61] distribution. Python codes for the model in the form of a Jupyter notebook are available for download [36]. In the following section, mass and energy flows through the different components of HDRI-EAF system will be described.

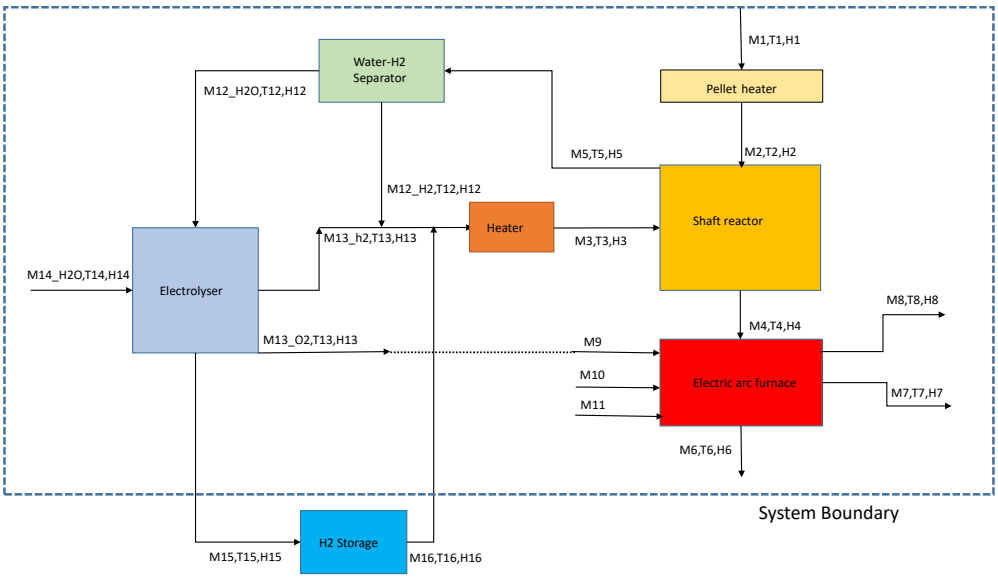

Figure 2. Schematic of the Hydrogen direct reduction shaft furnace coupled with an electric arc furnace. An electrolyzer is considered for hydrogen production.

3.1. Pellet Heating

It has been assumed that an electrical heating unit is used to heat iron ore pellets to 800 °C. Mass and energy flow through the electrical heating unit is depicted in Figure 3. The amount of iron ore required for producing one ton of steel was calculated using Equation (7). Equations (8) and (9) describe the mass and energy flow through the pellet electrical heating system.

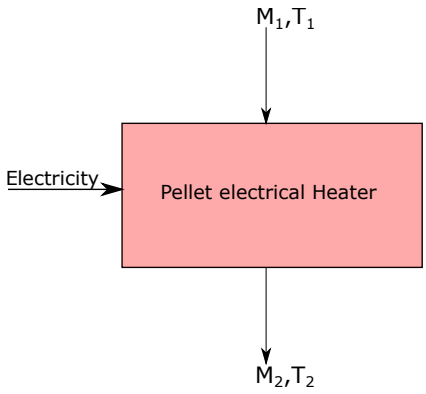

Figure 3. Mass and energy flows through the pellet heating unit.

$$M_1 = \frac{1}{(Fe_2O_{3pure} * FeO_{ratio})}. \tag{7}$$

Mass balance

$$M_1 = M_2. \tag{8}$$

Energy balance

$$M_1 * h_1 + EL_{pel\ heater} = M_2 * h_2 + \delta_{heat\ losses}, \tag{9}$$

3.2. Direct Reduction Shaft Furnace

The DRI shaft furnace is a counter-current solid-gas reactor, where pre-heated iron ore pellets at 800 °C are fed from the top to react with hydrogen stream entering from the bottom of the reactor. The reduction reaction is endothermic with a reaction enthalpy of 99.5 kJmol^{-1}. Iron ore particles need to be completely submerged in hydrogen for the optimal reaction rate. The ratio of actual flow rate of hydrogen to the stoichiometric flow rate of hydrogen required for the reduction reaction is represented by lambda λ [34]. The stoichiometric flow rate of hydrogen per ton of liquid steel is calculated by Equation (10). Actual mass flow of hydrogen in the reactor is the product of λ and stoichiometric quantity of hydrogen required to reduce 1 ton of hematite ore, as depicted in Equation (11). The mass and energy flow through the reactor are shown in Figure 4.

$$M_{H_2} = \frac{H_{2_{per\ mole}} * H_{2_{molecular\ weight}} * 10^3}{Fe_{molecular\ weight}} \tag{10}$$

$$M_3 = \lambda * M_{H_2}. \tag{11}$$

Metalization rate (α), is defined as the percentage of metallic iron (Fe) leaving the shaft furnace in the iron stream. DRI contains metallic iron along with FeO (wustite), which needs to be reduced inside the EAF. Metalization rate of 94% has been assumed for the base case. The amount of Fe, and FeO (Wustite) in the stream exiting the shaft furnace is calculated by using Equations (12) and (13). The mass balance of the shaft furnace is represented by Equation (16).

$$M_{4_{FeO}} = M_1 * Fe_2O_{3_{pure}} * FeO_{ratio} * (1 - \alpha) \tag{12}$$

$$M_{4_{Fe}} = 1000 - M_{4_{FeO}} \tag{13}$$

$$M_{4_{im}} = M_1 - (M_{4_{FeO}} + M_{4_{Fe}}). \tag{14}$$

It is assumed that the waste gas stream is a mixture of unreacted hydrogen and water/steam produced from the reduction reaction as shown in Equation (15). The amount of water produced depends on the metallization rate. For ease of calculations, it is assumed that metallization is complete. The amount of unused hydrogen in the waste stream depends on the amount of hydrogen entering the shaft furnace. A thorough understanding of the kinetics of the reaction and design of the shaft furnace is required to calculate the exact composition and temperature of the waste gas stream. Typically, the exhaust gases in a DRI shaft furnace exit the furnace at a temperature of 275 °C to 400 °C [42]. An exhaust gas temperature of 250 °C has been considered in the model to account for the endothermic reaction between hydrogen and iron ore.

$$M_5 = M_{5_{H_2}} + M_{5_{H_2O}}. \tag{15}$$

More energy is required for 100% hydrogen-based DRI production compared to reduction with syngas, as hydrogen reduction of iron ore is an endothermic reaction, whereas, reduction of iron ore with CO is an exothermic reaction. Energy in the form of heat is lost to the environment due to heat transfer from the shaft furnace walls. The energy flows through the reactor represented by Equation (17).

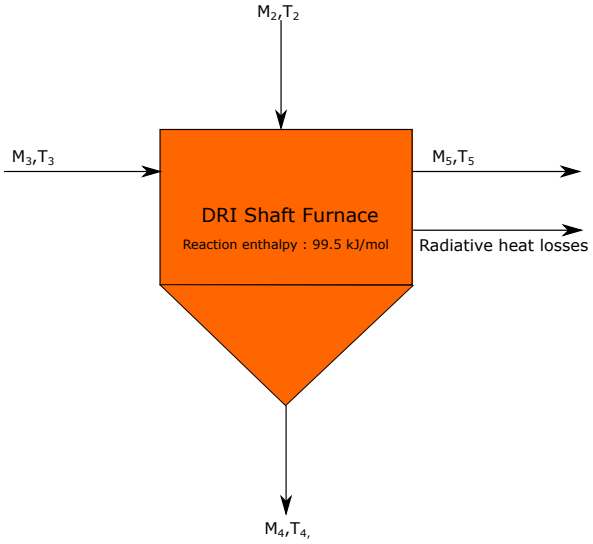

Figure 4. Mass and energy flow through the DRI shaft furnace.

Mass balance

$$M_3 + M_2 = M_4 + M_5. \tag{16}$$

Energy balance

$$M_2 * h_2 + M_3 * h_3 = M_4 * h_4 + M_5 * h_5 + H_{reaction} + \delta_{heat\ losses}. \tag{17}$$

3.3. Electric Arc Furnace

It is assumed that DRI with a metallic content of 94% enters the EAF at a temperature of 700 °C. The EAF is operated with 100% hot DRI. EAF temperature is assumed to be 1650 °C to ensure complete melting of metallic iron. The efficiency of the electric arc furnace, β_{el}, is assumed to be 0.6 to account for losses in the transformer, rectifier, electrodes and other sub-systems [51]. Carbon is added in the EAF for CO production. Oxygen, produced in the water electrolyzer could be added in the EAF for the production of CO to reduce the FeO in the EAF. It is assumed that 70% of the FeO entering the EAF is reduced and the rest is removed as slag. The dissolution of carbon in molten metal is an endothermic reaction and 3.59 KWh/kg of energy is used in the process. Exhaust gas stream from the EAF is assumed to be a mixture of CO and CO_2. Additional elements are added in the molten iron to improve its thermo-physical properties. They have not been considered in this analysis. Mass and energy flow through the EAF are shown in Figure 5. The mass and energy flow through the EAF are shown in Equations (18) and (19).

Mass balance

$$M_4 + M_9 + M_{10} + M_{11} = M_6 + M_8 + M_7. \tag{18}$$

Energy balance

$$M_4 * h_4 + \beta_{el} * EL_{EAF} = M_6 * h_6 + M_8 * h_8 + M_7 * h_7 + \delta_{heat\ losses} \tag{19}$$

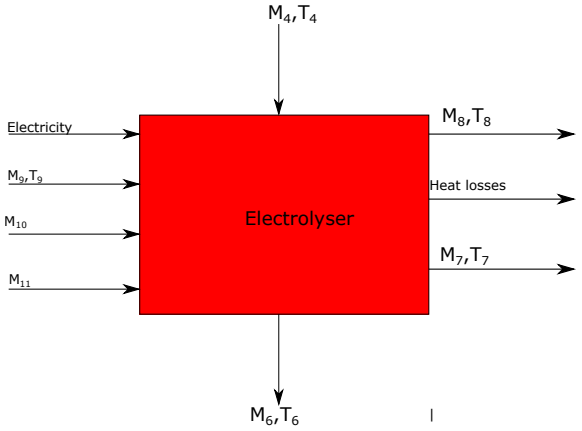

Figure 5. Mass and energy flow through the electric arc furnace.

3.4. Electrolyzer

Alkaline or PEM electrolyzers could be used in the system configuration presented in the model for hydrogen production. An alkaline electrolyzer has been considered in the present model owing to the lower capital cost of alkaline electrolysers [62] and their use in HYBRIT project [63] for a pilot project on hydrogen-based direct reduction of iron ore in Sweden. Technical specifications of the electrolyzer have been taken from 20 MW electric alkaline electrolyzer module produced by Thyssenkrupp industries [64]. Excess hydrogen produced during off-peak hours could be fed into the pressurized hydrogen storage tank. Dynamic operation of the electrolyzer has not been considered in the model. Electricity from the grid or from a dedicated renewable energy generation system could be utilized in the electrolyzer [65]. Mass and energy flow through the electrolyzer is presented in Figure 6.

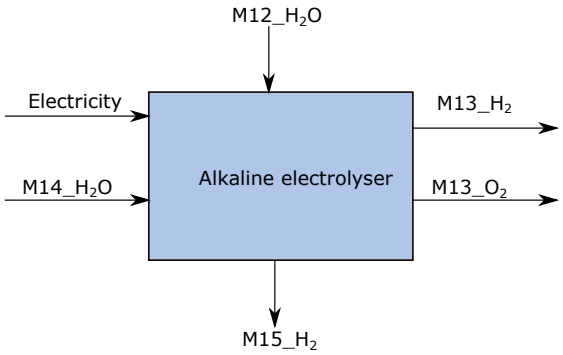

Figure 6. Mass and energy flow through the electrolyzer.

Mass balance

$$M_{12_{H_20}} + M_{14_{H_20}} = M_{13_{H_2}} + M_{15_{H_2}} + M_{13_{O_2}} \quad (20)$$

$$M_{13} = M_{13_{H_2}} + M_{13_{O_2}}. \quad (21)$$

Energy balance

Energy consumption of the electrolyzer (EL_spec) is assumed to be 45 KWh/kgH_2. In practice, efficiency of the electrolyzer varies with current density and hydrogen output. For a more detailed analysis of the operations and energy balance of the electrolsyer, readers could refer to [65–67].

$$EL_{elec} = (M_{13_{H_2}} + M_{15_{H_2}}) * EL_{spec}. \quad (22)$$

3.5. Waste Gas Separation Unit

Unreacted hydrogen is separated from the waste gas stream using a pressure swing adsorber [68,69]. Mass and energy flows through the pressure swing adsorber are shown in Figure 7. Pressure swing adsorbers have been used for industrial production of hydrogen in ammonia plants [70,71]. The temperature of the incoming waste gas stream was assumed to be 250 °C. Water separated from the waste stream is fed back to the electrolyzer. The energy required to run the pressure swing adsorber has not been considered in this model. It has been assumed that the water and hydrogen stream are free of impurities.

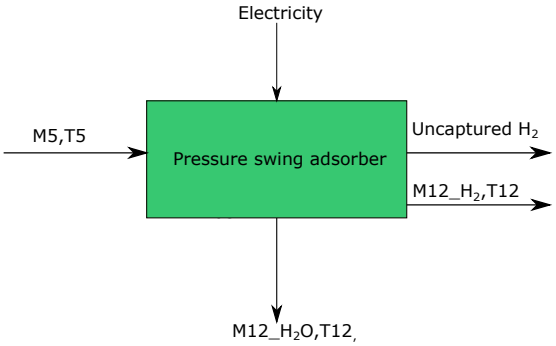

Figure 7. Mass and energy flow through the waste gas separation unit.

Mass balance

$$M_{5_{H_2}} + M_{5_{H_2O}} = M_{12_{H_2}} + M_{12_{H_2O}} + \delta_{H_2}. \tag{23}$$

Energy balance

$$M_5 * h_5 + El_{separator} = M_{12_{H_2}} * h_{12_{H_2}} + M_{12_{H_2O}} * h_{12_{H_2O}} + \delta_{heat\ losses} + \gamma_{H_2}. \tag{24}$$

3.6. Electric Heater for Hydrogen Stream

Electrical heater, with an efficiency of 0.6 has been considered for heating the hydrogen gas stream entering the shaft furnace to a temperature of 500 °C. Hydrogen gas stream entering the electrical heater is a mixture of hydrogen coming from the electrolyser at 90 °C and hydrogen separated in the pressure swing adsorbers at 250 °C. The mass and energy flow of the electrical heating unit is shown in Figure 8.

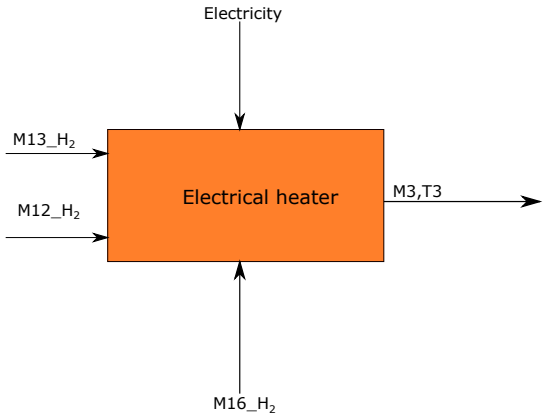

Figure 8. Mass and energy balance through the electrical heating unit for hydrogen stream.

Mass balance

$$M_3 = M_{13_{H_2}} + M_{12_{H_2}} \tag{25}$$

Energy balance

$$M_{12_{H_2}} * h_{12_{H_2}} + M_{13_{H_2}} * h_{13_{H_2}} + EL_{heating} = M_3 * h_3 + \delta_{heat\ losses} \tag{26}$$

4. Results and Discussions

The modeling results are presented in this section. It has been assumed that the ore contains five percent impurities and the metallization rate of 0.94 is achieved in the DRI shaft furnace in the base case [34]. Modeling results have been compared with the energy consumption and emission values reported in the literature for the HDRI-EAF system.

4.1. Mass and Energy Flow

Mass and energy flow through the different components of the HDRI-EAF system are presented in Table 1. Hydrogen entering the shaft furnace was considered to be 1.5 times the stoichiometric value ($\lambda = 1.5$). Exhaust stream from the EAF, M_8, comprising of CO_2 and CO was not calculated as the composition and temperature are dependent on the operation of the EAF. Carbon, M_{10}, was added to the system at a fixed rate of 10 kg/tls. It was assumed that 50 kg/tls of Lime and MgO, M_{11}, is added to the EAF. Oxygen, M_9, was added in the EAF for production of CO. Hydrogen flow from the storage, M_{15} and M_{16}, was not considered in the model.

Table 1. Mass and energy flow through the DRI-EAF system. N.A refers to not available or not calculated.

Stream	Mass Flow (ton/tls)	Temperature (°C)	Energy (KWh)	Short Description	Process Step
M_1	1.599	25	N.A	Iron ore pellets	Pellet heater
M_2	1.599	800	370.78	Heated iron ore pellets	Pellet heater
M_3	0.0812	500	155.59	H_2 entering the shaft furnace	Shaft furnace
M_4	1.063	700	107.498	Metallic stream exiting the shaft furnace	Shaft furnace
$M_{5_{H_2}}$	0.027	250	24.45	H_2 from waste stream	Shaft furnace
$M_{5_{H_2O}}$	0.483	250	82.18	H_2O from Waste stream	Shaft furnace
M_6	1	1650	239.15	Molten steel exiting the EAF	EAF
M_7	0.149	1650	54.25	Slag exiting the EAF	EAF
$M_{12_{H_2}}$	0.021	250	5.613	H_2 exiting the adsorber	Adsorber
$M_{12_{H_2O}}$	0.483	90	N.A	H_2O exiting the adsorber	Adsorber
$M_{13_{H_2}}$	0.059	90	53.80	H_2 from electrolyzer	Electrolyzer
M_{14}	0.171	25	N.A	H_2O entering the electrolyzer	Electrolyzer

4.2. Electricity Consumption

Variation of electricity consumption with a change in the mass flow of hydrogen is shown in Figure 9. Total energy consumption varied from 3.4 to 5.91 MWh/tls, as λ is varied from one to five. Specific energy consumption (SEC) of the HDRI-EAF system at 3.72 MWh/tls ($\lambda = 1.5$) system was higher than the BF-BOF based steel production, which has an SEC of 3.48 MWh. All the energy in the HDRI-EAF system was consumed in the form of electricity. Electricity is required for pellet heating, hydrogen production, heating the hydrogen stream entering the shaft furnace and melting of iron in the electric arc furnace. Switching from BF-BOF to HDRI-EAF based steel production would lead to an additional electricity demand of 375 TWh in the EU. It was observed that increasing the mass flow of hydrogen in the DRI shaft furnace, increases energy consumption in the electrolyzer and in the electric heater for hydrogen heating.

Approximately, 436 KWh/tls of electricity was used for heating the iron ore pellets to the reaction temperature of 800 °C. Waste gases exiting the DRI shaft furnace could be used for pre-heating the iron ore pellets. Endothermic reduction reaction of iron oxide with hydrogen requires 334 KWh of energy. Pre-heating the hydrogen stream entering the shaft furnace requires 160 KWh of electricity.

The electrolyzer consumed 2680 KWh of electricity, which was approximately 70% of the total energy consumed in the HDRI-EAF system. The performance of electrolyzer and mass flow of hydrogen has a significant impact on the overall energy consumption of the system. As stated in Section 2, the type of raw material, temperature of the reduction reaction and design of the reactor have an impact on the mass flow of hydrogen for optimal reaction rate. In order to reduce the energy consumption, design of the reactor and the operating conditions could be optimized for a lowering the λ value. EAF consumes 445 KWh/tls of electrical energy. EAF energy consumption increases at lower metallization rates. If the amount of impurities in the iron ore pellet increased, a similar trend in energy consumption of the EAF could be observed. The value of EAF energy consumption decreases at higher DRI temperatures.

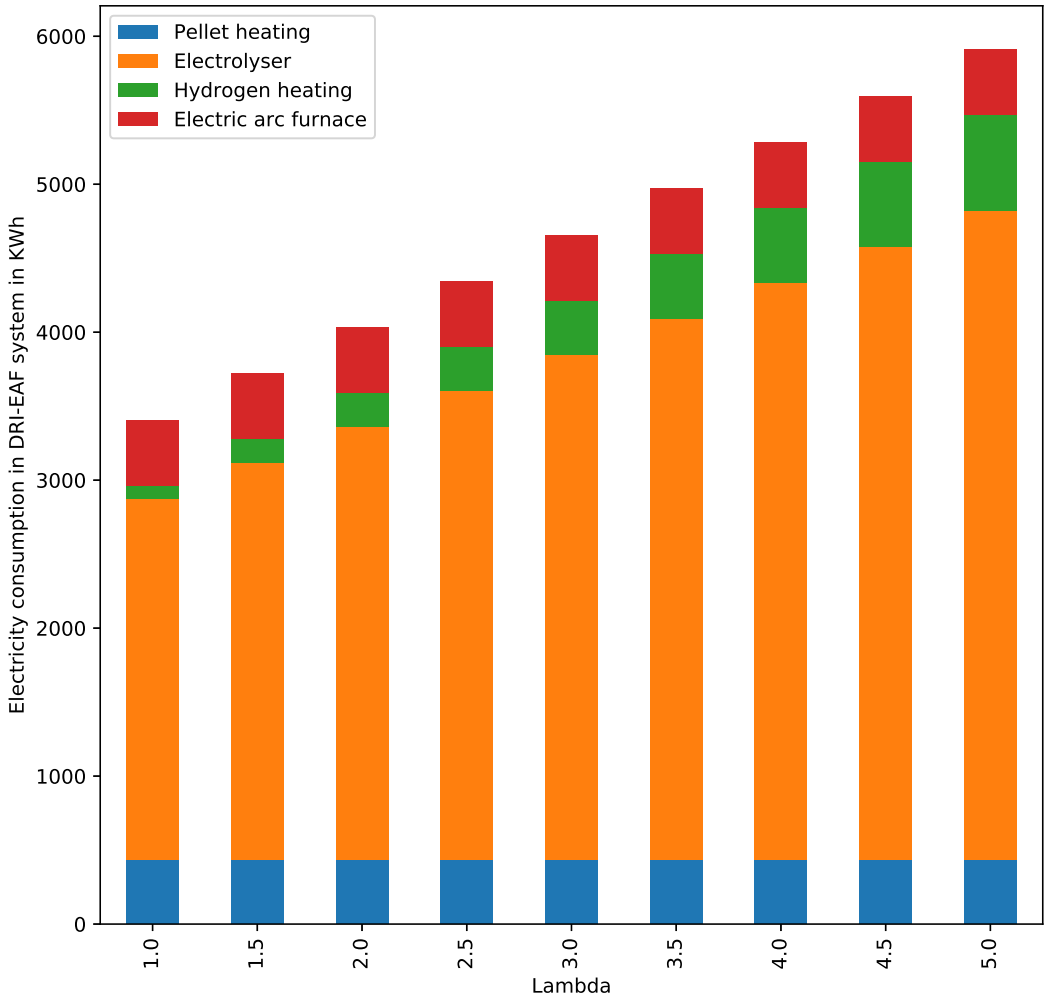

Figure 9. Variation of electricity demand (in KWh) in DRI-EAF system with varying mass flow rate of hydrogen in the DRI shaft furnace.

Waste Gas Enthalpy

The enthalpy of waste gas exiting the shaft furnace varies with temperature and flow rate of incoming hydrogen stream, as shown in Figure 10. Although majority of the outgoing energy could be captured by mixing the incoming hydrogen stream with the waste gas hydrogen stream, an optimal design of the shaft furnace and operating conditions would ensure lower losses through the waste stream.

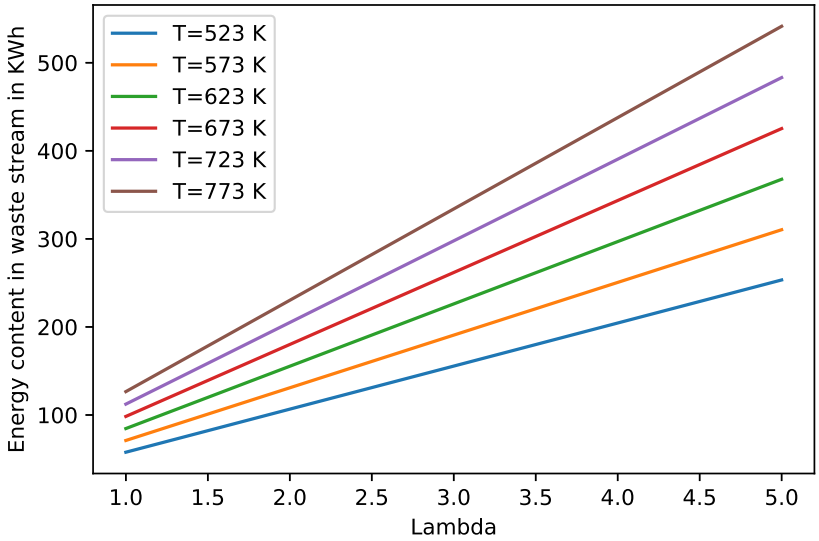

Figure 10. Waste gas enthalpy variation with temperature and mass flow rate of input hydrogen.

4.3. Emissions from the HDRI-EAF System

Emissions are directly related to the amount of electricity used in the HDRI-EAF system. A small amount of emission is also produced in the EAF, as a result of the reduction of wustite with carbon and from the oxidation of carbon to CO and to CO_2 subsequently. These emissions were not considered. The emission intensity of the system varies with the grid emission factor of the countries, as shown in Figure 11.

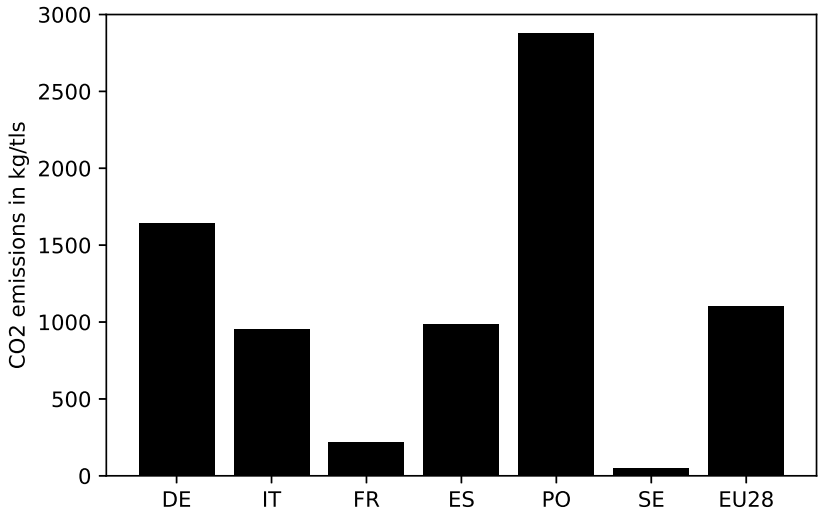

Figure 11. CO_2 emission variation with countries in kgCO2/tls.

Emission intensity of BF-BOF process is 1688 $kgCO_2$/tls in the EU [72], which is much higher than the HDRI-EAF's emission intensity of 1101 $kgCO_2$/tls (at EU's grid emission factor of 295 kgC_2/MWh). Modeling results show that the emissions from the production of steel in the HDRI-EAF system would be lower in most EU countries at present grid emission levels, except Poland. The grid emission factor of Poland is 773 gCO_2/KWh, which is more than twice the EU average of 295 gCO_2/KWh. The emission intensity of HDRI-EAF based steel production could be reduced to 415 $kgCO_2$/tls in countries with low grid emission factors like Sweden. If electricity is provided from renewable energy sources then it would result in a reduction of 170.26 $MtCO_2$ annually. The use of HDRI-EAF based steel production could increase the emissions from steel production in countries with a grid emission factor higher than 456 gCO_2/KWh.

4.4. Comparison with Literature Values

Specific energy consumption (SEC) and emission for production of 1 ton of liquid steel have been compared with the results available in the literature, shown in Figure 12. The grid emission factor of the German electricity grid has been considered for emission calculations, which is 440.9 gCO_2/KWh. Emission values were not reported by Vogl et al. [34] and Fischedick et al. [7], emissions associated with the use of electricity from the German electric grid have been considered for comparison. The mass flow rate of hydrogen was not specified by Otto et al. [32] and Fischedick et al. [7], the λ value of 1.5 was assumed as specified by Vogl et al. [34]. SEC of 3.72 MWh, corresponding to λ value of 1.5 has been considered for the comparison.

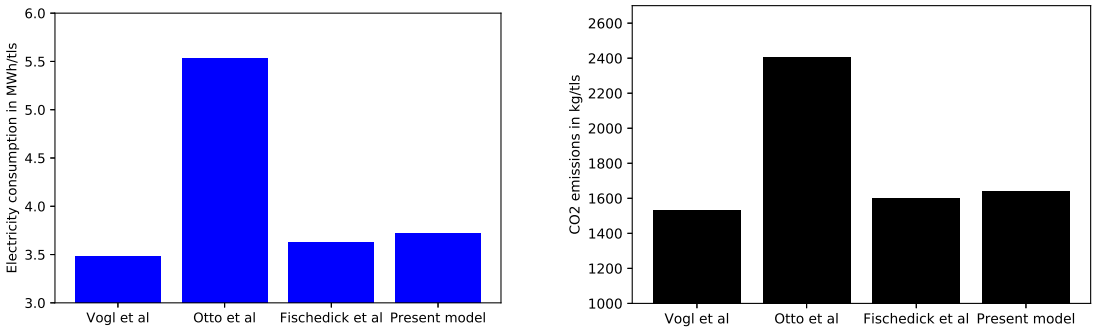

Figure 12. (**a**) Comparison of energy demand for hydrogen direct reduction of iron ore with literature values. (**b**) Comparison of CO_2 emission from hydrogen direct reduction of iron ore with literature values.

The difference in the SEC and emission intensity could stem from the different system configurations considered. Otto et al. [32] have considered the Circored process, which uses a fluidized bed reactor instead of a shaft furnace. The use of natural gas for pellet heating and other process steps increases the energy and emission intensity in the circored process. Electric energy has been considered for pre-heating the pellets and incoming hydrogen stream, instead of a waste heat utilization unit as described by Vogl et al. [34]. It has been assumed that 80% of the hydrogen gas available in the waste stream will be adsorbed, and the remaining 20% will be generated in the electrolyzer.

4.5. Energy Consumption and Emissions in EU Countries

The impact of transitioning to HDRI-EAF based primary steel production on energy demand and emissions in different EU countries has been evaluated in this section. Steel production data has been taken from the integrated database of the European energy sector(IDEES) [72]. The reference year for the steel production data is 2015. Additional energy consumption and emissions arising from pellet making, sintering, and steel finishing processes have also been considered in this analysis. The results are presented in Figure 13. The energy requirement for steel production could increase from 493 TWh to 517 TWh for EU-28 by switching to HDRI-EAF based steel production. At the same time, emissions from steel production could be reduced from 193 million tonnes of CO_2/year to approximately 134 million tonnes of CO_2/year. Considering the price of carbon to be 30 €/ton of CO_2 in the EU, it is estimated that HDRI-EAF based steel production could lead to a saving of 18 €/ton of steel, at present grid emission levels in the EU. The savings could be much higher in the future with increasing CO_2 prices and a reduction in the grid emission factor.

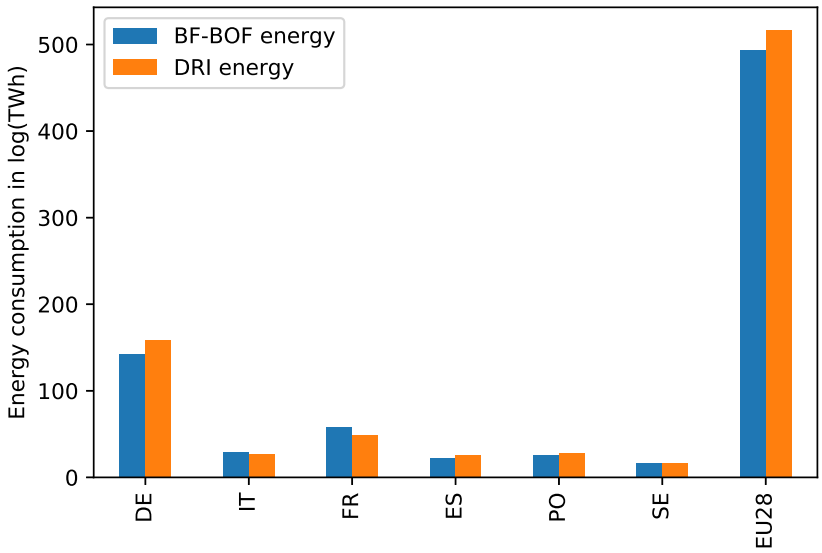

(**a**)

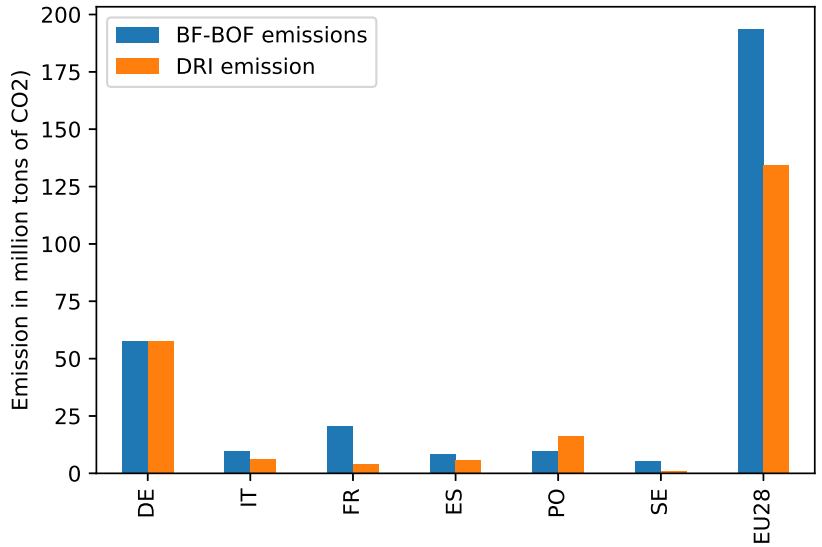

(**b**)

Figure 13. (**a**) Comparison of present energy demand from primary steel production in EU countries and projected energy demand for conversion to hydrogen direct reduction of iron ore (HDRI)-EAF based steel production. (**b**) Comparison of present emissions from primary steel production in EU countries and projected emissions for complete conversion to HDRI-EAF based steel production.

4.6. Sensitivity Analysis

Local sensitivity analysis [73] was carried out by varying the input parameters by ±5 %, ±10 %, ±15 %, ±20 % one-at-a-time and keeping other parameters fixed. The parameters considered for the sensitivity analysis are hydrogen mass flow rate (λ), electrolyzer efficiency, hydrogen input temperature(T3), EAF input temperature (T4), adsorber efficiency and the grid emission factor. The results of the sensitivity analysis are presented in Figure 14.

Sensitivity analysis revealed that electrolyzer output affects the electricity consumption of the EAF-DRI system. Electrolyzer output is an indicator of the electrolyzer efficiency in terms of the amount of electricity required for the production of one kg of hydrogen (KWh/kgH_2). Another important parameter affecting the electricity consumption is λ, which is a ratio of the actual hydrogen required for production of one ton of liquid steel to the stoichiometric requirement of hydrogen. The

value of λ is related to the design of the shaft furnace reactor and operating conditions. Electricity requirement of the system decreases as the adsorption efficiency increases in the pressure swing adsorption system. Emissions from the system are strongly correlated with the grid emission factor. Electrolyzer output, lambda and the adsorption factor are important factors, which decide the overall emissions from the system, as they are directly related to the electricity consumption of the HDRI-EAF system. Hydrogen input temperature (T3) and the EAF input temperature (T4) do not have a major impact on the energy requirement and emissions from the HDRI-EAF system.

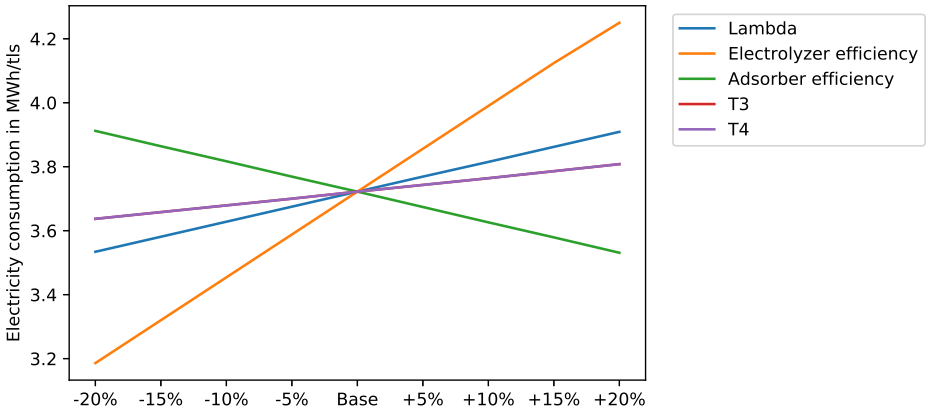

(**a**)

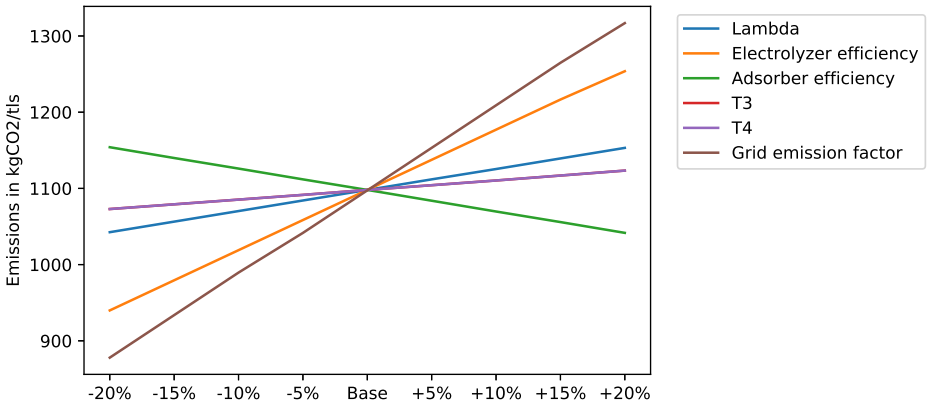

(**b**)

Figure 14. (**a**) Sensitivity analysis to identify the parameters affecting the electricity requirements of the HDRI-EAF system. (**b**) Sensitivity analysis to identify the most important parameters affecting the CO_2 emission from the HDRI-EAF system.

5. Conclusions

HDRI-EAF based steel production is a viable alternative to BF-BOF based steel production, but adoption of the technology would depend on the future cost of electrolyzers and electricity. Sensitivity analysis revealed that electrolyzer efficiency is the most important factor affecting the system energy consumption, while the grid emission factor is strongly correlated with the overall system emissions. Recent improvements in the performance of electrolyzers could reduce the energy consumption and emissions from the HDRI-EAF based steel production. The iron and steel industry could play a major role in the transition to the hydrogen economy by creating a demand for large quantities of hydrogen, which could lead to the development of infrastructure for generation, storage, and safe transport of hydrogen. The use of hydrogen in steel making coupled with hydrogen storage could provide flexibility to the electricity grid to integrate intermittent renewable energy sources and open new

opportunities for revenue generation for steel companies by participating in the power reserve markets. Other strategies for flexible operation of the HDRI-EAF system could be explored by storing the DRI and operating the EAF according to electricity prices. Dynamic modeling of the HDRI-EAF system could quantify the potential of the steel industry to participate in the demand response market.

6. Future Work

In the future works, the techno-economical performance of DRI-EAF based system coupled with different hydrogen production technologies will be compared under different scenarios. The price of electricity and carbon costs would be varied to see their impact on the cost of steel production. The impact of using grid electricity on the costs and performance of the system would be compared with using dedicated renewable energy generators. Different hydrogen production technologies with varying system configurations like solid oxide electrolysis, methane pyrolysis and steam methane reforming with CCS would be considered for the production of hydrogen. Large scale generation and storage of hydrogen for steel production could have a substantial impact on other sectors of the energy system like energy generation, transport, buildings etc. The integration of HDRI-EAF based steel production in an energy system model could highlight these interactions, which could assist policy-makers to make more informed decisions.

Author Contributions: All authors have contributed equally in the work. All authors have read and agreed to the published version of the manuscript.

Funding: This project has received funding from the European Unions Horizon 2020 research and innovation programme under the Marie Skłodowska–Curie grant agreement No 765515.

Conflicts of Interest: The authors declare no conflict of interest.

Abbreviations

The following abbreviations and symbols are used in this manuscript:

Abbreviations	
DRI	Direct reduced iron
HDRI	Hydrogen direct reduced iron
EAF	Electric arc furnace
BF-BOF	Blast furnace basic oxygen furnace
SMR	Steam methane reforming
BASF	Badische Anilin und Soda Fabrik
SSAB	Svenskt Stål AB
LKAB	Luossavaara-Kiirunavaara Aktiebolag
MMBTU	Metric Million British Thermal Unit
SEC	Specific energy consumption
TLS	Ton of liquid steel
$kgCO_2$	Kilogram of carbon dioxide
$GtCO_2$	Gigaton of carbon dioxide
kg	kilogram
kJ	KiloJoule
KWh	Kilowatthour
MWh	Megawatthour
$	US Dollar
€	Euro

Symbols

M_1	Mass of iron ore at heater inlet for production of 1 ton of liquid steel in kg/tls
M_2	Mass of iron ore at heater outlet for production of 1 ton of liquid steel in kg/tls
$Fe_2O_{3\,pure}$	Percentage of pure iron ore in the iron ore stream (assumed to be 0.95)
FeO_{ratio}	Ratio of molecular weight of iron contained in iron oxide (0.7)
$EL_{pel\ heater}$	Electrical energy required for heating the pellets in kJ
h_1	Specific enthalpy of iron ore at ambient temperature in kJ/kg
h_2	Specific enthalpy of iron ore at reactor temperature in kJ/kg
η_{el}	Efficiency of the electrical heater
M_{H_2}	Stoichiometric mass flow of hydrogen in kg/tls
$H_{2_{per\ mole}}$	1.5 Moles of hydrogen required for production of one mole of iron
$H_{2_{molecular\ weight}}$	2.015 g/mol
$Fe_{molecular\ weight}$	55.845 g/mol
$M_{4_{FeO}}$	Mass of FeO exiting the shaft furnace in kg/tls
M_{4Fe}	Mass of Fe exiting the shaft furnace in kg/tls
$M_{4_{im}}$	Mass of impurities exiting the shaft furnace
α	Metallization rate
M_5	Mass flow of exhaust gases from the shaft furnace in kg/tls
$M_{5_{H_2}}$	Mass of unused hydrogen as exhaust from the DRI shaft furnace in kg/tls
$M_{5_{H_2O}}$	Mass of water/steam produced as exhaust from the DRI shaft furnace in kg/tls
h_3	Specific enthalpy of hydrogen entering the shaft furnace in kJ/kg
h_4	Specific enthalpy of metallic stream exiting the shaft furnace in kJ/kg
h_5	Specific enthalpy of DRI exhaust gases in kJ/kg
$h_{5_{H_2}}$	Enthalpy of unreacted hydrogen from the DRI shaft furnace in kJ/kg
$h_{5_{H_2O}}$	Enthalpy of water/steam from the DRI shaft furnace in kJ/kg
$H_{reaction}$	Reaction enthalpy of the reduction reaction in kJ/kg
δ	Heat losses
M_6	Mass of molten metal from the EAF in Tons
h_6	Specific enthalpy of molten metal exiting the EAF in kJ/kg
M_7	Mass of scrap from the scrap in kg/tls
h_7	Specific enthalpy of scrap exiting the EAF in kJ/kg
M_8	Mass of exhaust gases exiting the EAF in kg/tls
h_8	Specific enthalpy of exhaust gases exiting the EAF in kJ/kg
M_9	Mass of oxygen entering the EAF in kg/tls
M_{10}	Mass of carbon added in the EAF in kg/tls
M_{11}	Mass of lime and dolomite added in the EAF in kg/tls
β_{el}	Efficiency of the EAF for conversion from electricity to heat
EL_{EAF}	Electricity supplied to the EAF in KWh/tls
M_{12H_20}	Mass of water entering the electrolyzer from the waste gas separation unit in kg
M_{12H_2}	Mass of hydrogen entering the electric heater in kg
h_{12H_2}	Enthalpy of hydrogen entering the electrolyzer from the waste gas separation unit in kg
M_{14H_20}	Mass of water supplied to electrolyzer externally in kg
M_{13H_2}	Mass of hydrogen produced in the electrolyzer and supplied to the DRI shaft furnace in kg
h_{13H_2}	Enthalpy of hydrogen produced in the electrolyzer and supplied to the DRI shaft furnace in kg
M_{15H_2}	Mass of hydrogen produced in the electrolyzer and supplied to the hydrogen storage in kg
M_{13O_2}	Mass of oxygen produced in the electrolyzer in kg
EL_{spec}	Specific energy consumption of the electrolyzer in KWh kg^{-1}
EL_{elec}	Electricity consumption in the electrolyzer in KWh
γ_{H_2}	Uncaptured hydrogen exiting the pressure swing adsorber
$EL_{heating}$	Electricity consumed for heating the hydrogen stream in KWh/tls

Appendix A

Some of the important assumptions made for the model are listed below:

1. All calculations are done for the production of 1 ton of liquid steel from the system.
2. Energy consumption and emissions related to iron ore mining, pellet making, and downstream steel finishing steps were not considered in this analysis.
3. 5% impurities are present in the raw materials. The assumption is consistent with the plant data available in the literature. The primary components of the impurities are silica and alumina.
4. The iron ore pellets are heated from ambient temperature to 800 °C, through an electrical heater of efficiency, $\eta_{thermal} = 0.85$.
5. Output from the shaft furnace would be metallic Fe and FeO. The remaining FeO will be reduced to pure iron in the electric arc furnace. Although, in practice, some amount of FeO does not get reduced and becomes a part of the EAF slag.
6. The flow rate of hydrogen is considered to be higher than the stoichiometric requirements.
7. Apparent activation energy of 35 kJ/mole has been considered in this model.
8. Hydrogen produced from electrolyzers is heated in an electrical heater with an efficiency of $\eta_{thermal} = 0.6$.
9. DRI stream exiting the shaft furnace is considered to be at a temperature of 800 °C.
10. The exhaust gas stream is assumed to be composed of hydrogen and water. The waste stream enthalpy varies with exhaust gas temperature and λ_{h2}.
11. Energy required to separate hydrogen and water from the waste stream is not considered in the present calculations.
12. 100% DRI is fed into the furnace without any scrap. The quality of scrap has a significant effect on energy consumption in a DRI.
13. Hot DRI is fed into the DRI at 700 °C as it saves a considerable amount of electrical energy in the EAF.
14. Natural gas is not used for heating the material as its the general practice to use natural gas with scrap for initial heating.
15. As DRI is reduced only with Hydrogen, it is assumed that it does not contain any ferric carbide. Carbon required for reduction of remaining FeO in the EAF is supplied externally as coal or coke.
16. Temperature of the DRI being fed into the EAF is not taken into account into empirical energy models [74]. Thermodynamic modeling of the EAF has been done to get the specific energy consumption of the EAF with 100% DRI.
17. Iron ore pellets generally contain elements such as silicon, manganese, chromium, aluminium, sulphur, phosphorus, molybdenum etc. They get oxidized inside the electric arc furnace, releasing heat and assist in the melting of the iron ore. As iron ore pellets containing only alumina and silica have been considered in this model, additional energy supplied from the oxidation of these elements has not been considered, but a provision for their inclusion in future work has been made in the code.
18. Carbon is added into the EAF to reduce the remaining FeO in the mix and also to generate CO for froth formation, which is essential for the operation of the EAF and to extend the life of the graphite electrodes and the refractory.
19. CaO and MgO are added in the EAF as slag formers to maintain the basicity of the EAF. The weights of CaO and MgO used are according to data published in the literature [51].
20. Efficiency parameters used in the EAF model for electrical and chemical energy are according to the reference [51].

References

1. Arens, M.; Worrell, E.; Eichhammer, W.; Hasanbeigi, A.; Zhang, Q. Pathways to a low-carbon iron and steel industry in the medium-term—The case of Germany. *J. Clean. Prod.* **2017**, *163*, 84–98. [CrossRef]
2. UNFCCC's Technology Executive Commitee; UNFCCC. *Industrial Energy and Material Efficiency in Emission-Intensive Sectors*; Technical report, United nations framework convention for climate change; UNFCCC's Technology Executive Commitee: Copenhagen, Denmark, 2017. Available online: https://bit.ly/332v3jl (accessed on 5 January 2020).
3. World Steel Association Statistics. 2017. Available online: https://www.worldsteel.org/internet-2017/steel-by-topic/statistics/steel-data-viewer/P1{_}crude{_}steel{_}total/CHN/IND/WORLD{_}ALL/JPN/DEU (accessed on 13 November 2019).
4. Arcelor Mittal: Climate Action Report. Available online: https://corporate.arcelormittal.com/sustainability/arcelormittal-climate-action-report?frommobile=true (accessed on 8 September 2019).
5. Bataille, C.; Åhman, M.; Neuhoff, K.; Nilsson, L.J.; Fischedick, M.; Lechtenböhmer, S.; Solano-Rodriquez, B.; Denis-Ryan, A.; Stiebert, S.; Waisman, H.; et al. A review of technology and policy deep decarbonization pathway options for making energy-intensive industry production consistent with the Paris Agreement. *J. Clean. Prod.* **2018**, *187*, 960–973. [CrossRef]
6. Åhman, M.; Nilsson, L.J.; Johansson, B. Global climate policy and deep decarbonization of energy-intensive industries. *Clim. Policy* **2017**, *17*. [CrossRef]
7. Fischedick, M.; Marzinkowski, J.; Winzer, P.; Weigel, M. Techno-economic evaluation of innovative steel production technologies. *J. Clean. Prod.* **2014**, *84*, 563–580. [CrossRef]
8. Sarkar, S.; Bhattacharya, R.; Roy, G.G.; Sen, P.K. Modeling MIDREX Based Process Configurations for Energy and Emission Analysis. *Steel Res. Int.* **2018**, *89*, 1700248. [CrossRef]
9. Pardo, N.; Moya, J.A.; Vatopoulos, K. *Prospective Scenarios on Energy Efficiency and CO_2 Emissions in the EU Iron & Steel Industry*; Technical Report LD-NA-25543-EN-C; Joint Research Council, European Union: Luxemburg City, Luxemburg, 2012. [CrossRef]
10. Wiencke, J.; Lavelaine, H.; Panteix, P.J.; Petitjean, C.; Rapin, C. Electrolysis of iron in a molten oxide electrolyte. *J. Appl. Electrochem.* **2018**, *48*, 115–126. [CrossRef]
11. Stel, J.V.D.; Hattink, M.; Sert, D.; Zagaria, M.; Eklund, N.; Pettersson, M.; Sundqvist, L.; Mefos, B.S.; Feilmayr, C.; Kinnunen, K.; et al. Developments of the ULCOS Low CO_2 Blast Furnace Process at the LKAB Experimental BF in Luleå Abstract Key Words History of Recycling of Blast Furnace Top Gas. In Proceedings of the 1st International Conference on Energy Efficiency and CO_2 Reduction in the Steel Industry, Dusseldorf, Germany, 1 July 2011; pp. 1–8.
12. IEA. *Technology Roadmap Carbon Capture and Storage in Industrial Applications*; IEA: Paris, France, 2011; p. 43.
13. Hydrogen Future Fuel Cell and Hydrogen Joint Undertaking. Technical Report June. 2019. Available online: https://www.fch.europa.eu/sites/default/files/Hydrogen%20Roadmap%20Europe_Report.pdf (accessed on 5 January 2020).
14. The Future of Hydrogen: Seizing Today's Opportunities. Technical Report June. 2019. Available online: https://webstore.iea.org/the-future-of-hydrogen (accessed on 5 January 2020).
15. Hydrogen for Australia's Future. Technical Report August, Austrlian Government Chief Scientist. 2018. Available online: https://bit.ly/2O0ASJA (accessed on 5 January 2020).
16. Philibert, C. *Renewable Energy for Industry From Green Energy to Green Materials and Fuels*; Technical report; International Energy Agency: Paris, France, 2017. Available online: https://webstore.iea.org/search?q=renewable+energy+for (accessed on 5 January 2020).
17. Nuber, D.; Eichberger, H.; Rollinger, B. Circored fine ore direct reduction. *Millenium Steel* **2006**, *2006*, 37–40.
18. Elmquist, S.A.; Weber, P.; Eichberger, H. Operational results of the Circored fine ore direct reduction plant in Trinidad. *STAHL UND EISEN* **2002**, 59–64. Available online: https://www.researchgate.net/publication/288144463_Operational_results_of_the_Circored_fine_ore_direct_reduction_plant_in_Trinidad (accessed on 5 January 2020). [CrossRef]
19. Duarte, P. *Hydrogen-Based Steelmaking*; Technical report; TenovaHYL: San Nicolás de los Garza, Mexico, 2015.
20. Armijo, J.; Philibert, C. Flexible production of green hydrogen and ammonia from variable solar and wind energy. Case study of Chile and Argentina. *ResearchGate* **2019**. [CrossRef]

21. Glenk, G.; Reichelstein, S. Economics of converting renewable power to hydrogen. *Nat. Energy* **2019**, *4*, 216–222. [CrossRef]
22. *The Future of Hydrogen*; Number June; OECD: Paris, France, 2019; p. 203. Available online: https://www.oecd-ilibrary.org/energy/the-future-of-hydrogen{_}1e0514c4-en (accessed on 5 February 2020).
23. Hybrit Project—Pilot Projects. Available online: http://www.hybritdevelopment.com/articles/three-hybrit-pilot-projects (accessed on 5 January 2020).
24. H2future. h2future. Available online: https://www.h2future-project.eu/technology (accessed on 8 September 2019).
25. Salcos Salzgitter. Available online: https://salcos.salzgitter-ag.com/ (accessed on 8 September 2019).
26. Green Indsustrial Hydrogen: GrInHy2.0. Available online: https://www.green-industrial-hydrogen.com/ (accessed on 8 September 2019).
27. Windh2. Available online: https://www.windh2.de/ (accessed on 8 September 2019).
28. Brook, D. Tata Steel's European Operations Take Major Step Towards Becoming Carbon Neutral. 2018. Available online: https://www.tatasteeleurope.com/en/news/news/tata-steel-european-operations-take-major-step-towards-becoming-carbon-neutral (accessed on 8 September 2019).
29. ArcelorMittal. World First for Steel: ArcelorMittal Investigates the Industrial Use of Pure Hydrogen—ArcelorMittal. 2019. Available online: https://corporate.arcelormittal.com/news-and-media/news/2019/mar/28-03-2019 (accessed on 5 January 2020).
30. Langner, A.; Lorraine, L. ArcelorMittal Commissions Midrex to Design Demonstration Plant for Hydrogen Steel Production in Hamburg. 2019. Available online: https://corporate.arcelormittal.com/news-and-media/news/2019/sep/16-09-2019 (accessed on 18 November 2019).
31. Thyssenkrupp. World First in Duisburg as NRW Economics Minister Pinkwart Launches Tests at Thyssenkrupp Into Blast Furnace Use of Hydrogen. 2019. Available online: https://www.thyssenkrupp-steel.com/en/newsroom/press-releases/world-first-in-duisburg.html (accessed on 13 November 2019).
32. Otto, A.; Robinius, M.; Grube, T.; Schiebahn, S.; Praktiknjo, A.; Stolten, D. Power-to-steel: Reducing CO_2 through the integration of renewable energy and hydrogen into the German steel industry. *Energies* **2017**, *10*, 451. [CrossRef]
33. Cavaliere, P.; Cavaliere, P. *Direct Reduced Iron: Most Efficient Technologies for Greenhouse Emissions Abatement*; Springer: New York, NY, USA, 2019; pp. 419–484. [CrossRef]
34. Vogl, V.; Åhman, M.; Nilsson, L.J. Assessment of hydrogen direct reduction for fossil-free steelmaking. *J. Clean. Prod.* **2018**, *203*, 736–745. [CrossRef]
35. Wagner, D.; Devisme, O.; Patisson, F.; Ablitzer, D. A laboratory study of the reduction of iron oxides by hydrogen. *2006 TMS Fall Extr. Process. Divis. Sohn Int. Symp.* **2006**, *2*, 111–120.
36. Abhinav, B. Hydrogen Direct Reduction of Iron Ore Using Green Hydrogen. Available online: https://zenodo.org/record/3562399#.XjpcSvkzaUk (accessed on 5 January 2020).
37. Spreitzer, D.; Schenk, J. Reduction of Iron Oxides with Hydrogen—A Review. *Steel Res. Int.* **2019**, *90*, 1900108. [CrossRef]
38. Hasanbeigi, A.; Price, L.; Chunxia, Z.; Aden, N.; Xiuping, L.; Fangqin, S. Comparison of iron and steel production energy use and energy intensity in China and the U.S. *J. Clean. Prod.* **2014**, *65*, 108–119. [CrossRef]
39. Small, M. Direct Reduction of Iron Ore. *J. Metals* **1981**, *33*, 67–75. [CrossRef]
40. Battle, T.; Srivastava, U.; Kopfle, J.; Hunter, R.; McClelland, J. The Direct Reduction of Iron. *Treatise Process Metall.* **2014**, *3*, 89–176. [CrossRef]
41. Anameric, B.; Kawatra, S.K. Properties and features of direct reduced iron. *Mineral Process. Extr. Metall. Rev.* **2007**, *28*, 59–116. [CrossRef]
42. Béchara, R.; Hamadeh, H.; Mirgaux, O.; Patisson, F. Optimization of the iron ore direct reduction process through multiscale process modeling. *Materials* **2018**, *11*, 1094. [CrossRef]
43. MIDREX. *World Direct Reduction Statistics*; Midrex Technologies, Inc.: Charlotte, NC, USA, 2013; p. 14.
44. Cheap Gas to Increase US Direct Reduced Iron Self Sufficiency. 2019. Available online: https://www.reuters.com/article/iron-gas-usa/cheap-gas-to-increase-us-direct-reduced-iron-self-sufficiency-idUSL5N0AYFSC20130129 (accessed on 25 October 2019).
45. Carlos, P.E.; Martinis, A.D.; Jorge, B.; Lizcano, C. Energiron direct reduction ironmaking—Economical, flexible, environmentally friendly. *Steel Times Int.* **2010**, *34*, 25–30.

46. Chen, Z.; Dang, J.; Hu, X.; Yan, H. Reduction kinetics of hematite powder in hydrogen atmosphere at moderate temperatures. *Metals* **2018**, *8*, 751. [CrossRef]
47. Van Der Walt, S.; Colbert, S.C.; Varoquaux, G. The NumPy array: A structure for efficient numerical computation. *Comput. Sci. Eng.* **2011**, *13*, 22–30. [CrossRef]
48. Alhumaizi, K.; Ajbar, A.; Soliman, M. Modelling the complex interactions between reformer and reduction furnace in a midrex-based iron plant. *Canad. J. Chem. Eng.* **2012**, *90*, 1120–1141. [CrossRef]
49. Cárdenas, J.G.G.; Conejo, A.N.; Gnechi, G.G. Optimization of Energy Consumption in Electric Arc Furnaces Operated with 100% Dri. *Metal* **2007**, *2007*, 1–7.
50. Rojas-Cardenas, J.C.; Hasanbeigi, A.; Sheinbaum-Pardo, C.; Price, L. Energy efficiency in the Mexican iron and steel industry from an international perspective. *J. Clean. Prod.* **2017**, *158*, 335–348. [CrossRef]
51. Dİlmaç, N.; Yörük, S.; Gülaboğlu, Ů.M. Investigation of Direct Reduction Mechanism of Attepe Iron Ore by Hydrogen in a Fluidized Bed. *Metall. Mater. Trans. B Process Metall. Mater. Process. Sci.* **2015**, *46*, 2278–2287. [CrossRef]
52. Pineau, A.; Kanari, N.; Gaballah, I. Kinetics of reduction of iron oxides by H_2. Part II. Low temperature reduction of magnetite. *Thermochim. Acta* **2007**, *456*, 75–88. [CrossRef]
53. Teplov, O.A. Kinetics of the low-temperature hydrogen reduction of magnetite concentrates. *Russian Metall. (Metally)* **2012**, *2012*, 8–21. [CrossRef]
54. Fruehan, R.J.; Li, Y.; Brabie, L.; Kim, E.J. Final stage of reduction of iron ores by hydrogen. *Scand. J. Metall.* **2005**, *34*, 205–212. [CrossRef]
55. Guo, D.; Hu, M.; Pu, C.; Xiao, B.; Hu, Z.; Liu, S.; Wang, X.; Zhu, X. Kinetics and mechanisms of direct reduction of iron ore-biomass composite pellets with hydrogen gas. *Int. J. Hydr. Energy* **2015**, *40*, 4733–4740. [CrossRef]
56. Ranzani da Costa, A.; Wagner, D.; Patisson, F. Modelling a new, low CO_2 emissions, hydrogen steelmaking process. *J. Clean. Prod.* **2013**, *46*, 27–35. [CrossRef]
57. Zuo, H.-B.; Wang, C.; Dong, J.-J.; Jiao, K.-X.; Xu, R.-S. Reduction kinetics of iron oxide pellets with H_2 and CO mixtures. *Int. J. Miner. Metall. Mater.* **2015**, *22*, 688–696. [CrossRef]
58. Pérez, F.; Granger, B.E. IPython: A system for interactive scientific computing. *Comput. Sci. Eng.* **2007**, *9*, 21–29. [CrossRef]
59. McKinney, W. Data Structures for Statistical Computing in Python. In Proceedings of the 9th Python in Science Conference, Austin, TX, USA, 28 June–3 July 2010; pp. 51–56.
60. Hunter, J.D. Matplotlib: A 2D graphics environment. *Comput. Sci. Eng.* **2007**, *9*, 99–104. [CrossRef]
61. Anaconda software distribution, Computer software. 2016. Available online: https://www.anaconda.com/ (accessed on 5 January 2020).
62. Schmidt, O.; Gambhir, A.; Staffell, I.; Hawkes, A.; Nelson, J.; Few, S. Future cost and performance of water electrolysis: An expert elicitation study. *Int. J. Hydr. Energy* **2017**, *42*, 30470–30492. [CrossRef]
63. Hydrogen, N. Nel ASA: Receives 4.5 MW Electrolyzer Purchase Order for Fossil Free Steel Production. 2019. Available online: https://nelhydrogen.com/press-release/nel-asa-receives-4-5-mw-electrolyzer-purchase-order-for-fossil-free-steel-production/ (accessed on 12 November 2019).
64. Thyssenkrupp. Hydrogen from Large-Scale Electrolysis—Efficienct Solutions for Sustainable Chemicals and Energy Storage. Available online: https://d13qmi8c46i38w.cloudfront.net/media/UCPthyssenkruppBAISUhdeChlorineEngineers/assets.files/products/water{_}electrolysis/thyssenkrupp{_}electrolytic{_}hydrogen{_}brochure.pdf (accessed on 5 January 2020).
65. Santos Diogo, M.F.; Sequeira Cesar, A.C.; Figueiredo, J.L. Hydrogen production by alkaline water electrolysis. *Quim. Nova Rev.* **2013**, *36*, 1176–1193. [CrossRef]
66. Rashid, M.M.; Mesfer, M.K.A.; Naseem, H.; Danish, M. Hydrogen Production by Water Electrolysis: A Review of Alkaline Water Electrolysis, PEM Water Electrolysis and High Temperature Water Electrolysis. *Int. J. Eng. Adv. Technol.* **2015**, *4*, 2249–8958.
67. Zeng, K.; Zhang, D. Recent progress in alkaline water electrolysis for hydrogen production and applications. *Progress Energy Combust. Sci.* **2010**, *36*, 307–326. [CrossRef]
68. Zare, A.; Khanipour, M.; Sarverstani, H.K.; Kakavandi, I.A.; Shokroo, E.J.; Farniaei, M.; Baghbani, M. Hydrogen and carbon dioxide recovery from the petrochemical flare gas to methanol production using adsorption and absorption combined high-efficient method. *Appl. Petrochem. Res.* **2019**, *9*, 127–145. [CrossRef]

69. Grande, C.A. Advances in Pressure Swing Adsorption for Gas Separation. *ISRN Chem. Eng.* **2012**, *2012*, 1–13. [CrossRef]
70. Song, C.; Liu, Q.; Ji, N.; Kansha, Y.; Tsutsumi, A. Optimization of steam methane reforming coupled with pressure swing adsorption hydrogen production process by heat integration. *Appl. Energy* **2015**, *154*, 392–401. [CrossRef]
71. Mondal, M.; Datta, A. Energy transfer in hydrogen separation from syngas using pressure swing adsorption (PSA) process: A thermodynamic model. *Int. J. Energy Res.* **2017**, *41*, 448–458. [CrossRef]
72. Mantzos, L.; Wiesenthal, T.; Matei, N.A.; Tchung-Ming, S.; Rozsai, M.; Russ, H.P.; Soria Ramirez, A. *JRC-IDEES: Integrated Database of the European Energy Sector: Methodological Note*; Technical report; Joint Research Council, European Union: Luxemburg, 2017. [CrossRef]
73. Hamby, D.M. A review of techniques for parameter sensitivity analysis of environmental models. *Environ. Monit. Assess.* **1994**, *32*, 135–154. [CrossRef] [PubMed]
74. Pfeifer, H.; Kirschen, M. Thermodynamic analysis of EAF energy efficiency and comparison with a statical model of electric energy model of demand. *Engineering* **2003**, *2003*, 1–16.

2. Abhinav Bhaskar, Mohsen Assadi, Homam Nikpey Somehsaraei, Can methane pyrolysis based hydrogen production lead to the decarbonisation of iron and steel industry?, Energy Conversion and Management: X, Volume 10,2021,100079, ISSN 2590-1745, https://doi.org/10.1016/j.ecmx.2021.100079

Energy Conversion and Management: X 10 (2021) 100079

Contents lists available at ScienceDirect

Energy Conversion and Management: X

journal homepage: www.sciencedirect.com/journal/energy-conversion-and-management-x

Can methane pyrolysis based hydrogen production lead to the decarbonisation of iron and steel industry?

Abhinav Bhaskar *, Mohsen Assadi, Homam Nikpey Somehsaraei

University of Stavanger, 4036, Norway

ARTICLE INFO

Keywords:
Industrial decarbonisation
Hydrogen direct reduction
Methane Pyrolysis
Water electrolysis
Green steel

ABSTRACT

Decarbonisation of the iron and steel industry would require the use of innovative low-carbon production technologies. Use of 100% hydrogen in a shaft furnace (SF) to reduce iron ore has the potential to reduce emissions from iron and steel production significantly. In this work, results from the techno-economic assessment of a H_2-SF connected to an electric arc furnace(EAF) for steel production are presented under two scenarios. In the first scenario H_2 is produced from molten metal methane pyrolysis in an electrically heated liquid metal bubble column reactor. Grid connected low-temperature alkaline electrolyser was considered for H_2 production in the second scenario. In both cases, 59.25 kgH_2 was required for the production of one ton of liquid steel (tls). The specific energy consumption (SEC) for the methane pyrolysis based system was found to be 5.16 MWh/tls. The system used 1.51 MWh/tls of electricity, and required 263 kg/tls of methane, corresponding to an energy consumption of 3.65 MWh/tls. The water electrolysis based system consumed 3.96 MWh/tls of electricity, at an electrolyser efficiency of 50 KWh/kgH_2. Both systems have direct emissions of 129.4 kgCO2/tls. The indirect emissions are dependent on the source of natural gas, pellet making process and the grid-emission factor. Indirect emissions for the electrolysis based system could be negligible, if the electricity is generated from renewable energy sources. The levellized cost of production(LCOP) was found to be $631, and $669 respectively at a discount rate of 8%, for a plant-life of 20 years. The LCOP of a natural gas reforming based direct reduction steelmaking plant of operating under similar conditions was found to be $414. Uncertainty analysis was conducted for the NPV and IRR values.

1. Introduction

Global greenhouse gas(GHG) emissions need to be reduced by 45% by 2030 from 2010 levels and to net zero by 2050 to limit global mean temperature rise to 1.5 °C [1]. Energy intensive industries (EII) like iron and steel, aluminum, cement, chemicals etc. are responsible for large share of the global GHG emissions. Decarbonisation of EII's is essential to achieve the 2050 emission reduction targets. Iron and steel production contributes to 7% of the global GHG emissions [2]. The use of demand reduction measures like material efficiency, material substitution and product service-life extension are important in achieving emission reductions from the steel industry [3]. However, in the short and medium term, as living standards improve in developing countries, the demand for steel could increase. The demand for primary steel is projected to increase by 30% in the next three decades [4]. At present majority of the primary steel is produced through the blast furnace-basic oxygen furnace(BF-BOF) route, where coke is used to reduce Fe_2O_3 to Fe in the BF and is converted to steel in the BOF. Approximately 1.8 ton(t) of CO_2 is released to produce ton of liquid steel (tls) [5]. An alternative production route is the reduction of solid Fe_2O_3 by a mixture of CO and H_2 in a direct reduction shaft furnace [6]. The direct reduced iron (DRI) could be processed in an electric arc furnace (EAF) to produce steel. The reducing gas is produced from reforming of natural gas or through coal gasification. The specific energy consumption (SEC) of a natural gas(NG) reforming based DRI-EAF systems varies from 2.9–3.5 MWh/tls, and direct emissions vary from 0.9 to 1.2 tCO_2/tls [7]. Efficiency improvement measures have reduced the energy and emission intensity of the steel industry in the past decades. However, complete decarbonisation of the iron and steel industry, while meeting the increasing steel demand, would require the introduction of innovative production technologies [8,9].

Fischedick et al. evaluated the techno-economic feasibility of three innovative iron production technologies i.e. blast furnace with carbon capture and storage (CCS), low and high-temperature iron ore electrolysis (electrowining), and H_2-direct reduction (DR) [10]. They found

* Corresponding author.
E-mail address: abhinav.bhaskar@uis.no (A. Bhaskar).

https://doi.org/10.1016/j.ecmx.2021.100079

Available online 10 March 2021

Nomenclature

Following abbreviations were used in the manuscript

H_2-SF-EAF	Hydrogen-shaft furnace-electric arc furnace
DRI-EAF	Direct reduced iron-electric arc furnace
BF-BOF	Blast furnace-Basic oxygen furnace
SMR	Steam methane reforming
CCS	Carbon capture and storage
DR	Direct reduction
GHG	Green house gas
EII	Energy intensive industry
LTE	low-temperature electrolyser
HTE	High-temperature electrolyser
SMR	Steam methane reforming
BASF	Badische Anilin und Soda Fabrik
SSAB	Svenskt Stål AB
LKAB	Luossavaara-Kiirunavaara Aktiebolag
LMBR	Liquid metal bubble column reactor
PSA	Pressure swing adsorber
EAF	Electric arc furnace
HEX	Heat exchanger
SF	Shaft furnace
TRL	Technology readiness level
TDM	Thermal decomposition of methane
SEC	Specific energy consumption
MWh	Megawatt hour
KWh	Kilowatt hour
kJ	Kilojoule
MJ	Megajoule
MMBTU	Metric Million British Thermal Unit
$	US dollar
tls	Ton of liquid steel
kg	Kilogram
kgH_2	Kilogram of hydrogen
kt	Kiloton
Mt/y	Million ton per year
t	ton
kta^{-1}	Kiloton per annum
tCO_2	Ton of carbon dioxide
K	Kelvin
°C	Celsius
CF	Cash flow
NPV	Net present value
IRR	Internal rate of return
LCOP	Levellized cost of production
ACC	Annualized capacity factor or annuity factor
capex	Capital expenditure
opex	Operational expenditure
GEF	Grid emission factor
H_2	Hydrogen
O_2	Oxygen
H_2O	Water
CH_4	Methane
CO_2	Carbon dioxide
CO	Carbon Monoxide
N_2	Nitrogen
Fe	Iron
FeO	Iron oxide
Fe_2O_3	Iron oxide (Hematite)
Fe_3O_4	Iron oxide (Magnetite)
Al_2O_3	Alumina
SiO_2	Silica
CaO	Calcium oxide (lime)
MgO	Magnesium oxide
NG	Natural gas

that H_2-DR and electrolysis based production routes have the highest potential to decarbonise the steel industry in the future. A multi-criteria analysis of primary steelmaking technologies was conducted by Weigel et al. [11]. Electrolysis and H_2-DR were rated as the most promising technologies for low-carbon steel production. Toktarova et al. conducted a techno-economic pathway analysis for low-carbon transition of the Swedish steel industry. They found that H_2-DR-EAF based steel production has the highest decarbonisation potential and could reduce total CO_2 emissions in Sweden by 10% [12]. Under the Ultra-Low Carbon Dioxide Steelmaking (ULCOS) research program, two iron-ore electrolysis processes were studied [13,6]. These processes are still at lab-scale and are not expected to be available for commercial deployment before 2040, and are hence not included in this analysis [10]. DR of iron ore with 100% H_2 was carried out at commercial scale using fluidized-bed reactors at an industrial plant in Trinidad and Tobago in the early 1990's [14]. The plant produced steel with 95% metallization rate, at a production capacity of 65 ton of liquid steel per hour (tls/hr) in a shaft-furnace(SF) reactor [15]. Direct reduction with more than 90% H_2 was conducted by Energiron at a test facility in Hysla, Monterrey [16]. A H_2-(SF) plant with an output capacity of one ton/day was commissioned under the HYBRIT project (consortium of Luossavaara-Kiirunavaara Aktiebolag (LKAB), Svenskt Stål AB (SSAB), and Vattenfall) in August 2020 in Sweden [17]. The project also aims to the develop a fossil fuel free pellet making process and a H_2 storage unit for continuous functioning of the plant. All major steel companies are involved in building industrial demonstration plants for H_2-SF based plants [18–22]. The largest producers of DRI shaft furnces, MIDREX and ENERGIRON, have indicated that their shaft furnace designs can be easily modified to use 100% H_2 as the reducing agent [23,16].

H_2 required for steel production could be produced by water electrolysis or from fossil fuels like natural gas or coal. 95% of H_2 is produced by steam methane reforming (SMR) at present. However, SMR process has a high carbon-footprint, and it's continued use would be an obstacle in achieving the emission reduction goals. In recent times, the role of green H_2 produced from water electrolysis, using renewable electricity has become increasingly prominent in decarbonising the energy system. It has the potential to decarbonise hard-to-abate sectors like industries (steel, ammonia, methanol etc.), heavy transport, shipping and aviation [24]. Although renewable electricity powered water electrolysis produces emission-free H_2, limited availability, and high-prices of renewable electricity are a deterrent to the large-scale deployment of industrial decarbonisation projects [2,5]. For example, converting existing steel production units in the EU to H_2-SF-EAF would require an additional 300–400 TWh/year of renewable electricity [25]. In the short and medium term, low-carbon H_2 produced from natural gas could pave the way for industrial H_2 projects [23]. SMR coupled with carbon capture and storage (CCS) has been proposed as an alternative for low-carbon H_2 production. However, there are concerns about the cost, safety and social acceptability of CCS [26]. Another alternative for low-carbon H_2 production is methane pyrolysis, where CH_4 is decomposed to solid-carbon and CH_4 [27]. Methane pyrolysis could act as a bridge technology until large-amounts of cheap renewable electricity becomes available, while infrastructure and end-use applications are deployed [28]. Parkinson et al. evaluated the costs of carbon mitigation from a life-cycle perspective of 12 different hydrogen production technologies, and found methane pyrolysis as the most cost-effective short-term carbon abatement solution [29].

To the best of the knowledge of the authors, integration of methane

pyrolysis with H_2-SF-EAF system based steel production has not been evaluated previously. In this work, techno-economic assessment of H_2-SF-EAF system based steel production has been conducted for two scenarios. Iron ore reduction is carried out in a H_2-SF and an EAF is used for steelmaking in both cases. H_2 is produced from methane pyrolysis in the first scenario and water electrolysis in the second. The analysis was conducted to answer the following questions.

1. Is it techno-economically feasible to integrate methane pyrolysis with H_2-SF-EAF system based steel making process?
2. How does methane pyrolysis compare with water electrolysis based H_2-SF-EAF system system in terms of SEC, emissions, and economic parameters?
3. Which factors have the maximum impact on the economic performance of H_2-SF-EAF system based steel production systems in both the scenarios?

The rest of the paper is structured as following. A brief review of the literature is presented in Section 2. Section 3, describes the methodology used to develop the techno-economic assessment model. The modelling and simulation results of the analysis are presented in Section 4. Discussions and inferences from the analysis are collated in Section 5, followed by the conclusions in Section 6.

2. Literature review

Vogl et al. conducted a techno-economic analysis of H_2-SF-EAF based steel production route, a low-temperature electrolyser(LTE) was used for hydrogen generation [30]. Their assessment revealed that the production costs vary from €361–640/t of steel, and is highly dependent on the price of electricity and the carbon emission prices. In a recent article, Krüger et al. analyzed the techno-economics of integrating a high-temperature electrolyser(HTE) to the H_2-SF-EAF system [31]. They calculated a 21% reduction in the energy consumption of a HTE based system. Some researchers haves evaluated the use of methanol produced from co-electrolysis of H_2O and CO_2 in the shaft furnace for steel production [32].

Methane pyrolysis is an endothermic reaction and requires high-temperatures (1273–1773 K) to achieve high-conversion rates. Solid-carbon, produced as a by-product of methane pyrolysis has many industrial applications, and could be sold at $0.4/kg -$2/kg to generate additional revenue [33]. Excess unsold carbon could be stored in geological storage or unused coal mines [29]. It can be handled, transported and stored at a fraction of the cost of gaseous CO_2. Schneider et al. reviewed different technologies for production of H_2 from methane pyrolysis, thermal decomposition, plasma decomposition and catalytic decomposition. Keipi et al. compared the economic feasibility of hydrogen production by methane pyrolysis with SMR and water electrolysis. H_2 produced by pyrolysis was found to have the lowest specific CO_2 emissions, and the economic feasibility was found to be dependent on the market price of solid-carbon [27]. Monolith materials has commissioned a methane pyrolysis plant in Nebraska, United states, primarily for carbon-black production [34]. They intend to use the by-product H_2 for industrial scale low-carbon ammonia production. The company uses plasma decomposition process powered by renewable electricity [35].

High-temperatures required for pyrolysis leads to complex reactor designs and higher costs. Thermo-catalytic reduction of CH_4 could lower the reaction temperature, leading to simpler reactor design. Metallic catalysts, carbonaceous catalysts like activated carbon and carbon black have been investigated previously for the production of H_2 from methane pyrolysis [36]. High-conversion rates were achieved at temperaures lower than 1273 K, but deposition of carbon on the surface of the catalysts reduces their activity, and can clog the fluid-bed and packed-bed reactors used for thermo-catalytic conversion of CH_4 to H_2 and solid-carbon [37–39].

2.1. Molten metal methane pyrolysis

Molten metal pyrolysis, utilizes the low-density and insolubility of solid-carbon in liquids for effective separation of carbon, and could solve the problem of reactor clogging by carbon deposition [40]. CH_4 is passed through a molten metal in a liquid metal bubble column reactor(LMBR), decomposing it to solid-carbon and H_2. Serban et al. achieved a methane conversion of 57% using molten tin in a LMBR at 1023 K [41]. Several experimental studies have recorded high-conversion rates, and low-concentration of intermediate products [42,43]. Upham et al. developed a conceptual process model and evaluated the techno-economic feasibility of molten-metal methane pyrolysis [44]. They proposed the use molten Fe as the heat transfer medium, and found the cost of H_2 to be comparable to SMR-based H_2 production. Gregory et al. conducted an optimization-based techno-economic analysis of an LMBR system to produce H_2 for an industrial boiler, and a petrochemical plant in California [45]. They reported that in locations with high emission prices, levellized cost of H_2 could be $0.39/kg$H_2$, much lower than the cost of hydrogen produced from SMR, which varies $1.5-$2/kgH_2. An industrial project to demonstrate molten-metal methane pyrolysis is being developed jointly by Wintershall and Karlsruhe University of technology in Germany [46].

3. Methodology

The techno-economic assessment framework, developed for assessing green chemical technologies at low technology readiness level (TRL) was used in this work [47]. Market demand and future projections were assessed in the first step. Conceptual process models, and material and energy balance models were developed to get preliminary estimates (30% accuracy) of the specific energy demand, emissions, and component sizes in the second step. This was followed by an economic analysis i.e. calculation of the NPV and IRR of the proposed production plants from an investor's perspective. The final step involved conducting a sensitivity and uncertainty analysis, with NPV and IRR as the target variables.

3.1. Market analysis and demand assessment

Steel demand is projected to increase by 30% in 2050 [4]. However, the market for low-carbon steel technologies is not well-established. The recent policy shift towards decarbonisation of all sectors of the economy, and emphasis on the use of climate-neutral industrial products could increase the demand for low-carbon steel in the future [48–50]. Steel demand has traditionally come from the infrastructure sector i.e. construction, shipping, power-generators etc. Achieving a zero-carbon footprint across the value chain is becoming an important strategic objective for different manufacturing industries i.e as the transport sector transitions from internal combustion engines based vehicles to battery electric vehicles, the demand for low-carbon steel to manufacture automotive body parts could increase. Similarly, electricity sector's transition from fossil fuel based power plants to wind and solar generators could lead to an increased demand for low-carbon steel. Iron and steel is used to build the wind tower structure, gearbox, generator and turbine transformers. The steel intensity of existing wind turbine models varies from 107 to 132 t/MW of installed capacity [51]. Solar photovoltaic (PV) plants require 67.9 t/MW of steel [51]. According to estimates by the international renewable energy agency (IRENA), 6 Terawatt (TW) of wind and 9 TW of solar generators should be installed by 2050, increasing the share of renewable electricity generation to 61% from the current 10% to limit the harmful impacts of anthropogenic climate change [52]. This target could translate into a huge demand for low-carbon steel.

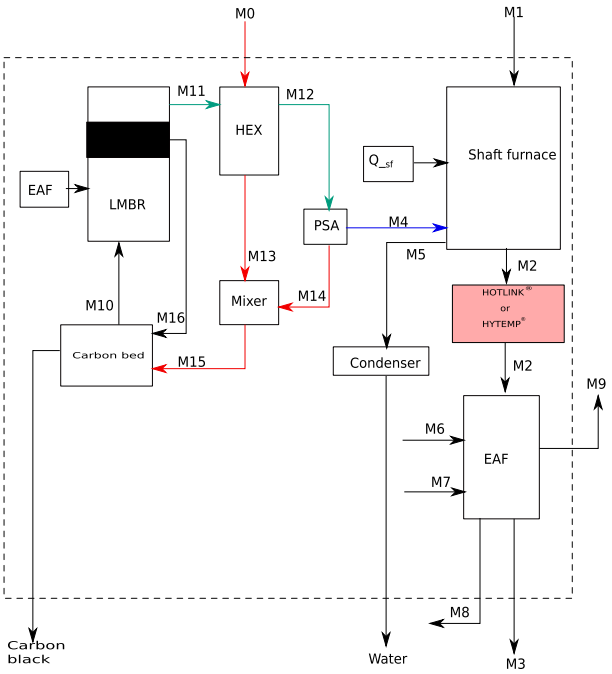

(a) Scenario 1 : H_2-SF-EAF system, H_2 is produced in a liquid metal bubble column reactor(LMBR), through methane pyrolysis. The heat is supplied by an EAF.

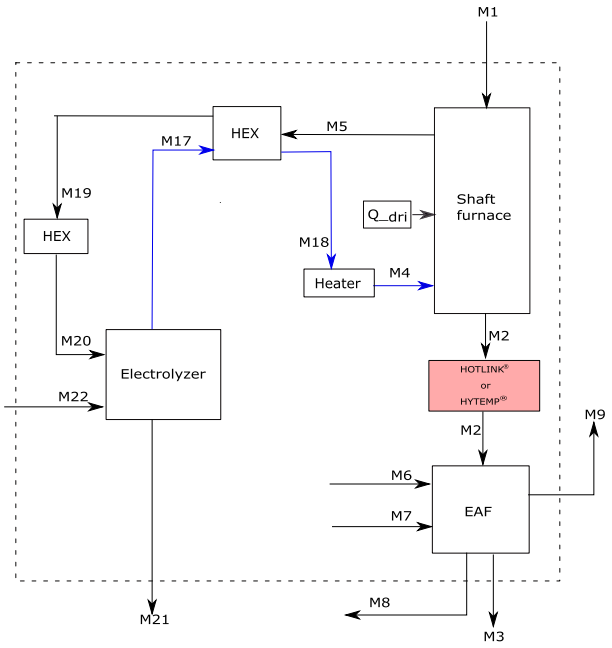

(b) Scenario 2: H_2-SF-EAF system, H_2 is produced by water electrolysis in a low-temperature alkaline electrolyser.

Fig. 1. (a) Scenario 1 : H_2-SF-EAF system, H_2 is produced in a liquid metal bubble column reactor(LMBR), through methane pyrolysis. The heat is supplied by an EAF. (b) Scenario 2: H_2-SF-EAF system, H_2 is produced by water electrolysis in a low-temperature alkaline electrolyser.

3.2. *Conceptual process modelling*

Conceptual process models were developed for both scenarios to calculate the material and energy balances. Calculations are based on the production of one ton of liquid steel under steady state conditions. Integrated material and energy balance calculations were performed across the control volumes of major components of the proposed systems. The process schematics of the systems considered in scenario 1 and scenario 2, used for developing the models are presented in Fig. 1a and Fig. 1b respectively. The steel production process can be divided into three sub-processes i.e. production of reducing agent (hydrogen), iron production in the shaft furnace, and conversion of iron to steel in the

Table 1
The reactor dimensions (M), temperature (°C), pressure, conversion factors (%), methane feed rate (kg/s) have been taken from [65]

Length	Diameter	Volume(Tin)	Temperature	Pressure	Conversion factor	CH_4 feed	H_2 flow
m	m	Tons	K	Bar	percentage	kg/hr	ton/hr
8.66	5.21	850	1443	19	0.90	29.39	24.03

EAF. The conceptual process flow diagram for the iron and steel production process using a shaft furnace and an EAF, is similar to the ones proposed by [30,17,5]. The difference in the overall material and energy balance of the two systems is attributed to the hydrogen production subprocess. Material flow through the components was evaluated using stoichiometric values of the reactants and products. It is assumed that the reactions reach completion in a single-pass, unless it is stated otherwise. The specific heat and enthalpy of the different species were calculated using the Shomate equation, as described in Eqs. (1) and (2). The coefficients of the Shomate equations were taken from NIST webBook [53].

$$C_p^{\circ} = A + B^*t + D^*t^2 + D^*t^3 + E/t^2 \tag{1}$$

$$H^{\circ} - H^{\circ}_{298.15} = A^*t + B^*t^2/2 + D^*t^3/3 + D^*t^4/4 - E/t + F - H \tag{2}$$

3.2.1. Iron production in the shaft furnace

The shaft furnace is a counter current flow reactor [54]. The iron ore pellet enter the shaft furnace from the top, through the stream **M1** at ambient temperature. Impurities have an adverse impact on the reaction kinetics, and should be limited to less than 5% [55]. The impurities are primarily composed of Al_2O_3 and SiO_2. The iron ore pellets react with the hydrogen gas, which enters the shaft furnace from the bottom of the furnace at 1173 K, represented by **M4**. The reduction of iron oxide to metallic iron occurs in three steps, where hematite (Fe_2O_3) is reduced to magnetite(Fe_3O_4), followed by magnetite's reduction to wustite (FeO), and subsequently to metallic Fe. The reduction steps are presented in the Eqs. (3)–(5). The heat of the reaction under standard conditions is 99.5 kJ/mol [56].

$$3Fe_2O_3(s) + H_2(g) \rightarrow 2Fe_3O_4(s) + H_2O(g) \tag{3}$$

$$Fe_3O_4(s) + H_2(g) \rightarrow 3FeO(s) + H_2O(g) \tag{4}$$

$$FeO(s) + H_2(g) \rightarrow Fe(s) + H_2O(g) \tag{5}$$

The reduction of Fe_2O_3 by H_2 is a non-catalytic, heterogeneous solid–gas endothermic reaction, where the overall reaction rate is dependent on the heat and mass transfer phenomena, and the rate of chemical reaction [57]. At higher temperatures, the chemical reaction rate increases exponentially, and diffusion of hydrogen through the laminar layer of hematite pellet is the rate limiting step [58]. Detailed analysis of the parameters affecting the overall reaction kinetics can be found in the literature [59,57,58,60].

Metallization rate of 94% is achieved in the H_2-SF [59]. The reduced iron exits the shaft furnace through stream **M2**, which is composed of metallic iron, wustite and impurities. The stream **M2** could be charged to the EAF at 873 K through the HOTLINK® or HYTEMP® process developed by MIDREX and ENERGIRON technologies respectively [61,62]. Energy consumed for the transfer of hot-metal to the EAF has not been considered in the present model. Although it's difficult to implement a hot-metal transport system in an existing steel plant, arrangements for gravity based transfer of hot-metal could be included in the design phase of a greenfield plant. The unreacted hydrogen, and steam produced as a by-product of the reduction reaction exit the reactor through the exhaust stream, **M5**, at 573 K [31]. A condenser is used to separate hydrogen, and water from the exhaust stream. Electrical resistance heaters are used to supply thermal energy to the shaft furnace.

3.2.2. Steel production in an EAF

The EAF is charged with 100% hot-DRI, and is heated to 1923 K. It exits the EAF, through the stream **M3**. The value of **M3** is fixed to one ton. Carbon fines of biogenic origin are added to the EAF through the stream **M6**. Carbon is required for the conversion of iron to steel, reduction of wustite to iron, and for the formation of CO. CO promotes froth formation, which is crucial for effective slag removal. The presence of CO gas improves the overall heat transfer rate from the graphite electrodes to the melt. It is assumed that 20 kg/tls of carbon is added [63]. Slag formers, **M7**, (mixture of CaO and MgO) are added to remove impurities, and to increase the life of the refractory lining of the furnace [64]. The slag exits the EAF through **M8**. The exhaust gases, composed primarily of CO_2,O_2 and N_2, exit the EAF through stream **M9** at 1773 K. Assumptions related to the air -infiltration, graphite electrode consumption etc. were taken from the literature [63].

Thermal energy is supplied by the electric arc formed between the graphite electrodes, and exothermic oxidation reactions. The reduction reactions of FeO and C, and the reaction between carbon and O_2 have been considered in the present model. The reactions are presented in Eqs. (6)–(8) respectively. An electrical efficiency of 0.85 has been considered for the EAF to account for losses from the transformer, rectifier, electrodes, radiative and convective heat transfer etc. Kirschen et al. presented a similar approach to calculate the energy consumption of an EAF [64].

$$FeO(s) + C(s) \rightarrow Fe(s) + CO(g) \tag{6}$$

$$2C(s) + O_2(g) \rightarrow 2CO(g) \tag{7}$$

$$C(s) + O_2(g) \rightarrow CO_2(g) \tag{8}$$

3.2.3. Scenario 1: LMBR subsystem

Catalan et al. designed an LMBR system for the production of 200 kta^{-1} using a coupled hydrodynamic and kinetic model [65]. Molten tin was used as the heat transfer medium in the LMBR and ten different configurations of the LMBR were presented by the authors. Configuration with the highest conversion factor, and smallest volume was evaluated in this model. The mass flow rates of H_2, CH_4, solid-carbon were converted to the mass flows per ton of liquid steel (kg/tls). LMBR dimensions and operational parameters are presented in Table 1. Thermodynamic properties of liquid tin were calculated using correlation provided by [66], and are presented in Eq. (9). The correlation is valid in the temperature range of $800 \leqslant T \leqslant 3000K$. The density of liquid tin was calculated using Eq. (10) [67].

$$\Delta H = -1285.372 + 28.4512^*T \tag{9}$$

$$\rho_{tin} = C_3 - C_4(T - T_{ref}) \tag{10}$$

Where $C_3 = 6979\ kgm^{-3}$,$C_4 = 0.652\ kgm^{-3}\ K^{-1}$, and $T_{ref} = 505.08$ K is the melting point of tin. Eq. (10) is valid in the temperature range of $506 \leqslant T \leqslant 1950$ K.

Natural gas (100% CH_4) enters the system through the stream **M0**, at high pressure and ambient temperature. It is pre-heated in the heat recovery heat exchanger (HEX) by the stream **M11**, which is a mixture of H_2 and unreacted CH_4 exiting the LMBR at 1443 K. The stream **M11** exits the heat exchanger as **M12** at 1173 K. CH_4 is separated in the pressure swing adsorber(PSA), and exits as stream **M14**. The stream **M13** and **M14** are mixed and enter the carbon-bed at an elevated temperature, through the stream **M15**. The carbon-bed can be visualized as a

solid–gas tubular heat exchanger [44]. The stream **M15** is heated to 973 K by the incoming stream of solid-carbon(**M16**). **M10**, enters the LMBR from the bottom, where a sparger disperses the pressurised gas into bubbles. Gas bubbles rise through the LMBR. They contain the solid-carbon particles, H_2, and CH_4 inside them, which are released at the top of the liquid tin surface. Molten metal acts as a heat transfer medium, providing heat for the endothermic decomposition of methane. The low-density carbon is insoluble in liquid tin, it can be readily removed in a continuous process in a manner similar to a floatation cell as is done routinely in slag removal. LMBR is made of 120 mm stainless steel, and is lined with a refractory layer of 600 mm, made of MgO bricks to sustain the high-temperatures inside the reactor [38]. An EAF is used for melting tin, and providing thermal energy to the LMBR [44].

3.2.4. Scenario 2: water electrolysis for hydrogen production

H_2 is produced using a low-temperature alkaline electrolsyer, consuming 50 KWh/kgH_2. The hydrogen stream, **M17** exiting the electrolyser is pre-heated in the heat recovery heat exchanger to **M18**. Heat is recovered from the shaft-furnace exhaust stream, **M5**, in the heat exchanger. An electrical heater is used to raise the temperature of the stream **M18** to the 1173 K. The shaft-furnace exhaust gases enter the condenser through the stream **M19**, lowering it's temperature from 393 K to 343 K. Purified condensed water enters the electrolyser through the stream **M20**. Additional water requirements are met through the stream **M22**, to account for losses in the circuit. O_2 is produced as a by-product of the water-electrolysis and exits the electrolyser through the stream **M21**.

3.3. Economic evaluation

Preliminary sizing of the main process equipment (reactors, pressure vessels, EAF) was done for a 3.35 Mta^{-1}) steel production plant, which is comparable to the size of NG-reformer based DRI-EAF plants in operation [68]. H_2 production capacity of 200 kta^{-1} was considered in both scenarios. Preliminary costs of the main process equipment were converted to the total capital costs using Lang factors from Sinnot [69]. The H_2-SF-EAF system plants were modelled as first-of-its-kind plants. A Lang-factor of five was considered for the H_2-SF-EAF system system, while a Lang factor of ten was used for the LMBR based hydrogen production system. The operational costs are comprised of the cost of iron ore, electricity, natural gas, and shaft furnace and EAF operational costs. A fixed price of electricity has been used to calculate the financial parameters for the plant. Only the direct emissions from the plants were used to evaluate the annual emissions cost. The annual maintenance cost was considered to be 2% of the capital cost, and a labour cost of 20$/tls was considered in the model [69]. The levellized cost of production (LCOP) was calculated for both scenarios by considering the annualized capital, operational, labour, maintenance, and emission costs of the system, using Eqs. (11) and (12).

$$LCOP = \frac{C_{capex}{}^{*}ACC + C_{opex} + C_{maint} + C_{labour} + C_{emission}}{Annual\,steel\,production} \tag{11}$$

$$ACC = \frac{r^{*}(1+r)^{n}}{(1+r)^{n}-1} \tag{12}$$

A discounted cash flow analysis was conducted to compare the NPV and IRR of the investment. NPV was calculated using Eq. (13). IRR is calculated as the discount rate at which the NPV of the cash flow is zero. The salvage value of the equipment after the end of plant life was assumed to be zero, and a linear depreciation rate has been considered. A tax rate of 25% was assumed for the calculations.

$$NPV = \sum_{n=1}^{n} \frac{CF}{(1+r)^{n}} \tag{13}$$

Where, ACC, CF, r, and n refer to the annuity factor, cumulative cash flow, discount rate, and the project life respectively. The economical parameters used for the calculations are presented in Table 2.

Table 2
Economical parameters considered for the H_2-SF-EAF system system.

Plant life	Plant construction	Discount rate	Tax rate	Depreciation	Steel output	H_2 output
Years	Years	%	%	N.A	Mt/year	Kt/year
20	2	8	25	linear	3.07	200

Table 3
Assumptions used in the techno-economic assessment model.

Capital cost assumptions			
Equipment	Cost ($)	Lifetime	Reference/remark
Electrolyser (Million $/MW H_2)	0.704	90000 h	[70]
Stack replacement (Million $/MW H_2)	0.540	100000 h	[70]
Shaft furnace ($\$t^{-1}$DRI/year)	240	20 years	[31]
Electric arc furnace ($\$t^{-1}$ steel/year)	140	20 years	[31]
Operational cost assumptions			
Item	Cost	Unit	Reference/remark
Iron ore	90	$/t	[71]
Electricity	56	$/MWh	[72]
Natural gas	6.58	$/MMBTU	[72]
DRI OPEX	12	$/tls	[73]
EAF OPEX	33	$/tls	[73]
CO_2 emission	35	$/t$CO_2$	[74]
Revenue stream assumptions			
Product	Price	Unit	Reference/remark
Carbon steel	700	$/t	[71]
Carbon	200	$/t	[44]
Oxygen	40	$/t	Market price of O_2

Revenue is generated from the sale of steel and by-products. Solid-carbon and oxygen are produced as a by-products of methane pyrolysis and water electrolysis respectively. Both by-products could be sold to generate additional revenue. Solid-carbon produced during methane pyrolysis is used in the manufacturing industries i.e. automobile tires, graphite electrodes, printer ink pigments, graphite electrodes etc. [27]. O_2 has many industrial applications. Assumptions related to the costs, and revenue used in the model are presented in Table 3.

3.4. Sensitivity and uncertainty analysis

There are different sources of uncertainty in the model inputs. They arise from the fluctuations in the price of internationally traded commodities (iron ore, natural gas, carbon price etc.), and price of input parameters such as electricity cost, emission costs. The technologies analyzed in this work are at low TRL, hence values of input parameters such as electrolyser efficiency and cost are uncertain. Local and global sensitivity analysis were conducted to apportion the uncertainty in the model output to different model inputs [75]. The NPV and IRR of the system were selected as the target variables. In the first step a local parametric sensitivity analysis was conducted [76]. The input parameters (uncertain factors) were varied by ±20% from their base values, and percentage change in the output values were evaluated.

A global sensitivity analysis was conducted using the sobol sensitivity indices approach to ascertain the uncertainty of the NPV and IRR values, based on the global uncertainty in the input parameter values [77]. Sobol sensitivity analysis determines the contribution of each input parameter, and their interactions to the overall model output

Table 4
Lower and upper bounds of input parameters used for the global sensitivity analysis.

Target Parameters: NPV and IRR			
Parameter	Lower bound	Upper bound	Unit
Tax rate	25	35	Percentage
Interest rate	0.06	0.12	Percentage
Electricity price	20	60	USD/MWh
Natural gas price	4	10	USD/MMBTU
Iron ore cost	75	120	USD/ton
Emission cost	35	200	Euro/tCO_2
Carbon steel price	600	700	USD/ton
Carbon price	100	300	USD/ton
Electrolyser efficiency	45	60	KWh/kgH_2
Electrolyser capital cost	0.2	0.7	Million \$/MWH_2

variance. The global sensitivity analysis was carried out using the SALib library to evaluate the Sobol first-order and Sobol total-order sensitivity indices [78]. The selected input parameters, and their lower and upper bounds are provided in Table 4.

4. Results

This section outlines the results of the techno-economic assessment. The material and energy balance, specific energy consumption, emissions, economic parameters, and results of the local and global sensitivity analysis are presented.

4.1. Material and energy balance

The material and energy flows through the different components of the steel production systems in presented in Table 5. It has been divided into three sub-processes as described in Section 3.2. The streams **M1** to **M9** represent the iron and steel production sub-process. Material and energy flows through the LMBR based H_2 production sub-system are presented by the streams **M0**, and **M10** to **M16**. The streams **M17** to **M22** depict the material and energy flows through the electrolyser based hydrogen production subsystem.

Approximately 59 kg of H_2 is required for the reduction of 1.5 ton of iron ore, required for one ton of steel production, considering a metallization rate of 94%, and impurity content of 5% in the iron ore pellets. Stoichiometric requirement of H_2 for iron oxide reduction is 54 kg/tls (considering 100% conversion of FeO in the EAF). A higher quantity of H_2 is considered in this model to account for 10% losses, owing to leakage, dissolution in water and other solid streams. The H_2 requirement is similar to the ones reported in the literature [31,30,25,5]. For the methane pyrolysis based system 261.6 kg of CH_4 is required, resulting in the production of 178 kg of solid-carbon as a by-product. In the electrolyser based system, the stream **M18** is heated to the shaft furnace temperature of 1173 K.

4.2. Specific energy consumption

Both systems were assumed to be connected to the electricity grid, and all energy requirements of the plants (except CH_4 used in the LMBR) were met by grid-electricity. The SF and the EAF have a combined electricity consumption of 0.79 MWh/tls. The endothermic reduction of Fe_2O_3 in the shaft furnace results in an additional electrical energy demand of 0.252 MWh/tls ($\eta = 0.85$). The EAF uses 0.537 MWh/tls ($\eta = 0.8$) of electricity. The total electricity requirements are higher than the NG-reformer based DRI-EAF unit, which requires approximately 0.680 MWh/tls. Thermal energy demand in the NG-reformer based DRI units is met by the exothermic reaction between CO and Fe_2O_3.

In scenario one, the SEC was found to be 5.16 MWh/tls. CH_4 entering the reactor is pre-heated to 973 K by exchanging heat with the streams **M11**, **M16** and **M14**. 55% of the thermal energy contained in the solid-carbon stream, **M16**, is recovered. The LMBR consumes 0.71 MWh/tls of electricity at an EAF efficiency of 80 %, which is slightly higher than 0.51 MWh/tls ((reported as 31 MJ/kgH_2) calculated by Upham et al. for a similar system [44]. They considered 90% sensible heat recovery from the H_2 stream exiting the reactor and solid-carbon stream, along with an EAF efficiency of 90 % leading to slightly lower electricity consumption. In addition, CH_4 used in LMBR as a chemical feedstock, corresponds to

Table 5
Material and energy flows through the different components of the steel production systems, considering a metallization rate of 0.94 and an impurity content of 5% in the iron ore pellets. Reaction enthalpy values are not presented in this table. More details about the calculations can be found in the Jupyter notebooks [79].

Stream	Description	Mass flow in kg/tls	Temperature in K	Enthalpy in KWh/tls
	Shaft furnace-Electric arc furnace subsystem			
M1	Fe_2O_3 pellets and impurities	1527.91	298	0.00
M2	Fe, FeO, and impurities	1089.48	873	99.02
M3	Liquid steel	1000.00	1923	324.84
M4	H_2 stream (reducing gas)	59.25	1173	211.99
M5	Shaft furnace exhaust	489.31	573	76.65
M6	Carbon fines	20.00	298	0.00
M7	Slag formers	50	298	0.00
M8	EAF slag stream	126.39	1923	75.07
M9	EAF exhaust stream	230.00	1173	105.22
M_{air}	Infiltrated air	250.00	298	0.00
	Liquid metal bubble column reactor subsystem			
M0	Natural gas from pipeline	263.37	298	0.00
M10	Pre-heated methane	263.37	973	166.07
M11	H_2 and CH_4 at LMBR outlet	85.38	1443	316.48
M12	H_2 and CH_4 from HEX	85.38	1173	235.20
M13	Pre-heated incoming CH_4 stream	263.37	585	83.96
M14	CH_4 stream from PSA	26.12	1173	23.17
M15	Mixed CH_4 stream	263.37	616	96.33
M16	Carbon stream from LMBR	177.77	1443	100.37
	Electrolysis subsystem			
M17	H_2 from electrolyser	59.56	343	1.12
M18	Heated H_2	59.56	448	31.85
M19	H_2O after HEX	486.82	393	25.47
M20	Condensed H_2O	481.43	343	85.85
M21	O_2 from electrolyser	476.49	343	6.63
M22	H_2O for electrolysis	52	298	0.0

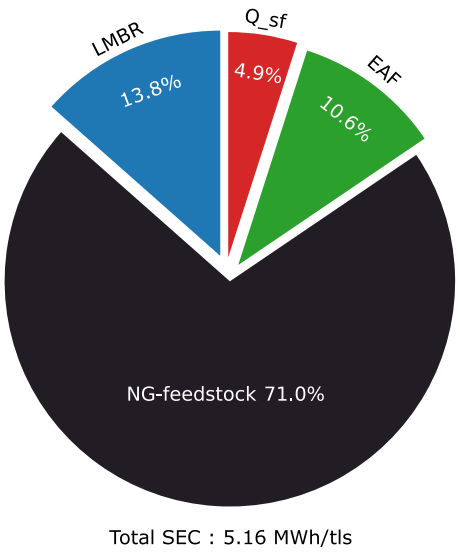

(a) Energy consumption of the methane pyrolysis based H_2-SF-EAF system system

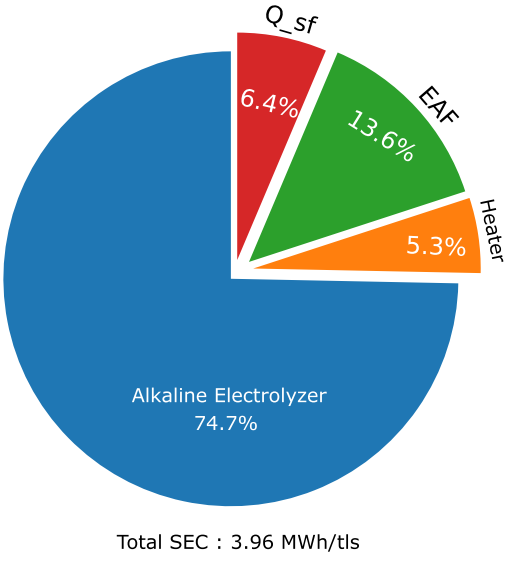

(b) Energy consumption of the electrolyser based H_2-SF-EAF system system

Fig. 2. (a) Energy consumption of the methane pyrolysis based H_2-SF-EAF system system. (b) Energy consumption of the electrolyser based H_2-SF-EAF system system.

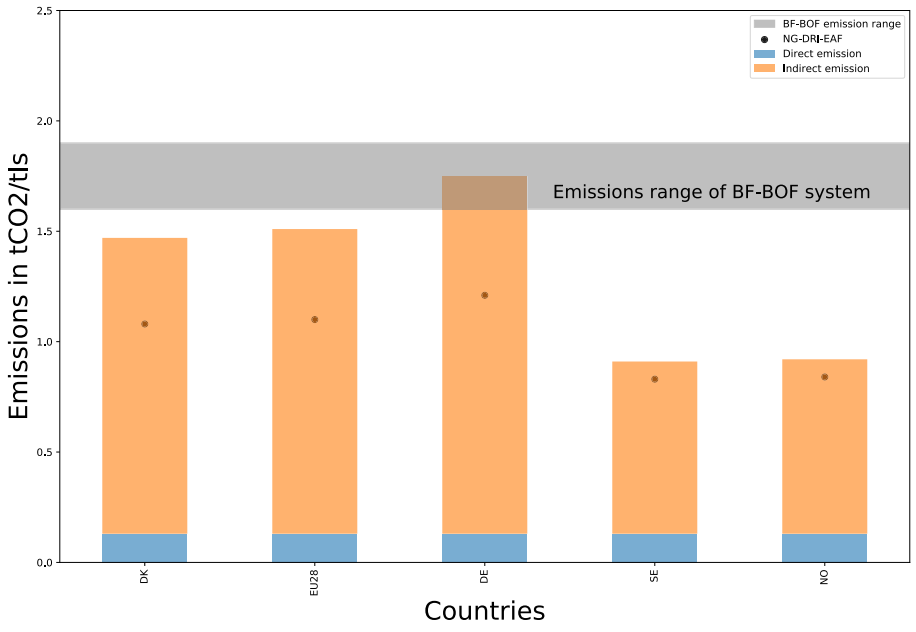

(a)

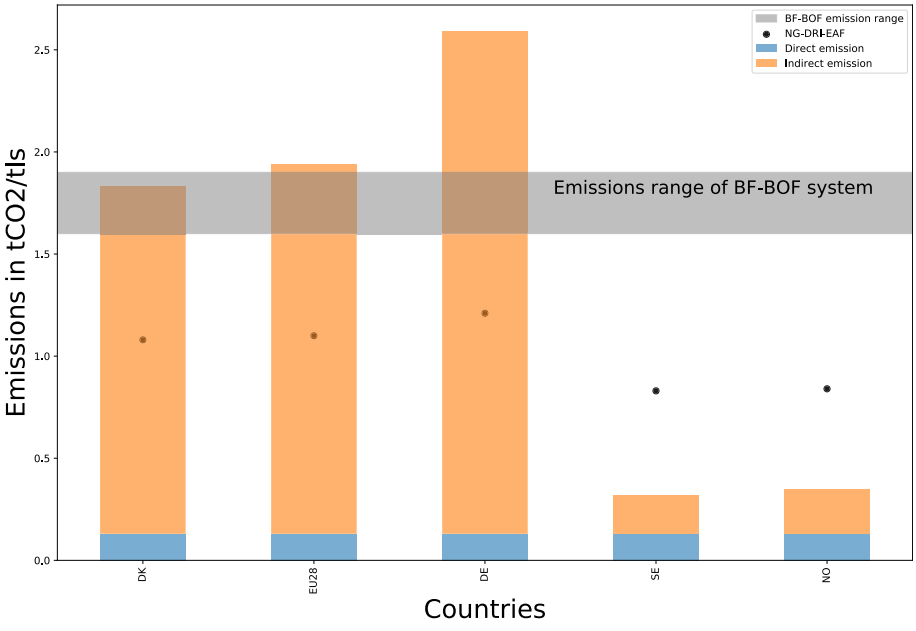

(b)

Fig. 3. (a) Direct and indirect emissions from the methane pyrolysis based H_2-SF-EAF system. (b) Direct and indirect emissions from the electrolysis based H_2-SF-EAF system. The grey band on the top of chart depicts the range of emissions from BF-BOF based steel production. The black dots represent the total emissions a NG-reformer based DRI-EAF system.

an energy consumption of 3.65 MWh/tls at lower heating value of 48 MJ/kg of CH_4. The SEC of a NG-reformer based DRI-EAF system is much lower at 3.26 MWh/tls [16].

The water electrolysis based H_2-SF-EAF system system has an SEC of 3.96 MWh/tls, at an electrolyser efficiency of 50 KWh/kgH_2. Electrolysers consume 2.96 MWh/tls or 74.7% of the total electricity. The H_2stream, exiting the electrolyser is pre-heated by exchanging heat with the SF exhaust gases. It exits the heat exchanger at a 448 K. The H_2 stream is subsequently heated to the reactor temperature of 1173 K °C in an electrical heater consuming 0.211 MWh/tls of electricity ($\eta = 0.85$. In the literature, the SEC value of comparable systems vary from 3.48 MWh/tls [30,17] to 3.95 MWh/tls [31]. The difference in the SEC's originate from the use of different values of electrolyser efficiency (depends on the projected installation year of the plant), use of scrap in the EAF, thermal energy requirements of the shaft-furnace, purge-gas requirements etc. The energy consumption of the different components for both scenarios is depicted in Fig. 2a, and Fig. 2.

4.3. Emissions

4.3.1. Direct emissions

Direct emissions of 129.4 kgCO_2/tls have been considered for both scenarios, which are related to CO_2 emissions from the EAF. The EAF emissions originate from the use of carbon fines, graphite electrodes and

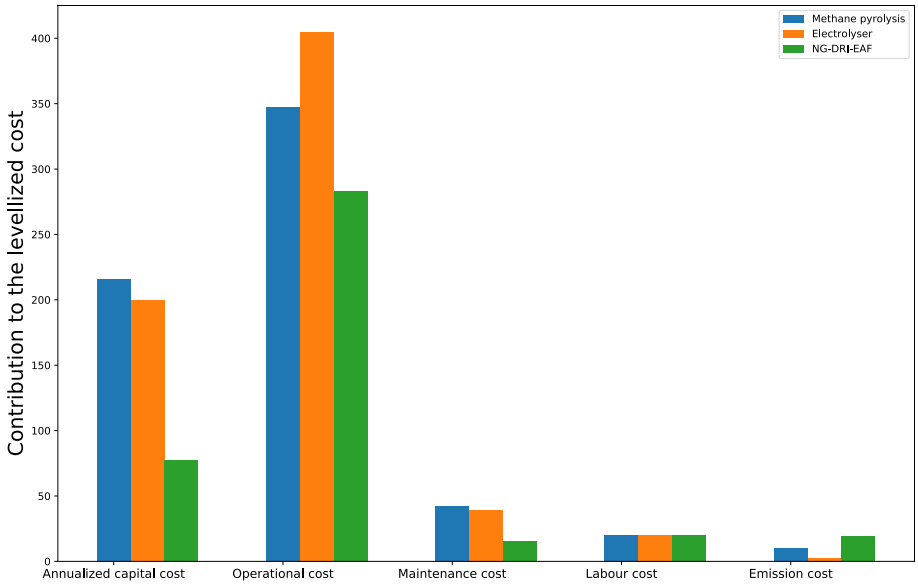

Fig. 4. Breakup of levellized cost of production of steel for both scenarios. The costs are compared with an NG reformer based DRI-EAF based system, operating under similar conditions.

the production of lime.

4.3.2. Indirect emissions

The indirect emissions are related to the use of electricity and natural gas. The pellet making process accounts for the release of 120 $kgCO_2$/tls of emissions. In the HYBRIT project, new production methods are being developed to decarbonise the pellet making process [17]. An upstream emission of 17 gCO_2/MJ has been considered for natural gas, taking into account the fugitive emissions caused by production, transport and distribution of natural gas [80]. Indirect emissions associated with electricity use are dependent on the electricity mix of the region, and is represented by the grid emission factor (GEF) [81].

4.3.3. Total emissions

The total emissions were calculated as the sum of the direct and indirect emissions. Considering a GEF of 412 $kgCO_2$/MWh, corresponding to the GEF of EU-28 [81]. The total emissions in scenario one were 0.90 tCO_2/tls. The value is comparable to the emissions of 0.98 tCO_2/tls from a reforming based NG-DRI-EAF system. More natural gas is consumed in the LMBR, for the production of reducing agent (H_2) resulting in a higher amount of indirect upstream emissions. The impact of variation in the GEF on emissions for LMBR system is depicted in Fig. 3a.

The total emissions from the electrolyser based H_2-SF-EAF system system were found to be 1.93 tCO_2/tls. In countries with cleaner electricity mix, the total emissions for electrolyser based H_2-SF-EAF system system were found to be much lower than NG-reformer based DRI-EAF systems. If electricity is supplied from renewable energy generators, the total emissions in the second scenario could be much lower, as can be seen in Fig. 3b from the lower emissions in Norway and Sweden.

4.4. Economic analysis

The methane pyrolysis based system has a lower LCOP of 631 $/t, compared to the LCOP of 669 $/t for the electrolyser based H_2-SF-EAF system. The LCOP value is at the higher end of values reported in the literature, as we have considered first-of-its kind plants, resulting in higher capital costs [30,31]. Additionally, we have considered maintenance, labour and emission costs in LCOP calculations, which were not included in the previous studies. The NG reformer based DRI-EAF system has a much lower LCOP of 414 $/t. The break-up of the LCOP is presented in Fig. 4. The annual operational costs contribute to more than 50% of the production costs in all three scenarios. Annualized capital costs have a significant contribution to the LCOP of methane pyrolysis based system. Compared to the low-carbon steel production routes, emission costs have the highest impact on the production costs of the NG reformer based DRI-EAF system. In a carbon constrained world, rising emission prices could increase production costs significantly for the NG reformer based DRI-EAF systems.

4.5. Discounted cash flow analysis

A discounted cash flow analysis was conducted for both the scenarios, under the economical assumptions presented in Table 2 and Table 3. The NPV was $1.07 billion for the first scenario, and $-5 million in the second scenario. At 10.01 %, the IRR of the methane pyrolysis based steelmaking unit was higher than the discount rate of 8%. The IRR of the electrolyser based H_2-SF-EAF system based steelmaking unit was found to be 7.98 %. A NG reformer based DRI-EAF system operating under the same conditions was found to have an NPV of $5.9 billion, and an IRR of 33.1%.

4.5.1. Local sensitivity analysis

The results of the local sensitivity analysis reveal that the NPV of the methane pyrolysis based H_2-SF-EAF system system are highly sensitive to changes in the carbon steel price and discount rate. The IRR of the system is sensitive to the carbon steel price, and the iron ore costs. The other significant factors are the electricity prices, and the natural gas price. The NPV and IRR of the electrolyser based H_2-SF-EAF system system are sensitive to changes in the carbon steel price, electricity cost, and the electrolyser efficiency. The results of the sensitivity analysis are presented in Fig. 5a, 5b, 6a, and 6b.

4.5.2. Global sensitivity analysis

The results of the global sensitivity analysis in the form of first order Sobol indices, and total order Sobol indices are presented in Fig. 7a and Fig. 7b. The values of the second order Sobol indices were found to be insignificant, indicating weak interaction between the input variables. It can be inferred that the interest rate, and carbon steel price have maximum contribution to the variance of methane pyrolysis system's NPV. The variance in the IRR value of the methane pyrolysis system stems from the uncertainty in carbon steel price, electricity price, and the cost of emissions. Variations in electricity cost, and carbon steel price

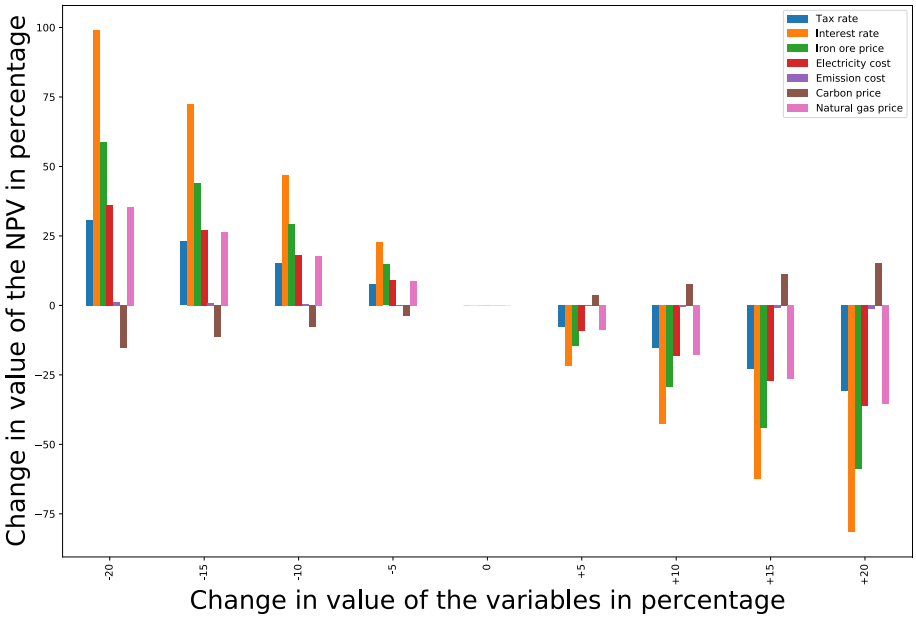

(a)

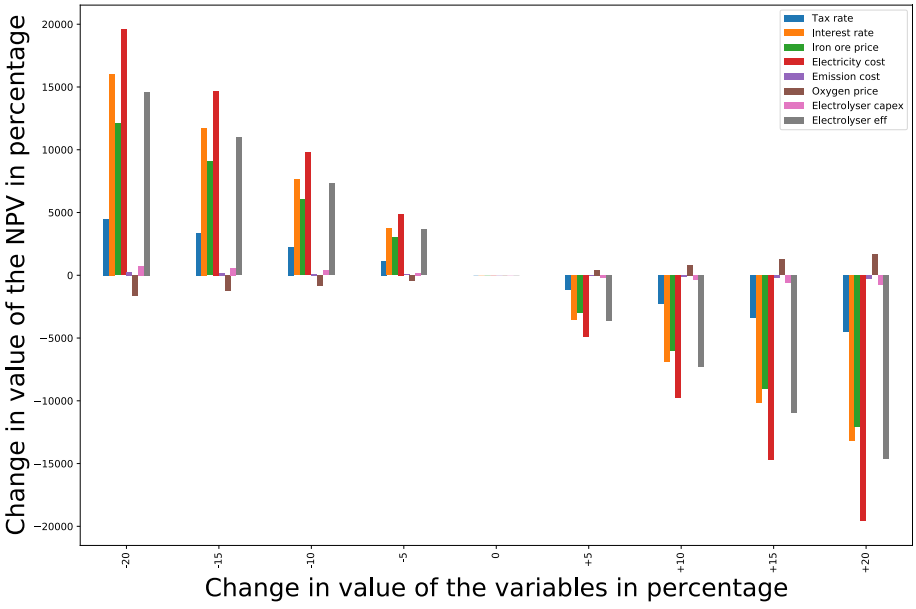

(b)

Fig. 5. The sensitivity of different parameters with NPV (a) Scenario one (b) Scenario two.

can be attributed with the maximum contribution to the variance in the NPV and IRR values of the electrolyser based system.

5. Discussion

Economic feasibility of the LMBR system is highly sensitive to the discount rate, owing to the higher capital costs of the system. The total capital cost of the methane pyrolysis based system was found to be $7.1 billion. LMBR system capex was $743 million and the H_2-SF-EAF system had a capex of $6.4 billion. Capital costs of the H_2-SF-EAF system steelmaking unit could reduce in the future as new plants are installed. The use of EAF for heating the LMBR has a major contribution to the LMBR capital costs. Tank-lined electric resistive heating elements made of silicon carbide could heat the reactor and lead to reduction in LMBR system costs [45]. The capital costs of the LMBR could be reduced by using a cheaper heat-transfer metal, or by using catalytic metals to lower the reaction temperature [82].

The operational costs of the electrolyser based system have the highest impact on the economic feasibility. The operational costs could be reduced by selecting regions with low electricity prices for installation of the plant. Improvements in the electrolyser efficiency could also reduce the operational costs. Using solid oxide electroysers (SOEC) for H_2 generation could reduce the electricity consumption, by utilizing heat from the shaft-furnace exhaust gases for steam generation [31]. Waste heat recovery from the EAF exhaust gases to heat the iron ore pellets could reduce the energy consumption, as they leave the EAF at 1773 K. Integration of renewable generators, with optimally sized electrolysers, and H_2 storage could allow the use of cheap renewable electricity for steelmaking [83]. Additional revenue generated by providing demand-response services to the electricity grid could also

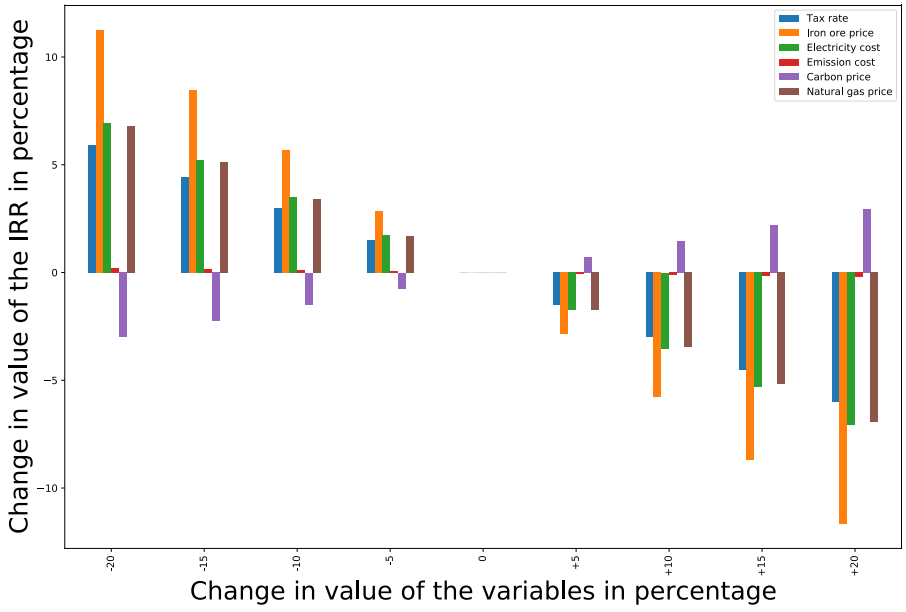

(a)

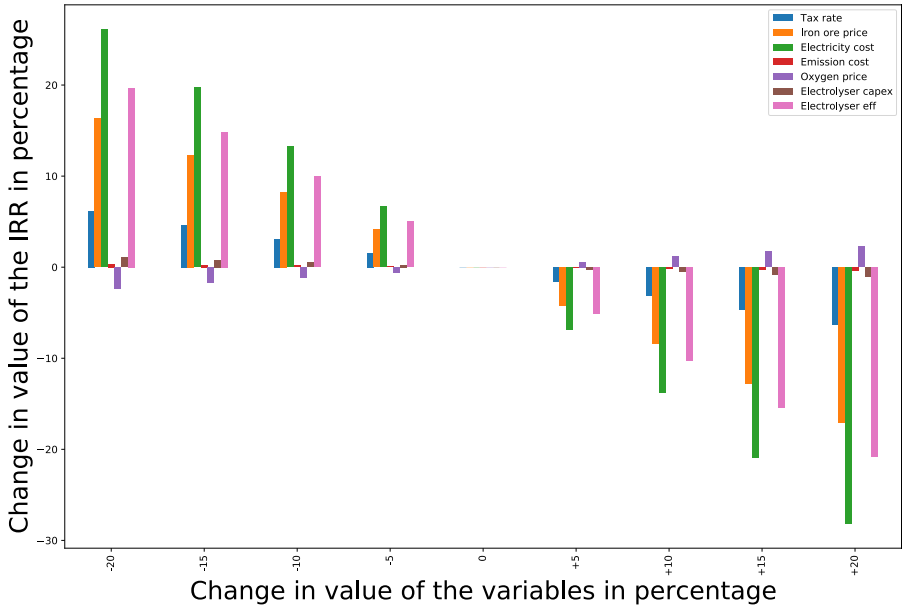

(b)

Fig. 6. The sensitivity of different parameters with IRR (a) Scenario one (b) Scenario two.

lower the cost of operation of the plants in the future by producing and storing large quantities of H_2 during times of low-electricity prices. However, availability of geological storage in close proximity to the steel production facilities is integral to leveraging the variations in the electricity prices as other storage alternatives are quite expensive.

6. Conclusion

A techno-economic assessment was conducted to evaluate the viability of integrating methane pyrolysis for H_2-SF-EAF system based low-carbon steel production. The assessment was conducted under two scenarios, and the results were compared. In the first scenario, hydrogen is produced by methane pyrolysis in a liquid metal bubble column reactor, and by low- temperature water electrolysis in the second scenario. The analysis was conducted from an investor's perspective for first-of-its-kind plants, leading to higher capital costs. In scenario one, the specific energy consumption was 5.15 MWh/tls, comprising of 1.37 MWh/tls of electricity, and 3.65 MWh/tls of natural gas consumption. In scenario two, 3.96 MWh/tls of electricity was consumed. The direct emission in both cases were found to be 128 kg/tls. Total emissions for electrolyser based steel production were found to be lower in regions with a cleaner electricity mix. The levellized costs of production were found to be $659 and $651 respectively, which are higher than the production costs from a reformer based NG-DRI-EAF system. The main results of the techno-economic assessment are presented in Table 6.

Integrating methane pyrolysis with an H_2-SF-EAF system system is techno-economically feasible and could play an important role in decarbonising steel production in the short and medium term. The authors recommend the development of a consortium of steel companies, natural gas companies, researchers, and universities to further develop

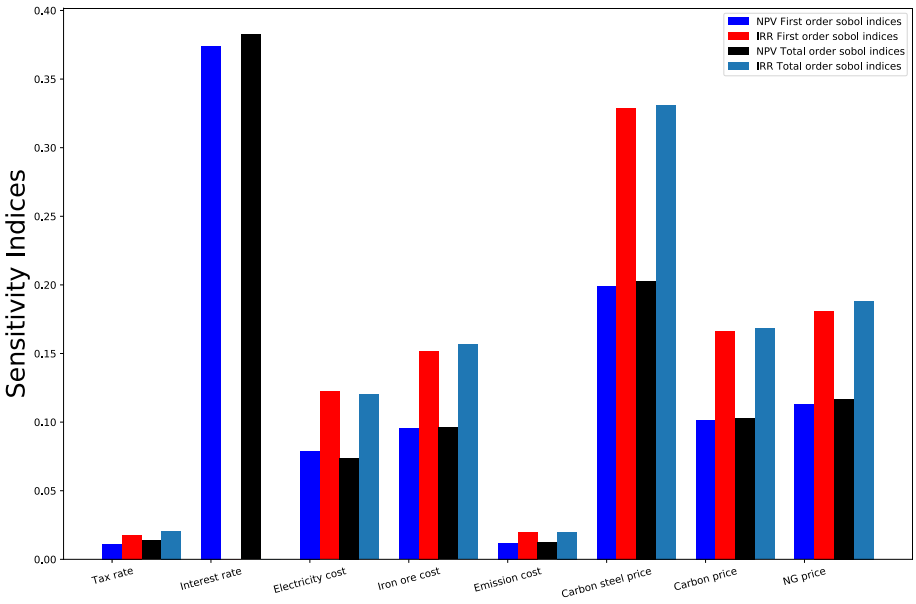

(a)

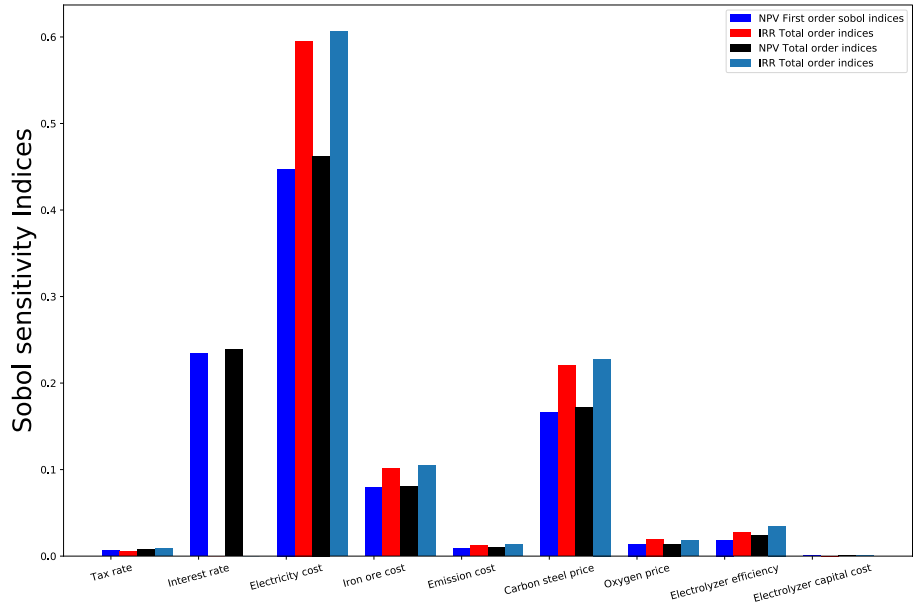

(b)

Fig. 7. (a) First order and total order Sobol indices calculated to quantify the uncertainty propagation in NPV and IRR values of the methane pyrolysis based H_2-SF-EAF system system. (b) First order and total order Sobol indices calculated to quantity the uncertainty propagation in NPV and IRR values of the water electrolyser based H_2-SF-EAF system system.

Table 6
Results from the techno-economic assessment analysis.

	SEC	Direct Emissions	CAPEX	OPEX	LCOP	NPV	IRR
Units	MWh/tls	$KgCO_2$/tls	$ Billion	$ Billion	$	$ Billion	%
LMBR-H_2-SF-EAF	5.16	129.42	7.15	1.17	631	1.07	10.09
Electrolyser-H_2-SF-EAF	3.96	129.42	6.6	1.38	669	−0.005	7.98
NG-DRI-EAF	3.26	541	2.56	0.95	414	5.9	33.1

the technology, especially in regions with access to cheap natural gas and clean grid electricity.

Data availability

The software codes developed for the analysis are hosted on Zenodo. The model is written in the Python programming language [79].

CRediT authorship contribution statement

Abhinav Bhaskar: Conceptualization, Methodology, Software, Writing - original draft, Visualization. **Mohsen Assadi:** Supervision, Validation. **Homam Nikpey Somehsaraei:** Supervision, Validation.

Declaration of Competing Interest

The authors declare that they have no known competing financial interests or personal relationships that could have appeared to influence the work reported in this paper.

Acknowledgement

This project has received funding from the European Union's Horizon 2020 research and innovation programme under the Marie Skłodowska-Curie grant agreement No 765515.

References

[1] IPCC. IPCC 2018: Summary for Policymakers. In: Global Warming of 1.5C. An IPCC Special Report on the impacts of global warming of 1.5C above pre-industrial levels and related global greenhouse gas emission pathways, in the context of strengthening the global, Tech. rep., IPCC; 2018.
[2] Flores-Granobles M, Saeys M. Minimizing CO_2 emissions with renewable energy: a comparative study of emerging technologies in the steel industry. Energy Environ Sci.https://doi.org/10.1039/d0ee00787k.
[3] M. Fischedick, J. Roy, A. Abdel-Aziz, A. Acquaye, J. M. Allwood, J.-p. Ceron, Y. Geng, H. Kheshgi, A. Lanza, D. Perczyk, L. Price, E. Santalla, C. Sheinbaum, K. Tanaka, Industry, Tech. rep., IPCC (2014).
[4] International Energy Agency. Iron and Steel Technology roadmap: Towards more sustainable steelmaking, Tech. rep., International energy agency; 2020. URL www.iea.org.
[5] Patisson F, Mirgaux O. Hydrogen ironmaking: how it works. Metals 2020;10(7):1–15. https://doi.org/10.3390/met10070922.
[6] Birat J-P. Society, Materials, and the Environment: The Case of Steel. Metals 2020;10(3):331. https://doi.org/10.3390/met10030331.
[7] Sarkar S, Bhattacharya R, Roy GG, Sen PK. Modeling MIDREX Based Process Configurations for Energy and Emission Analysis. Steel Research International, 89; 2018. p. 1700248. https://doi.org/10.1002/srin.201700248.
[8] Arens M, Worrell E, Eichhammer W, Hasanbeigi A, Zhang Q. Pathways to a low-carbon iron and steel industry in the medium-term – the case of Germany. J Clean Prod 2017;163:84–98. https://doi.org/10.1016/J.JCLEPRO.2015.12.097.
[9] Quader MA, Ahmed S, Ghazilla RAR, Ahmed S, Dahari M. A comprehensive review on energy efficient CO2 breakthrough technologies for sustainable green iron and steel manufacturing. Renew Sustain Energy Rev 2015;50(October):594–614. https://doi.org/10.1016/j.rser.2015.05.026.
[10] Fischedick M, Marzinkowski J, Winzer P, Weigel M. Techno-economic evaluation of innovative steel production technologies. J Clean Prod 2014;84(1):563–80. https://doi.org/10.1016/j.jclepro.2014.05.063.
[11] M. Weigel, M. Fischedick, J. Marzinkowski, P. Winzer, Multicriteria analysis of primary steelmaking technologies, Journal of Cleaner Production 112 (May 2013) (2016) 1064–1076. doi:10.1016/j.jclepro.2015.07.132.
[12] Toktarova A, Karlsson I, Rootzén J, Göransson L, Odenberger M, Johnsson F. Pathways for Low-Carbon Transition of the Steel Industry—A Swedish Case Study. Energies 13 (15).https://doi.org/10.3390/en13153840.
[13] Lopes DV, Ivanova YA, Kovalevsky AV, Sarabando AR, Frade JR, Quina MJ. Electrochemical reduction of hematite-based ceramics in alkaline medium: challenges in electrode design. Electrochim Acta 2019;327:135060. https://doi.org/10.1016/j.electacta.2019.135060.
[14] Nuber D, Eichberger H, Rollinger B. Circored fine ore direct reduction, Millenium steel 2006. URL http://millennium-steel.com/wp-content/uploads/articles/pdf/2006/pp37-40 MS06.pdf http://millennium-steel.com/wp-content/uploads/articles/pdf/2006/pp37-40 MS06.pdf.
[15] Elmquist H, Weber SA, Eichberger P. Operational results of the Circored fine ore direct reduction plant in Trinidad, STAHL UND EISEN (2002) 59–64 doi:0340-4803.
[16] Duarte P. Hydrogen-based steelmaking, Tech. rep., TenovaHYL; 2015. URLhttps://www.millennium-steel.com/wp-content/uploads/2019/05/MS2019-22-MS19-16.pdf.
[17] Pei M, Petäjäniemi M, Regnell A, Wijk O. Toward a fossil free future with hybrit: Development of iron and steelmaking technology in Sweden and Finland. Metals 2020;10(7):1–11. https://doi.org/10.3390/met10070972.
[18] Karakaya E, Nuur C, Assbring L. Potential transitions in the iron and steel industry in Sweden: Towards a hydrogen-based future? J Clean Prod 2018;195:651–63. https://doi.org/10.1016/j.jclepro.2018.05.142.
[19] Keys A, Van Hout M, Daniëls B. Decarbonisation options for the dutch steel industry. PBL Netherlands Environmental Assessment Agency 2019. Tech. Rep. november, URL www.pbl.nl/en.
[20] Langner LL, Arne, ArcelorMittal commissions Midrex to design demonstration plant for hydrogen steel production in Hamburg; 2019.https://corporate.arcelormittal.com/news-and-media/news/2019/sep/16-09-2019.
[21] Posdziech O, Schwarze K, Brabandt J. Efficient hydrogen production for industry and electricity storage via high-temperature electrolysis. Int J Hydrogen Energy 2019;4:19089–101. https://doi.org/10.1016/j.ijhydene.2018.05.169.
[22] Thyssenkrupp. World first in Duisburg as NRW economics minister Pinkwart launches tests at thyssenkrupp into blast furnace use of hydrogen; 2019.https://www.thyssenkrupp-steel.com/en/newsroom/press-releases/world-first-in-duisburg.html.
[23] ArcelorMittal. World first for steel: ArcelorMittal investigates the industrial use of pure hydrogen – ArcelorMittal; 2019. URLhttps://corporate.arcelormittal.com/news-and-media/news/2019/mar/28-03-2019.
[24] European Commission (EC), A hydrogen strategy for a climate-neutral Europe, Tech. rep., European commission, Brussels; 2020.
[25] Rechberger K, Spanlang A, Sasiain Conde A, Wolfmeir H, Harris C. Green Hydrogen-Based Direct Reduction for Low-Carbon Steelmaking, Steel Res Int 91 (11).https://doi.org/10.1002/srin.202000110.
[26] Whitmarsh L, Xenias D, Jones CR. Framing effects on public support for carbon capture and storage. Palgrave Commun 5(1).https://doi.org/10.1057/s41599-019-0217-x.
[27] Keipi T, Tolvanen H, Konttinen J. Economic analysis of hydrogen production by methane thermal decomposition: Comparison to competing technologies. Energy Convers Manage 2018;159(January):264–73. https://doi.org/10.1016/j.enconman.2017.12.063.
[28] Weger L, Abánades A, Butler T. Methane cracking as a bridge technology to the hydrogen economy. Int J Hydrogen Energy 2017;42(1):720–31. https://doi.org/10.1016/J.IJHYDENE.2016.11.029.
[29] Parkinson B, Balcombe P, Speirs JF, Hawkes AD, Hellgardt K. Levelized cost of CO_2 mitigation from hydrogen production routes. Energy Environ Sci 2019;12(1):19–40. https://doi.org/10.1039/c8ee02079e.
[30] Vogl V, Åhman M, Nilsson LJ. Assessment of hydrogen direct reduction for fossil-free steelmaking. J Clean Prod 2018;203:736–45. https://doi.org/10.1016/j.jclepro.2018.08.279.
[31] Krüger A, Andersson J, Grönkvist S, Cornell A. Integration of water electrolysis for fossil-free steel production. Int J Hydrogen Energyhttps://doi.org/10.1016/j.ijhydene.2020.08.116.
[32] Andersson J, Krüger A, Grönkvist S. Methanol as a carrier of hydrogen and carbon in fossil-free production of direct reduced iron. Energy Convers Manage: X 2020;7 (April):100051. https://doi.org/10.1016/j.ecmx.2020.100051.
[33] Wang IW, Kutteri DA, Gao B, Tian H, Hu J. Methane Pyrolysis for Carbon Nanotubes and COx -Free H2 over Transition-Metal Catalysts. Energy Fuels 2019;33(1):197–205. https://doi.org/10.1021/acs.energyfuels.8b03502.
[34] Monolith Materials, Monolith Materials: Olive Creek Plant; 2019. URLhttps://monolithmaterials.com/olive-creek/.
[35] M. Materials, Monolith plans carbon free ammonia plant.https://monolithmaterials.com/news/monolith-plans-carbon-free-ammonia-production-plant.
[36] Abbas HF, Wan Daud WMA. Hydrogen production by methane decomposition: a review. Int J Hydrogen Energy 2010;35(3):1160–90. https://doi.org/10.1016/j.ijhydene.2009.11.036.
[37] D. C. Upham, V. Agarwal, A. Khechfe, Z. R. Snodgrass, M. J. Gordon, H. Metiu, E. W. McFarland, Catalytic molten metals for the direct conversion of methane to

hydrogen and separable carbon, Science 358 (6365). doi:10.1126/science.aao5023.
[38] Parkinson B, Tabatabaei M, Upham DC, Ballinger B, Greig C, Smart S, McFarland E. Hydrogen production using methane: Techno-economics of decarbonizing fuels and chemicals. Int J Hydrogen Energy 2018;43(5):2540–55. https://doi.org/10.1016/j.ijhydene.2017.12.081.
[39] Abánades A, Rathnam RK, Geißler T, Heinzel A, Mehravaran K, Müller G, Plevan M, Rubbia C, Salmieri D, Stoppel L, Stückrad S, Weisenburger A, Wenninger H, Wetzel T. Development of methane decarbonisation based on liquid metal technology for CO2-free production of hydrogen. Int J Hydrogen Energy 2016;41(19):8159–67. https://doi.org/10.1016/j.ijhydene.2015.11.164.
[40] Palmer C, Tarazkar M, Kristoffersen HH, Gelinas J, Gordon MJ, McFarland EW, Metiu H. Methane Pyrolysis with a Molten Cu-Bi Alloy Catalyst, ACS Catal 9 (9). https://doi.org/10.1021/acscatal.9b01833.
[41] Serban M, Lewis MA, Marshall CL, Doctor RD. Hydrogen production by direct contact pyrolysis of natural gas. Energy Fuels 2003;17(3):705–13. https://doi.org/10.1021/ef020271q.
[42] Plevan M, Geißler T, Abánades A, Mehravaran K, Rathnam RK, Rubbia C, Salmieri D, Stoppel L, Stückrad S, Wetzel T. Thermal cracking of methane in a liquid metal bubble column reactor: experiments and kinetic analysis. Int J Hydrogen Energy 2015;40(25):8020–33. https://doi.org/10.1016/j.ijhydene.2015.04.062.
[43] Geißler T, Abánades A, Heinzel A, Mehravaran K, Müller G, Rathnam RK, Rubbia C, Salmieri D, Stoppel L, Stückrad S, Weisenburger A, Wenninger H, Wetzel T. Hydrogen production via methane pyrolysis in a liquid metal bubble column reactor with a packed bed. Chem Eng J 2016;299:192–200. https://doi.org/10.1016/j.cej.2016.04.066.
[44] Parkinson B, Matthews JW, McConnaughy TB, Upham DC, McFarland EW. Techno-economic analysis of methane pyrolysis in molten metals: decarbonizing natural gas. Chem Eng Technol 2017;40(6):1022–30. https://doi.org/10.1002/ceat.201600414.
[45] Von Wald GA, Masnadi MS, Upham DC, Brandt AR. Optimization-based technoeconomic analysis of molten-media methane pyrolysis for reducing industrial sector CO 2 emissions. Sustain Energy Fuels 2020;4(9):4598–613. https://doi.org/10.1039/D0SE00427H.
[46] U. MICHAELIS, Hydrogen from Natural Gas without CO2 Emissions; 2019. URL shorturl.at/jzBMS.
[47] Thomassen G, Van Dael M, Van Passel S, You F. How to assess the potential of emerging green technologies? Towards a prospective environmental and techno-economic assessment framework. Green Chem 2019;21(18):4868–86. https://doi.org/10.1039/c9gc02223f.
[48] E. Directorate-General for Internal Market, Industry, S. E. Commission), Masterplan for a competitive transformation of EU energy intensive industries enabling a climate-neutral, circular economy by 2050, Tech. rep., European commission; 2019.https://doi.org/10.2873/854920.
[49] Gielen D, Saygin D, Taibi E, Birat JP. Renewables-based decarbonization and relocation of iron and steel making: a case study. J Ind Ecol 2020;24(5):1113–25. https://doi.org/10.1111/jiec.12997.
[50] Rissman J, Bataille C, Masanet E, Aden N, Morrow WR, Zhou N, Elliott N, Dell R, Heeren N, Huckestein B, Cresko J, Miller SA, Roy J, Fennell P, Cremmins B, Koch Blank T, Hone D, Williams ED, de la Rue S, du Can B, Sisson M, Williams J, Katzenberger D, Burtraw G, Sethi H, Ping D, Danielson H, Lu T, Lorber J, Dinkel J Helseth. Technologies and policies to decarbonize global industry. Appl Energy 2020;266:114848. https://doi.org/10.1016/j.apenergy.2020.114848. Review and assessment of mitigation drivers through 2070.
[51] European Commission, Raw materials demand for wind and solar PV technologies in the transition towards a decarbonised energy system, Tech. rep., European commission; 2020.https://doi.org/10.2760/160859.
[52] IRENA. Global Renewables Outlook: Energy transformation 2050. Available at: https://www.irena.org/publications/2020/Apr/Global-Renewables-Outlook-2020, Tech. rep., International renewable energy agency; 2020.https://www.irena.org/publications/2020/Apr/Global-Renewables-Outlook-2020.
[53] Chase MW. NIST-JANAF thermochemical Tables, 4th ed., vol. 9, American Chemical Society; American institute of Physics for the National institute of standards and technology; 1998.
[54] Béchara R, Hamadeh H, Mirgaux O, Patisson F. Optimization of the iron ore direct reduction process through multiscale process modeling. Materials 2018;11(7):1094. https://doi.org/10.3390/ma11071094.
[55] Lu L, Pan J, Zhu D. Quality requirements of iron ore for iron production. In: Iron Ore, Elsevier; 2015. p. 475–504.https://doi.org/10.1016/B978-1-78242-156-6.00016-2.
[56] Wagner M. Thermal Analysis in Practice, Collected Applications Thermal Analysis.
[57] Spreitzer D, Schenk J. Reduction of iron oxides with hydrogen—a review. Steel Res Int 2019;90(10):1900108. https://doi.org/10.1002/srin.201900108.
[58] Shao L, Wang Q, Qu Y, Saxén H, Zou Z. A Numerical Study on the Operation of the H2 Shaft Furnace with Top Gas Recycling. Metall Mater Trans Bhttps://doi.org/10.1007/s11663-020-02020-6.
[59] Ranzani da Costa A, Wagner D, Patisson F. Modelling a new, low CO2 emissions, hydrogen steelmaking process. J Clean Prod 2013;46:27–35. https://doi.org/10.1016/J.JCLEPRO.2012.07.045.
[60] Kawasaki E, Sanscrainte J, Walsh TJ. Kinetics of reduction of iron oxide with carbon monoxide and hydrogen. AIChE J 1962;8(1):48–52. https://doi.org/10.1002/aic.690080114.
[61] Midrex. MIDREX Hotlink process.https://www.kobelco.co.jp/english/products/ironunit/dri/dri04.html.
[62] Duarte P, Pauluzzi D. Premium Quality DRI Products from ENERGIRON; 2019. https://www.energiron.com/wp-content/uploads/2019/05/Premium-Quality-DRI-Products-from-ENERGIRON.pdf.
[63] Pfeifer H, Kirschen M. Thermodynamic analysis of EAF energy efficiency and comparison with a statical model of electric energy model of demand. Engineering 2003:1–16.
[64] Kirschen M, Badr K, Pfeifer H. Influence of direct reduced iron on the energy balance of the electric arc furnace in steel industry. Energy 2011;36(10):6146–55. https://doi.org/10.1016/j.energy.2011.07.050.
[65] Catalan LJ, Rezaei E. Coupled hydrodynamic and kinetic model of liquid metal bubble reactor for hydrogen production by noncatalytic thermal decomposition of methane. Int J Hydrogen Energy 2020;45(4):2486–503. https://doi.org/10.1016/j.ijhydene.2019.11.143.
[66] Oleinik KI, Bykov AS, Pastukhov EA. Refinement of the thermophysical properties of liquid tin at high temperatures. Russian Metallurgy (Metally) 2018;2018(2):110–3. https://doi.org/10.1134/S0036029518020143.
[67] Assael MJ, Kalyva AE, Antoniadis KD, Michael Banish R, Egry I, Wu J, Kaschnitz E, Wakeham WA. Reference data for the density and viscosity of liquid copper and liquid tin. J Phys Chem Ref Data 2010;39(3):1–8. https://doi.org/10.1063/1.3467496.
[68] Ho MT, Bustamante A, Wiley DE. Comparison of CO2 capture economics for iron and steel mills. Int J Greenhouse Gas Control 2013;19:145–59. https://doi.org/10.1016/j.ijggc.2013.08.003.
[69] Gavin Towler RS. Chemical Engineering Design. 2nd ed. Elsevier; 2013. https://doi.org/10.1016/C2009-0-61216-2.
[70] Cihlar J, Lejarreta AV, Wang A, Melgar F, Jens J, Rio P, van der Leun K. Hydrogen generation in Europe: Overview of costs and key benefits, Tech. rep., European Commission, Luxembourg; 2020.https://doi.org/10.2833/122757.
[71] OECD. Steel Market Developments Q2 2020, Tech. Rep. June, OECD; 2020. URLhttps://www.oecd.org/sti/ind/steel-market-developments-Q2-2020.pdf.
[72] European Commission. Composition and Drivers of Energy Prices and Costs in Energy Intensive Industries., Tech. Rep. January, Directorate general for internal Market,Industry, Entrepreneurship and SMEs; 2018.https://doi.org/10.2873/004141.
[73] Cavaliere P. Direct Reduced Iron: Most Efficient Technologies for Greenhouse Emissions Abatement. In: Clean Ironmaking and Steelmaking Processes. Cham: Springer International Publishing; 2019. p. 419–84. https://doi.org/10.1007/978-3-030-21209-4_8.
[74] E. commission. Report from the commission to the European parliament and the council, report on the functioning of the European carbon market, Tech. rep., European commission, Brussels; 2020.
[75] Saltelli A, Annoni P, Azzini I, Campolongo F, Ratto M, Tarantola S. Variance based sensitivity analysis of model output. Design and estimator for the total sensitivity index. Comput Phys Commun 2010;181(2):259–70. https://doi.org/10.1016/j.cpc.2009.09.018.
[76] Hamby DM. A review of techniques for parameter sensitivity analysis of environmental models. Environ Monit Assess 1994;32(2):135–54. https://doi.org/10.1007/BF00547132.
[77] Sobol I. Global sensitivity indices for non-linear mathematical models and their Monte carlo estimates. Math Comput Simul 2001;5(2):271–80.
[78] Herman J, Usher W. SALib: an open-source python library for sensitivity analysis. J Open Source Software 2017;2(9):97. https://doi.org/10.21105/joss.00097.
[79] Bhaskar A. Material and energy balance model of the H-SF-EAF system using methane pyrolysis and water electrolysis; 2020.https://doi.org/10.5281/zenodo.4504841.
[80] Timmerberg S, Kaltschmitt M, Finkbeiner M. Hydrogen and hydrogen-derived fuels through methane decomposition of natural gas – GHG emissions and costs. Energy Convers Manage: X 2020;7(April):100043. https://doi.org/10.1016/j.ecmx.2020.100043.
[81] Moro A, Lonza L. Electricity carbon intensity in European Member States: Impacts on GHG emissions of electric vehicles, Transp Res Part D: Transp Environ 64 (July 2017) (2018) 5–14.https://doi.org/10.1016/j.trd.2017.07.012.
[82] Palmer C, Upham DC, Smart S, Gordon MJ, Metiu H, McFarland EW. Dry reforming of methane catalysed by molten metal alloys. Nat Catal 2020;3(1):83–9. https://doi.org/10.1038/s41929-019-0416-2.
[83] Mallapragada DS, Gençer E, Insinger P, Keith DW, O'Sullivan FM. Can industrial-scale solar hydrogen supplied from commodity technologies be cost competitive by 2030? Cell Reports Physical Science 2020:100174. https://doi.org/10.1016/j.xcrp.2020.100174.

3. Abhinav Bhaskar, Rockey Abhishek, Mohsen Assadi, Homam Nikpey Somehesaraei, Decarbonizing primary steel production : Techno-economic assessment of a hydrogen based green steel production plant in Norway, Journal of Cleaner Production, Volume 350, 2022, 131339, ISSN 0959-6526,
https://doi.org/10.1016/j.jclepro.2022.131339

Journal of Cleaner Production 350 (2022) 131339

Contents lists available at ScienceDirect

Journal of Cleaner Production

journal homepage: www.elsevier.com/locate/jclepro

Decarbonizing primary steel production : Techno-economic assessment of a hydrogen based green steel production plant in Norway

Abhinav Bhaskar *, Rockey Abhishek, Mohsen Assadi, Homam Nikpey Somehesaraei

University of Stavanger, 4036, Norway

ARTICLE INFO

Handling Editor: Kathleen Aviso

Keywords:
Industrial decarbonization
Hydrogen direct reduction
Water electrolysis
Green steel
Climate change
Norway
Optimization
Day ahead electricity market

ABSTRACT

High electricity cost is the biggest challenge faced by the steel industry in transitioning to hydrogen based steelmaking. A steel plant in Norway could have access to cheap, emission free electricity, high-quality iron ore, skilled manpower, and the European market. An open-source model for conducting techno-economic assessment of a hydrogen based steel manufacturing plant, operating in Norway has been developed in this work. Levelized cost of production (LCOP) for two plant configurations; one procuring electricity at a fixed price, and the other procuring electricity from the day-ahead electricity markets, with different electrolyzer capacity were analyzed. LCOP varied from $622/tls to $722/tls for the different plant configurations. Procuring electricity from the day-ahead electricity markets could reduce the LCOP by 15%. Increasing the electrolyzer capacity reduced the operational costs, but increased the capital investments, reducing the overall advantage. Sensitivity analysis revealed that electricity price and iron ore price are the major contributors to uncertainty for configurations with fixed electricity prices. For configurations with higher electrolyzer capacity, changes in the iron ore price and parameters related to capital investment were found to affect the LCOP significantly.

1. Introduction

The Inter-governmental panel on climate change(IPCC) has estimated that the total human contribution to global surface temperature increase is in the range of 0.8 °C–1.3 °C, with a best estimate of 1.07 °C (V et al., 2021). The evidence for human-induced climate change affecting the extreme weather events such as heatwaves, heavy precipitation, droughts, tropical cyclones, and in particular their attribution to human influence has strengthened. High concentration of greenhouse gases such as carbon dioxide, methane, nitrous and nitrogen oxides, halogenated gases and volatile organic compounds in the atmosphere are the main contributors to the increased radiative forcing and consequent rise in global mean surface temperatures. Rapid decarbonization of all sectors of the economy is imperative to limit the global mean surface temperature increase to 1.5 °C by the end of the century (Fischedick et al., 2014).

Approximately 1.86 billion tonnes of crude steel were produced in 2019 (Worldsteel, 2020). Production of 1.34 billion tons of steel, with an average emission of 1.8 tCO_2/tls, contributed 2.4 $GtCO_2$ emissions in 2019, which corresponds to 7% of the global energy related CO_2 emissions (IEA, 2021). While improved material efficiency, product service life extension, increased share of recycling and material substitution are viable measures to reduce steel demand, and hence the associated emissions, steel demand is likely to increase in the short and medium term (IEA, 2020). Incremental efficiency improvements are likely to contribute to emission reduction but would not be sufficient in meeting the emission reduction targets required to meet the goals of the Paris climate agreement (Rissman et al., 2020).

Introduction of alternative production technologies with zero carbon-footprint would be essential to decarbonize the iron and steel sector (Åhman et al., 2018). Mitigation technologies can be broadly divided in carbon capture utilization and storage or carbon direct avoidance technologies. The former aim to capture the CO_2, and either utilize it, or store it in geological reservoirs. Portho et al. identified three main alternatives for the utilization of off-gases in the steelmaking plant i.e. use for thermal energy, recovery of valuable compounds for selling and the synthesis of a high-added value product (Uribe-Soto et al., 2017). Through the Carbon2chem project, thyssenkrupp aims to use the top gases from the blast furnace at Duisburg, Germany to produce value added chemicals like methanol and higher alcohols (Wich et al., 2020). The project consortium includes chemical companies and industrial research institutes. Arcelor Mittal, another leading steel manufacturer aims to use the off-gases produced at its steel plant in Ghent, Belgium to produce 63,000 tonnes of ethanol per year (Birat, 2020).

With carbon direct avoidance technologies, the focus has been on technologies which can replace coke as the reducing agent (Fischedick

* Corresponding author.
E-mail address: abhinav.bhaskar@uis.no (A. Bhaskar).

https://doi.org/10.1016/j.jclepro.2022.131339
Received 27 September 2021; Received in revised form 8 March 2022; Accepted 11 March 2022
Available online 25 March 2022

et al., 2014). While a combination of CO and H_2 have been used since the 1970's for the direct reduction of iron ore, there has been interest in the use of electricity for reducing iron oxide, similar to the electrolysis of Alumina. Both high-temperature and low-temperature electrolysis pathways are being explored, but are currently at low technology readiness levels, and are constrained by the use of expensive catalysts (Bailera et al., 2021).

Hydrogen can replace coke as a reducing agent in a hydrogen direct reduction shaft furnace (H_2-SF) (da Costa et al., 2013). The resulting direct reduced iron (DRI) can be fed to an electric arc furnace (EAF) for the production of emission free steel. Weigel et al. (2016) conducted a multi-criteria analysis of four mitigation technologies, and found H_2-SF-EAF route for primary steel production to be the most competitive. Use of hydrogen in existing blast furnaces has also been studied by some researchers. Suer et al. (2021) analyzed the injection of natural gas or hydrogen into a blast furnace, addition of hot briquetted iron (HBI) into the blast furnace produced from direct reduction of iron ore using natural gas-based and use of 100% hydrogen in BF. Their analysis revealed that the use of HBI into a blast furnace is a reasonable way to reduce emissions in the short and medium term, and will allow the creation of the hydrogen market till the metallurgical challenges of H_2-SF-EAF based method are completely resolved. Vogl et al. (2018) conducted techno-economic assessment of a H_2-SF-EAF system powered by grid electricity, and found that hydrogen based steel production could be cost competitive with a BF-BOF based plant at an emission price in the range of €34 to €68/tCO_2, and at an electricity price of €40/MWh. Krüger et al. (2020) studied the integration of low and high temperature electrolyzers with the H_2-SF-EAF process, and found that high temperature electrolyzers could lower the specific energy consumption. Jacobasch et al. (2021) evaluated the economic feasibility of a hydrogen direct reduction steel plant, and calculated the carbon mitigation cost. Hydrogen production from three different electrolyzer technologies i.e. alkaline, proton electron membrane and solid oxide electrolysis was considered. They calculated the CO_2 mitigation cost to be 89 €/t. To alleviate the problems of storing large quantities of hydrogen, where geological storage sites are hard to find, hydrogen carriers could be used. Andersson (2021) evaluated the integration of four different hydrogen carriers for in the steelmaking process. They were compared based on their thermodynamic and economic data to estimate operational and capital costs. Methanol was found to be the most promising alternative.

Steel manufacturers have announced multiple projects to explore the technical and commercial feasibility of hydrogen based steelmaking. Under the HYBRIT project in Sweden, various aspects of the hydrogen based steelmaking's value chain are being tested. A pilot plant running on 100% hydrogen as reducing gas was commissioned in August, 2020 (Pei et al., 2020). Other aspects of the value chain such as hydrogen storage in rock caverns, production of emission free pellets etc. are also being explored. A hydrogen-based fine-ore reduction (HYFOR) pilot plant developed by Primetals Technologies was commissioned in Donawitz, Austria in April, 2021. The HYFOR technology could enable the use of iron ore fines in the direct reduction process, which could reduce the operatiing costs (Primemetals, 2022). Green steel tracker is an open-source database to track the recent development in the decarbonization of the iron and steel industry (Vogl et al., 2021b). The project database shows that hydrogen based steelmaking is increasingly becoming the technology of choice for decarbonizing, among the largest steelmakers i.e. Baowu steel, Arcelor Mittal, thyssenkrupp, Tata steel, Posco etc. New entrants in the steel sector, such as H2green steel in Sweden, plan to use hydrogen based steelmaking. It has plans to produce five million tons of green steel by 2030 (Vogl et al., 2021a).

1.1. Research context

Approximately 60 kg of hydrogen is required for the production of one ton of steel (Bhaskar et al., 2021). Hydrogen is currently produced from fossil fuels, which results in significant emissions (Howarth and Jacobson, 2021). In order to use hydrogen for decarbonizing the industry, zero emission hydrogen production technologies such as water electrolysis need to be considered. Water electrolysis is an energy intensive process, and availability of low cost electricity is a necessary condition for producing cost competitive H_2-SF-EAF based steel. This creates an opportunity to produce hydrogen at locations with low electricity prices, and high renewable energy potential (IRENA, 2022). Gielen et al. found that the relocation of iron and steel industry to regions with high renewable potential could increase renewable energy deployment, and create more value through sustainable industrial activities in resource-rich countries (Gielen et al., 2020). Bataille et al. analyzed the economic feasibility of producing Hydrogen based DRI in South Africa, and found that primary iron production with hydrogen could increase value added from local iron ore and solar energy resources, increase exports and initiate transformation to a more sustainable industry (Trollip et al., 2022).

Norway has one of the lowest wholesale electricity price and energy tax rates in Europe, and has a low grid emission factor, as majority of the electricity is supplied by hydroelectric power plants (Moro and Lonza, 2018). Many energy intensive manufacturing industries such as paper and pulp, ferro-alloys and non-ferrous metals (Aluminum) are operational in Norway. Almost one-third of Norway's total electricity was used by energy intensive industries in 2019. More than 60% of the industrial electricity demand came from the Aluminum industry (Norway, 2021). More recently, low-electricity prices, and high-renewable energy potential of Norway is being leveraged by the ammonia producers to reduce emissions from the ammonia value chain. A collaborative project between Yara, Aker Clean Hydrogen and Statkraft called HEGRA has been announced recently (YARA, 2021). Hydrogen will be produced from water electrolysis, and will decarbonize Yara's ammonia factory on Herøya in Porsgrunn. Notably, the first electricity based hydrogen production plants were commissioned in Norway in 1929, and many leading electrolyzer manufacturers such Nel Hydrogen ASA have manufacturing facilities in Norway (IRENA, 2022). Along with the availability of cheap, emission-free electricity, Norway has an additional advantage of having access to a highly skilled work force from the metallurgical industry. These factors could enable the establishment of a hydrogen based steelmaking industry in Norway. In order to assess this opportunity, techno-economic assessment model of a grid connected H_2-SF-EAF plant in Norway has been developed in this work. The techno-assessment model was developed to provide answers to the following research questions:

1. What are the enabling factors associated with the H_2-SF-EAF based steel production in Norway?
2. What is the levellized cost of hydrogen based steel production in Norway?
3. Which electricity procurement strategy; fixed power purchase agreements or procurement of electricity from day-ahead electricity markets is most cost-efficient?

Rest of the article is structured as follows. The research framework and methodology is presented in Section 2. Results of the analysis are presented in Section 3, followed by a discussion on the monthly and seasonal variation of electricity prices in Section 4. The results are further discussed, and contextualized in Section 5. Conclusions of this study are presented in Section 6.

2. Methodology

The model is based on the techno-economic assessment framework developed by Thomassen et al. for green chemical production technologies at low technology readiness level (Thomassen et al., 2019). First, market assessment for a green steel manufacturing plant in Norway was conducted. In the second step, a conceptual process model of a grid connected H_2-SF-EAF was developed to calculate the material and energy balance across different components. The model was used to calculate the annual energy consumption, emissions and material requirement for a steel plant with an output capacity One Million ton per annum (Mtpa) of liquid steel. In the third step, levellized cost of steel production was calculated for two electricity procurement strategies using discounted cash-flow analysis i.e. fixed electricity price power purchase agreement, and procurement of electricity from day-ahead markets. In the final step, global sensitivity analysis was conducted using the Sobol sensitivity indices based on the global uncertainty in the input parameter values (Sobol, 2001).

Open-source scientific computation software have been used in this work. The Pandas library was used for retrieving, and analyzing tabular data (McKinney, 2010). Numpy, was used for creating arrays and data handling (Walt et al., 2011). Matplotlib was used for data visualization, and creation of plots (Hunter, 2007). The Ipython notebook environment was used to write the python scripts (Perez and Granger, 2007). The optimization model was written in Python, using PYOMO, which is an open-source optimization framework (Sch et al., 2021). The optimization problem was solved using Gurobi (Gruobi, 2021). The Python scripts, and data used for the analysis are available on the Zenodo repository (Bhaskar, 2021). In the following sections, the different steps are detailed further.

2.1. Market assessment

More than 150 Million tons of steel were used in the European Union(EU) in 2019 (EUROFER, 2020). One-third of the demand originates from the construction sector. The automobile and machinery sector are the two other major demand segments. There has been an increased scrutiny of the embodied emissions of buildings and structures, which includes structural steel used in the construction sector. A global coalition of public and private organizations, called the Industrial deep decarbonization initiative (IDDI) was set up recently to stimulate demand for low carbon industrial materials (UNIDO, 2021). The objectives of IDDI include encouraging governments, and the private sector to buy low carbon steel and cement, and to share data and resources to set common standards and targets across member states. The recent announcements to lower the cap in the EU emission trading system, carbon border adjustment taxes, and emphasis on the use of climate-neutral industrial products could result in an increased demand for green steel in the construction sector in the future (Sartor et al., 2022). Leading automobile manufacturers are moving towards green steel. Volvo, which is a leading automobile manufacturer, and steel producer SSAB have signed a collaboration agreement on research, development, serial production and commercialization of the world's first vehicles to be made of hydrogen reduction based steel. Volvo plans to start the production of concept vehicles and components from hydrogen based green steel by 2021 (Volvo, 2021). Similar, plans have been announced by the Mercedes group, which has invested in an upcoming 5 Mtpa steel production facility in Sweden (Schäfer, 2021). Ørsted, a leading wind energy developer has joined the SteelZero global initiative to drive market demand for net-zero emission steel (Stougaard, 2021).

Norway's proximity to the steel demand centers in the EU could result in lower transportation costs for finished steel from the proposed plant. Interestingly, import of iron and steel, cement, ammonia, aluminum and electricity are included in EU's carbon-border adjustment mechanism (UNCTAD, 2021). Low-emission steel produced in Norway could become cost competitive with other exporters such as Russia, China, India etc. which are still reliant on emission-intensive manufacturing processes. Operations at a magnetite iron ore mining facility are set to resume in Northern Norway. Sydvaranger plans to produce magnetite iron ore concentrate from its mining and processing facilities, which could be used as a raw material input for the hydrogen based steel making (Sydvaranger, 2022). Using domestic iron ore could reduce emission footprint from shipping, and hedge against price fluctuations, which have recently plagued the iron and steel industry. Apart from abundant hydro-power resources, Norway has very good wind electricity potential (both onshore and offshore). The theoretical potential of Norway's offshore is close to 12000 TWh/year, although most of it is located in deep waters and hence costlier to exploit (Bosch et al., 2018). The recent 4.5 GW tenders for fixed bottom plants in Sørlige Nordsjø-II, and floating bottom offshore wind projects in Utsira Nord are an example of the new developments in the Norwegian offshore wind industry. Additional renewable generators could reduce the electricity prices, and reduce operational costs for the proposed H_2-SF-EAF plant.

2.2. Conceptual process model

Hydrogen based steel production can be divided into three distinct sub-processes i.e. hot metal (iron) production in the shaft furnace, conversion of iron to steel in the EAF, and the production and storage of reducing agent (hydrogen). Material and energy flows through the different components were calculated for the production of one ton liquid steel. The specific heat and enthalpy of the different species were calculated using the Shomate equation, as described in Eqs. (1) and (2). The coefficients of the Shomate equations were taken from NIST webBook (Chase, 1998). A conceptual model of the system is presented in Fig. 1.

$$C_p^\circ = A + B * t + D * t^2 + D * t^3 + E/t^2 \quad (1)$$

$$H^\circ - H_{298.15}^\circ = A * t + B * t^2/2 + D * t^3/3 + D * t^4/4 - E/t + F - H \quad (2)$$

2.2.1. Hot metal production in SF

The DRI shaft furnace is counter current solid–gas reactor, where the iron ore pellets, at ambient temperature are fed from the top through a hopper. The iron ore pellet stream is depicted by **M1**. It is assumed that the impurity content in the pellets is 5%, and the impurities are composed of Al_2O_3 and SiO_2. In practice other impurities could be present in the iron ore pellets. Composition of the pellets have an impact on reduction kinetics and thermodynamics. Since, there are no gangue separation processes in the SF-EAF process, it is imperative that the impurity content in the pellets is low. The higher purity requirement has an implication on the cost of the iron ore, and DRI pellets are relatively more expensive compared to raw materials used for blast furnace based iron production. The pelletization process uses fossil fuels as a source for thermal energy, and an upstream emission of 56 kg CO2/t of pellets has been assumed in this study (LKAB, 2017). The reducing gas stream, **M4**, composed of 100% hydrogen enters the shaft furnace at a temperature of 900 °C. The SF operates at a pressure of 6–8 Bar (Maggiolino, 2019). Although SF can operate at atmospheric pressure as well, increasing the pressure could have a positive impact on the diffusivity of the reducing gas, and lead to faster kinetics.

Reduction occurs in three steps, where Hematite (Fe_2O_3) is first converted to Magnetite (Fe_3O_4). In subsequent steps, magnetite is converted to Wüstite (FeO), and finally metallic iron (eFe). Kim et al. found that the easy nucleation, and fast diffusion through the iron oxide product layer are the main reasons for the fast reduction kinetics of hematite to Wüstite conversion (Kim et al., 2021). The conversion from Wüstite to metallic iron is an order of magnitude slower due to sluggish mass transport, particularly of the oxygen through the iron layers. The reduction kinetics of is positively correlated with temperature in the range of 800–1000 °C. Increase in kinetics is attributed to the increase

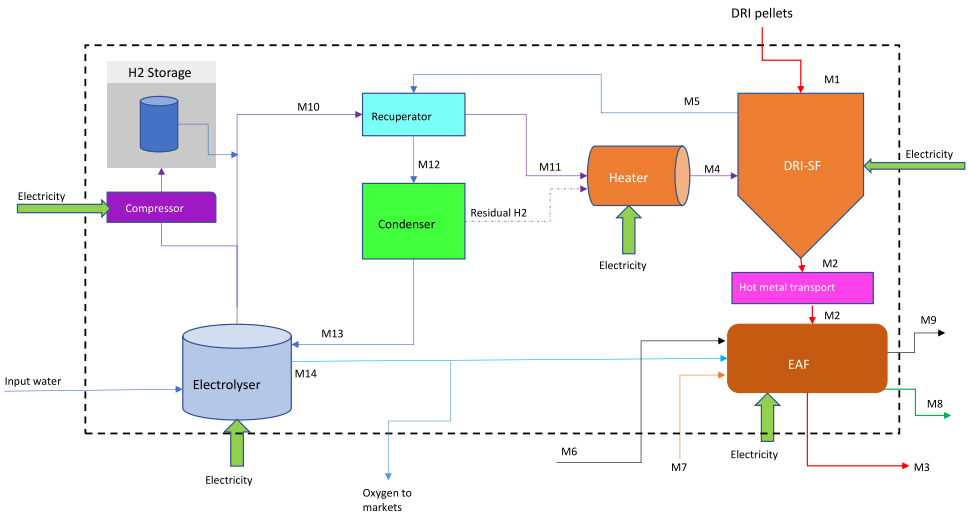

Fig. 1. Schematic of a grid connected H_2-SF-EAF based steel production system.

in diffusivity and reaction rate (Heidari et al., 2021). Reduction kinetics of H_2 was found to be higher than CO, and could result in SF with smaller dimensions (Wagner, 2009). The reduction reaction between hydrogen and iron oxide is endothermic, requiring 99.5 KJ/mol of energy (da Costa et al., 2013). The reduction steps are presented in the Eqs. (3), (4) and (5).

$$3Fe_2O3(s) + H_2(g) \rightarrow 2Fe_3O_4(s) + H_2O(g) \quad (3)$$

$$Fe_3O_4(s) + H_2(g) \rightarrow 3FeO(s) + H_2O(g) \quad (4)$$

$$FeO(s) + H_2(g) \rightarrow Fe(s) + H_2O(g) \quad (5)$$

Hydrogen can be combusted in the DRI shaft furnace to provide the thermal energy required for the endothermic reaction (Duarte and Pauluzzi, 2019). This would require input of higher flow rate of hydrogen than the stoichiometric requirement. For this analysis, a flow rate 10% excess hydrogen has been considered. However, the exact flow rate would depend on the process kinetics, thermodynamics, iron ore characteristics (diffusivity), heat transfer rate from the reactor walls etc, which is outside the scope of this analysis. The unreacted hydrogen can be fed back to the reactor, as has been depicted through the stream **Residual H_2**. Metallization rate of 94% is achieved in the SF. Metallization rate refers to the ratio of metallic iron entering and leaving the shaft furnace. The metallic stream (mixture of Fe, FeO and impurities) exits the shaft furnace at a temperature of 700 °C. It is depicted by **M2** in the figure. Unreacted hydrogen and water leave the SF at a temperature of 300 °C from the shaft furnace through the stream **M5**.

2.2.2. Hot metal transport

The metallic stream, **M2**, can be either cooled down to form cold direct reduced iron (CDRI) or can be fed to a briquetting machine to form hot briquetted iron (HBI). The CDRI and HBI can be shipped to other locations where they can be fed to an EAF or BF for steel production. However, in this analysis, the hot iron feed at 700 °C is directly fed into the EAF. This reduces the energy consumption of the EAF. Since the energy consumption of DRI with zero carbon is higher than in the EAF, it is beneficial to take advantage of the hot metal stream and produce molten steel in the integrated process. Feeding the burden at 700 °C results in an energy saving of approximately 140 KWh/tls. An additional advantage is the extended lifetime of graphite electrodes, and refractory layer of the EAF. The largest DRI-SF reactor manufacturers, ENERGIRON and MIDREX offer solutions for the transport of hot metal from the SF to the EAF. Energiron's HYTEMP™ system uses a pneumatic transport system (Energiron, 2022). The HOTLINK™ system designed by MIDREX on the other hand uses gravitational forces for the transfer of the burden from the SF to the EAF (Midrex, 2021).

2.2.3. Electric arc furnace

The incoming metallic stream is heated to a temperature of 1650 °C inside the EAF. The EAF operates with a charge of 100% hot DRI from the SF. Carbon fines, **M6**, are added to the EAF to reduce the FeO, and for the production of CO, which is essential for froth formation, and slag removal inside the EAF. Froth formation extends the life of the refractory lining, graphite electrodes and reduces downtime of the EAF (Kirschen et al., 2011). Slag is removed from the EAF by using slag formers(CaO, MgO). The slag stream,**M8**, leaves the EAF at a temperature of 1650 °C. Oxygen produced as a by-product of the electrolysis, finds application in the EAF, where it helps in the oxidation of carbon fines to CO. The oxidation reaction is exothermic, and contributes in reducing the overall electricity consumption of the EAF. Air enters the EAF during opening and closing of the roof for material input. Combination of CO_2, NO_2, NO leave the EAF as exhaust gases through **M9** at a temperature of 1500 °C. Energy from the exhaust stream could be used to heat the SF or the hydrogen stream, but this process integration has not been considered in this analysis. The molten metal stream, **M3**, leaves the EAF at a temperature of 1650 °C. The molten metal could either be converted to billets for export or processed further. Subsequent processing of the steel would require additional capital investment and energy inputs. This has not been considered in the present analysis.

2.2.4. Hydrogen production

Alkaline electrolyzers are the most advanced electrolyzers systems, have been deployed at industrial scale previously, and are available in MW scale module sizes at present. Their costs are significantly lower than the other electrolyzer technologies such as polymer electrolyte membrane(PEM), and solid oxide electrolyzers, and their large-scale production is not constrained by availability of rare-earth materials like Platinum or Iridium (used for PEM electrolyzers) (David et al., 2019). A 4.5 MW Alkaline electrolyzer system, supplied by Nel Hydrogen, is being used to produce hydrogen for the H_2-SF demonstration plant commissioned in Sweden in August, 2020 (Pei et al., 2020). Alkaline electrolyzer have been considered for hydrogen production in this analysis.

The technical specifications of multi-MW scale alkaline electrolyzer modules available in the market is presented in Table 1. The average stack-life time of 80,000–100,000 h, and system life of 20–25 years has

Table 1
Technical specification of Alkaline electrolyzer systems available in the market.

Company	Units	Nel Hydrogen	thyssenkrupp	Sunfire	Tianjin Mainland Hydrogen Equipment
Electrolyzer model		A4000	20 MW module	HYLINK Alkaline	FDQ800
Net production rate	Nm^3/h	2400–3800	4000	2230	400–1000
Production capacity dynamic range	%	15–100	10–100	20–100	40–100
Power rating	MW		20	10	N.A
Power consumption at stack	KWh/Nm^3	3.8 to 4.4	4.5	N.A	4.4
Power consumption system level	KWh/Nm^3	N.A	N.A	4.7	N.A
System electrical efficiency(LHV)	%	N.A	N.A	64	N.A
Purity	%	99.99	99.99	99.99	99.99
Delivery pressure	Bar(gauge)	1 to 200	0.5	30	30
Electrolyte		25% KOH	N.A	N.A	30% KOH
Feedwater consumption	L/Nm^3	1	<1	1.9	N.A
Reference		nelhydrogen (2022)	thyssenkrupp (2022)	sunfire (2022)	TianjinMainlandHydrogenEquipment (2022)

been widely reported in the academic and gray literature (Matute et al., 2019). The reported system efficiency is in the range of 60%–67%, but can improve to 75%–80% in the future, based on improvements in the design of different electrolyzer components (IRENA, 2020). The electrolyzer system comprises of the electrolyzer stack, balance of plant systems like the gas separators, compressors(if required), electricity conversion devices (transformers and rectifiers), hydrogen purification system, water supply purification system, cooling equipment etc. High pressure compressors could be required on the storage loop. The reported cost of alkaline electrolyzer system including the balance of plant costs are in the range of $\$500–1000/kW_{el}$ (IRENA, 2020). The costs of engineering, shipping the equipment, civil works and site preparations are additional to these costs. With the combined effects of technology learning, standardization of manufacturing components, automation of production processes, and improvements in performance parameters (lifetime, efficiency and durability), the capital costs of the electrolyzer systems could reduce substantially. Vartiainen et al. have projected the electrolyzer system cost to decline with a learning rate of 18% annually, and reach a capital cost of approximately $\$275/kW_{el}$ by 2030 (Vartiainen et al., 2021). Standardization and technology learning from the Chlor-alkali industry could be directly applicable to the water–electrolyzer industry. Some of the largest chlor-alkali salt–electrolyzer manufacturers like thyssenkrupp uhde chlorine engineers, Asahi Kasie, De Nora etc. are venturing into the water electrolysis business.

Hydrogen stream exiting the electrolyzer, **M10** is pre-heated in the recuperator, by exchanging heat with the SF exhaust stream. The pre-heated H_2 stream, **M11** is heated to the reactor inlet temperature of 800 °C in the electrical heater. The SF exhaust stream, exit the recuperator at a temperature of 120 °C to ensure no condensation inside the heat exchanger tubes, through the stream **M12**. Excess H_2 dissolved in the exhaust stream is separated in the condenser and is fed back to the heater. Electrical gas heaters have been considered in this analysis, however it is possible to use hydrogen as a fuel. A final decision regarding the selection of the heaters would depend on both the capex and efficiency of gas heaters. Fossil fuel fired gas heaters are used in the industry quite frequently but would lead to the release of emissions, and have thus not been considered in this analysis. Water stream exiting the condenser at 70 °C, as **M13** can be fed back to the electrolyzer. Oxygen is produced as a by-product in the electrolyzers, and the exits the electrolyzer as **M14**. Part of it is used within the EAF and the remaining can be sold in market to generate additional revenue. In Norway, fish farms have high demand for Oxygen, and deploying a supply chain for the same could be beneficial for the overall plant economics. Purified water stream enters the electrolyzer for the production of Hydrogen.

2.2.5. Hydrogen storage

Hydrogen produced from the electrolyzer can be directly fed to the DRI shaft reactor or stored in the hydrogen storage unit. Hydrogen storage systems can be divided into two broad categories i.e. physical storage and chemical-based storage. Physical storage of H_2 refers to storing it under high pressure (60–960 Bar) or cryogenic storage of hydrogen at −253 C. Until now physical storage of hydrogen is the most widely deployed mode for commercial storage of hydrogen. Chemical-based storage systems, such as metal hydrides (AlH_3, MgH_2), ammonia, methanol, formic acid, or liquid organic hydrogen carriers are still at an early stage of development. Most of them require conversion and re-conversion processes, which require additional capital investment, and would lead to additional operational costs. Liquefaction of hydrogen at −253 °C, increases the volumetric energy density of H_2 significantly, but is an energy intensive process, requiring close to 10 KWh/kgH2 or one-third of the energy content of the hydrogen. Issues related to boil-off gases result in complicated insulation design requirements for the liquid H_2 storage tanks. In this analysis, compressed hydrogen storage has been considered as a viable alternative for storing hydrogen.

Compressed hydrogen can be stored in above-ground steel tanks or in underground geological reservoirs like salt and rock caverns, aquifers, or depleted oil and gas wells. Salt caverns are most suited for hydrogen storage and have been used in Texas (USA) since 1983 and in Teesside (UK) since 1972 (Abdin et al., 2021). Dilara et al. studied the technical potential of hydrogen storage in salt caverns in Europe (Gulcin et al., 2020). They estimated the total onshore and off-shore H_2 storage potential to be 84.8 PWh_{H_2}. Equinor and SSE thermal are building a salt cavern based hydrogen storage facility With an initial expected capacity of at least 320 GWh at Aldbrough. The storage plant is likely to be commissioned by 2028, and will comprise of nine salt caverns (Equinor, 2021). Under the HYBRIT project in Sweden, a lined rock cavern is being developed for hydrogen storage (Pei et al., 2020). Ahluwalia et al. calculated the levellized cost of hydrogen storage for underground pipe storage, salt caverns and lined rocks caverns. They found that storage in caverns gets cheaper as the storage capacity increases (Papadias and Ahluwalia, 2021). For a more detailed analysis on the levellized cost of storage, the readers are referred to the work of (Lord et al., 2014). While the cost of hydrogen storage in geological reservoirs is quite low, and reduces with increase in storage capacity, their availability is constrained by geographical formations.

Iberdola, which is building a 800 MW electrolyzer plant for green ammonia production in Puertollano, Spain will use steel tanks for Hydrogen storage (Iberdola, 2022). Each tank has a volume of 133 m^3, height of 23 meters and a diameter of 2.8 m, and can store 2.7 ton of hydrogen at a pressure of 60 Bar. Eleven such tanks will be installed at the plant. In order to meet the storage requirements of the proposed system, above-surface storage tanks made of austenitic stainless steels or aluminum have been considered in this analysis (Elberry et al., 2021). A capital cost of 1500 USD/kgH_2 has been considered for the system comprising of the compressors and storage tank (DEA, 2020). The operating pressure of the storage tank is considered to be 200 Bar. Transport of hydrogen within the plant can be done through the pipes made from L415ME/X60 grade steel, which is designed for oil and other combustible liquids, natural gas and other gaseous media. Arcelor Mittal is supplying pipes with similar grade of steel for a 440 kilometer, high-pressure hydrogen pipeline network across Italy, which could operate with 100% hydrogen (ArcelorMittal, 2022). Although the low-pressure pipes within the plant (except the storage lines) could be constructed with cheaper grades of steel.

Table 2
Capital cost assumptions.

Capital cost assumptions			
Equipment	Cost($)	Unit	Reference
Electrolyzer	$/kW	700	Vartiainen et al. (2021)
Stack replacement cost	$/kW	300	Vartiainen et al. (2021)
Shaft furnace	$t/steel/year	250	Krüger et al. (2020)
Electric arc furnace	$t/steel/year	160	Vogl et al. (2018)
Hydrogen storage tank	$kg/$H_2$	500	Hampp et al. (2021)
Hydrogen compressor	$kg/$H_2$	2545	Christensen (2020)

Table 3
Operational cost assumptions.

Operational cost assumptions			
Item	Cost	Unit	Reference/remark
Iron ore	120	$/t	OECD (2020)
Electrolyzer effciency(2020)	53	KWh/kgH_2	David et al. (2019)
Electrolyzer efficiency(2030)	45	KWh/kgH_2	David et al. (2019)
DRI OPEX	12	$/tls	Cavaliere (2019)
EAF OPEX	33	$/tls	Cavaliere (2019)
Emission price	100	$/t$CO_2$	EC (2020)
Grid emission factor(Norway)	16	gCO_2/KWh	EC (2020)

2.3. Economic evaluation

A discounted cash flow analysis was conducted to calculate the levellized cost of production for the proposed system. The levellized cost of production (LCOP) was calculated using Eqs. (6) and (7).

$$LCOP = \frac{C_{capex} * ACC + C_{opex} + C_{maint} + C_{labor} + C_{emission}}{Annual\ steel\ production} \quad (6)$$

Where, LCOP is the levelized cost of production, C_{capex} and ACC are the total capital investments, and annuity factor respectively. Annual operational, maintenance, labor and emission costs are represented by C_{opex}, C_{maint}, C_{labor} and $C_{emission}$ respectively.

$$ACC = \frac{r * (1+r)^n}{(1+r)^n - 1} \quad (7)$$

Where, r represents the discount rate used for the calculation and n refers to the plant life. A discount rate of 10% was considered in the base case to account for investments in an early stage technology. Plant life of 20 years, which is widely reported in the literature was considered for the calculations (Pimm et al., 2021).

The CO_2 mitigation cost was calculated for the different configurations, compared to the BF-BOF process using Eq. (8).

$$M_{cost} = \frac{LCOP_{SF-EAF} - LCOP_{BF-BOF}}{E_{BF-BOF} - E_{SF-EAF}} \quad (8)$$

In Eq. (8), M_{cost} is the mitigation calculated in $/tCO2. The numerator represents the difference in LCOP of the SF-EAF and BF-BOF system of similar capacity. The LCOP of the SF-EAF system is calculated using Eq. (6). For the BF-BOF system the LCOP has been varied between 400–500 $/t, based on widely reported literature values (Levi et al., 2022). E_{SF-EAF}, represents the sum of direct and indirect emissions from the SF-EAF system, and is calculated in tCO_2/tls. For the BF-BOF system, E_{BF-BOF}, represents the total emissions. A value of 2.1 tCO_2/tls has been used in this calculation (Backes et al., 2021).

2.3.1. Capital costs

The capital costs for the main plant components were calculated for a one Mtpa steel production plant, based on the material and energy balance from the conceptual process model. Equipment costs were converted to total capital costs using the Lang factors approach described by Sinnott et al. (Towler, 2013). A Lang factor of two was considered for the entire system. The electrolyzer installed capacity was calculated based on the flow rate of hydrogen, and corresponding efficiency. It was assumed that only the stacks, which are 60% of the electrolyzer system cost would be replaced after 90,000 h of operation. Compressor size was calculated based on the ideal gas equation, and outlet pressure of 200 Bar (Christensen, 2020). Capital cost assumptions for the main equipment are presented in Table 2.

2.3.2. Operational costs

To calculate the operational costs, price of iron ore, electricity, emission, and shaft furnace and EAF operational costs were considered. The electricity costs were determined using the optimization framework described in Section 2.3.3. Direct emissions from the plant were used to evaluate the annual emissions cost. The annual maintenance cost was considered to be 1.5% of the capital cost, and a labor cost of 20$/tls was allocated (Towler, 2013). Assumptions for evaluating the operational costs are presented in Table 3. It is assumed that the SF consumes 80 KWh/tls for the operation of the pneumatic system for the transport of iron ore from the hopper, operation of valves and transport of hot metal from SF to the EAF.

2.3.3. Electricity price

In this article, two scenarios for electricity procurement have been considered. In the first scenario electricity is procured based on long-term power purchase agreements. A fixed price of $60/MWh of electricity has been considered in the fixed electricity price scenario. For the second scenario, historical day-ahead prices for Bergen were retrieved from Nordpool (2020). Electricity prices are available at an hourly resolution for the different bidding zones in the Nordic electricity markets, including Oslo, Kristiansand, Bergen, Molde, Trondheim, and Tromsø. Bergen was chosen for the present analysis as it has the largest maritime port in Norway, handling more than 36% of the total cargo. As most of the iron ore will be imported, and the finished products would be shipped to EU countries, access to shipping routes could play a pivotal role in site selection. Historical day-ahead electricity prices were used to develop an optimal production schedule for the electrolyzers. Storage sizes were calculated based on the electrolyzer operation profile. Five different electrolyzer configurations were evaluated in this work. In the base case, the output of the electrolyzer system was considered to be equal to the hydrogen demand from the steel plant. The hydrogen output capacity was increased to two times the hourly hydrogen demand in the highest configuration to evaluate the impact of increasing the electrolyzer size on the financial feasibility of the plant.

Optimization framework:. The operation scheduling of the electrolyzers has been formulated as a linear optimization problem, shown in Eq. (9). Linear optimization formulation was chosen to avoid computational complexity. Other approaches such as mixed integer linear programming, quadratic programming, stochastic decision making using Markov chain method have been used by other researchers for a more detailed analysis optimal control strategies. As the focus of this study is to present an initial assessment, linear optimization was found to be an adequate solution. Scheduling of grid connected electrolyzers have been solved using linear optimization models previously (Nguyen et al., 2019).

$$\begin{aligned} \text{Minimize} \quad & c_1 x_1 + \ldots + c_n x_n \\ \text{subject to} \quad & a_{11} x_1 + \ldots + a_{1n} x_n \geq b_1 \\ & \vdots \\ & a_{m1} x_1 + \ldots + a_{mn} x_n \geq b_m \end{aligned} \quad (9)$$

The objective of the optimization framework is to minimize the operating cost by utilizing the fluctuations in electricity prices. Electricity price is the cost vector c_i, which varies each hour, based on the historical day ahead prices. At each hour, a decision has to be made regarding the amount of hydrogen to be produced, which is represented

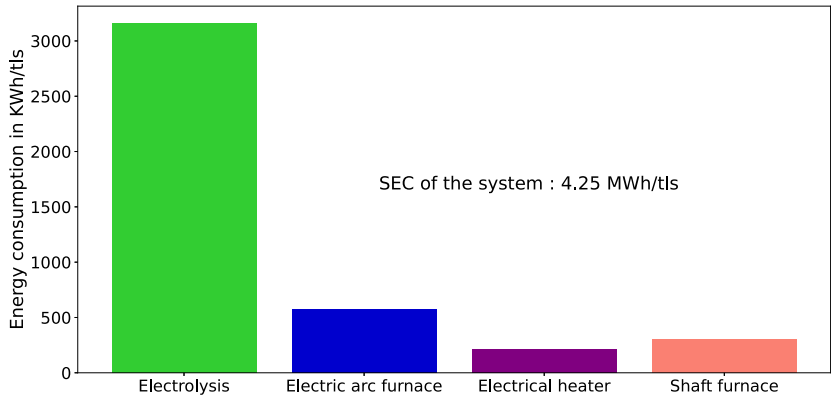

Fig. 2. Electricity consumption of different components of the H_2-SF-EAF system.

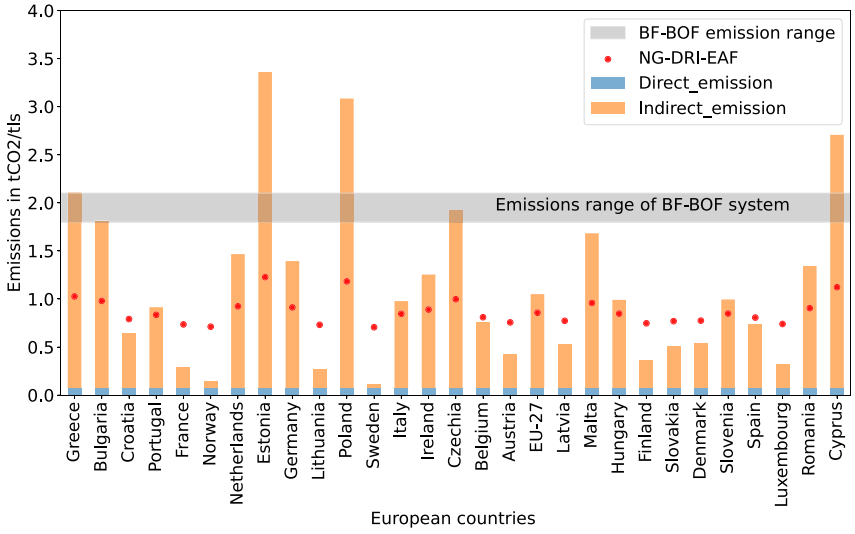

Fig. 3. Emissions from the hydrogen SF-EAF system in European countries.

Table 4
Lower and upper bounds of input variables for sensitivity analysis.

Input Variable	Units	Lower Bound	Upper Bound
Discount rate	%	0.06	0.12
Plant life	Years	20	40
Lang factor	Number	1	2
Electrolyzer efficiency 2020[a]	KWh/kgH2	60	45
Electrolyzer efficiency 2030[a]	KWh/kgH2	50	40
Electrolyzer capex 2020	USD/kW	600	800
Electrolyzer capex 2030	USD/kW	300	500
EAF capex	USD/t/Year	100	200
DRI-SF capex	USD/t/Year	200	300
Iron ore cost	USD/t	80	150
Electricity price[b]	USD/MWh	40	100
Grid emission factor	tCO2/KWh	0.015	0.250
Emission price	USD/tCO2	50	250
Storage unit cost[c]	USD/kGH2	100	500

[a]In the model, the lower bound has to be numerically lower.
[b]Electricity price was varied for configuration with fixed power prices.
[c]Storage input costs were varied only for the configuratons purchasing electricity from the day-ahead market.

by the decision variable x_i. The optimization is done for every twenty four hours, since day-ahead prices are available for the next 24 h. In order to get the annual hydrogen generation profile, the slice of the cost vector is passed to the optimization function, which generates an instance of the optimization problem for every 24 h. To calculate the annual operational cost the code is run 365 times, as the optimization interval is fixed at 24 h. The analysis was conducted for all five electrolyzer configurations. The quantity of hydrogen produced per hour is constrained by the installed electrolyzer capacity, defined in Eq. (10).

$$0 \leq x_i \leq \text{electrolyzer capacity} \tag{10}$$

The second constraint pertains to the meeting the demand of hydrogen. At each hour, the demand for hydrogen, represented by b_i has to be met. Hydrogen could be supplied by the electrolyzer or through the hydrogen storage unit. Considering the fixed demand of hydrogen for steel making to be d tons/hour, the demand vector is presented in Eq. (11):

$$b_j = \sum_{n=1}^{24} d * n; \text{where j varies from 1 to 24} \tag{11}$$

The generation profile was used to evaluate the storage status by transferring all excess hydrogen generated to the storage unit. Energy consumption of 0.4 MWh/t of hydrogen has been used for the compression process (Penev et al., 2019). The storage status at each instance can be calculated using Eq. (12)

$$s_k = \sum_{n=1}^{k} x_k - d_k; \tag{12}$$

Where $s = 0, t = 0$, k is the hour, which varies from 1 to 8760.

Table 5
Material and Energy flows through the system.

Stream	Stream description	Material flow (kg/tls)	Temperature (°C)	Enthalpy (KWh/tls)
M1	Raw iron ore input	1504.99	25	0.0
M2	Metallic stream at SF outlet	1075.25	700	116.38
M3	Molten metal at EAF outlet	1000.0	1650	324.85
M4	Hydrogen stream at SF inlet	59.56	900	213.08
M5	SF exhaust stream	484.49	300	71.72
M6	Carbon fines added to EAF	20.0	25	0.0
M7	Slag formers added to EAF	75.0	25	0.0
M8	EAF exhaust gas stream	150.0	1500	89.09
M9	EAF slag stream	200.0	1650	49.29
M10	Hydrogen at electrolyzer outlet	59.56	70	1.12
M11	Hydrogen stream at electric heater inlet	59.56	170	29.54
M12	SF exhaust at recuperator outlet	484.49	120	24.13
M13	Water stream at condenser outlet	483.89	70	86.29
M14	Oxygen stream at electrolyzer outlet	476.49	25	0.0

2.4. Uncertainty analysis

The global sensitivity analysis was carried out using the SALib library to evaluate the Sobol first-order and Sobol total-order sensitivity indices (Herman and Usher, 2017). The parameters used for calculating the levellized cost of production were varied between the lower and upper bounds. Uncertainty propagation was calculated by varying the value of the input variables between the lower and upper bounds, and determining the relationship between the input variables and output variable, as well as the inter-dependence of the input variables. To get convergence the model was run 16384 times. The lower and upper bounds of the input parameters are presented in the Table 4.

3. Results

3.1. Material and energy flows

The material and energy flows through the different components of the system are presented in the Table 5.

3.2. Energy consumption

The H_2-SF-EAF system has a specific energy consumption (SEC) of 4.25 MWh/tls, at an electrolyzer efficiency of 53 KWh/kgH_2. In the literature, the SEC of comparable systems vary from 3.48 MWh/tls (Vogl et al., 2018) to 3.95 MWH/tls (Krüger et al., 2020). The difference in the SEC's originate from the use of different electrolyzer types, values of electrolyzer efficiency (depends on the projected installation year of the plant), use of scrap in the EAF, thermal energy requirements of the shaft-furnace, purge-gas requirements etc. Water electrolysis was found to consume 75.7% of the total energy. Consumption of electricity from different components of the system is presented in Fig. 2.

3.3. Emissions

The total emissions from the system could be divided into direct and indirect emissions. Direct emissions from the EAF (lime production, carbon oxidation, FeO)reduction account for 73 kgCO_2/tls. Indirect emissions from pellet production, and lime production contribute to 167 kgCO_2/tls. While the upstream emissions do not vary substantially with location, the indirect emissions from electricity consumption vary with the electricity mix of the region where the plant is located. The indirect emissions from electricity consumption were found to be 67 kgCO_2/tls. A comparison of the total emissions from the H_2-SF-EAF operation in different countries is shown in Fig. 3. The red dots represent the average emissions from a natural gas based DRI-EAF plant, whereas the gray band represents the emission range of the BF-BOF process. It can be inferred from this chart that countries with low grid emission factor like Norway and Sweden are well suited for the installation of H_2-SF-EAF plants, in terms of total emission reduction.

3.4. Hydrogen production and storage status

The H_2-SF-EAF plant was found to have an hourly hydrogen demand of 7.55 tons/h. The hourly demand is met either through production or from hydrogen produced earlier and stored in the storage tanks. In Fig. 4, histogram of the hydrogen production and storage status for different configurations is presented. The configuration with constant production, and no storage have been excluded from the plot for brevity. Hydrogen production profile have been presented on the left and the associated storage status at each hour is on the right hand of the chart. It can be observed from that the number of idle hours increase, as the capacity increases. By increasing the installed hydrogen output capacity from 7.55 t/h to 15.11 t/h, electricity demand could be shifted for more than 43% of the time. Shifting industrial electricity demand, often referred to as demand response, has the potential to increase the flexibility of the grid, and allow integration of intermittent renewable electricity generators (Stöckl et al., 2021). Hydrogen storage tanks remain empty for shorter duration, only 16% of the time for configurations with higher hydrogen output. To double the hydrogen production capacity from 7.55 t/h to 15.11 t/h, hydrogen storage tanks with a capacity of 90 tons would be required.

3.5. Levelized cost of steel production

LCOP of $714/t was calculated for the configuration with fixed electricity price of $60/MWh. For the systems procuring electricity from the day-ahead markets, the LCOP varied from $622-$722/t. The LCOP values, for all configurations, were found to be significantly higher than the LCOP of the plants based on BF-BOF process. LCOP of the different configurations is shown in Fig. 5. The configurations are shown on the *x*-axis, according to their hydrogen output capacity. The right most column(7.55-ppa) represents the configuration with a hydrogen out put capacity of 7.55 t/h, while purchasing electricity at under a fixed power purchase agreement. Almost 73% of the LCOP is comprised of the operational cost, which is primarily composed of the electricity costs and iron ore costs. While the operational costs have the maximum contribution to the production costs at lower hydrogen output capacities, the contributions from capex become more prominent for the configurations with higher electrolyzer capacities. The maintenance costs increase with higher capacities, while the labor and emission costs remain constant for all configurations at $20 million and $7.64 million respectively. The emission costs were calculated only for the direct emissions from the H_2-SF-EAF system.

Capital cost. The capital cost of the system configurations with higher hydrogen flow rates were found to be significantly higher, owing to the need for larger installed capacity of electrolyzer, storage tanks and compressor systems. It was found that doubling the electrolyzer capacity, and subsequent shifting of operating hours, would require 90 tons of storage capacity, and a compressor of 13.6 MW electrical capacity

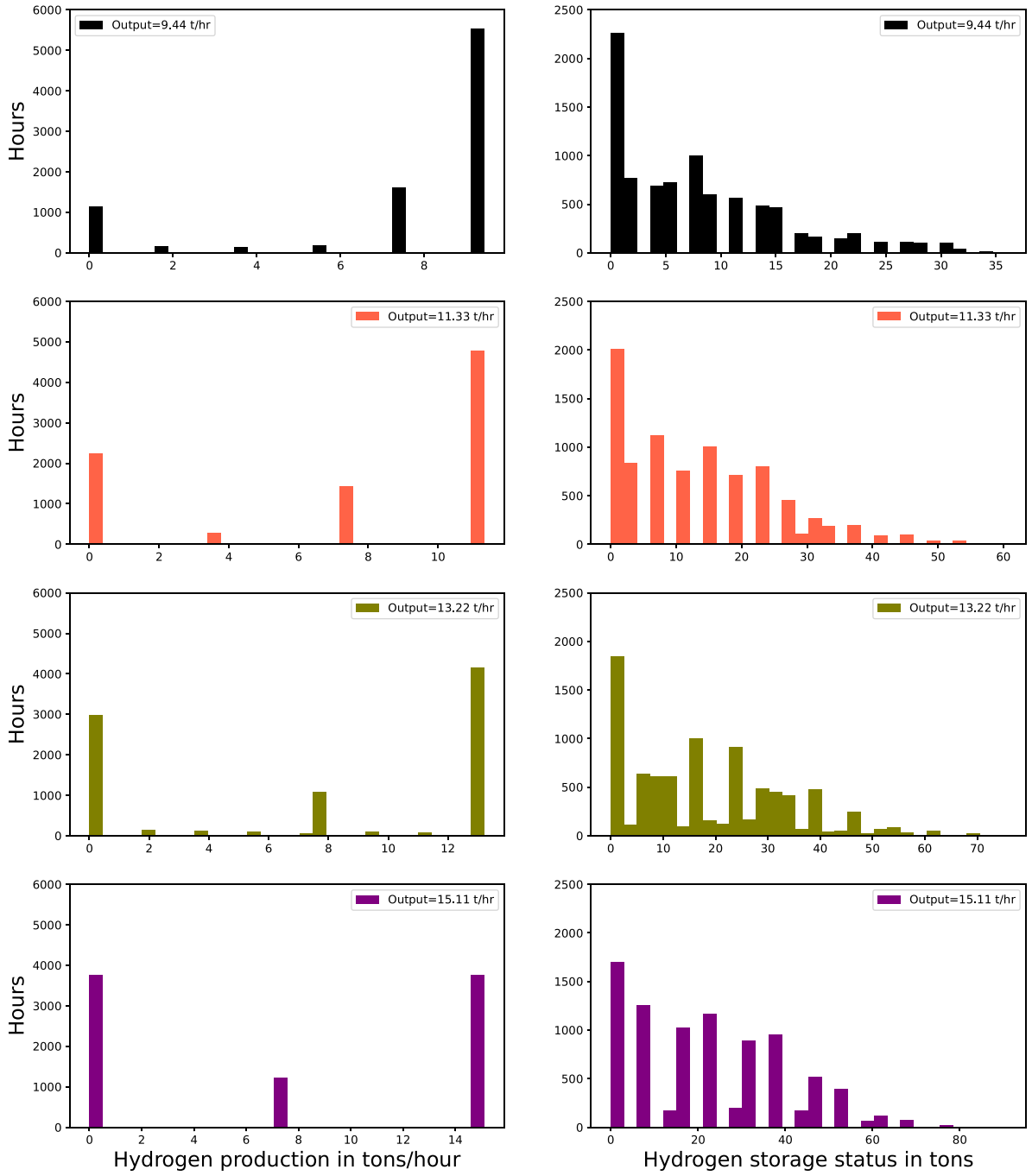

Fig. 4. Histograms of production and storage status of different electrolyzer configurations.

Table 6
Capital cost distribution of different plant configurations.

Configurations	Electrolyzer	Stack replacement	DRI-EAF capex	Storage capex	Compressor capex
7.55	280.10	61.15	410,00	0,00	0,00
9.44	350.22	76.46	410,00	17.95	9.57
11.33	420.34	91.77	410,00	30.02	19.1
13.22	490.46	107.08	410,00	37.75	28.71
15.11	560.581	122.39	410,00	45.3	38.28
7.55 _PPA	280.10	61.15	410,00	0,00	0,00

*All costs are in Million USD.

to deliver the required flow rate. The distribution of capital costs for the six different configurations analyzed in this work is presented in Table 6.

Electricity cost. The electricity costs where found to be highest for the configuration purchasing electricity at a fixed electricity price. Purchasing electricity from the day-ahead market could reduce the procurement cost of electricity by 38%, if the electrolyzer capacity

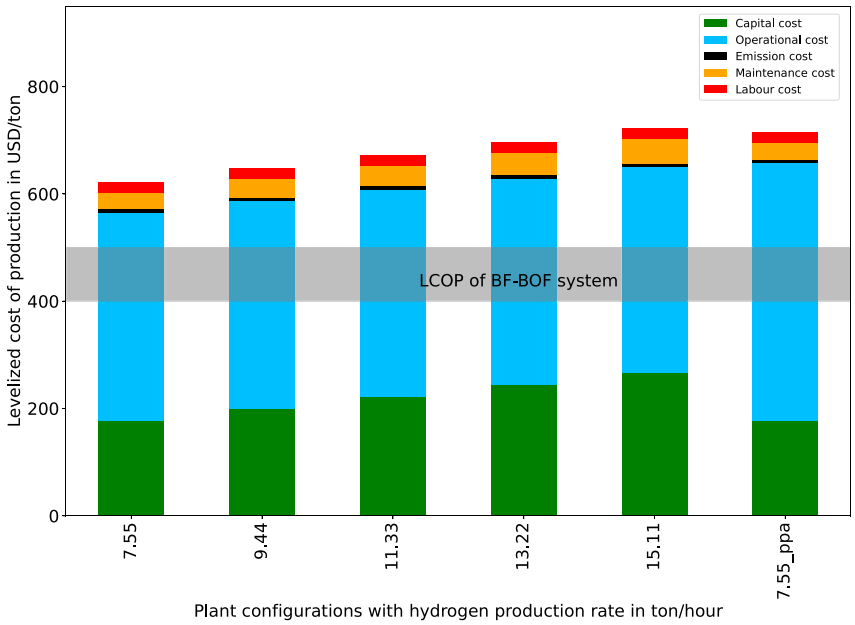

Fig. 5. Levelized cost of production for different plant configurations.

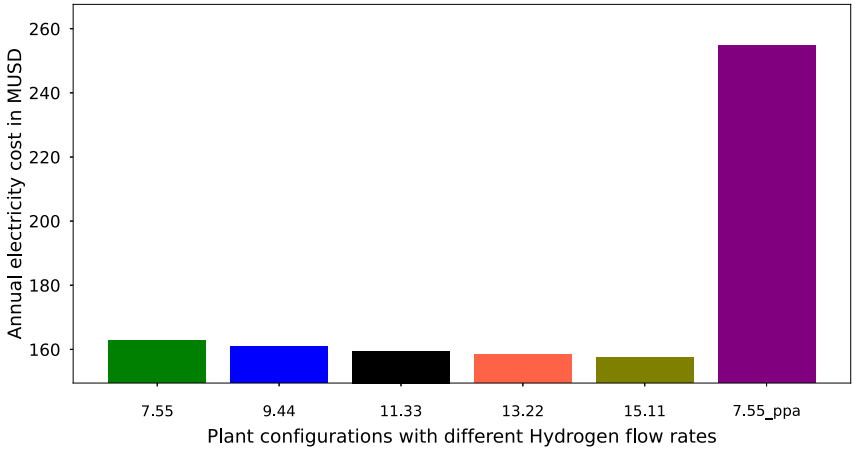

Fig. 6. Annual electricity costs for different configurations.

is doubled, and storage tanks are installed at the facility. However, even at the same electrolyzer capacity, procuring electricity from the markets instead of fixed power purchase agreements could bring down annual electricity costs from $254 million to $160 million. In Fig. 6 for the different configurations is presented.

3.6. Sensitivity analysis

The results of the global sensitivity analysis in the form of first order Sobol indices, and total order Sobol indices are presented in this section. The values of the second order Sobol indices were found to be insignificant, indicating weak interaction between the input variables, and hence have not been included in this analysis.

3.6.1. Configuration with fixed PPA

For the system procuring electricity at fixed price, variation in the price of electricity could have the maximum impact on the LCOP. Iron ore price, Lang factor, and electrolyzer capex are the other important parameters. For configurations with lower electrolyzer capacity, iron ore prices have a higher contribution to the total uncertainty. The lower impact of the interest rate indicate that LCOP is heavily dependent on the operational costs (see Figs. 7 and 8).

3.6.2. Configurations purchasing electricity from day-ahead markets

Fluctuation in iron ore price affects the systems with lower hydrogen output capacity, and hence lower capital investments, while configurations with higher output of hydrogen show higher sensitivity to installation costs(Lang factor), and the interest rate (discount rate). Plant life also becomes a significant factor for the plants with increased capital investments, as it a part of the annuity calculations. Longer lifetime of plants could reduce the LCOP. Storage cost does not have a huge impact owing to the relatively smaller size.

4. Electricity price data characteristics

The current work focuses on developing an optimization model, based on linear optimization techniques for operational scheduling based on day ahead electricity prices. Further insights can be derived by understanding the seasonal variation in electricity prices which can aid in developing an optimal strategy for plant/storage sizing as well.

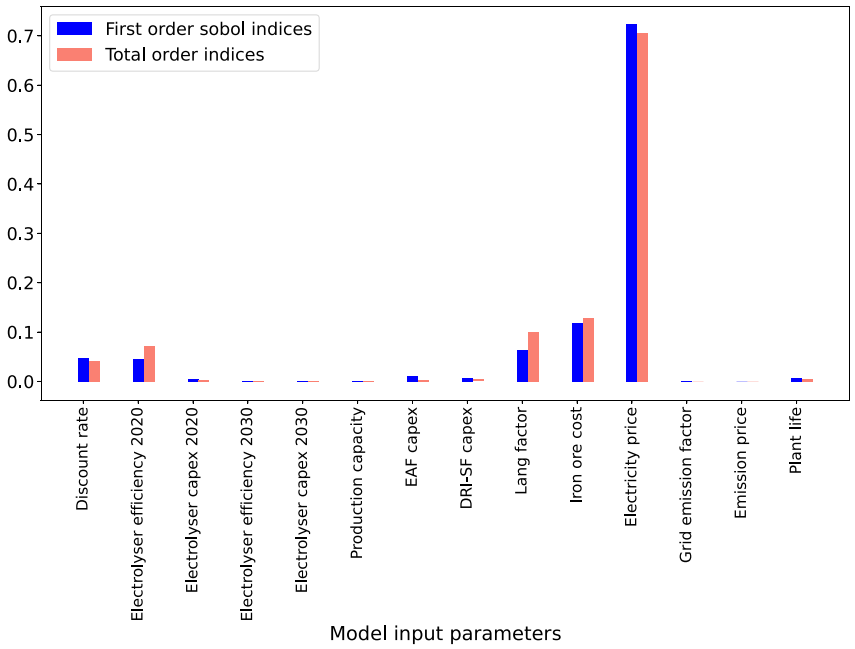

Fig. 7. Sensitivity analysis for the configuration purchasing electricity at fixed price.

The combination of high degree of variability in electricity demand and supply creates a regional price environment that may have daily, weekly, seasonal or yearly characteristics. This section provides a brief of the price characteristics in Bergen region of Norway for the year 2019 which has been used for the optimization performed in this study.

The electricity prices for the Bergen region in the year 2019 is shown in Fig. 9. Analyzing a time series like the electricity prices shown in Fig. 9 involves data mining to extract knowledge from the data. One of the methods to gain a deeper understanding of the data and extract patterns and anomalies embedded in the dataset, is Time Series sub-sequences All-Pairs-Similarity-Search (TSAPSS). Matrix profile is a innovative and fast technique for performing TSAPSS proposed by researchers at University of California, Riverside and University of New Mexico (Yeh et al., 2017) in 2016. Briefly, the Matrix profile of a time series of length n is itself a time series that contains the z-normalized Euclidean distance normalized distance of a sub-sequence of length m to its nearest neighbor in the original time series (Yeh et al., 2018). Annotating the original time series with the matrix profile can help locate the motifs (closely repeated patterns) and discords (anomalies). Further, the matrix profile allows us to perform semantic segmentation and identify the existence of regimes in a time series based on the calculation of a Corrected Arc Crossing (CAC) for every data point in the series (Gharghabi et al., 2017).

The matrix profile for the time series in this study was computed with a sub-sequence length of 1 week ($m = 24 * 7 = 168$ hours). Based on the matrix profile, the CAC and the locations of the regime change has been plotted in the lower half of Fig. 9. Fig. 9 shows that the major seasons (summer and winter) form a distinct price regime, while the shoulder seasons are split roughly in the middle indicating a transition period. A future work could investigate leveraging the existence of these seasonal regimes for calculating optimum storage sizing and exploring the possibility of incorporating large scale sub-surface storage. Large scale storage systems like salt caverns which are cycled seasonally enable continuous production of Hydrogen for extended periods. Additionally, this can be an effective strategy for de-risking against price fluctuations in the electricity market.

The motif and discords extracted form the price data are shown in Fig. 10. From the pattern matches obtained in Figs. 10(a) and 10(b) we can see that these weekly periods represent periods with very low daily fluctuation on prices with bi-modal peaks. The twice daily peaks can be attributed to morning and evening peak load periods, however, it is interesting to note that the dips between these periods remains relatively low. The third motif (Fig. 10(c)) has similar characteristics however, the peaks during the first two days are much higher. The black anomaly shown in Fig. 10(d) is interesting since there is no clear daily pattern in this period and very high variability. A future work could also explore the utilization of motifs (repeated patterns) and discords (anomalies) in the price data. The current analysis has been done for patterns of sub-sequence length: 1 week. Performing the analysis at varying sub-sequence lengths relevant to the operation of the plant could lead to significant insights. For instance identifying the nature of anomalous periods and linking them to prevailing regional and environmental conditions can help us predict these periods. As mentioned previously, over one-third of electricity generation in Norway is used for energy intensive industrial applications. Performing a similar analysis with electricity price data overlaid with wind/ solar energy generation potential on a regional basis can further aid the case for greater investments in renewable energy production to facilitate the development of decarbonized heavy industries in Norway.

5. Discussion

BF-BOF based steelmaking process has been optimized for several decades, and has an advantage over the H_2-SF-EAF process in terms of cost. However, in a carbon constrained world, the cost of operating a BF-BOF based steel mill could increase substantially. With increasing carbon taxes, as envisaged in the revised EU emission trading system, the LCOP of BF-BOF based could increase substantially. Increase in cost of raw materials such as coking coal has increased the production costs considerably for steel producers in recent times (Levi et al., 2022). Reduction in electrolyzer capex, efficiency improvements, and reduced cost of finance could bring down production costs for H_2-SF-EAF based steel based route The emission price at which an alternatively technology could become economically feasible is often used as a metric to evaluate different decarbonizing technologies. The CO_2 mitigation cost range for the different configurations is presented in Fig. 11. The mitigation costs were found to vary from \$68/tCO_2 to \$180/tCO_2. The emission trading price in the EU has increased from \$40/tCO_2 to \$90/tCO_2 in the past year, and the increasing trend is likely to continue in the coming years, on the back of ambitious climate policies.

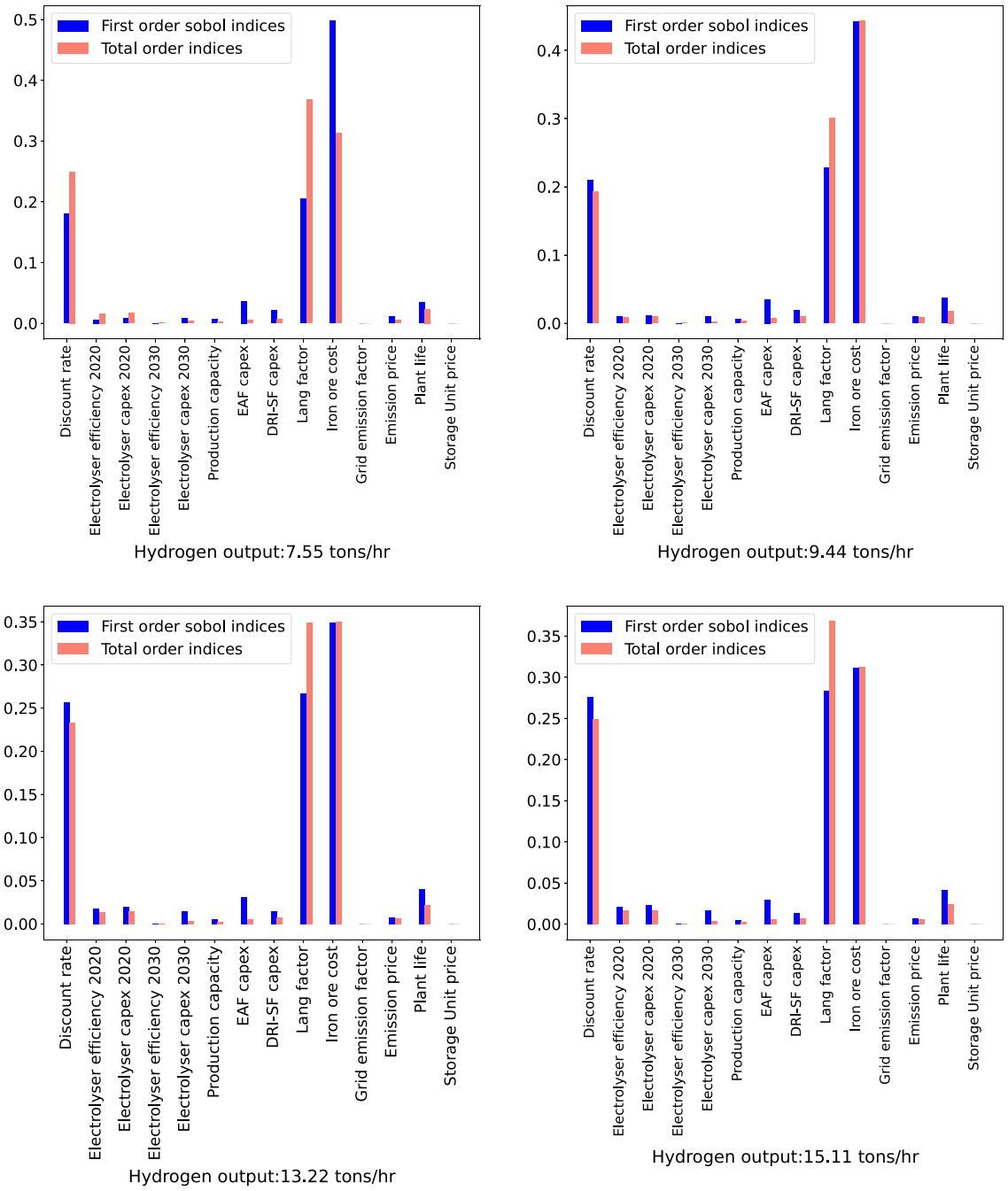

Fig. 8. Sensitivity analysis for the configuration purchasing electricity from the day-ahead electricity markets.

6. Conclusion

In this work, techno-economic assessment of a grid connected H_2-SF-EAF plant in Bergen, Norway was conducted to answer a set of research questions. An open-source model was developed to calculate the levelized cost of production for two configurations i.e. one purchasing electricity at a fixed price, and the other procuring electricity from the day-ahead electricity markets. The main findings, in light of the research questions are discussed below.

What are the enabling factors associated with the H_2-SF-EAF based steel production in Norway?. The main influencing factors identified in this analysis are availability of cheap and low-emission electricity, access to magnetite iron ore from northern Norway(Varanger), access to the EU market, and availability of a highly-skilled workforce. Some of the other factors, which could further add to the attractiveness of Norway as a hydrogen based steel manufacturing destination are its offshore wind energy potential, and a need for the economy to transition from the oil and gas industry.

What is the levellized cost of hydrogen based steel production in Norway?. The levellized cost of steel production varied from $ 622 to $722 for the different configurations. The production costs were found to be 40% higher than the BF-BOF based steel production route. CO_2 mitigation cost was found to vary between \$68/tCO_2 to \$180/tCO_2.

Which electricity procurement strategy; fixed power purchase agreements or procurement of electricity from day-ahead electricity markets is most cost-efficient?. Participating in the electricity markets could reduce production costs by 14,7% compared to a plant with similar capacity,

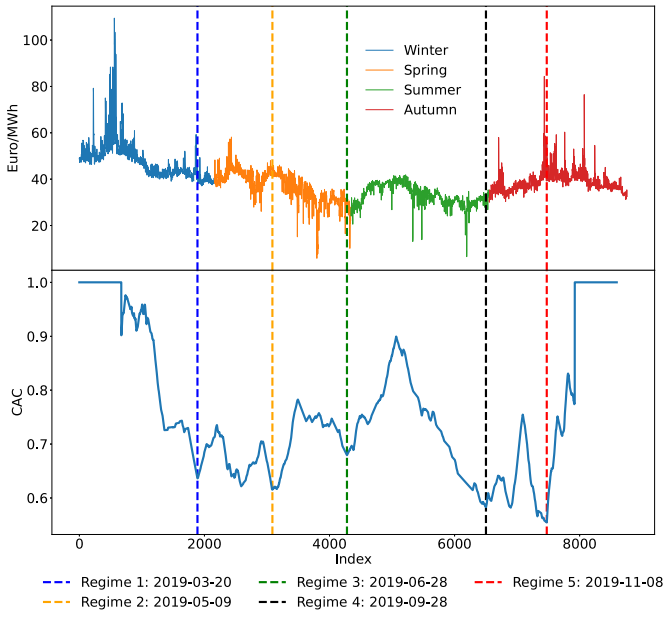

Fig. 9. Seasonal variation of electricity prices in Bergen (2019) and the regime changes based on the Corrected Arc Crossings (CAC).

operating with fixed electricity prices. Increasing the electrolyzer capacity reduced the operational costs. However, the reduction was not enough to justify investments in additional electrolyzer, and hydrogen storage capacity. Access to underground geological storage such as salt cavern, rock cavern or depleted oil wells could make it economically feasible to store large quantities of hydrogen at cheaper costs, and allow the plant to leverage the seasonal fluctuation in electricity costs. It would also open opportunity for the steel plant to participate in the electricity capacity markets and generate additional revenue. Analyzing the historical price trends could help in detection of seasonal patterns in electricity prices, which could be leveraged for designing a plant with optimal plant capacity and operation schedule.

Abbreviations

EU	European Union
USA	United States of America
UK	United kingdom
IDDI	Industrial deep decarbonization initiative1
DRI	Direct reduced iron
HBI	Hot briquetted iron
SF	Shaft furnace
HDRI	Hydrogen direct reduced iron
HYFOR	Hydrogen-based fine-ore reduction
NIST	National institute of standards
EAF	Electric arc furnace
BF-BOF	Blast furnace basic oxygen furnace
SMR	Steam methane reforming
CAC	Corrected Arc Crossings
LCOP	Levelized cost of production
IPCC	Inter-governmental panel on climate change
SSAB	Svenskt Stål AB
LKAB	Luossavaara-Kiirunavaara Aktiebolag
MMBTU	Metric Million British Thermal Unit
IDDI	Industrial deep decarbonization initiative
SEC	Specific energy consumption
tls	Ton of liquid steel
$kgCO_2$	Kilogram of carbon dioxide
tCO_2	Tonn of carbon dioxide
$GtCO_2$	Gigaton of carbon dioxide
kg	Kilogram
kJ	KiloJoule
GJ	GigaJoule
kW	kilowatt
kW_{el}	kilowatt electric
MW	Megawatt
GW	Gigawatt
KWh	Kilowatthour
MWh	Megawatthour
TWh	Terrawatthour
Mtpa	Million ton per annum
mol	moles
L	Liter
NM^3	Normal cubic meter
h	hour
CO	Carbon Monoxide
H_2	Hydrogen
O_2	Oxygen
Al_2O_3	Aluminum oxide (Alumina)
SiO_2	Silicon dioxide(Sillica)
Fe_2O_3	Hematite
Fe_3O_4	Magnetite
Fe	Iron
FeO	Iron Oxide
Fe_3C	Iron carbide
C	Carbon
CO_2	Carbon dioxide
NO_2	Nitrous Oxide
MgO	Magnesium Oxide
CaO	Calcium Oxide

Symbols

$	US Dollar
USD	US Dollar
°C	Celsius
€	Euro
$M1$	Iron ore stream entering the shaft furnace in kg/tls
$M2$	Metallic stream exiting the shaft furnace in kg/tls
$M3$	Molten steel exiting the electric arc furnace kg/tls
$M4$	Hydrogen stream entering the shaft furnace in kg/tls
$M5$	By-product Water and unreacted Hydrogen exiting the shaft furnace in kg/tls
$M6$	Carbon fines added to the electric arc furnace in kg/tls
$M7$	Slag formers added to the electric arc furnace in kg/tls
$M8$	Slag stream exiting the electric arc furnace in kg/tls
$M9$	By-product gases exiting the electric arc furnace in kg/tls
$M10$	Hydrogen stream exiting the electrolyzer in kg/tls
$M11$	Hydrogen stream exiting the recuperator in kg/tls
$M12$	By-product Water and unreacted Hydrogen exiting the recuperator in kg/tls
$M13$	Water stream exiting the condenser in kg/tls
$M14$	Oxygen stream exiting the electrolyzer in kg/tls
$H1$	Enthalpy of stream M1 in KWh/tls
$H2$	Enthalpy of stream M2 in KWh/tls
$H3$	Enthalpy of stream M3 in KWh/tls
$H4$	Enthalpy of stream M4 in KWh/tls
$H5$	Enthalpy of stream M5 in KWh/tls
$H6$	Enthalpy of stream M6 in KWh/tls
$H7$	Enthalpy of stream M7 in KWh/tls

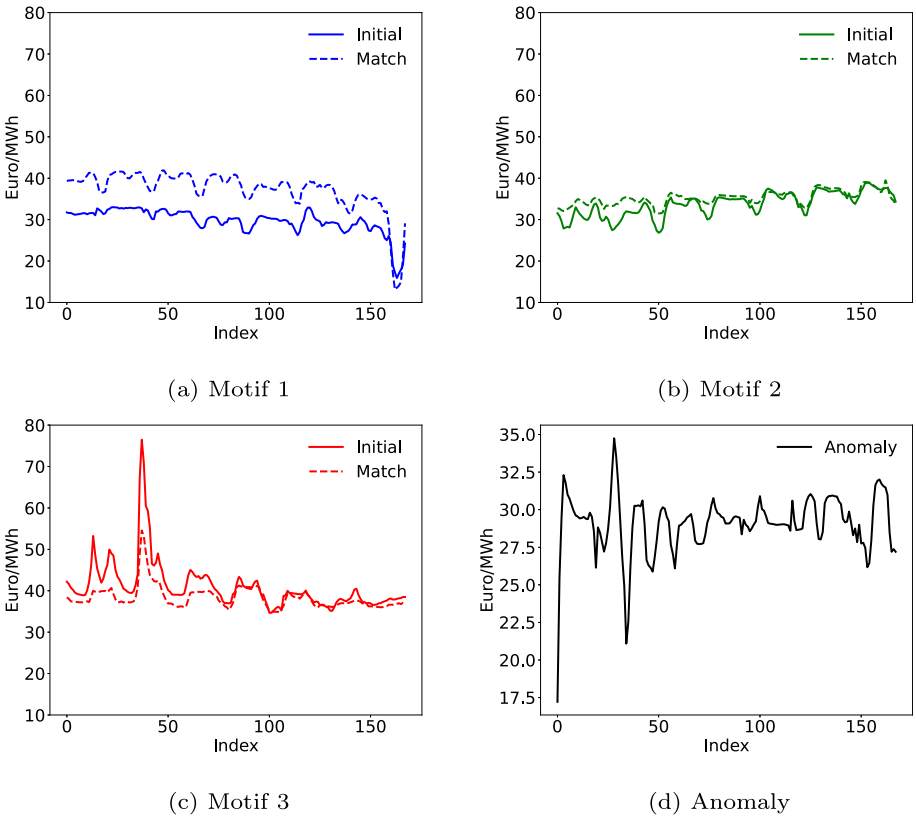

Fig. 10. Closely repeating patterns (a–c) of length 1 week and an anomalous (d) 1 week period with high variability detected in the 2019 Bergen day ahead electricity prices.

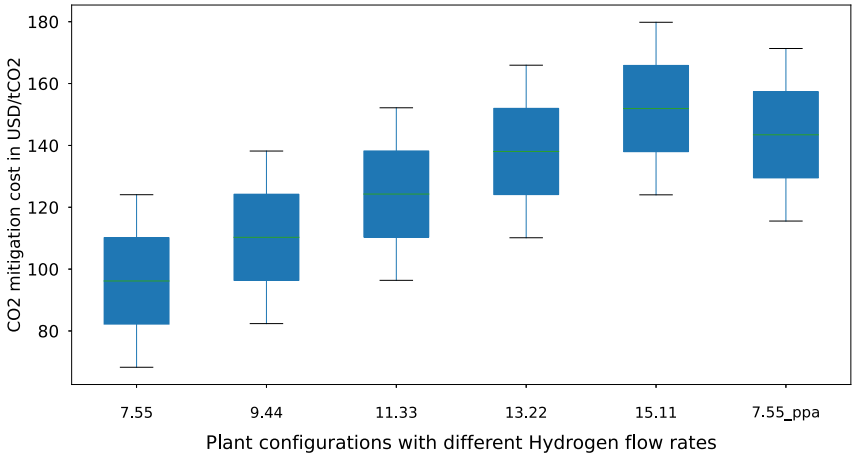

Fig. 11. CO_2 mitigation costs for different configurations.

$H8$	Enthalpy of stream M8 in KWh/tls
$H9$	Enthalpy of stream M9 in KWh/tls
$H10$	Enthalpy of stream M10 in KWh/tls
$H11$	Enthalpy of stream M11 in KWh/tls
$H12$	Enthalpy of stream M12 in KWh/tls
$H13$	Enthalpy of stream M13 in KWh/tls
$H14$	Enthalpy of stream M14 in KWh/tls

Funding

This project has received funding from the European Union's Horizon 2020 research and innovation programme under the Marie Skłodowska-Curie grant agreement No 765515.

CRediT authorship contribution statement

Abhinav Bhaskar: Conceptualization, Methodology, Software, Visualization, Investigation, Data curation, Writing – review & editing. **Rockey Abhishek:** Data curation, Writing – original draft, Investigation, Software, Visualization. **Mohsen Assadi:** Supervision, Funding. **Homam Nikpey Somehesaraei:** Supervision, Funding.

Declaration of competing interest

The authors declare that they have no known competing financial interests or personal relationships that could have appeared to influence the work reported in this paper.

Data availability

Python codes used for modeling the H_2 -SF-EAF system and calculating the optimal electrolyzer production schedule are available at Zenodo repository (Bhaskar, 2021).

Acknowledgments

The authors would like to thank Kevin Gould from Statkraft for his valuable inputs and advice. The authors appreciate the feedback and suggestions received from anonymous reviewers.

References

Åhman, M., Olsson, O., Vogl, V., Nyqvist, B., Maltais, A., Nilsson, L.J., Hallding, K., Skånberg, K., Nilsson, M., 2018. Hydrogen steelmaking for a low-carbon economy: A joint LU-SEI working paper for the HYBRIT project. p. 28, Stockholm environment institute and Lund University, Stockholm, URL: https://www.sei.org/wp-content/uploads/2018/09/hydrogen-steelmaking-for-a-low-carbon-economy.pdf.

Abdin, Z., Tang, C., Liu, Y., Catchpole, K., 2021. Large-scale stationary hydrogen storage via liquid organic hydrogen carriers. IScience 24, 102966. http://dx.doi.org/10.1016/j.isci.2021.102966.

Andersson, J., 2021. Application of liquid hydrogen carriers in hydrogen steelmaking. Energies 14, 1392. http://dx.doi.org/10.3390/en14051392, URL: https://www.mdpi.com/1996-1073/14/5/1392.

ArcelorMittal, 2022. Arcelormittal steels used in first hydrogen-certified pipeline.

Backes, J.G., Suer, J., Pauliks, N., Neugebauer, S., Traverso, M., 2021. Life cycle assessment of an integrated steel mill using primary manufacturing data: Actual environmental profile. Sustainability (Switzerland) 13, http://dx.doi.org/10.3390/su13063443.

Bailera, M., Lisbona, P., Peña, B., Romeo, L.M., 2021. A review on CO2 mitigation in the iron and steel industry through power to x processes. J. CO2 Util. 46, 101456. http://dx.doi.org/10.1016/j.jcou.2021.101456, URL: https://linkinghub.elsevier.com/retrieve/pii/S2212982021000238.

Bhaskar, A., 2021. Levellized cost of prodution of hydrogen based steel production in bergen Norway, using a cost optimization framework for optimal scheduling of hydrogen electrolyzers. http://dx.doi.org/10.5281/zenodo.5520046, Zenodo, Oslo.

Bhaskar, A., Assadi, M., Somehsaraei, H.N., 2021. Energy conversion and management : X can methane pyrolysis based hydrogen production lead to the decarbonisation of iron and steel industry ? Energy Convers. Manage.: X 10, 100079. http://dx.doi.org/10.1016/j.ecmx.2021.100079.

Birat, J.-P., 2020. Society, materials, and the environment: The case of steel. Metals 10, 331. http://dx.doi.org/10.3390/met10030331, URL: https://www.mdpi.com/2075-4701/10/3/331.

Bosch, J., Staffell, I., Hawkes, A.D., 2018. Temporally explicit and spatially resolved global offshore wind energy potentials. Energy 163, 766–781. http://dx.doi.org/10.1016/j.energy.2018.08.153.

Cavaliere, P., 2019. Direct reduced iron: most efficient technologies for greenhouse emissions abatement. In: Clean Ironmaking and Steelmaking Processes. Springer International Publishing, Cham, pp. 419–484. http://dx.doi.org/10.1007/978-3-030-21209-4_8.

Chase, M., 1998. NIST-JANAF Thermochemical Tables, 4 9, American Chemical Society;American institute of Physics for the National institute of standards and technology, p. 1961,

Christensen, A., 2020. Assessment of hydrogen production costs from electrolysis: united states and Europe. URL:.

da Costa, A.R., Wagner, D., Patisson, F., 2013. Modelling a new, low CO2 emissions, hydrogen steelmaking process. J. Cleaner Prod. 46, 27–35. http://dx.doi.org/10.1016/J.JCLEPRO.2012.07.045, URL: https://www.sciencedirect.com/science/article/pii/S0959652612003836.

David, M., Ocampo-Martínez, C., na, R.S.-P., 2019. Advances in alkaline water electrolyzers: A review. J. Energy Storage 23, 392–403. http://dx.doi.org/10.1016/j.est.2019.03.001, URL: https://linkinghub.elsevier.com/retrieve/pii/S2352152X18306558.

DEA, 2020. Technology descriptions and projections for long term energy system planning. p. 234, Danish energy agency, URL: http://www.ens.dk/teknologikatalog.

Duarte, P., Pauluzzi, D., 2019. Premium quality DRI products from ENERGIRON. pp. 1–19, URL: https://www.energiron.com/wp-content/uploads/2019/05/Premium-Quality-DRI-Products-from-ENERGIRON.pdf Energiron.

EC, 2020. Report from the commission to the European parliament and the council, report on the functioning of the European carbon market. European Commission, Brussels, URL: https://eur-lex.europa.eu/legal-content/EN/TXT/?uri=CELEX%3A52020DC0740.

Elberry, A.M., Thakur, J., Santasalo-aarnio, A., 2021. Large-scale compressed hydrogen storage as part of renewable electricity storage systems. Int. J. Hydrogen Energy 46, 15671–15690. http://dx.doi.org/10.1016/j.ijhydene.2021.02.080.

Energiron, 2022. Hytemp -ENERGIRON hot metal transport. URL: https://www.energiron.com/hytemp-system/.

Equinor, 2021. Sse thermal and equinor developing plans for world-leading hydrogen storage facility in yorkshire. p. 1, URL: https://www.equinor.com/en/where-we-are/united-kingdom/sse-thermal-and-equinor-developing-plans-for-world-leading-hydrogen-storage-facility-in-yorkshire.html.

EUROFER, 2020. European steel in figures 2020. p. 74, EUROFER, URL: https://www.eurofer.eu/assets/Uploads/European-Steel-in-Figures-2020.pdf.

Fischedick, M., Marzinkowski, J., Winzer, P., Weigel, M., 2014. Techno-economic evaluation of innovative steel production technologies. J. Cleaner Prod. 84, 563–580. http://dx.doi.org/10.1016/j.jclepro.2014.05.063.

Gharghabi, S., Ding, Y., Yeh, C.C.M., Kamgar, K., Ulanova, L., Keogh, E., 2017. Matrix profile VIII: Domain agnostic online semantic segmentation at superhuman performance levels. In: Proceedings - IEEE International Conference on Data Mining. ICDM, 2017-Novem, pp. 117–126. http://dx.doi.org/10.1109/ICDM.2017.21.

Gielen, D., Saygin, D., Taibi, E., Birat, J.-P., 2020. Renewables-based decarbonization and relocation of iron and steel making: A case study. J. Ind. Ecol. 24, 1113–1125. http://dx.doi.org/10.1111/jiec.12997, URL: https://onlinelibrary.wiley.com/doi/10.1111/jiec.12997.

Gruobi, 2021. Gurobi optimizer reference manual.

Gulcin, D., Weber, N., Heinrichs, H.U., Linßen, J., Robinius, M., Kukla, P.A., Stolten, D., 2020. Technical potential of salt caverns for hydrogen storage in Europe. Int. J. Hydrogen Energy 45, 6793–6805. http://dx.doi.org/10.1016/j.ijhydene.2019.12.161.

Hampp, J., Düren, M., Brown, T., 2021. Import options for chemical energy carriers from renewable sources to Germany import options for chemical energy carriers from renewable sources to Germany.

Heidari, A., Niknahad, N., Iljana, M., Fabritius, T., 2021. A review on the kinetics of iron ore reduction by hydrogen. Materials 14, 7540. http://dx.doi.org/10.3390/ma14247540, URL: https://www.mdpi.com/1996-1944/14/24/7540.

Herman, J., Usher, W., 2017. SALib: An open-source Python library for sensitivity analysis. J. Open Source Softw. 2, 97. http://dx.doi.org/10.21105/joss.00097.

Howarth, R.W., Jacobson, M.Z., 2021. How green is blue hydrogen? Energy Sci. Eng. 1–12. http://dx.doi.org/10.1002/ese3.956.

Hunter, J.D., 2007. Matplotlib: A 2D graphics environment. Comput. Sci. Eng. 9, 90–95. http://dx.doi.org/10.1109/MCSE.2007.55.

Iberdola, 2022. Compressed hydrogen storage tanks. URL: https://www.iberdrola.com/press-room/news/detail/storage-tanks-green-hydrogen-puertollano.

IEA, 2020. Iron and steel technology roadmap : Towards more sustainable steelmaking. 3, p. 190,

IEA, 2021. IEA (2021) global energy review 2021, IEA, Paris. URL: https://www.iea.org/reports/global-energy-review-2021.

IRENA, 2020. Green hydrogen cost reduction: Scaling up electrolysers to meet the 1.5c climate goal. p. 106, IRENA, Abu Dhabi.

IRENA, 2022. Geopolitics of the energy transformation: The hydrogen factor. International Renewable Energy Agency.

Jacobasch, E., Herz, G., Rix, C., Müller, N., Reichelt, E., Jahn, M., Michaelis, A., 2021. Economic evaluation of low-carbon steelmaking via coupling of electrolysis and direct reduction. J. Cleaner Prod. 328, 129502. http://dx.doi.org/10.1016/j.jclepro.2021.129502, URL: https://linkinghub.elsevier.com/retrieve/pii/S0959652621036817.

Kim, S.H., Zhang, X., Ma, Y., Filho, I.R.S., Schweinar, K., Angenendt, K., Vogel, D., Stephenson, L.T., El-Zoka, A.A., Mianroodi, J.R., Rohwerder, M., Gault, B., Raabe, D., 2021. Influence of microstructure and atomic-scale chemistry on the direct reduction of iron ore with hydrogen at 700° c. Acta Mater. 212, http://dx.doi.org/10.1016/j.actamat.2021.116933.

Kirschen, M., Badr, K., Pfeifer, H., 2011. Influence of direct reduced iron on the energy balance of the electric arc furnace in steel industry. Energy 36, 6146–6155. http://dx.doi.org/10.1016/j.energy.2011.07.050.

Krüger, A., Andersson, J., Grönkvist, S., Cornell, A., 2020. Integration of water electrolysis for fossil-free steel production. Int. J. Hydrogen Energy http://dx.doi.org/10.1016/j.ijhydene.2020.08.116.

Levi, P., m'barek, B.B., Lu, H., Tao, J.Y., Xiuping, L., Swalec, C., Myllyvirta, L., Hasanbeigi, A., Zhang, Q., 2022. Global steel production costs. Transition zero, URL: https://www.transitionzero.org/reports/global-steel-production-costs.

LKAB, 2017. Lkab pellet steel vs. average European primary steel methodological appendix. URL: https://www.lkab.com/sv/SysSiteAssets/documents/blandat/lkab-value-chain-comparison-methodological-annex.pdf.

Lord, A.S., Kobos, P.H., Borns, D.J., 2014. Geologic storage of hydrogen: Scaling up to meet city transportation demands. Int. J. Hydrogen Energy 39, 15570–15582. http://dx.doi.org/10.1016/j.ijhydene.2014.07.121, URL: https://linkinghub.elsevier.com/retrieve/pii/S0360319914021223.

Maggiolino, S., 2019. Hyl newsletter 2019. URL: www.tenova.comandwww.energiron.com.

Matute, G., Yusta, J., Correas, L., 2019. Techno-economic modelling of water electrolysers in the range of several MW to provide grid services while generating hydrogen for different applications: A case study in Spain applied to mobility with FCEVs. Int. J. Hydrogen Energy 44, 17431–17442. http://dx.doi.org/10.1016/j.ijhydene.2019.05.092, URL: https://linkinghub.elsevier.com/retrieve/pii/S0360319919319482.

McKinney, W., 2010. Data structures for statistical computing in python. In: van der Walt, S., Millman, J. (Eds.), Proceedings of the 9th Python in Science Conference. pp. 51–56.

Midrex, 2021. Midrex hotlink process. URL: https://www.kobelco.co.jp/english/products/ironunit/dri/dri04.html.

Moro, A., Lonza, L., 2018. Electricity carbon intensity in European member states: Impacts on GHG emissions of electric vehicles. Transp. Res. D: Transp. Environ. 64, 5–14. http://dx.doi.org/10.1016/j.trd.2017.07.012.

nelhydrogen, 2022. Nel electrolysers-brochure. URL: https://nelhydrogen.com/product/atmospheric-alkaline-electrolyser-a-series/.

Nguyen, T., Abdin, Z., Holm, T., Mérida, W., 2019. Grid-connected hydrogen production via large-scale water electrolysis. Energy Convers. Manage. 200, 112108. http://dx.doi.org/10.1016/j.enconman.2019.112108, URL: https://www.sciencedirect.com/science/article/pii/S0196890419311148.

Nordpool, 2020. Nordpool historical electricity spot prices. URL: https://www.nordpoolgroup.com/historical-market-data/.

Norway, S., 2021. Statistics Norway. URL: https://www.ssb.no/en/energi-og-industri/energi/statistikk/elektrisitet.

OECD, 2020. Steel market developments Q2 2020. OECD, URL: https://www.oecd.org/sti/ind/steel-market-developments-Q2-2020.pdf.

Papadias, D.D., Ahluwalia, R.K., 2021. Bulk storage of hydrogen. Int. J. Hydrogen Energy 46, 34527–34541. http://dx.doi.org/10.1016/j.ijhydene.2021.08.028.

Pei, M., Petäjäniemi, M., Regnell, A., Wijk, O., 2020. Toward a fossil free future with hybrit: Development of iron and steelmaking technology in Sweden and Finland. Metals 10, 1–11. http://dx.doi.org/10.3390/met10070972.

Penev, M., Zuboy, J., Hunter, C., 2019. Economic analysis of a high-pressure urban pipeline concept (HyLine) for delivering hydrogen to retail fueling stations. Transp. Res. D: Transp. Environ. 77, 92–105. http://dx.doi.org/10.1016/j.trd.2019.10.005, URL: https://www.sciencedirect.com/science/article/pii/S1361920918311982.

Perez, F., Granger, B.E., 2007. IPython: A system for interactive scientific computing. Comput. Sci. Eng. 9, 21–29. http://dx.doi.org/10.1109/MCSE.2007.53.

Pimm, A.J., Cockerill, T.T., Gale, W.F., 2021. Energy system requirements of fossil-free steelmaking using hydrogen direct reduction. J. Cleaner Prod. 312, http://dx.doi.org/10.1016/j.jclepro.2021.127665.

Primemetals, 2022. Zero-carbon hyfor direct-reduction pilot plant starts operation. URL: https://magazine.primetals.com/2021/06/24/zero-carbon-hyfor-direct-reduction-pilot-plant-commences-operation-in-donawitz-austria/.

Rissman, J., Bataille, C., Masanet, E., Aden, N., Morrow, W.R., Zhou, N., Elliott, N., Dell, R., Heeren, N., Huckestein, B., Cresko, J., Miller, S.A., Roy, J., Fennell, P., Cremmins, B., Blank, T.K., Hone, D., Williams, E.D., de la Rue du Can, S., Sisson, B., Williams, M., Katzenberger, J., Burtraw, D., Sethi, G., Ping, H., Danielson, D., Lu, H., Lorber, T., Dinkel, J., Helseth, J., 2020. Technologies and policies to decarbonize global industry: Review and assessment of mitigation drivers through 2070. Appl. Energy 266, 114848. http://dx.doi.org/10.1016/j.apenergy.2020.114848.

Sartor, O., Sourrisseau, S., Mari, E., Peter, F., Buck, M., Graf, A., Vangenechten, D., 2022. Getting the transition to CBAM right: Finding pragmatic solutions to key implementation questions IMPULSE.

Sch, N., Bau, U., Reuter, M.A., Dahmen, M., Fritz, T.C.R., 2021. Decarbonizing copper production by power-to-hydrogen : A techno- economic analysis. J. Cleaner Prod. 306, http://dx.doi.org/10.1016/j.jclepro.2021.127191.

Schäfer, M., 2021. From 2025: “green” steel for Mercedes-Benz. URL: https://www.daimler.com/sustainability/climate/green-steel.html.

Sobol, I., 2001. Global sensitivity indices for non-linear mathematical models and their Monte carlo estimates. Math. Comput. Sumul. 5, 271–280.

Stöckl, F., Schill, W.P., Zerrahn, A., 2021. Optimal supply chains and power sector benefits of green hydrogen. Sci. Rep. 11, 1–14. http://dx.doi.org/10.1038/s41598-021-92511-6.

Stougaard, A., 2021. Ørsted joins the SteelZero initiative to support transition to low-carbon steel. URL: https://orsted.com/en/media/newsroom/news/2020/12/633975720078575.

Suer, J., Traverso, M., Ahrenhold, F., 2021. Carbon footprint of scenarios towards climate-neutral steel according to ISO 14067. J. Cleaner Prod. 318, 128588. http://dx.doi.org/10.1016/j.jclepro.2021.128588.

sunfire, 2022. Sunfire-hylink alkaline electrolyzer. URL: https://www.sunfire.de/files/sunfire/images/content/Sunfire.de%20(neu)/Sunfire-Factsheet-HyLink-Alkaline-20210305.pdf.

Sydvaranger, 2022. Norwegian Iron ore mine in northern Norway. URL: https://www.sydvarangergruve.no/home-eng.

Thomassen, G., Dael, M.V., Passel, S.V., You, F., 2019. How to assess the potential of emerging green technologies? Towards a prospective environmental and techno-economic assessment framework. Green Chem. 21, 4868–4886. http://dx.doi.org/10.1039/c9gc02223f.

thyssenkrupp, 2022. Thyssenkrupp electrolyzer brochure. URL: https://ucpcdn.thyssenkrupp.com/_binary/UCPthyssenkruppBAISUhdeChlorineEngineers/en/products/water-electrolysis-hydrogen-production/210622-gH2-product-brochure.pdf.

TianjinMainlandHydrogenEquipment, 2022. Tianjin mainland hydrogen equipment brochure. URL: http://www.cnthe.com/en/product_detail-35-43-30.html.

Towler, R.S.G., 2013. Chemical Engineering Design, second ed. Elsevier, http://dx.doi.org/10.1016/C2009-0-61216-2.

Trollip, H., McCall, B., Bataille, C., 2022. How green primary iron production in South Africa could help global decarbonization. Climate Policy 1–12. http://dx.doi.org/10.1080/14693062.2021.2024123.

UNCTAD, 2021. A European union carbon border adjustment mechanism : Implications for developing countries. United Nations Conference on Trade and Development, URL: https://unctad.org/system/files/official-document/osginf2021d2_en.pdf.

UNIDO, 2021. Industrial deep decarbonisation initiative. URL: https://www.unido.org/IDDI.

Uribe-Soto, W., Portha, J.-F., Commenge, J.-M., Falk, L., 2017. A review of thermochemical processes and technologies to use steelworks off-gases. Renew. Sustain. Energy Rev. 74, 809–823. http://dx.doi.org/10.1016/j.rser.2017.03.008, URL: https://linkinghub.elsevier.com/retrieve/pii/S1364032117303234.

V, M., Zhai, P., Pirani, A., Connors, S.L., Péan, C., Berger, S., Caud, N., Chen, Y., Goldfarb, L., Gomis, M.I., Huang, M., Leitzell, K., Lonnoy, E., Matthews, J., Maycock, T.K., Waterfield, T., Yelekçi, O., Yu, R., Zhou, B., 2021. Ipcc,2021: Climate change 2021: The physical science basis. contribution of working group I to the sixth assessment report of the intergovernmental panel on climate change. Cambridge University Press.

Vartiainen, E., Breyer, C., Moser, D., Medina, E.R., Busto, C., Masson, G., Bosch, E., Jäger-Waldau, A., 2021. True cost of solar hydrogen. Solar RRL http://dx.doi.org/10.1002/solr.202100487.

Vogl, V., Åhman, M., Nilsson, L.J., 2018. Assessment of hydrogen direct reduction for fossil-free steelmaking. J. Cleaner Prod. 203, 736–745. http://dx.doi.org/10.1016/j.jclepro.2018.08.279.

Vogl, V., Åhman, M., Nilsson, L.J., 2021a. The making of green steel in the EU: a policy evaluation for the early commercialization phase. Climate Policy 21, 78–92. http://dx.doi.org/10.1080/14693062.2020.1803040, URL: https://www.tandfonline.com/doi/full/10.1080/14693062.2020.1803040.

Vogl, V., Sanchez, F., Gerres, T., Lettow, F., Bhaskar, A., Swalec, C., Mete, G., Åhman, M., Lehne, J., Schenk, S., Witecka, W., Olsson, O., Rootzén, J., 2021b. Green steel tracker. URL: https://www.sei.org/featured/green-steel-tracker/.

Volvo, 2021. Volvo group and SSAB to collaborate on the world’s first vehicles of fossil-free steel. URL: https://www.volvogroup.com/en/news-and-media/news/2021/apr/news-3938822.html.

Wagner, M., 2009. Thermal analysis in practice. Collect. Appl. Thermal Anal..

Walt, S.V.D., Colbert, S.C., Varoquaux, G., 2011. The numPy array: A structure for efficient numerical computation. Comput. Sci. Eng. 13, 22–30. http://dx.doi.org/10.1109/MCSE.2011.37.

Weigel, M., Fischedick, M., Marzinkowski, J., Winzer, P., 2016. Multicriteria analysis of primary steelmaking technologies. J. Cleaner Prod. 112, 1064–1076. http://dx.doi.org/10.1016/j.jclepro.2015.07.132.

Wich, T., Lueke, W., Deerberg, G., Oles, M., 2020. Carbon2chem®-CCU as a step toward a circular economy. Front. Energy Res. 7, http://dx.doi.org/10.3389/fenrg.2019.00162, URL: https://www.frontiersin.org/article/10.3389/fenrg.2019.00162/full.

Worldsteel, A., 2020. Major steel-producing countries 2018 and 2019 million. pp. 1–8, 2020 World Steel in Figures, Worldsteel Association, URL: http://www.worldsteel.org/wsif.php.

YARA, 2021. Green ammonia from HEGRA to secure Norwegian competitiveness. URL: https://www.yara.com/corporate-releases/green-ammonia-from-hegra-to-secure-norwegian-competitiveness/.

Yeh, C.C.M., Zhu, Y., Ulanova, L., Begum, N., Ding, Y., Dau, H.A., Silva, D.F., Mueen, A., Keogh, E., 2017. Matrix profile I: All pairs similarity joins for time series: A unifying view that includes motifs, discords and shapelets. In: Proceedings - IEEE International Conference on Data Mining, ICDM. IEEE, pp. 1317–1322. http://dx.doi.org/10.1109/ICDM.2016.89.

Yeh, C.-C.M., Zhu, Y., Ulanova, L., Begum, N., Ding, Y., Dau, H.A., Zimmerman, Z., Silva, D.F., Mueen, A., Keogh, E., 2018. Time series joins, motifs, discords and shapelets: a unifying view that exploits the matrix profile. Data Min. Knowl. Discov. 32, 83–123. http://dx.doi.org/10.1007/s10618-017-0519-9.